Faculty of Physics, Astronomy and Applied Computer Science
Jagellonian University

# Beyond the standard $t$–$J$ model

Krzysztof Wohlfeld

A thesis, written under the supervision of Prof. Dr. Andrzej M. Oleś, presented in part fulfilment of the requirements for the degree of Doctor of Philosophy in the Jagellonian University

Cracow, May 2009

# Contents

# List of abbreviations and remarks on notation

1D – one-dimensional
2D – two-dimensional
3D – three-dimensional
AF – antiferromagnetic
AO – alternating orbital
CDW – charge density wave
FM – ferromagnetic
FO – ferro-orbital
LOW – linear orbital wave
LSW – linear spin wave
SCBA – self-consistent Born approximation
VCA – variational cluster approach

Throughout the thesis:
(i) we use $\mathcal{H}$ (possibly with some indices) to denote any type of the Hubbard Hamiltonian,
(ii) we use $H$ (possibly with some indices) to denote any component of the (standard or extended) $t$–$J$ model,
(iii) we use $H^{eff}$ (possibly with some indices) to denote any component of the effective model obtained from the (standard or extended) $t$–$J$ model by introducing slave fermions or slave bosons,
(iv) the main Hamiltonians of the chapters (Hubbard, $t$–$J$, and possibly the effective one) do not have any index,
(v) the lattice constant is set to unity,
(vi) $\sum_{\langle ij \rangle}$ means taking summation over the *bond* formed between site $i$ and $j$.

Despite the above mentioned common features of the notation used in the thesis the notation in each chapter is independent of the other chapters and is logically consistent only within each chapter.

We call the spin $t$–$J$ model of Refs. [1, 2, 3] the *standard* $t$–$J$ model [see Eq. (1.22) in this thesis] to distinguish it from various other $t$–$J$–type models discussed in this thesis.

# Preface

In this thesis we discuss and present solutions of three related problems which arise in strongly correlated electron systems:

*1. Explaining charge order in* $Sr_{14-x}Ca_xCu_{24}O_{41}$.— The first problem concerns the explanation of the peculiar charge order observed experimentally at low temperature $T = 20$K in the coupled ladders $Cu_2O_5$ in $Sr_{14-x}Ca_xCu_{24}O_{41}$ [4, 5, 6, 7, 8]. On the one hand, the resonant soft x-ray scattering shows that the charge order there is formed by a charge density wave (CDW) phase with odd period and is stable for $x = 0$ and $x = 11$ in $Sr_{14-x}Ca_xCu_{24}O_{41}$ presumably due to the on-site Coulomb repulsion [7, 8]. On the other hand, a CDW phase with even period has not been observed in these systems [8]. These are striking results as they contradict the theoretical prediction of a stable CDW phase with even period for $x = 4$ and no CDW order for other values of $x$ [9, 10, 11].

*2. Verifying the idea of orbitally induced hole localization.*— The next problem is more general and 'touches' the idea that the mere presence of orbital degeneracy in the transition metal oxides could lead to the hole confinement in the strongly correlated electron system. This idea can be backed by the following facts: (i) the manganites show a colossal magnetoresistive effect [12, 13, 14, 15] which can be attributed to the orbital degeneracy [16, 17, 18], (ii) the transition metal oxides with orbital degeneracy (e.g. manganites or vanadates) have much more stable insulating phases in the regime of hole doping [15, 19] than the cuprates without orbital degeneracy [20]. However, in strongly correlated systems without orbital degeneracy (and described by the simple Hubbard model) the hole had been thought to be localized for a very long time [21] and only much later [22, 23] it was shown that the hole was mobile. This suggests that the verification of the idea of orbitally induced hole localization should be performed rather carefully.

*3. Understanding hole motion in* $LaVO_3$.— The last problem is devoted to the understanding of the behaviour of the single hole doped into the *ab* plane of $LaVO_3$. This system is a Mott insulator and superexchange interactions stabilize the spin antiferromagnetic (AF) and alternating orbital (AO) ordered ground state [19, 24, 25]. The problem which arises here can be in short formulated as follows: upon doping this plane with holes (which is possible by substituting lantanium for strontium in $La_{1-x}Sr_xVO_3$) the orbital dynamics seems to influence the hole motion much more than the spin dynamics (see conjecture in the Introduction to Chapter 5 of this thesis based on the experimental results from Ref. [19]). Thus, the question is: why the spin dynamics is quenched in the hole doped AF and AO state.

*Common feature of the three problems.*— Although all of the three topics belong to the strongly correlated transition metal oxides [20], 'at first glance'

it is hard to imagine that there is something more which connects *all three* of them.[1] However, a closer look (taken in the consecutive chapters) will show that the three simplest models, formulated to solve these problems, will have a lot in common. Actually, all three of them will turn out to be merely a more or less elaborate version of the *standard* $t$–$J$ model [1, 2, 3] although the standard $t$–$J$ model itself will become evident not to be enough to explain these phenomena. More precisely, it will turn out that the simplest models capable of explaining the above problems will be: (i) the $t$–$J$ model for *coupled* ladders for the first problem, (ii) the $t_{2g}$ orbital $t$–$J$ model *with* three-site terms for the second one and (iii) the $t_{2g}$ *spin-orbital* $t$–$J$ model with three-site terms for the third one. Thus, we will show that, as the title of the thesis suggests, one indeed has to go *beyond the standard* $t$–$J$ *model* to be able to understand the physics behind all these three phenomena.

*Aim of the thesis.*— The purpose of this thesis is to give answers to the three problems using the above mentioned extensions of the $t$–$J$ models. As 'a side effect' one will see how powerful is the concept of the $t$–$J$ model and the canonical perturbation expansion [1, 2] or the Zhang-Rice scheme [26]: merely slight modifications of the model mean that it is still capable of explaining a huge variety of phenomena present in the transition metal oxides.

*Structure of the thesis.*— The thesis is organized as follows. Chapter 1 contains a preliminary material concerning the standard $t$–$J$ model: (i) the Hubbard model, (ii) its derivation from the Hubbard model by the canonical perturbation expansion, and finally (iii) its form and range of applicability. This chapter may be easily skipped by the reader familiar with the standard $t$–$J$ model [1, 2, 3], though a quick look at this chapter would be always of great help in understanding the results presented in this thesis. Next in the three consecutive chapters (which are called the *main* chapters of the thesis) we discuss the three problems mentioned above: (i) in Chapter 2 we explain the charge order in $Sr_{14-x}Ca_xCu_{24}O_{41}$ using the $t$–$J$ model for *coupled* ladders, (ii) in Chapter 3 we verify the idea of orbitally induced hole localization using the $t_{2g}$ orbital $t$–$J$ model *with* three-site terms, and (iii) in Chapter 4 we try to understand hole motion in $LaVO_3$ using the the $t_{2g}$ *spin-orbital* $t$–$J$ model with three-site terms. Finally, in Summary we briefly discuss the solutions of the problems and the common features of the new $t$–$J$ models. The thesis is supplemented by two appendices (which contain some mathematical derivation needed in Chapter 3), Bibliography, 'Streszczenie' (summary in Polish), and the list of publications which were published during my PhD studies. Finally, in the end we mention those people without whose support it would have never been possible to complete this thesis.

The organization of material serves the main idea of the thesis. First, in each of the three main chapters: (i) we discuss the problem in more detail in the introduction (first section), (ii) we introduce the new $t$–$J$ model by carefully discussing its differences with respect to the standard $t$–$J$ model (second section), (iii) we derive the new $t$–$J$ model from the Hubbard-type model appropriate for the considered problem using the canonical perturbation expansion [1, 2] or the Zhang-Rice scheme [26] (third section). Second, as the methods of solving each $t$–$J$ model differ, we introduce the slave bosons (Chapter 2) or slave

[1] Although, the reader familiar with the strongly correlated electron systems will immediately note that the second and third problem has a lot in common. See also Sec. 4.7 for a more detailed discussion of the similarities between them.

fermions (Chapters 3 and 4) to overcome the constraint of the restricted hopping present in any $t$–$J$ model and only then we solve the effective model written in the slave particle language using the mean-field in Chapter 2 or self-consistent Born approximation (SCBA) in Chapter 3 and 4 (fourth section). Finally, we discuss the results including its validity (fifth section), and we draw some conclusions (sixth section). Furthermore, each main chapter is supplemented by a Postscriptum (seventh section) in which we discuss some side issues which are interesting but are not central for the main message and can be easily skipped in first reading. We would like to stress that the ability to build a common structure of the three main chapters reflects (practically) the above mentioned common origin of the three problems discussed in the thesis.

# Chapter 1

# Motivation: The standard $t$–$J$ model

## 1.1 The Hubbard model

*Hamiltonian.*— The (arche)typical model which describes the strongly correlated electrons is the Hubbard model described by the Hamiltonian [27]

$$\mathcal{H} = -t \sum_{\langle \mathbf{ij} \rangle, \sigma} \left( c^{\dagger}_{\mathbf{i}\sigma} c_{\mathbf{j}\sigma} + \text{H.c.} \right) + U \sum_{\mathbf{i}} n_{\mathbf{i}\uparrow} n_{\mathbf{i}\downarrow}, \tag{1.1}$$

where $\langle \mathbf{ij} \rangle$ denotes the bond formed between site $\mathbf{i}$ and $\mathbf{j}$, $c^{\dagger}_{\mathbf{i}\sigma}$ operator creates an electron at site $\mathbf{i}$ with spin $\sigma$, and the electron density operator is defined as $n_{\mathbf{i}\sigma} = c^{\dagger}_{\mathbf{i}\sigma} c_{\mathbf{i}\sigma}$. Here the first term is responsible for the hopping $\propto t$ of electrons on a hypercubic lattice while the second term describes the Coulomb repulsion $\propto U$ between two electrons with opposite spins on the same site. This model is introduced to describe a common situation which takes place in various transition metal oxides [20]: the lattice potential is very strong and one needs to calculate the Coulomb interaction between electrons in the (almost) atomic wavefunctions. This leads to a modification of the bare Coulomb potential: it is short range (i.e. merely on-site) but strongly amplified. This naturally means that the physical regime of the model is when $U > W$ (where $W = 2zt$ is the bandwidth and $z$ is the coordination number for the hypercubic lattice) and throughout the thesis we will assume that one is always in this regime.

Actually the more general definition of the Hubbard model (1.1) would contain the chemical potential. However, it is customary to omit that term and instead to specify the number of electrons per site $n$ present in the system separately. This can take the values $0 \leq n \leq 2$ due to the Pauli principle.

*Space dimensions of the lattice.*— Finally, let us note that the model Eq. (1.1) can be defined as well in the one-dimensional (1D), two-dimensional (2D) and three-dimensional (3D) version. However, due to its most interesting (in my opinion) application concerns the 2D copper oxide layers of high-$T_c$ cuprates [28]. Moreover, as we will be interested either in layered structures (Chapter 2) or in situations where the orbital order (Chapter 3) or spin and orbital order (Chapter 4) contains two spatial dimensions, we restrict the discussion to the 2D Hubbard model.

*Drawbacks and advantages of the model.*— It is worth mentioning that the model Eq. (1.1) has been indeed very successful in describing various properties of the strongly correlated electron systems [28]. However, there are two main drawbacks of the model. First, despite its simplicity it is hard to solve it in the interesting regime $n \neq 1$ as the Monte Carlo simulations often break down due to the 'sign problem' whereas all other methods are also not reliable due to the huge dimensions of the Hilbert space of the model (which in the half-filled case is $[N!/(N/2)!(N/2)!]^2$ where $N$ is the number of lattice sites) [28]. Second, let us remark that many systems are too complicated to have the electron correlations described by the Hubbard model in a reliable way: e.g. the orbital degeneracy regime can change the matters drastically [29].

On the one hand, to overcome the first difficulty one performs the canonical perturbation expansion[1] of the Hubbard model which hugely reduces the dimensionality of the Hilbert space by neglecting the high-energy states in the regime $U > W$. This is done in the next two sections and the model which is obtained after such an expansion is the standard $t$–$J$ model. On the other hand, one should add extra terms and/or modify the two existing ones in Eq. (1.1) to make the Hubbard model more realistic. Actually, in the next three chapters of this thesis we will combine both of the approaches: we will modify the Hubbard model to make it more realistic and reduce it to the appropriate $t$–$J$ model using the canonical perturbation expansion.

## 1.2 The canonical perturbation expansion

*Hubbard subbands.*— One of the main features of the model (1.1) is the split of the Hilbert space (spanned by the Hubbard Hamiltonian) into the so-called Hubbard subbands [1, 2, 31]. This can be understood in the following way. Let us assume that $n \leq 1$ (the case $n > 1$ follows from the particle-hole symmetry of the model) and switch off the hopping $t = 0$ for a moment. Then the ground state of the model will clearly have no sites with two electrons as each site occupied by two electrons costs energy $U$. This condition defines the lowest Hubbard subband with zero total energy which consists of all (degenerate) states with no double occupancies. Next, all of the states with just one single site occupied by two electrons (and the rest singly occupied or empty) define the second Hubbard subbands with the total energy $U$. Repeating this procedure further, one splits up the Hilbert space into the Hubbard subbands spanned by the states with $m$ doubly occupied sites and energy $mU$.

Switching on hopping $t$ obviously changes the situation: not only the states within the Hubbard subband are no longer degenerate but more importantly the Hubbard Hamiltonian are no longer 'diagonal in the Hubbard subbands' (more precisely the hopping $t$ connects the states from different Hubbard subbands). However, as long as $W < U$ the Hubbard subbands do not overlap, in order to obtain the behaviour of the system in the low energy limit it is enough to concentrate on the lowest Hubbard subband and treat the hopping to the states from higher Hubbard subbands as a perturbation.

[1] Note that the more standard perturbation expansion of the Hubbard model [30], where the entire hopping term is treated as a small perturbation, is very tedious for the Hubbard model and yields results which are very hard to interpret [2].

*Deriving the Hamiltonian within the Hubbard subband.*— The canonical perturbation expansion sets the above described procedure on the mathematical grounds [1, 2] (see also Refs. [32, 33]). In the beginning one rewrites the Hubbard Hamiltonian $\mathcal{H}$ in the following way:

$$\mathcal{H} = \mathcal{H}_0 + \mathcal{H}_1, \tag{1.2}$$

where $\mathcal{H}_0$ describes the physics within the Hubbard subband ($\bar{\sigma} = -\sigma$):

$$\begin{aligned}
\mathcal{H}_0 &= \mathcal{V} + \mathcal{T}_0, \\
\mathcal{V} &= U \sum_{\mathbf{i}} n_{\mathbf{i}\uparrow} n_{\mathbf{i}\downarrow} \\
\mathcal{T}_0 &= -t \sum_{\langle \mathbf{ij} \rangle, \sigma} \left\{ (1 - n_{\mathbf{i}\bar{\sigma}}) c^{\dagger}_{\mathbf{i}\sigma} c_{\mathbf{j}\sigma} (1 - n_{\mathbf{j}\bar{\sigma}}) + n_{\mathbf{i}\bar{\sigma}} c^{\dagger}_{\mathbf{i}\sigma} c_{\mathbf{j}\sigma} n_{\mathbf{j}\bar{\sigma}} + \text{H.c.} \right\},
\end{aligned} \tag{1.3}$$

while $\mathcal{H}_1$ is responsible for hopping processes between different Hubbard subbands:

$$\begin{aligned}
\mathcal{H}_1 &= \mathcal{T}_+ + \mathcal{T}_-, \\
\mathcal{T}_+ &= -t \sum_{\langle \mathbf{ij} \rangle, \sigma} \left\{ n_{\mathbf{i}\bar{\sigma}} c^{\dagger}_{\mathbf{i}\sigma} c_{\mathbf{j}\sigma} (1 - n_{\mathbf{j}\bar{\sigma}}) + \text{H.c.} \right\} \\
\mathcal{T}_- &= -t \sum_{\langle \mathbf{ij} \rangle, \sigma} \left\{ (1 - n_{\mathbf{i}\bar{\sigma}}) c^{\dagger}_{\mathbf{i}\sigma} c_{\mathbf{j}\sigma} n_{\mathbf{j}\bar{\sigma}} + \text{H.c.} \right\}.
\end{aligned} \tag{1.4}$$

Next, the task is to construct a canonical transformation $S$ of the Hamiltonian $\mathcal{H}$

$$\tilde{H} = e^{S} \mathcal{H} e^{-S}, \tag{1.5}$$

where $S^{\dagger} = -S$. If $\tilde{H}$ is calculated from the above equation *exactly* then the unitarity of this transformation would mean that the observables calculated using the spectrum spanned by $\tilde{H}$ will be identical to the ones calculated using the spectrum spanned by $\mathcal{H}$.

The explicit form of $S$ is calculated from the single requirement that the Hamiltonian $\tilde{H}$ would not connect states from two different Hubbard subbands. *A priori* this can always be done as long as the Hubbard subbands do not overlap, i.e. when $W < U$ (which is the case here). Obviously, this means that the observables calculated using the spectrum spanned by $\tilde{H}$ will *not* be identical to the ones calculated using the spectrum spanned by $\mathcal{H}$. However, the bigger distances one has between the Hubbard subbands, the more similar the observables are. Explicitly one calculates $\tilde{H}$ and $S$ using the following steps (compare Ref. [33]):

(i) One makes the Ansatz that $S$ is of the order of $t/U$ so that one can write

$$e^{S} = 1 + S + \frac{1}{2} S^2 + O\left( \frac{t^3}{U^3} \right). \tag{1.6}$$

Since $t \ll U$ the terms of the order $O(\frac{t^3}{U^3})$ should be much smaller than 1 (e.g. $U = 12t$ in the high-$T_c$ cuprates [28] yields $\frac{t^3}{U^3}$ smaller than $10^{-3}$) and can be skipped. Then Eq. (1.5) can be rewritten using Eq. (1.6) as

$$\tilde{H} = \mathcal{H} + [S, \mathcal{H}] + \frac{1}{2} [S, [S, \mathcal{H}]] + O\left( \frac{t^3}{U^2} \right), \tag{1.7}$$

to the order $O(\frac{t^3}{U^2})$ (which is again enough in the regime $t \ll U$) since $\mathcal{H}$ is (maximally) of the order of $U$.

(ii) Let us first calculate $S$ to first order in $t/U$ $[S^{(1)}]$. Then Eq. (1.7) to the order $O(\frac{t^2}{U})$ is

$$\tilde{H}^{(1)} = \mathcal{H} + [S^{(1)}, \mathcal{H}]. \tag{1.8}$$

Now, one demands that $\mathcal{H}_1$ is not present in $\tilde{H}^{(1)}$: this is due to the fact that with one hop one leaves the Hubbard subband under consideration and one prohibits that $\tilde{H}$ in any order describes processes which couple various Hubbard subbands. Then in this order one needs to have:

$$\mathcal{T}_+ + \mathcal{T}_- + [S^{(1)}, \mathcal{H}] \equiv 0. \tag{1.9}$$

However, $\mathcal{T}_+ + \mathcal{T}_-$ is $\propto t$ while $S^{(1)}$ is $\propto t/U$. Thus one can only have $\mathcal{V}$ in the commutator:

$$[S^{(1)}, \mathcal{V}] = -\mathcal{T}_+ + \mathcal{T}_-. \tag{1.10}$$

One can check that:

$$S^{(1)} = \frac{1}{U}(\mathcal{T}_+ - \mathcal{T}_-), \tag{1.11}$$

fulfills Eq. (1.10).

(iii) Having determinded $S$ to first order in $t/U$ $[S^{(1)}]$ one can now proceed further and calculate $S$ to the second order $[S^{(2)}]$. For convenience one defines $S'$

$$S^{(2)} = S^{(1)} + S'. \tag{1.12}$$

Then $S'$ is calculated from [compare Eq. (1.8)]:

$$\tilde{H}^{(2)} = \mathcal{H}_0 + [S^{(1)}, \mathcal{T}_+ + \mathcal{T}_-] + [S^{(1)}, \mathcal{T}_0] + \frac{1}{2}[S^{(1)}, [S^{(1)}, \mathcal{V}]] + [S', \mathcal{V}], \tag{1.13}$$

where we used the substitution $[S', \mathcal{H}] \to [S', \mathcal{V}]$ similarly as when going from Eq. (1.9) to Eq. (1.10). Next using Eq. (1.11) we reduce Eq. (1.13) to

$$\tilde{H}^{(2)} = \mathcal{H}_0 + \frac{1}{U}[\mathcal{T}_+, \mathcal{T}_-] + [S^{(1)}, \mathcal{T}_0] + [S', \mathcal{V}]. \tag{1.14}$$

However, the term $[S^{(1)}, \mathcal{T}_0]$ is not allowed to appear in $\tilde{H}^{(2)}$ because it is responsible for transitions between Hubbard subbands and one prohibits that $\tilde{H}$ in any order describes processes between various Hubbard subbands. Thus one needs to have

$$[S^{(1)}, \mathcal{T}_0] + [S', \mathcal{V}] \equiv 0, \tag{1.15}$$

which defines $S'$. From this equation one can calculate $S'$ – however it is not needed (see below).

(iv) To determine $H^{(2)}$ one needs only the explicit form of $S^{(1)}$. In fact, it is straightforward to determine it by substituting Eq. (1.15) to Eq. (1.14). One obtains

$$\tilde{H}^{(2)} = \mathcal{H}_0 + \frac{1}{U}[\mathcal{T}_+, \mathcal{T}_-]. \tag{1.16}$$

This describes the physics of a particular Hubbard subband up to second order in $t/U$ and one can write

$$\tilde{H} = \mathcal{T}_0 + \mathcal{V} + \frac{1}{U}[\mathcal{T}_+, \mathcal{T}_-] + O\left(\frac{t^3}{U^2}\right). \tag{1.17}$$

*Hamiltonian for the lowest Hubbard subband.*— If one is interested in $\tilde{H}$ describing merely the lowest Hubbard subband in the case $n \leq 1$ (called $H$), one can skip $\mathcal{T}_+\mathcal{T}_-$ and $\mathcal{V}$ terms in Eq. (1.17) and one arrives at

$$H = \mathcal{T}_0 - \frac{1}{U}\mathcal{T}_-\mathcal{T}_+ + O\left(\frac{t^3}{U^2}\right). \tag{1.18}$$

One can now plug in the explicit forms of $\mathcal{T}_0$, $\mathcal{T}_+$, and $\mathcal{T}_-$ to obtain the explicit form of $H$. This is done in the next section. Note that due to the particle-hole symmetry a similar Hamiltonian as written above describes the case $n > 1$.

## 1.3 The standard $t$–$J$ Hamiltonian

*Explicit form.*— After inserting Eqs. (1.3-1.4) into Eq. (1.18) one obtains the explicit form of the effective low-energy Hamiltonian for the lowest Hubbard subband

$$\begin{aligned} H = &- t \sum_{\langle \mathbf{ij} \rangle, \sigma} \left\{ (1 - n_{\mathbf{i}\bar{\sigma}}) c^\dagger_{\mathbf{i}\sigma} c_{\mathbf{j}\sigma} (1 - n_{\mathbf{j}\bar{\sigma}}) + \text{H.c.} \right\} \\ &- \frac{1}{4} J \sum_{\langle\langle \mathbf{mij} \rangle\rangle, \sigma, \sigma'} \left\{ (1 - n_{\mathbf{m}\bar{\sigma}'}) c^\dagger_{\mathbf{m}\sigma'} c_{\mathbf{i}\sigma'} n_{\mathbf{i}\bar{\sigma}'} n_{\mathbf{i}\bar{\sigma}} c^\dagger_{\mathbf{i}\sigma} c_{\mathbf{j}\sigma} (1 - n_{\mathbf{j}\bar{\sigma}}) + \text{H.c.} \right\}, \end{aligned} \tag{1.19}$$

where $\langle\langle \mathbf{mij} \rangle\rangle$ means the paths built of the three nearest neighbour sites. Here the first term is responsible for hopping within the lowest Hubbard subband while the second term, which arises from the virtual hoppings to the upper Hubbard subband, is the so-called superexchangeb term[2] with the energy scale $J = 4t^2/U$.

Equation (1.19) can be simplified by replacing the electron operators in the superexchange term by the $S = 1/2$ spin operators:

$$\begin{aligned} S^z_{\mathbf{i}} &= \frac{1}{2}(\tilde{n}_{\mathbf{i}\uparrow} - \tilde{n}_{\mathbf{i}\downarrow}), \\ S^+_{\mathbf{i}} &= \tilde{c}^\dagger_{\mathbf{i}\uparrow} \tilde{c}_{\mathbf{i}\downarrow}, \\ S^-_{\mathbf{i}} &= \tilde{c}^\dagger_{\mathbf{i}\downarrow} \tilde{c}_{\mathbf{i}\uparrow}, \end{aligned} \tag{1.20}$$

where we defined the constrained electron operators

$$\tilde{c}^\dagger_{\mathbf{i}\sigma} = c^\dagger_{\mathbf{i}\sigma}(1 - n_{\mathbf{i}\bar{\sigma}}). \tag{1.21}$$

[2] Note that we use here the term 'superexchange' instead of the more proper 'kinetic exchange' as typically $t$ is merely the *effective* hopping [33].

Then one obtains the 2D version of the standard $t$–$J$ Hamiltonian [1, 2, 3]

$$H = -t \sum_{\langle \mathbf{ij} \rangle, \sigma} (\tilde{c}^{\dagger}_{\mathbf{i}\sigma} \tilde{c}_{\mathbf{j}\sigma} + \text{H.c.}) + J \sum_{\langle \mathbf{ij} \rangle} \left( \mathbf{S_i} \cdot \mathbf{S_j} - \frac{1}{4} \tilde{n}_{\mathbf{i}} \tilde{n}_{\mathbf{j}} \right), \tag{1.22}$$

where $\tilde{n}_{\mathbf{i}} = \tilde{c}^{\dagger}_{\mathbf{i}\uparrow} \tilde{c}_{\mathbf{i}\uparrow} + \tilde{c}^{\dagger}_{\mathbf{i}\downarrow} \tilde{c}_{\mathbf{i}\downarrow}$ and we assumed that $\mathbf{m} = \mathbf{j}$ in Eq. (1.19). The 1D and 3D version of the standard $t$–$J$ Hamiltonian follow in a natural way from the above equation.

*The kinetic and superexchange terms.*— The first term $\propto t$ describes the hopping of electrons in the constrained Hilbert space with no double occupancies (i.e. the lowest Hubbard subband). Thus, it can be viewed as an effective hopping of holes as such a hopping of electrons is possible only if there is a hole at the site to which the electron hops. Note that the operators $\tilde{c}^{\dagger}_{\mathbf{i}\sigma}$ do not fulfill the fermionic commutation rules [32]. Thus one cannot treat these objects as electrons and e.g. one cannot introduce the Fermi energy or momentum in this case. Therefore, even without the second term (as obtained for $U \to \infty$), Eq. (1.22) constitutes a nontrivial problem.

The second term $\propto J$ describes the interaction between the spins which is of the AF character since $J > 0$. The meaning of this term can be easily seen in the half-filled case ($n = 1$) when Eq. (1.22) reduces to the Heisenberg Hamiltonian since then there are no holes in the system and the kinetic term does not contribute. Thus instead of having strongly correlated electrons, see Eq. (1.1), one is left with interacting spin degrees of freedom as the charge degrees of freedom are integrated out. This striking result means that the interactions are so strong in this case (due to $U > W$ in the Hubbard model) that the electrons are localized (charge degrees of freedom are frozen) and only the virtual hoppings of electrons (described by $\mathcal{T}_+$ and $\mathcal{T}_-$ processes) lead to a 'residual' interaction between electron spins. This is the physical explanation of the canonical perturbation expansion. Note also, that naturally the dimensionality of the Hilbert space is now reduced: e.g. in the half-filled case there are only spin degrees of freedom and the dimension of the Hilbert space is $2^N$.

*The three-site terms.*— The assumption $\mathbf{m} = \mathbf{j}$ needs further explanation. It means that the electron, which is virtually excited to the upper Hubbard subband by $\mathcal{T}_+$ process, returns (by the $\mathcal{T}_-$ process) to the same site from where it was excited in the lowest Hubbard band. Thus, one omits here the so-called three-site terms. These contribute merely if there are holes in the lowest Hubbard band since the electron excited from site $\mathbf{j}$ in the lowest Hubbard subband can return to a different site $\mathbf{m}$ in the lowest Hubbard subband only when there is a hole on site $\mathbf{m}$ (because otherwise a double occupancy would be created which is prohibited in the lowest Hubbard subband). Thus similarly as the kinetic term $\propto t$ in Eq. (1.22) the three-site terms will describe the hopping of holes in the lowest Hubbard subband. However, unlike the kinetic term they scale as $\propto J$. Thus, altogether the three-site terms contribute to the total energy of the system as $\propto J\delta$ where $\delta$ is the number of holes in the system. If $\delta \ll 1$ (which is the typical regime for the $t$–$J$ model) and since $J < t$ (as $t \ll U$), then this contribution to the total energy is very small. In particular, it is much smaller than both the contribution of the kinetic term $\propto t\delta$ and the superexchange term $\propto J(1-\delta)^2$.

*Application.*— The application of the $t$–$J$ model follows from two facts: (i) as shown above, in the low energy but strongly correlated regime, it describes

essentially the same physics as the widely used Hubbard model, (ii) it is much easier to solve than the Hubbard model since the dimensionality of its Hilbert space is considerably reduced in comparison with the one of the Hubbard model. The latter property means that: (i) all the numerical calculations, such as the Lanczos or exact diagonalization techniques are more easily done, and (ii) the spins are much easier to treat analytically as the ground states of the spin models are typically more classical [33]. Consequently there have been a tremendous number of papers on the $t$–$J$ model, its solutions, and applications. For further details we refer to the review articles of Ref. [28] or [20] or to Ref. [32] for the more 'personal perspective on the $t$–$J$ model from the pioneering times'.

# Chapter 2

# Explaining charge order in $Sr_{14-x}Ca_xCu_{24}O_{41}$

*This chapter is based on the following publications: (i) K. Wohlfeld, 'Doped Spin Ladder: Zhang-Rice Singlets or Rung-centred Holes?', AIP Conference Proceedings* **918**, *337-341 (2007); (ii) K. Wohlfeld, A. M. Oleś, G. A. Sawatzky, 'Origin of charge density wave in the coupled spin ladders of* $Sr_{14-x}Ca_xCu_{24}O_{41}$*', Physical Review B* **75**, *180501(R)/1-4 (2007); (iii) K. Wohlfeld, A. M. Oleś, G. A. Sawatzky, 'The t-J-V Model for Coupled Ladders', in preparation to be submitted to Physical Review B (Rapid Communication).*

## 2.1 Introduction

*Crystal structure of* $Sr_{14-x}Ca_xCu_{24}O_{41}$*.* — The telephone number compound, as $Sr_{14-x}Ca_xCu_{24}O_{41}$ is often called due to its chemical formula which resembles a telephone number 14-24-41, is a layered material with two distinctly different types of 2D copper oxide planes separated by Sr/Ca atoms [4]: (i) the planes with almost decoupled $CuO_2$ chains and (ii) the $Cu_2O_3$ planes formed by $Cu_2O_5$ coupled ladders (see Fig. 2.1). Although in principle there could be some interaction between the ladder subsystem, the chain subsystem and the Sr/Ca atoms[1] we would assume that the ladder subsystem can be treated independently, i.e. the Hamiltonians for each subsystem are independent one from another, except for the chemical potential which should be determined to conserve a particular number of electrons in the whole 3D crystal (see below).

*Number of carriers in* $Sr_{14-x}Ca_xCu_{24}O_{41}$*.* — The complicated chemical formula leads to the problems with determining the number of electrons present in the system. Let us first concentrate on the $x = 0$ case. Actually, the ionic picture suggests that one has in the formula unit: 14 $Sr^{2+}$ ions, 24 $Cu^{2+}$ ions and 41 $O^{2-}$ ions with all of these ions having filled shells, except for copper (where

[1] In particular the substitution of strontium by calcium yields structural modulations in the ladder subsystem, see Ref. [34]. However, this modulation grows with calcium doping $x$ and cannot explain the onset of charge order for small $x$ and large $x$ (while the charge order is unstable for intermediate $x$), see discussion below. Furthermore, the influence of the chain subsystem on the ladder subsystem can be reduced to the chains being the charge reservoir for the planes, see also Ref. [34].

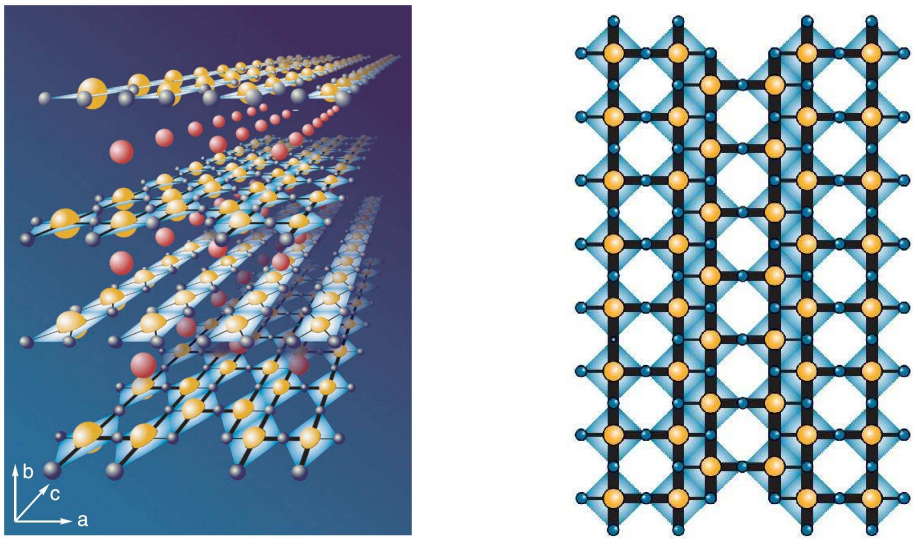


Figure 2.1: Left panel: the 3D structure of $Sr_{14}Cu_{24}O_{41}$. Right panel: the $Cu_2O_5$ coupled ladders which form one of the two types of planes in $Sr_{14}Cu_{24}O_{41}$. The big yellow spheres depict copper atoms, the big red spheres strontium atoms, the small blue spheres oxygen atoms. Both panels are reproduced after Ref. [4].

the $3d$ shell is naturally unfilled). Thus, one obtains from the ionic picture that there is one hole per $Cu^{2+}$ ion,[2] similarly as in the $CuO_2$ planes of $La_2CuO_4$ [28].

However, one sees that such ionic picture considerations lead to the 6 extra holes present in the formula unit and the compound is self-doped already at $x = 0$. As the forumula unit consists of 7 $Cu_2O_3$ units in the ladder plane, 14 strontium atoms and 10 $CuO_2$ units in the chain plane, a natural question arises: how these 6 extra holes are distributed between the ladders and the chains. Actually, the answer to this question is nontrivial (see Refs. [35, 36, 37] for various scenarios) and it was only recently that the x-ray absorption spectroscopy results suggested [9] that there are 2.8 extra holes in the formula unit in the ladders (which means that there are 0.2 holes per copper site) and 3.2 extra holes in the formula unit in the chains (i.e. 0.32 holes per copper site). In what follows, we adopt the latter results as they seem to agree best with other experimental data for this system [9].

Let us now turn to the $x \neq 0$ case. Here, the ionic picture suggests that again there are 6 extra holes in the formula unit: this is because calcium is isovalent with strontium. However, it has been suggested that introducing calcium leads to the gradual increase of the number of these extra holes in the ladder subsystem [9]. Indeed the same x-ray absorption spectroscopy results as for the $x = 0$ case [9] revealed that for the interesting case (see below) of $x = 4$ the number of holes in the ladders is 3.4 (i.e. ca. 0.24 per copper site) and 2.6 in the chains (i.e. ca. 0.26 per copper site) while for $x = 11$ the number of holes

[2] Since it is easier to talk about one hole per copper site than about 9 electrons per copper site, we will use the hole language throughout this chapter.

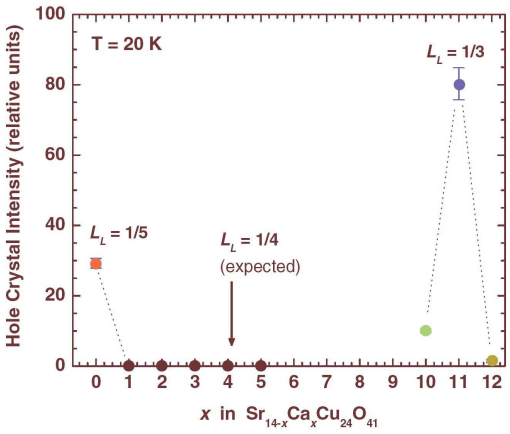


Figure 2.2: The intensity of the scattering at the oxygen $K$ 'mobile carrier peak' (528.6 eV, see Ref. [8] for detailed explanation) in the resonant soft x-ray scattering for various values of calcium doping $x$ in $Sr_{14-x}Ca_xCu_{24}O_{41}$ at temperature $T = 20$K. CDW is observed for $x = 0$ (with period $\lambda = 5$, depicted as $L_L = 1/5$ on the figure) and $x = 11$ (with period $\lambda = 3$, depicted as $L_L = 1/5$ on the figure). A small intensity is also visible for $x = 10$ and even smaller for $x = 12$ which also corresponds to a (small) CDW with period $\lambda = 3$. For $0 < x < 6$ no reflections are observed and in particular no CDW is seen at $x = 4$ where $n_h = 1.24$ would suggest a CDW with period $\lambda = 4$ ($L_L = 1/4$) to be stable. The figure is reproduced after Ref. [8].

in the ladders is 4.4 (i.e. ca. 0.31 per copper site) and 1.6 in the chains (i.e. ca. 0.16 per copper site).

*Peculiar charge order in the ladder subsystem.*— While the ladder subsystem exhibits the non-BCS superconducting phase for $x = 13.6$ under pressure larger than 3 GPa [38], in broad range of $x$ and under normal pressure a spin-gaped insulating CDW states was discovered in the ladders [5, 6]. By means of the resonant soft x-ray scattering it was found [7] that this CDW state is driven by many-body interactions (presumably just Coulomb on-site interactions since the long-range interactions are screened in copper oxides [39]), and it cannot be explained by a conventional Peierls mechanism. Hence, the observed competition between the CDW phase (also referred to as the 'hole crystal' due to its electronic origin) and superconducting states in spin ladders resembles the one between stripes and the superconducting phase in $CuO_2$ planes of a high-$T_c$ superconductor [40]. This is why the problem of the origin of the CDW phase in the ladder subsystem of $Sr_{14-x}Ca_xCu_{24}O_{41}$ is both generic and of general interest.

Furthermore, recently it was found [8] that the only stable CDW states in the low temperature regime ($T = 20$K) are with period $\lambda = 5$ for $x = 0$, and with period $\lambda = 3$ for $x = 11$ (and with a much smaller intensity for $x = 10$ and 12), see Fig. 2.2. Even more striking results show that such a CDW order could not be stable for $1 \leq x \leq 5$, see also Fig. 2.2. These striking results, which contradict the previous suggestion [6] that the CDW order occurs in the

entire range of $0 \leq x < 10$, need to be explained by considering hole density per copper site increasing with $x$. As written above $x = 0$ case with CDW state with period $\lambda = 5$ corresponds to $n_h = 1.20$ (*total* number of holes per copper ion) while the $x = 11$ case with CDW order with period $\lambda = 3$ corresponds to $n_h = 1.31$. Interestingly, the $x = 4$ case (with no CDW phase) corresponds to $n_h = 1.24$, i.e. to the case where the number of extra doped holes is very close to $1/4$ and where one could intuitively expect a CDW state with period $\lambda = 4$.

*Main goals of the chapter.*— The main aim of this chapter is to explain theoretically (at temperature $T = 0$K) the onset of the CDW order in the telephone number compound for only selected values of $x$ while using a model which merely contains on-site Coulomb interactions. In particular the questions to be answered in this chapter are: (i) what the proper $t$–$J$ model for the coupled $Cu_2O_5$ ladders, which would arise due to the on-site Coulomb interactions, looks like, and (ii) whether this model can explain the onset of the CDW phase with particular periods for particular values of $x$.

*Structure of the chapter.*— The chapter is organized as follows. In Sec. 2.2 we start the analysis by looking at the anticipated features of the new $t$–$J$ model which is derived in Sec. 2.3. Next, we solve the model for the three interesting hole dopings $n_h = 4/3$, $n_h = 5/4$ and $n_h = 6/5$: (i) using the slave boson language we reduce the model to the effective Hamiltonian with the constraints of 'no double occupancies' (always present in any $t$–$J$ model) released – see Sec. 2.4.1, (ii) we introduce the mean-field approximation for the effective Hamiltonian – see Sec. 2.4.2 , (iii) we solve the mean-field equations on a finite mesh of $k$ points (Sec. 2.4.3). In Sec. 2.5 the results are discussed, with a particular emphasis on the approximations made in obtaining the correct $t$–$J$ model. Finally, we draw some conclusions in Sec. 2.6 and add a peculiar example of a toy-model for coupled chains in which the even-period CDW can become unstable in the *Postscriptum* in Sec. 2.7.

## 2.2 The $t$–$J$ model for *coupled* ladders

*'Rough' predictions of the new $t$–$J$ model.*— Let us first look at the anticipated features of the new $t$–$J$ model without going deeply into mathematical details (such calculations will be performed in the next section). Actually, the biggest problem with deriving such a model is that the $Cu_2O_5$ coupled ladders belong to a class of copper oxides which are classified as charge transfer systems [41]. On the one hand, in these systems the Hubbard repulsion $U$ between holes in the $3d$ orbitals on the copper sites is still the largest energy scale in the system and it is much bigger than the largest hopping $t_{pd}$ between the copper $3d_{x^2-y^2}$ and the oxygen $2p_\sigma$ orbitals [39]. On the other hand, the on-site energies $\Delta$ for the holes in the oxygen $2p_\sigma$ orbitals are smaller than the Hubbard repulsion $U$ on the copper sites [39]. Therefore, when the number of holes is bigger than one per one copper ion, some holes tend to occupy oxygen sites. Thus, unlike in the Mott-Hubbard system, here the oxygen atoms cannot be easily integrated out and the Hubbard model (called then the charge transfer model [42, 43]) should not only contain orbitals on the copper sites but also the ones on the oxygen sites [41]. Nevertheless, Zhang and Rice [26] showed that for the $CuO_2$ plane it is still possible to integrate out the oxygen atoms and the $t$–$J$ model, which results from such an itinerant model, is capable of describing the low energy

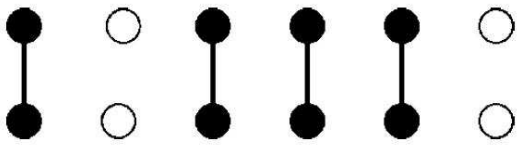

Figure 2.3: The artist's view of the CDW with period $\lambda = 4$ for a single ladder as obtained from the density matrix renormalization group calculations for the $t$–$J$ model on a single ladder with $J = 0.25t$ [10]. Black filled circles depict a copper site occupied by a hole, unfilled circles depict a copper site with the Zhang-Rice singlet centred around it, i.e. where the extra hole (situated symmetrically on the four oxygen sites surrounding the copper site) formed a singlet state with the hole on the copper site. In this way number of holes $n_h = 1.25$ in the $Cu_2O_5$ single ladder corresponds to the $n = 0.75$ filling (number of spins per site) in the $t$–$J$ model on the two-leg ladder. The figure is reproduced after Ref. [10].

physics of charge transfer systems. Note however, that the meaning of $J$ is then different and $J \neq 4t^2/U$.

Although the above mentioned reduction of the charge transfer model to the standard $t$–$J$ model is done for the $CuO_2$ plane [26], a similar derivation should in principle be possible for a single $Cu_2O_5$ ladder. The difference would be that in this case one will be left with a $t$–$J$ model defined on a two-leg ladder but otherwise the $t$–$J$ model would be exactly the same as the standard one, known from Chapter 1. Indeed, it is widely believed [11, 44] that a two-leg ladder described by the $t$–$J$ model captures the essential physical properties of the plane with $Cu_2O_5$ ladders in $Sr_{14-x}Ca_xCu_{24}O_{41}$. Furthermore such a model has been extensively studied (see e.g. Refs. [45, 46, 47, 48, 49]): in particular White *et al.* [10] found using the density matrix renormalization group, that a CDW of period $\lambda = 4$ is the (possibly spin gaped) ground state at $n_h = 1.25$ ($n = 0.75$ filling in the $t$–$J$ model, see caption of Fig. 2.3 and discussion in the end of Sec. 2.3.3 for further details). Besides, only recently it was shown in Ref. [11] that a CDW is possible for such a model merely for number of holes $n_h = 1.25$ ($n = 0.75$) and $n_h = 1.5$ ($n = 0.5$).

*Reason for wrong predictions.*— However, one immediately sees that the above results are totally incompatible with the experimental ones described in Sec. 2.1: there the CDW was stable in the $Cu_2O_5$ ladders in $Sr_{14-x}Ca_xCu_{24}O_{41}$ for $n_h = 1.31$ ($x = 11$) and $n_h = 1.2$ ($x = 0$) whereas it was *not* stable for $n_h = 1.24$ ($x = 4$), i.e. around the only point (apart from $n_h = 1.5$) where the density matrix renormalization group predicted the CDW to be stable. One may thus wonder what may be wrong with the above $t$–$J$ model? Actually, it is easy to see that the validity of the $t$–$J$ model for the plane with $Cu_2O_5$ ladders is far from obvious due to the specific geometry. In particular: (i) unlike the $CuO_2$ plane of a high-$T_c$ superconductor, a single $Cu_2O_5$ ladder lacks the $D_{4h}$ symmetry which makes the Zhang-Rice derivation [26] of the $t$–$J$ model questionable and (ii) $Cu_2O_5$ spin ladders are coupled through the on-site Coulomb interactions between holes in different O($2p$) orbitals, so new interactions could arise.

*More careful approach needed.*— Thus, instead of taking the $t$–$J$ model for

'granted', i.e. assuming that the derivation of the $t$–$J$ model from the charge transfer model valid for the $CuO_2$ would work also for the coupled $Cu_2O_5$ ladders and would give a $t$–$J$ model on the two-leg ladder, one should follow the Zhang and Rice scheme [26] step-by-step in the case of this specific ladder geometry. More precisely, one should take the charge transfer model for copper oxide planes [42, 43], adopt it to the coupled $Cu_2O_5$ ladders, and then following the Zhang and Rice scheme [26] derive the proper $t$–$J$ model. We present such a derivation in the next section.

## 2.3 The model

### 2.3.1 The $t$–$J$–$V_1$–$V_2$ Hamiltonian

*The Hubbard-type model.*— As the starting point we choose the Hubbard-type model relevant for the charge transfer systems (and thus called also charge transfer model [41]). It follows from the multiband charge transfer Hamiltonian [41] and is adapted to the $Cu_2O_5$ coupled ladder geometry, similarly as the one introduced earlier for $CuO_2$ planes [42] or $CuO_3$ chains [50], the structural units of high-$T_c$ superconductors. As parameters the charge transfer model includes: the energy for oxygen $2p$ orbital $\Delta$ (measured with respect to the energy for the $3d$ orbital), the $d$-$p$ hopping $t_{pd}$ between the nearest neighbour copper and oxygen sites, and the on-site Coulomb repulsion $U$ ($U_p$) on the copper (oxygen) sites, respectively. Note that the charge transfer regime naturally leads to $\Delta < U$ since otherwise the oxygen atoms could be easily integrated out. Indeed, the typical parameters are $U \sim 8t_{pd}$, $\Delta \sim 3t_{pd}$, and $U_p \sim 3t_{pd}$, see e.g. Ref. [51]. Then the model in hole notation reads,

$$\begin{aligned}
\mathcal{H} = -t_{pd}\Big\{ \sum_{i\sigma}\Big( & - d^\dagger_{iL\sigma}x_{iL\sigma} + d^\dagger_{iR\sigma}x_{iR\sigma} + d^\dagger_{iL\sigma}b_{i\sigma} - d^\dagger_{iR\sigma}b_{i\sigma} + \text{H.c.}\Big) \\
& + \sum_{i\alpha\sigma}\Big(d^\dagger_{i\alpha\sigma}y_{i\alpha\sigma} - d^\dagger_{i+1,\alpha\sigma}y_{i\alpha\sigma} + \text{H.c.}\Big)\Big\} \\
& + \Delta\Big\{\sum_{i\alpha}\Big(n_{i\alpha x} + n_{i\alpha y}\Big) + \varepsilon\sum_i n_{ib}\Big\} \\
& + U_p\Big\{\sum_{i\alpha}\Big(n_{i\alpha x\uparrow}n_{i\alpha x\downarrow} + n_{i\alpha y\uparrow}n_{i\alpha y\downarrow}\Big) + \sum_i n_{ib\uparrow}n_{ib\downarrow}\Big\} \\
& + U_p\Big\{(1-2\eta)\sum_{i\alpha\sigma}\Big(n_{i\alpha x\sigma}\bar{n}_{i\bar{\alpha}y\bar{\sigma}} + n_{i\alpha y\sigma}\bar{n}_{i\bar{\alpha}x\bar{\sigma}}\Big) \\
& \quad + (1-3\eta)\sum_{i\alpha\sigma}\Big(n_{i\alpha x\sigma}\bar{n}_{i\bar{\alpha}y\sigma} + n_{i\alpha y\sigma}\bar{n}_{i\bar{\alpha}x\sigma}\Big)\Big\} \\
& + U \sum_{i\alpha} n_{i\alpha d\uparrow}n_{i\alpha d\downarrow},
\end{aligned} \tag{2.1}$$

where the phases of the orbitals were explicitly taken into account in the hopping elements, the index $\alpha \in \{R, L\}$ denotes the right or left leg of the ladder ($\bar{R} = L$ and $\bar{L} = R$), and $\bar{\sigma} = -\sigma$ for $\sigma \in \{\uparrow, \downarrow\}$. The parameter $\eta = J_H/U_p \sim 0.2$ stands for a realistic value of Hund's exchange on oxygen ions ($U_p$ is the intraorbital repulsion) [39]. Besides, $\varepsilon \sim 0.9$ yields the correct orbital energy ($\varepsilon\Delta$) at bridge positions on the rung of the ladder [52] but, unless explicitly stated differently,

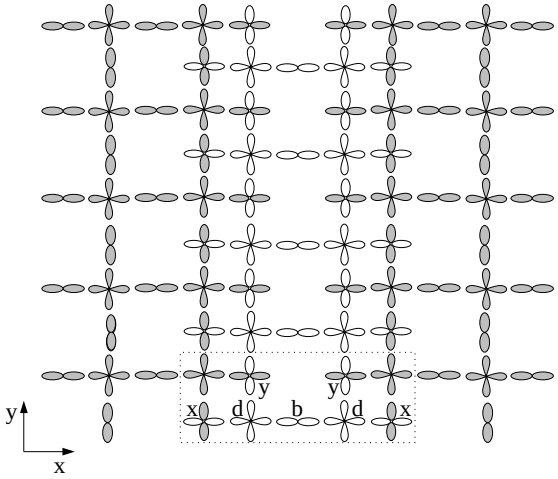


Figure 2.4: Three coupled $Cu_2O_5$ ladders. Only orbitals which are included in the model Eq. (2.1) are shown, see text. The dotted line depicts the unit cell of the single ladder under consideration; it consists of seven orbitals.

we will assume that $\varepsilon = 1$ for simplicity (see also Sec. 2.5.3 for a detailed discussion on this issue). The model of Eq. (2.1) includes seven orbitals per $Cu_2O_5$ ladder unit cell (see Fig. 2.4): two Cu($3d_{x^2-y^2} \equiv d$) orbitals on the $R/L$ leg, two O($2p_y \equiv y$) orbitals on the $R/L$ leg, two O($2p_x \equiv x$) side orbitals on the $R/L$ leg, and one O($2p_x \equiv b$) bridge orbital on the rung of the ladder.

*Spatial dimension of the Hubbard-type model.*— It should be emphasized that the terms in the fifth and sixth line of Eq. (2.1) account for interladder interaction – the holes within two different orbitals on a given oxygen ion in a leg belong to two neighbouring ladders (shown as white/grey orbitals in Fig. 2.4), and are described by charge operators $n_{i\alpha x(y)\sigma}$ with/without bar sign in Eq. (2.1). Thus, in principle one should define two other Hamiltonians $\mathcal{H}$ which describe the two neighbouring ladders and from which one can determine $\tilde{n}_{i\alpha x(y)\sigma}$. Then, these two Hamiltonians will be again coupled to two Hamiltonians and so on. In what follows, we will implicitly assume that such Hamiltonians are indeed defined and when needed we will use this feature to solve the *coupled ladder problem*. Obviously, such a notation is not very elegant. An alternative scenario would be to define a single Hamiltonian for all the ladders in the plane – however, this would complicate the notation even more and, in my opinion, would not make the physics more transparent.

*Central Hamiltonian of the chapter.*— Applying the Zhang-Rice procedure [26] adopted to the geometry of coupled ladders and finite value of the interaction $U_p$ we obtain the following $t$–$J$ model with intraladder interaction $V_1$ and interladder interaction $V_2$ (therefore called also $t$–$J$–$V_1$–$V_2$ Hamiltonian):

$$H = H_t + H_J + H_{V_1} + H_{V_2}. \tag{2.2}$$

Here $H_t$ stands for the kinetic term [see Eq. (2.13) in Sec. 2.3.3], $H_J$ is the superexchange term [see Eq. (2.5) in Sec. 2.3.2], while $H_{V_1}$ and $H_{V_2}$ are the intraladder and interladder terms, respectively [see Eq. (2.29) in Sec. 2.3.4 and

Eq. (2.39) in Sec. 2.3.5].

Note that, during the procedure suggested by Zhang and Rice not only the Hamiltonian changes but also the form and *number* of carriers changes as the form of the Hilbert space is changed drastically [26]. Whereas in the charge transfer model we denote by $n_h$ the number of holes per copper site, in the $t$–$J$–$V_1$–$V_2$ model the filling (number of spins per site) is $n = 2 - n_h$, see also discussion in the end of Sec. 2.3.3.

### 2.3.2 The superexchange term

*Single ladder in the undoped case.*— In the so-called half-filled case (i.e. when there is just one hole per copper site) and in the charge transfer regime (see above), the charge transfer model (2.1) can be easily reduced to the Heisenberg model using the perturbation theory to fourth order in $t_{pd}$ [53].[3] This is because, when $t_{pd} = 0$ the holes are localized on the copper sites, while for small $t_{pd}$ in comparison with the other energy scales in the in the charge transfer system the holes perform merely virtual excitations which involve the doubly occupied copper or oxygen site. Thus, the charge degrees are frozen and one is left merely with spin degrees of freedom, somewhat similarly as in the half-filled case of the Hubbard model of Chapter 1. One obtains [53]:

$$H_J(n_h = 1) = J \sum_{i\alpha} \Big( \mathbf{S}_{i\alpha} \cdot \mathbf{S}_{i+1,\alpha} - \frac{1}{4} \Big) + J \sum_{i} \Big( \mathbf{S}_{iR} \cdot \mathbf{S}_{iL} - \frac{1}{4} \Big), \qquad (2.3)$$

where the superexchange constant for finite $U_p$ case [53] is

$$J = \frac{4t_{pd}^4}{\Delta^2} \Big( \frac{1}{U} + \frac{2}{2\Delta + U_p} \Big). \qquad (2.4)$$

*Specific geometry of coupled ladders.*— The reader may wonder, whether the geometry of coupled ladders could influence the above result. Indeed, there exists a $90^0$ superexchange process between the holes on two neighbouring ladders which involves $\tilde{n}_{i\alpha x(y)\sigma}$ operators. However, according to the Goodenough-Kanamori-Anderson rules [54, 55, 56] such a superexchange process [which is ferromagnetic (FM) in contrast to the above AF interaction] is much weaker than the superexchange along the $180^0$ path in the single ladder and can be neglected. Thus, Eq. (2.3) should also be valid for coupled ladders.

*Coupled ladder in the doped case.*— Although when the system is not half-filled there are other processes which contribute to the low energy $t$–$J$ Hamiltonian (see below), the above result can be extended to the doped case. Actually, if there is no hole on one of the sites forming a bond between the copper sites, then the superexchange process does not occur. One can easily check that Eq. (2.3) for this particular bond does not contribute to the $t$–$J$ Hamiltonian provided one changes it into:

$$H_J = J \sum_{i\alpha} \Big( \mathbf{S}_{i\alpha} \cdot \mathbf{S}_{i+1,\alpha} - \frac{1}{4} \tilde{n}_{i\alpha d} \tilde{n}_{i+1,\alpha d} \Big) + J \sum_{i} \Big( \mathbf{S}_{iR} \cdot \mathbf{S}_{iL} - \frac{1}{4} \tilde{n}_{iRd} \tilde{n}_{iLd} \Big). \qquad (2.5)$$

[3] Note that in the half-filled case there is no need to perform the canonical perturbation expansion of Chapter 1 as there are no hopping processes within the lowest Hubbard subband.

| | symmetric ($\|P_{i\alpha\sigma}\rangle$) | antisymmetric | single oxygen |
|---|---|---|---|
| singlet | $-8(t_1+t_2)+2t_3$ | $-4t_1+2t_3$ | $-2(t_1+t_2)+2t_3$ |
| triplet | 0 | $-4t_1$ | 0 |

Table 2.1: Binding energy of the singlet and triplet state formed by the the hole on the copper site and the extra doped hole in one of the three various oxygen states: (i) symmetric plaquette $|P_{i\alpha\sigma}\rangle$ state, (ii) antisymmetric plaquette state with a similar combination of oxygen orbitals as in $|P_{i\alpha\sigma}\rangle$ but with *the same* signs before each oxygen orbital, and (iii) single oxygen orbital state. Here $t_1 = t_{pd}^2/\Delta \sim t_{pd}/3$, $t_2 = t_{pd}^2/(U-\Delta) \sim t_{pd}/5$, $t_3 = t_{pd}^2 U_p/(\Delta^2 + U_p\Delta) \sim t_{pd}/6$ where the estimations follow from the typical charge transfer parameters [51].

Here tilde above the number operator denotes the fact that the double occupancies on the copper sites are prohibited in the low energy limit of the charge transfer system.

### 2.3.3 The kinetic energy term

*Finite contribution only for doped case.*— As described above, in the half-filled case the holes localize on the copper sites with the charge degrees of freedom entirely gone and one is left with the Heisenberg Hamiltonian for the spins. Thus, there is no kinetic term at all in the half-filled case and it could only contribute in the doped case due to the restricted hopping.

*Zhang-Rice scheme needed.*— In the doped case a significant problem arises: where the extra hole doped into the half-filled system goes. Actually, if $t_{pd} = 0$, then the hole will for sure localize at one of the oxygen sites as the on-site energy $\Delta$ is smaller than the repulsion between two holes at the same copper site $U$. Therefore, in this regime one cannot integrate out the oxygen sites. It may be expected that such states will dominate also for finite $t_{pd}$.

Actually, for finite $t_{pd}$ in the $CuO_2$ plane, it occurs that the hole also tends to localize on oxygen sites but forms a peculiar bound state with the nearby hole on the copper site – the so-called Zhang-Rice singlet [26]. We now construct such a state step-by-step for the coupled ladder case (again starting with the single ladder and only later on discussing the coupled ladder problem), see Fig. 2.5 for an artist's view of the result obtained in this section.

*Nonorthogonal Zhang-Rice singlets.*— First, it is evident that placing a hole on the oxygen site and aligning its spin in the AF-way with respect to the spin of the hole on the copper site, one can gain some energy due to the virtual hopping processes by small but finite $t_{pd}$ (in the ferromagnetic case such charge excitations are not allowed due to Pauli principle). Second, however, one can gain even more binding energy if one uses the possibility of forming a phase coherent state out of the four oxygen orbitals surrounding the copper. More precisely it occurs that the singlet state formed by a hole on the copper site and a hole in one of the following *symmetric plaquette* state (different for the left and right leg of the ladder):

$$|P_{iL\sigma}\rangle = \frac{1}{2}(x^\dagger_{iL\sigma} - b^\dagger_{i\sigma} + y^\dagger_{i-1,L\sigma} - y^\dagger_{iL\sigma})|0\rangle, \tag{2.6}$$

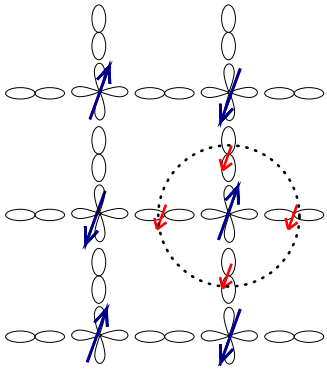

Figure 2.5: The artist's view of the Zhang-Rice singlet formation in the single ladder (the state depicted by a dotted ring). Large (small) arrows depict the hole spins for +1.0 (+0.25) charge. The red arrows stand for spins of doped holes while the blue arrows show the spins in the undoped case.

or

$$|P_{iR\sigma}\rangle = \frac{1}{2}(-x^{\dagger}_{iR\sigma} + b^{\dagger}_{i\sigma} + y^{\dagger}_{i-1,R\sigma} - y^{\dagger}_{iR\sigma})|0\rangle, \tag{2.7}$$

has a binding energy of $-8(t_1 + t_2) + 2t_3$. Actually, this binding energy is not only negative and huge in comparison with the effective hopping (which is of the order of $t_1$ or $t_2$ [26]) but it is also much bigger than the binding energy of some other possible bound states formed by a hole on the copper site and oxygen site, see Table 2.1. It may be verified that finite $U_p$, not considered in the Zhang and Rice paper [26], which results in finite $t_3$ term (see Table 2.1) does not change qualitatively the large binding energy of a symmetric singlet state.

At this stage one can already imagine that all of the doped holes (if their number is smaller than the number of copper sites) should be able to form such symmetric singlet states in the charge transfer systems and it would be possible to integrate out oxygen sites entirely. Although this conjecture will turn out to be true, it cannot be done so easily. A quick look at Eqs. (2.6-2.7) reveals that the above symmetric singlet states are nonorthogonal (they could be called the nonorthogonal Zhang-Rice singlets) as the neighbouring states share common oxygen orbitals.

*Orthogonalized Zhang-Rice singlets.*— The task is now to make the states defined in Eqs. (2.6-2.7) orthogonal. This is done by the following transformation in the single ladder case:

$$|\phi_{lL\sigma}\rangle = \frac{1}{N}\sum_{jk} e^{ikl}e^{-ikj}(\alpha_k|P_{jL\sigma}\rangle + \beta_k|P_{jR\sigma}\rangle), \tag{2.8}$$

and

$$|\phi_{lR\sigma}\rangle = \frac{1}{N}\sum_{jk} e^{ikl}e^{-ikj}(\beta_k|P_{jL\sigma}\rangle + \alpha_k|P_{jR\sigma}\rangle), \tag{2.9}$$

where

$$\alpha_k = \frac{1}{\sqrt{1-\frac{1}{2}\cos k - \frac{1}{4}}} + \frac{1}{\sqrt{1-\frac{1}{2}\cos k + \frac{1}{4}}}, \tag{2.10}$$

and

$$\beta_k = \frac{1}{\sqrt{1-\frac{1}{2}\cos k - \frac{1}{4}}} - \frac{1}{\sqrt{1-\frac{1}{2}\cos k + \frac{1}{4}}}. \tag{2.11}$$

One can check that the 'extended' symmetric states $|\phi_{i\alpha\sigma}\rangle$ are indeed orthogonal.

Let us note that it is at this point that the equations are truely distinct here than the ones considered by Zhang and Rice in Ref. [26]: there it was only shown how to 'orthogonalize' symmetric states for the 2D case. While that procedure could have been easily generalized (or one should rather say 'reduced') to the 1D case, the ladder case required a more careful consideration. Actually the easiest way to obtain equations for $\alpha_k$ and $\beta_k$ is to derive them first for merely a single rung of the ladder. In that case one can easily check $\alpha_k = 1/\sqrt{3} + 1/\sqrt{5}$ while $\beta_k = 1/\sqrt{3} - 1/\sqrt{5}$. Then one can generalize this result to the whole ladder.

Finally one can explicitly define the Zhang-Rice singlets as

$$|\psi_{i\alpha}\rangle = \frac{1}{\sqrt{2}}|\phi_{i\alpha\uparrow} d_{i\alpha\downarrow} - \phi_{i\alpha\downarrow} d_{i\alpha\uparrow}\rangle, \tag{2.12}$$

see also Fig. 2.5 for an artist's view of this state. In principle, one should also check how the binding energy changes when the Zhang-Rice singlets are orthogonalized. It was shown in Ref. [26] that the energy splitting changes only slightly when the singlets are orthogonalized. Obviously, the results in Ref. [26] are valid only for the 2D case. Fortunately, a similar result can be easily obtained for the 1D case. Actually, the energy splitting between the orthogonalized Zhang-Rice singlets and triplets can be defined as $16\chi^2 t_1$ (for the simplified case $t_1 = t_2$ and $t_3 = 0$) [26]. Then the crucial constant $\chi$ is very close to one — both in the 1D ($\chi = 0.98$) and in the 2D case ($\chi = 0.96$) [26]. One can safely argue that $\chi$ for the ladders takes some value in between 0.96 and 0.98 as there is no physical reason that the orthogonalization procedure for the ladders would lead to totally different behaviour than for the 1D chains or 2D case (despite the form which is slightly more complicated in the ladder case). Thus, the orthogonalized Zhang-Rice singlets have a huge binding energy also for the ladder. In what follows, we will refer to Zhang-Rice singlets having in mind merely their orthogonal version.

*Kinetic term for single ladder.*— Having shown that the Zhang-Rice singlets in the single ladder do not differ much from those in the 2D case, we can now safely assume that one can apply to the ladder case all the arguments used in Ref. [26] to derive the effective hopping of Zhang-Rice singlets due to finite $t_{pd}$. Thus, we obtain,

$$H_t = -t \sum_{i\alpha\sigma} \left( \tilde{d}^\dagger_{i\alpha\sigma} \tilde{d}_{i+1,\alpha\sigma} + \text{H.c.} \right) - t \sum_{i\sigma} \left( \tilde{d}^\dagger_{iR\sigma} \tilde{d}_{iL\sigma} + \text{H.c.} \right), \tag{2.13}$$

where again $\tilde{d}_{i\alpha\sigma} = d_{i\alpha\sigma}(1 - n_{i\alpha\bar{\sigma}})$ is the restricted fermion operator and as before $d_{i\alpha\sigma}$ creates a hole in the copper site $i\alpha$. This follows from the effective hopping of Zhang-Rice singlets $t$ by a hole-particle transformation. While we

do not show her the detailed expression for the effective hopping of Zhang-Rice singlets $t$, note that it is considerably smaller than $t_{pd}$ (ca. 30%). Note also that having two Zhang-Rice singlets on the same site costs energy $4t_2 + 2t_1$ (see Ref. [26]) and therefore we used the tilde operators above to prevent from having two Zhang-Rice singlets on the same site.

*Extension to coupled ladders.*— Since the interoxygen hopping $t_{pp'} < t_{pd}$ [39] in copper oxide systems, there is no possibility of hopping between the ladders. Thus, the above result will also be valid for coupled ladders provided the Zhang-Rice singlets can be constructed in that case. This is indeed the case, however it is somewhat subtle and we refer the reader to the next section for more details.

*Number of carriers in the $t$–$J$–$V_1$–$V_2$ model.*— Due to the Zhang-Rice procedure not only the nature of carriers but also their number is changed in the effective $t$–$J$–$V_1$–$V_2$ model. Since the number of extra holes which occupy the oxygen sites and form the Zhang-Rice singlets is equal to $n_h - 1$ per copper site (where $n_h$ is the number of holes per copper site), there are $n_e = n_h - 1$ per site empty states in the effective $t$–$J$–$V_1$–$V_2$ model. This means, that the filling $n$ in the $t$–$J$–$V_1$–$V_2$ model (i.e. the number of spins) is $n = 1 - n_e = 2 - n_h$ per site.

### 2.3.4 The intraladder repulsive term $V_1$

*Finite $U_p$ and the interaction between Zhang-Rice singlets in 2D case.*— In the original Zhang and Rice paper [26] the interaction on oxygen sites $U_p$ was entirely neglected. Here, we have already stated its rather minor role in the stability of the Zhang-Rice singlets (see e.g. Table 2.1 where $t_3$ is finite for finite $U_p$ as well as discussion in Sec. 2.3.3). However, this is not the full story [57, 58, 59]. Actually, due to the finite $U_p$ the two nonorthogonal Zhang-Rice singlets repel if they are situated on the nearest neighbour site. This is because these two nonorthogonal Zhang-Rice singlets share a common oxygen site and the two holes situated on this oxygen site and belonging to two neighbouring nonorthogonal Zhang-Rice singlets repel.

Obviously, this interaction is quite reduced as there is just 25% probability to find a hole forming a nonorthogonal Zhang-Rice state on the particular oxygen site (which is shared with the neighbouring Zhang-Rice singlet). Indeed detailed calculations for the *orthogonal* Zhang-Rice singlets, performed in Refs. [58, 59], showed that this repulsion is of the order of $0.029U_p$ (while the not-considered-here finite intersite Coulomb repulsion $V_{pd}$ between holes on oxygen sites and copper sites even further reduces this value [57]). Thus, the orthogonalization procedure reduces its value from the estimated $1/2(1/4 \times 1/4 + 1/4 \times 1/4) = 1/32 \sim 0.031$ (the factor $1/2$ before the equation originates from the Pauli principle) for nonorthogonal Zhang-Rice singlets. Therefore, one usually neglects the effective repulsion between holes in the $t$–$J$ model as it will be at maximum of the order of $0.2t$ (for parameters from [39] where $U_p = 4.18$ eV is rather large) while typically $J \sim 0.4t$ in copper oxides [23].

*Intraladder and interladder repulsion.*— In the coupled ladder geometry, however, the situation changes drastically. Although, within each single ladder the repulsion is somewhat similar as in the 2D case (this will be called the *intraladder* repulsion, see Fig. 2.6), a distinct situation occurs for the coupled ladder. Here, there is a much stronger repulsion between nearest neighbour

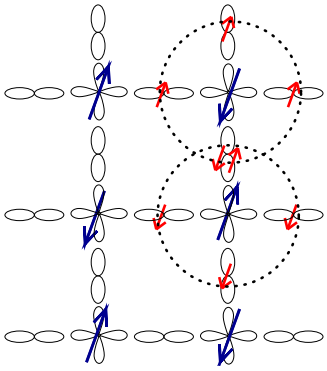

Figure 2.6: The artist's view of the intraladder repulsion between two nearest neighbour Zhang-Rice singlets. See Fig. 2.5 for further explanation of the symbols used here.

Zhang-Rice singlets on neighbouring ladders. This is because, such Zhang-Rice singlets share not one but two oxygen sites, see Fig. 2.7 in the next section. Thus, the *interladder* repulsion between Zhang-Rice singlets should naively be four times[4] as big as the intraladder repulsion and therefore it can happen that it could be of the order of $J$.

*Calculation of the intraladder repulsion.*— Whereas the significance of the interladder repulsion is discussed in the next section, let us now concentrate on the repulsion between the Zhang-Rice singlets within a single ladder (see Fig. 2.6 for the artist's view of the problem). Thus, the task is to calculate repulsion between orthogonalized Zhang-Rice singlets within the ladder due to the on-site interaction $U_p$:

$$\mathcal{H}' = U_p\Big\{\sum_{i\alpha}\Big(n_{i\alpha x\uparrow}n_{i\alpha x\downarrow} + n_{i\alpha y\uparrow}n_{i\alpha y\downarrow}\Big) + \sum_{i} n_{ib\uparrow}n_{ib\downarrow}\Big\}. \tag{2.14}$$

Thus, one needs to calculate the following matrix elements:

$$\langle\psi_{s\alpha},\psi_{r\alpha}|\mathcal{H}'|\psi_{h\alpha},\psi_{j\alpha}\rangle, \quad \langle\psi_{s\alpha},\psi_{r\bar{\alpha}}|\mathcal{H}'|\psi_{h\bar{\alpha}},\psi_{j\alpha}\rangle. \tag{2.15}$$

Let us note that the mixed terms such as for example $(RL, LL)$ give zero in the Zhang-Rice singlet basis – they could a priori lead to the destruction of the Zhang-Rice singlets but fortunately are much smaller than the respective binding energy.

*Intraladder repulsion along the leg.*— First, we calculate the matrix elements

[4]This is because here both the holes with the same and opposite spins can repel: $1/4 \times 1/4 + 1/4/4 = 1/8$. However, this factor will multiply smaller on-site repulsion, with respect to the intraladder case, due to Hund's exchange and altogether it will turn out that for $\eta = 0.2$ [39] the interladder repulsion is roughly twice stronger than the intraladder repulsion.

of $\mathcal{H}'$ between the orthogonal plaquette states Eqs. (2.8-2.9) along the leg:

$$\begin{aligned}\langle\phi_{s\alpha\sigma},\phi_{r\alpha\bar{\sigma}}|\mathcal{H}'|\phi_{h\alpha\bar{\sigma}},\phi_{j\alpha\sigma}\rangle =&\frac{1}{16}U_p\frac{1}{N^3}\sum_{kqf}e^{ik(h-r)}e^{iq(j-s)}e^{if(r-s)}\\ &\Big\{\frac{1}{16}\Big(\alpha_k\alpha_q+\beta_k\beta_q-\alpha_k\beta_q-\beta_k\alpha_q\Big)\\ &\Big(\alpha_{q-f}\alpha_{k+f}+\beta_{q-f}\beta_{k+f}-\alpha_{q-f}\beta_{k+f}-\beta_{q-f}\alpha_{k+f}\Big)\\ &+\Big(\sin\frac{k}{2}\sin\frac{q}{2}\sin\frac{q-f}{2}\sin\frac{k+f}{2}+\frac{1}{16}\Big)\\ &\Big(\alpha_k\alpha_q\alpha_{q-f}\alpha_{k+f}+\beta_k\beta_q\beta_{q-f}\beta_{k+f}\Big)\Big\},\end{aligned}\tag{2.16}$$

and

$$\langle\phi_{s\alpha\sigma},\phi_{r\alpha\bar{\sigma}}|\mathcal{H}'|\phi_{h\alpha\sigma},\phi_{j\alpha\bar{\sigma}}\rangle=-\langle\phi_{s\alpha\sigma},\phi_{r\alpha\bar{\sigma}}|\mathcal{H}'|\phi_{h\alpha\bar{\sigma}},\phi_{j\alpha\sigma}\rangle,\tag{2.17}$$

and

$$\langle\phi_{s\alpha\sigma},\phi_{r\alpha\sigma}|\mathcal{H}'|\phi_{h\alpha\sigma},\phi_{j\alpha\sigma}\rangle=0.\tag{2.18}$$

One can evaluate numerically the above expressions. It occurs that the largest positive element is the nearest neighbour interaction

$$\langle\phi_{j\alpha\sigma},\phi_{j+1,\alpha\bar{\sigma}}|\mathcal{H}'|\phi_{j+1,\alpha\bar{\sigma}},\phi_{j\alpha\sigma}\rangle=0.0544U_p,\tag{2.19}$$

while following Eq. (2.18) the absolute value of the largest negative element, which corresponds to spin-flip nearest neighbour interaction, is the same. Furthermore, the second largest element is the next nearest neighbour interaction and is over 20 times smaller, which means that it can be easily neglected.

Second, we calculate the matrix elements of $\mathcal{H}'$ between the nearest neighbour Zhang-Rice singlets. This introduces a factor 1/2 to the above estimations of the repulsion between orthogonal plaquette states: It is because there is a 50% probability to have opposite spins on a particular shared oxygen site occupied by two holes from two different Zhang-Rice singlets. Note that the spin-flip-plaquette terms do not give any contribution to the repulsion between Zhang-Rice singlets, although they could in principle destabilize the Zhang-Rice states themselves. Fortunately, this is not possible since the binding energy of the Zhang-Rice singlets is much larger. Thus altogether, we obtain

$$\langle\psi_{j\alpha},\psi_{j+1,\alpha}|\mathcal{H}'|\psi_{j+1,\alpha},\psi_{j\alpha}\rangle=0.0272U_p.\tag{2.20}$$

*Intraladder repulsion along the rung.*— Following a similar scheme, we calculate the repulsion between Zhang-Rice singlets on different legs. We obtain for the matrix elements of $\mathcal{H}'$ between the orthogonal plaquette states Eqs.

(2.8-2.9) on different legs

$$\begin{aligned}\langle\phi_{s\alpha\sigma},\phi_{r\bar{\alpha}\bar{\sigma}}|\mathcal{H}'|\phi_{h\bar{\alpha}\bar{\sigma}},\phi_{j\alpha\sigma}\rangle =&\frac{1}{16}U_p\frac{1}{N^3}\sum_{kqf}e^{ik(h-r)}e^{iq(j-s)}e^{if(r-s)}\\ &\Big\{\frac{1}{16}\Big(\alpha_k\beta_q+\beta_k\alpha_q-\alpha_k\alpha_q-\beta_k\beta_q\Big)\\ &\Big(\alpha_{q-f}\beta_{k+f}+\beta_{q-f}\alpha_{k+f}-\alpha_{q-f}\alpha_{k+f}-\beta_{q-f}\beta_{k+f}\Big)\\ &+\Big(\sin\frac{k}{2}\sin\frac{q}{2}\sin\frac{q-f}{2}\sin\frac{k+f}{2}+\frac{1}{16}\Big)\\ &\Big(\alpha_k\beta_q\alpha_{q-f}\beta_{k+f}+\beta_k\alpha_q\beta_{q-f}\alpha_{k+f}\Big)\Big\},\end{aligned}\tag{2.21}$$

and

$$\langle\phi_{s\alpha\sigma},\phi_{r\bar{\alpha}\bar{\sigma}}|\mathcal{H}'|\phi_{h\bar{\alpha}\sigma},\phi_{j\alpha\bar{\sigma}}\rangle=-\langle\phi_{s\alpha\sigma},\phi_{r\bar{\alpha}\bar{\sigma}}|\mathcal{H}'|\phi_{h\bar{\alpha}\bar{\sigma}},\phi_{j\alpha\sigma}\rangle,\tag{2.22}$$

and

$$\langle\phi_{s\alpha\sigma},\phi_{r\bar{\alpha}\sigma}|\mathcal{H}'|\phi_{h\bar{\alpha}\sigma},\phi_{j\alpha\sigma}\rangle=0.\tag{2.23}$$

Evaluating numerically the above expressions one obtains that the largest element is the nearest neighbour repulsion – this time between the orthogonal plaquette states on the same rung:

$$\langle\phi_{j\alpha\sigma},\phi_{j,\bar{\alpha}\bar{\sigma}}|\mathcal{H}'|\phi_{j,\bar{\alpha}\bar{\sigma}},\phi_{j\alpha\sigma}\rangle=0.0529U_p,\tag{2.24}$$

while the second largest element (the next nearest neighbour interaction) but is very small (over 15 times smaller) and can be neglected.

Finally, following the same steps we obtain the repulsion between the nearest neighbour Zhang-Rice singlets which is twice reduced:

$$\langle\psi_{j\alpha},\psi_{j,\bar{\alpha}}|\mathcal{H}'|\psi_{j,\bar{\alpha}},\psi_{j\alpha}\rangle=0.0265U_p.\tag{2.25}$$

*Intraladder repulsion between Zhang-Rice singlets.*— Hence, one can note that the interaction among the nearest neighbour Zhang-Rice singlets is almost isotropic. Thus, one can write the effective Hamiltonian for the repulsion between Zhang-Rice singlets (compare Fig. 2.6)

$$H_{V_1}=V_1\Big(\sum_{i\alpha}n_{\psi_{i\alpha}}n_{\psi_{i+1,\alpha}}+\sum_i n_{\psi_{iR}}n_{\psi_{iL}}\Big),\tag{2.26}$$

where $n_{\psi_{i\alpha}}=|\psi_{i\alpha}\rangle\langle\psi_{i\alpha}|$ and

$$V_1\sim 0.027U_p.\tag{2.27}$$

Thus the constant before $U_p$ is ca. 14% smaller than the nonorthogonal value $1/32=0.03125$. Note the trend of the renormalization factors: 0.023, 0.025, 0.027, 0.029 for single rung, 1D case, ladder, and 2D case, respectively (calculations are not shown; for 2D case a similar result was obtained in Ref. [58, 59]). This trend originates from the fact that in lower dimensions the charge escapes more from the main orbitals ($b$ or $y$) responsible for the interaction (and the contribution to the interaction due to the other orbitals is very small). In 2D it

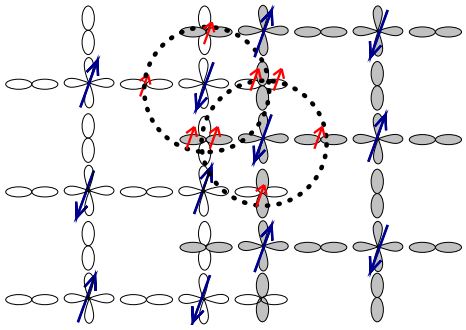

Figure 2.7: The artist's view of the interladder repulsion between two nearest neighbour Zhang-Rice singlets on two different ladders. See Fig. 2.5 for further explanation of the symbols used here.

does not escape in this way as *all* of the orbitals suffer from the orthogonality problem.

*Intraladder repulsion in terms of copper holes.*— Since Zhang-Rice singlets are 'particle-hole cousins' of copper holes (i.e. Zhang-Rice singlets correspond to empty sites on copper) one has

$$n_{\psi_{j\alpha}} = (1 - \tilde{n}_{j\alpha d}), \tag{2.28}$$

where everything happens in the constrained Hilbert space with no double occupancies on copper holes. Substituting this equation and shifting the chemical potential one obtains the intraladder repulsion between copper holes

$$H_{V_1} = V_1 \Big( \sum_{i\alpha} \tilde{n}_{i\alpha d} \tilde{n}_{i+1,\alpha d} + \sum_{i} \tilde{n}_{iRd} \tilde{n}_{iLd} \Big), \tag{2.29}$$

where $V_1$ defined as in Eq. (2.27).

### 2.3.5 The interladder repulsive term $V_2$

*Calculation of interladder repulsion.*— Finally, the task is to calculate the repulsion between two Zhang-Rice singlets sitting next to each other (and thus sharing the same oxygen sites but *not* the $p$ orbitals, see Fig. 2.7) due to the on-site repulsion on oxygen sites. However, again we will calculate the repulsion between arbitrarily located Zhang-Rice singlets and only then we will show which elements are negligible. Note that the plaquette states on two ladders are orthogonal to each other although they still have to be orthogonalized for the same ladder (as before).

Explicitly one needs to calculate the following matrix elements:

$$\langle \psi_{s\alpha}, \bar{\psi}_{r+\frac{1}{2},\bar{\alpha}} | \mathcal{H}'' | \bar{\psi}_{h+\frac{1}{2},\bar{\alpha}}, \psi_{j\alpha} \rangle, \tag{2.30}$$

and

$$\langle \psi_{s\alpha}, \bar{\psi}_{r+\frac{1}{2},\alpha} | \mathcal{H}'' | \bar{\psi}_{h+\frac{1}{2},\alpha}, \psi_{j\alpha} \rangle, \tag{2.31}$$

where

$$\mathcal{H}'' = U_p\Big\{(1-2\eta)\sum_{i\alpha\sigma}\Big(n_{i\alpha x\sigma}\bar{n}_{i\bar{\alpha}y\bar{\sigma}} + n_{i\alpha y\sigma}\bar{n}_{i\bar{\alpha}x\bar{\sigma}}\Big) + (1-3\eta)\sum_{i\alpha\sigma}\Big(n_{i\alpha x\sigma}\bar{n}_{i\bar{\alpha}y\sigma} + n_{i\alpha y\sigma}\bar{n}_{i\bar{\alpha}x\sigma}\Big)\Big\}. \tag{2.32}$$

Note that we introduced here a *bar* sign over the Zhang-Rice singlet states to denote the Zhang-Rice singlets formed on a *different* ladder than the one under consideration. Besides, since the other ladder is misaligned by a lattice constant 1/2 with respect to the ladder under consideration, we count the Zhang-Rice singlets on the neighbouring ladder with the index $j+1/2$ (note that the lattice constant in the single ladder is the copper-copper distance which we assume to be equal to 1, see Remarks at Notation in the beginning of the thesis).

*Interladder repulsion between plaquettes with the same spin.*— First, we calculate the matrix elements of $\mathcal{H}''$ between the orthogonal plaquette states Eqs. (2.8-2.9) with the same spin but situated on different legs:

$$\begin{aligned}\langle \phi_{r\alpha\sigma}, \bar{\phi}_{s+\frac{1}{2},\bar{\alpha}\sigma}|\mathcal{H}''|\bar{\phi}_{h+\frac{1}{2},\bar{\alpha}\sigma}, \phi_{j\alpha\sigma}\rangle =& \frac{1}{16}(1-3\eta)U_p\frac{1}{N^3}\sum_{kqf}\alpha_k\alpha_q\alpha_{q-f}\alpha_{k+f} \\ & \Big\{\frac{1}{4}\sin q\sin(q-f)+\frac{1}{4}\sin k\sin(k+f)\Big\} \\ & e^{ik(h-r)}e^{iq(j-s)}e^{if(r-s-\frac{1}{2})},\end{aligned} \tag{2.33}$$

while for the same legs we obtain

$$\begin{aligned}\langle \phi_{r\alpha\sigma}, \bar{\phi}_{s+\frac{1}{2},\alpha\sigma}|\mathcal{H}''|\bar{\phi}_{h+\frac{1}{2},\alpha\sigma}, \phi_{j\alpha\sigma}\rangle =& \frac{1}{16}(1-3\eta)U_p\frac{1}{N^3}\sum_{kqf}\alpha_k\beta_q\alpha_{q-f}\beta_{k+f} \\ & \Big\{\frac{1}{4}\sin q\sin(q-f)+\frac{1}{4}\sin k\sin(k+f)\Big\} \\ & e^{ik(h-r)}e^{iq(j-s)}e^{if(r-s-\frac{1}{2})}.\end{aligned} \tag{2.34}$$

As it might have been expected, it occurs that the biggest term is the repulsion between orthogonal plaquette states with the same spin situated on the closest possible sites in the neighbouring ladders (see Fig. 2.7):

$$\langle \phi_{j\alpha\sigma}, \bar{\phi}_{j\pm\frac{1}{2},\bar{\alpha}\sigma}|\mathcal{H}''|\bar{\phi}_{j\pm\frac{1}{2},\bar{\alpha}\sigma}, \phi_{j\alpha\sigma}\rangle = 0.1355(1-3\eta)U_p, \tag{2.35}$$

and all other terms are of the order of $10^{-3}(1-3\eta)U_p$ and can be neglected.

*Interladder repulsion between plaquettes with opposite spin.*— Second, an exactly similar calculation as above, but for the orthogonal plaquette states Eqs. (2.8-2.9) with opposite spins leads to the repulsion between orthogonal plaquette states with opposite spins and situated on the closest possible sites in the neighbouring ladders:

$$\langle \phi_{j\alpha\sigma}, \bar{\phi}_{j\pm\frac{1}{2},\bar{\alpha}\bar{\sigma}}|\mathcal{H}''|\bar{\phi}_{j\pm\frac{1}{2},\bar{\alpha}\bar{\sigma}}, \phi_{j\alpha\sigma}\rangle = 0.1355(1-2\eta)U_p, \tag{2.36}$$

while again all other longer-range repulsive terms can be neglected.

*Interladder repulsion between Zhang-Rice singlets.*— Combining the two results for the plaquette states, one can calculate repulsion between Zhang-Rice

singlets situated on nearest neighbour sites of the neighbouring ladders (see Fig. 2.7):

$$H_{V_2} = V_2 \sum_{i\alpha} \left( n_{\psi_{i\alpha}} n_{\bar{\psi}_{i+\frac{1}{2},\bar{\alpha}}} + n_{\psi_{i\alpha}} n_{\bar{\psi}_{i-\frac{1}{2},\bar{\alpha}}} \right), \tag{2.37}$$

where $n_{\psi_{i\alpha}}$ is defined as before and

$$V_2 \sim 0.1355(1 - 5\eta/2)U_p. \tag{2.38}$$

Note that we again neglected all spin-flip terms which are small in comparison with the Zhang-Rice binding energy and give zero when 'sandwiched' in the singlet states. Besides, the prefactor (equal to 0.1355) before the interaction between the Zhang-Rice singlets is slightly enhanced with respect to the expected $1/8 = 0.125$ value (unlike in the intraladder case). This is because quite a lot of charge escapes from the $b$ and $y$ orbitals to the $x$ orbitals due to the orthogonalization procedure.

*Interladder repulsion in terms of copper holes.*— Since Zhang-Rice singlets are 'particle-hole cousins' of copper holes one can easily write down the interladder repulsion in terms of copper holes:

$$H_{V_2} = V_2 \sum_{i\alpha} \left( \tilde{n}_{i\alpha d} \tilde{\bar{n}}_{i+\frac{1}{2},\bar{\alpha}d} + \tilde{n}_{i\alpha d} \tilde{\bar{n}}_{i-\frac{1}{2},\bar{\alpha}d} \right), \tag{2.39}$$

where $V_2$ defined as in Eq. (2.38). Note that to obtain Eq. (2.39) from Eq. (2.37) we again [see Eq. (2.29)] shifted the chemical potential.

## 2.4 Method and results

### 2.4.1 The slave-boson approach

*Slave-particle formalism.*— The first difficulty one encounters while trying to solve the $t$–$J$-type of Hamiltonian is to cope with the constraint of no double occupancies at each site [20]. While there are several methods which approximately implement these constraints (see the following chapters where the slave-*fermion* approach is used), in this chapter we choose the slave boson method [60] to obtain qualitative insights. The reason is that this method is rather reliable in describing properties of the relatively highly doped $t$–$J$ models [20].

*Introducing Kotliar-Ruckenstein slave bosons.*— In contrast to the Barnes slave-boson approach [61], the Kotliar-Ruckenstein slave-boson representation [60] correctly interpolates between the $U = 0$ and the $U = \infty$ limit and therefore we choose this slave-bosons approach in what follows. In this approximation one enlarges the Fock space by introducing three auxiliary boson fields. First, one decouples the constrained fermion creation operator $\tilde{d}^\dagger_{i\alpha\sigma}$ into a fermion creation operator $f^\dagger_{i\alpha\sigma}$ carrying the spin degree of freedom, a boson creation operator $p^\dagger_{i\alpha\sigma}$, and a boson annihilation operator $e_{i\alpha}$ carrying the charge degree of freedom (i.e. $e^\dagger_{i\alpha}$ creates a charged hole):

$$\tilde{d}^\dagger_{i\alpha\sigma} = f^\dagger_{i\alpha\sigma} p^\dagger_{i\alpha\sigma} e_{i\alpha}. \tag{2.40}$$

This means that in order to create a fermion at site $i\alpha$, one first has to destroy a hole at this site but then one also keeps track of the change of the boson

configuration by the extra boson $p^\dagger_{i\alpha\sigma}$. Consequently, one not only *cannot* create a fermion at site $i\alpha$, if there are no holes at this site but one also 'remembers' which type of the fermion was created at site $i\alpha$. However, in the $U = 0$ limit one recovers only 25% of the value of the uncorrelated hopping, which has to be corrected [60]. Thus, one further modifies the decoupling procedure in order to reproduce the correct $U = 0$ limit:

$$\tilde{d}^\dagger_{i\alpha\sigma} = f^\dagger_{i\alpha\sigma} z^\dagger_{i\alpha\sigma}, \tag{2.41}$$

where

$$z^\dagger_{i\alpha\sigma} = \frac{p^\dagger_{i\alpha\sigma} e_{i\alpha}}{\sqrt{(1 - e^\dagger_{i\alpha} e_{i\alpha} - p^\dagger_{i\alpha\bar{\sigma}} p_{i\alpha\bar{\sigma}})(1 - p^\dagger_{i\alpha\sigma} p_{i\alpha\sigma})}}. \tag{2.42}$$

Note, however, that we need to introduce the following constraints to get rid of the nonphysical states in the enlarged Fock space:

$$\forall_{i\alpha} \quad \sum_\sigma p^\dagger_{i\alpha\sigma} p_{i\alpha\sigma} + e^\dagger_{i\alpha} e_{i\alpha} = 1, \tag{2.43}$$

$$\forall_{i\alpha\sigma} \quad p^\dagger_{i\alpha\sigma} p_{i\alpha\sigma} = f^\dagger_{i\alpha\sigma} f_{i\alpha\sigma}. \tag{2.44}$$

Thus, the full transformation contains not only Eq. (2.41) but also Eq. (2.44).

*Bosonic condensation.*— A typical next step in the slave boson approach is to assume that the introduced auxiliary bosons condense, i.e. they could be regarded as classical fields [with their values determined either self-consistently or using Eq. (2.44)]. Therefore, we assume that

$$\begin{aligned} p^\dagger_{i\alpha\sigma} &\sim \sqrt{f^\dagger_{i\alpha\sigma} f_{i\alpha\sigma}} \sim \sqrt{\frac{n}{2}}, \\ p_{i\alpha\sigma} &\sim \sqrt{f^\dagger_{i\alpha\sigma} f_{i\alpha\sigma}} \sim \sqrt{\frac{n}{2}}, \\ e_{i\alpha} &\sim \sqrt{1 - n}, \\ e^\dagger_{i\alpha} &\sim \sqrt{1 - n}, \end{aligned} \tag{2.45}$$

where $n$ is the already mentioned 'filling factor', i.e. the number of copper spins created by $\tilde{d}_{i\alpha}$ operators in the effective $t$–$J$–$V_1$–$V_2$ model.

Substituting transformations Eq. (2.41) together with Eq. (2.45) to Eq.

(2.2) we obtain the following effective Hamiltonian for interacting fermions $f$

$$\begin{aligned}
H^{eff} &= -tg_t\Big\{\sum_{i\alpha\sigma}\Big(f^\dagger_{i\alpha\sigma}f_{i+1,\alpha\sigma}+\text{H.c.}\Big)+\sum_{i\sigma}\Big(f^\dagger_{iR\sigma}f_{iL\sigma}+\text{H.c.}\Big)\Big\}\\
&\quad -\frac{1}{2}Jg_J\Big\{\sum_{i\alpha\sigma}\Big(f^\dagger_{i\alpha\sigma}f_{i\alpha\sigma}f^\dagger_{i+1,\alpha\bar\sigma}f_{i+1,\alpha\bar\sigma}+f^\dagger_{i\alpha\sigma}f^\dagger_{i+1,\alpha\bar\sigma}f_{i\alpha\bar\sigma}f_{i+1,\alpha\sigma}\Big)\\
&\qquad +\sum_{i\alpha}\Big(f^\dagger_{iR\sigma}f_{iR\sigma}f^\dagger_{iL\bar\sigma}f_{iL\bar\sigma}+f^\dagger_{iR\sigma}f^\dagger_{iL\bar\sigma}f_{iR\bar\sigma}f_{iL\sigma}\Big)\Big\}\\
&\quad +V_1g_J\Big\{\sum_{i\alpha\sigma}\Big(f^\dagger_{i\alpha\sigma}f_{i\alpha\sigma}f^\dagger_{i+1,\alpha\bar\sigma}f_{i+1,\alpha\bar\sigma}+f^\dagger_{i\alpha\sigma}f_{i\alpha\sigma}f^\dagger_{i+1,\alpha\sigma}f_{i+1,\alpha\sigma}\Big)\\
&\qquad +\sum_{i\alpha}\Big(f^\dagger_{iR\sigma}f_{iR\sigma}f^\dagger_{iL\bar\sigma}f_{iL\bar\sigma}+f^\dagger_{iR\sigma}f_{iR\sigma}f^\dagger_{iL\sigma}f_{iL\sigma}\Big)\Big\}\\
&\quad +V_2g_J\Big\{\sum_{i\alpha\sigma}\Big(f^\dagger_{i\alpha\sigma}f_{i\alpha\sigma}\bar f^\dagger_{i+\frac12,\bar\alpha\bar\sigma}\bar f_{i+\frac12,\bar\alpha\bar\sigma}+f^\dagger_{i\alpha\sigma}f_{i\alpha\sigma}\bar f^\dagger_{i+\frac12,\bar\alpha\sigma}\bar f_{i+\frac12,\bar\alpha\sigma}\\
&\qquad +f^\dagger_{i\alpha\sigma}f_{i\alpha\sigma}\bar f^\dagger_{i-\frac12,\bar\alpha\bar\sigma}\bar f_{i-\frac12,\bar\alpha\bar\sigma}+f^\dagger_{i\alpha\sigma}f_{i\alpha\sigma}\bar f^\dagger_{i-\frac12,\bar\alpha\sigma}\bar f_{i-\frac12,\bar\alpha\sigma}\Big)\Big\},
\end{aligned}\tag{2.46}$$

where the *bar* sign denotes the fact that the fermion operators act in the Hilbert subspace of the Hamiltonian for the neighbouring ladder. Furthermore, the factors $g_t$ and $g_J$ are:

$$\begin{aligned}
g_t &= \frac{2-2n}{2-n},\\
g_J &= \frac{4}{(2-n)^2}.
\end{aligned}\tag{2.47}$$

The reader may wonder here whether we gained a lot by introducing the Zhang-Rice scheme and then the slave bosons: The calculations were pretty lengthy and we ended up with a Hamiltonian describing again the interacting problem. However, we gained quite a lot during the above procedure: (i) we integrated out the oxygen orbital degrees of freedom entirely, (ii) the interaction terms in Eq. (2.46) are much weaker than those in the original model since $J$, $V_1$ and $V_2$ are of the order of the effective hopping $g_t t$ while in the Hamiltonian (2.1) the interacting terms are much bigger than the kinetic terms.

*Agreement with Gutzwiller factors.*— Actually, the $g_t$ and $g_J$ factors are equal to the well-known Gutzwiller factors [62, 63]. Thus, we could have introduced here the Gutzwiller approach to obtain the effective Hamiltonian (2.46). However, the slave boson approach seems to us to be more transparent.

### 2.4.2 The mean-field approximation

*Mean-field decoupling.*— To solve the effective Hamiltonian Eq. (2.46) we introduce the mean-field decoupling:

$$\begin{aligned}
&f^\dagger_{i\alpha\sigma}f_{i\alpha\sigma}f^\dagger_{i\alpha\sigma'}f_{i\alpha\sigma'}\rightarrow\\
&\qquad f^\dagger_{i\alpha\sigma}f_{i\alpha\sigma}\langle f^\dagger_{i\alpha\sigma'}f_{i\alpha\sigma'}\rangle+\langle f^\dagger_{i\alpha\sigma}f_{i\alpha\sigma}\rangle f^\dagger_{i\alpha\sigma'}f_{i\alpha\sigma'}-\langle f^\dagger_{i\alpha\sigma}f_{i\alpha\sigma}\rangle\langle f^\dagger_{i\alpha\sigma'}f_{i\alpha\sigma'}\rangle,
\end{aligned}\tag{2.48}$$

where the classical fields $\langle f^\dagger_{i\alpha\sigma} f_{i\alpha\sigma}\rangle$ are to be determined self-consistently with the initial values for these fields chosen in the following way:

First, we assume that

$$\langle f^\dagger_{i\alpha\uparrow} f_{i\alpha\uparrow}\rangle = \langle f^\dagger_{i\alpha\downarrow} f_{i\alpha\downarrow}\rangle = \frac{1}{2}\sum_\sigma \langle f^\dagger_{i\alpha\sigma} f_{i\alpha\sigma}\rangle \equiv \frac{1}{2}\langle f^\dagger_{i\alpha} f_{i\alpha}\rangle. \tag{2.49}$$

Second, if the number of fermions $f$ per site is $n = 2/3$. then we assume that

$$\langle f^\dagger_{i\alpha} f_{i\alpha}\rangle = \begin{cases} n-p & \text{for } i/3 \in \mathbb{Z} \\ n+\frac{1}{2}p & \text{for } i/3 \notin \mathbb{Z} \end{cases}, \tag{2.50}$$

while if $n = 3/4$ then

$$\langle f^\dagger_{i\alpha} f_{i\alpha}\rangle = \begin{cases} n-p & \text{for } i/4 \in \mathbb{Z} \\ n+\frac{1}{3}p & \text{for } i/4 \notin \mathbb{Z} \end{cases}, \tag{2.51}$$

and finally if $n = 4/5$ then we assume that

$$\langle f^\dagger_{i\alpha} f_{i\alpha}\rangle = \begin{cases} n-p & \text{for } i/5 \in \mathbb{Z} \\ n+\frac{1}{4}p & \text{for } i/5 \notin \mathbb{Z} \end{cases}, \tag{2.52}$$

where $p$ is a real number (with its value to be determined self-consistently, see next section) such that $0 \le p \le n$.

*Decoupling for neighbouring ladder.*— Actually, a similar decoupling is done for $\bar{f}$ fermion operators. However, here we assume different initial values for the classical fields:

If the number of fermions $f$ per site is $n = 2/3$, then we assume that

$$\langle \bar{f}^\dagger_{i-\frac{1}{2}\alpha} \bar{f}_{i-\frac{1}{2}\alpha}\rangle = \begin{cases} n-p & \text{for } (i+1)/3 \in \mathbb{Z} \\ n+\frac{1}{2}p & \text{for } (i+1)/3 \notin \mathbb{Z} \end{cases}, \tag{2.53}$$

while if $n = 3/4$ then

$$\langle \bar{f}^\dagger_{i-\frac{1}{2}\alpha} \bar{f}_{i-\frac{1}{2}\alpha}\rangle = \begin{cases} n-p & \text{for } (i+1)/4 \in \mathbb{Z} \\ n+\frac{1}{3}p & \text{for } (i+1)/4 \notin \mathbb{Z} \end{cases}, \tag{2.54}$$

and finally if $n = 4/5$ then we assume that

$$\langle \bar{f}^\dagger_{i-\frac{1}{2}\alpha} \bar{f}_{i-\frac{1}{2}\alpha}\rangle = \begin{cases} n-p & \text{for } (i+2)/5 \in \mathbb{Z} \\ n+\frac{1}{4}p & \text{for } (i+2)/5 \notin \mathbb{Z} \end{cases}. \tag{2.55}$$

*Reasons for the assumed initial values of the fields.*— Note that we choose these particular values for the classical field in order to investigate the stability of the CDW state of period $\lambda = 3$ for $n = 2/3$ ($n_h = 4/3$), period $\lambda = 4$ for $n = 3/4$ ($n_h = 5/4$) and period $\lambda = 5$ for $n = 4/5$ ($n_h = 6/5$). Since we are merely interested in investigating whether the interladder interaction can at all lead to the stability of the CDW phase in the coupled ladder, we choose the simplest possible pattern of the CDW order in the ladders [see Eqs. (2.50)-(2.52)]. Furthermore, we choose that the CDW order in the neighbouring ladder is such that the rungs with lower densities in that ladder are as far away as possible from the rungs with lower densities in the ladder under consideration.[5]

[5] In the case of $n = 3/4$ we could have equally chosen $(i+2)$ as the shift in the CDW order in the neighbouring ladder.

In this way the classical energy (i.e. for $t = 0$) of the system will be minimized for $p = n$ with respect to the interladder interaction $V_2$. Obviously, finite $t$ (and also finite $V_1$ and $J$) could change this result and it is the task of the next section to verify this assumption self-consistently.

*Validity of the approximation.*— One may wonder whether the above decoupling is justified since values of the interaction parameters $J$, $V_1$, and $V_2$ are comparable with the effective kinetic energy and therefore cannot be assumed as being small terms. However, as discussed in detail in Ref. [33] what matters in such a mean-field decoupling is the strength of quantum fluctuations (which are neglected in the mean-field decoupling) while the strength of the interactions is not important at all.

### 2.4.3 The ground state properties

*Stability of the CDW order.*— We determine the value of the CDW order parameter $p$ (2.50-2.55) self-consistently by diagonalizing the effective Hamiltonian [Eq. (2.46)] of the model (2.2) rewritten using the mean-field decoupling (2.48). The diagonalization is done numerically in the single-particle $k$ space using 500 $k$ points along the single leg of the ladder. The result is shown in Fig. 2.8: it depicts the stability of the CDW order in the coupled ladders due to the interladder interaction $V_2$ for all three studied doping levels ($n = 2/3$, $n = 3/4$, and $n = 4/5$). Besides, the CDW ground state has a small gap at the Fermi level for $n = 3/4$ and $n = 4/5$ while the gap at the Fermi level does not open for $n = 2/3$ (although the bands are flattened in the CDW state).

In particular, let us note that the CDW state with $\lambda = 4, 5$ is stable for the realistic values of the parameters $J = 0.4t$, $V_1 = 0.2t$ and $V_2 = 0.5t$ [as calculated using Eqs. (2.4), (2.27), (2.38) and parameters from Refs. [39, 51]]. Furthermore, the CDW order state is stable for period $\lambda = 3$ for a somewhat enhanced value of the interladder interaction $V_2 \sim 0.9t$ which nevertheless could be obtained using the charge transfer parameters of Ref. [64].

*Role of superexchange $J$ and intraladder interaction $V_1$.*— While the stability of the CDW order is entirely due to the interladder interaction $V_2$, the superexchange $\propto J$ and the intraladder interaction $\propto V_1$ also slightly influence the order. Actually, in all three cases turning on these interactions reduces the magnitude of the CDW order and makes it a bit less stable (i.e. the CDW order is stable for larger values of the interladder interaction $V_2$). Besides, this effect is well visible for period $\lambda = 3, 5$ while for period $\lambda = 4$ it is rather suppressed, see Fig. 2.8.

First, let us try to understand what kind of (ordered) ground state is favoured by these interactions. On the one hand, the role of the superexchange $J$ in the mean-field decoupling (2.48) amounts to the Ising-like interaction. Furthermore, we assumed that the solution is nonmagnetic (2.49). Thus, the superexchange merely favours formation of pairs of charges along each bond. On the other hand, the intraladder interaction $V_1$ disfavours such pairs as it is a repulsive interaction between nearest neighbours. Since a typical value of the superexchange is $J = 0.4t$ and of the intraladder interaction is $V_1 = 0.2t$ (see above), the joint effect of these interactions is a suppression of pairs of charges (as they jointly contribute as $J - 4V_1$ to the effective mean-field Hamiltonian).

Second, one can try to understand how it influences the CDW state. This, however, strongly depends on the CDW period. In the simplest case $\lambda = 3$ we

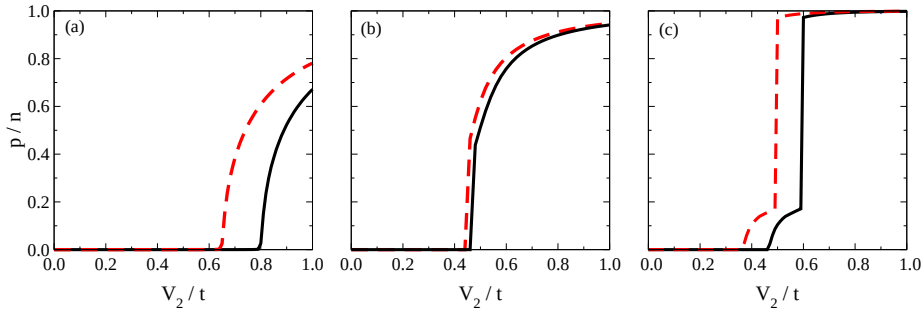


Figure 2.8: Stability of the CDW order due to the interladder interaction $V_2$ as obtained self-consistently from the mean-field decoupling (2.48) of the effective Hamiltonian [Eq. (2.46)] of the model (2.2). The panels depict the following cases: (a) filling $n = 2/3$ ($n_h = 4/3$) with period $\lambda = 3$ and order parameter $p$ as defined in Eqs. (2.50, 2.53), (b) filling $n = 3/4$ ($n_h = 5/4$) with period $\lambda = 4$ and order parameter $p$ as defined in Eqs. (2.51, 2.54), (c) filling $n = 4/5$ ($n_h = 6/5$) with period $\lambda = 5$ and order parameter $p$ as defined in Eqs. (2.52, 2.55). Solid lines are for realistic values of $J = 0.4t$ and $V_1 = 0.2t$ [see Eqs. (2.4), (2.27), (2.38) and Refs. [39, 51]] while dashed lines show results for $J = 0$ and $V_1 = 0$.

have two rungs with enhanced charge densities and therefore the joint effect is that the realistic $J$ and $V_1$ disfavour formation of the CDW order, see Fig. 2.8(a). On the other hand, when $\lambda = 4$ the situation is more complicated: we have three sites with enhanced charge density along the leg, while the pairs of charges are again formed along the rung. Together this yields that $J$ and $V_1$ interaction disfavour the onset of CDW states only marginally, see Fig. 2.8(b). Finally, the case with period $\lambda = 5$ is somewhat in between the two above cases as along the leg there are four sites with enhanced charge density, see Fig. 2.8(c).

*Understanding the results for $J = 0$ and $V_1 = 0$.*— Having understood the minor role of superexchange $J$ and intraladder interaction $V_1$, let us now turn to the understanding of the onset of the CDW order due to the interladder interaction $V_2$ for $J = 0$ and $V_1 = 0$ (see Fig. 2.8). First, the basic mechanism which supports the formation of the CDW order is rather simple. The onset of the CDW state lowers the energy interladder interaction $V_2$. This is because then the CDW states in the neighbouring ladders are arranged in such a way that the rungs with more charge in one ladder are the nearest neighbours of the rungs with less charge in the neighbouring ladder and vice versa, see Eqs. (2.50-2.55). Obviously, the onset of the CDW order is associated with the flattening of the bands (not shown) as then the mobility is reduced. Thus, in the CDW state the kinetic energy is higher and therefore the total energy of the system is lowered (and the transition to the CDW state takes place) only when the decrease in the interaction energy is higher than the decrease in the (negative) kinetic energy. When the nesting conditions are not satisfied (which is the case here but compare also Sec. 2.7) this can take place for finite value of the ratio $V_2/t$.

Second, there are relatively big differences between the onset of the CDW order for different doping levels $n$. However, with the exception of the 'cusp' for the CDW order with period $\lambda = 5$ (see below), this can be understood rather easily. The CDW state is more easily stabilized and has bigger amplitude $p/n$ when the number of $f$ fermions $n$ is bigger. This is because then the kinetic energy is reduced as there are less carriers in the system. Thus, for example the CDW order with period $\lambda = 4$ is stable already for smaller values of the ratio $V_2/t$ and has bigger amplitude $p/n$ than the CDW state with period $\lambda = 3$

*Understanding the 'cusp' for period* $\lambda = 5$.— Finally, the 'cusp' in Fig. 2.8(c) needs some explanation. Here, in the numerically most complicated case with period $\lambda = 5$, there is a competition between two different types of the CDW order: (i) the CDW state with a small amplitude $p$, rather unchanged electronic bands and small gap at the Fermi level, and (ii) the CDW state with a large charge modulation $p$, almost flat bands and a large gap at the Fermi level. While CDW state (ii) could be understood as a sort of 'analytic continuation' of the results obtained for period $\lambda = 3$ and $\lambda = 4$, the CDW state (i) is awkward and needs some further understanding.

In fact, the existence of the possibility (i) is the result of the complex interplay of the complicated band structure for the CDW state with period $\lambda = 5$ (where the effective Brillouin zone is 'five-folded') and the complicated effective mean-field potential from the neighbouring ladder. Actually, the latter mean-field potential from the neighbouring ladder is due to the fact that the CDW order in the neighbouring ladder acts as a negative potential merely on three rungs (out of five in the unit cell) in the ladder under consideration. Thus, this potential itself contains competing terms and therefore the 'interpolating' CDW state with small amplitude $p$ is formed.

## 2.5 Discussion

### 2.5.1 Validity of the results

*Possible shortcomings of the present approach.*— In order to obtain results shown in Fig. 2.8 we introduced a number of approximations to the $t$–$J$–$V_1$–$V_2$ Hamiltonian. In particular, we introduced: (i) the slave-boson approach to overcome the problem of the constraint of double occupancies, (ii) the mean-field decoupling. Whereas the first approximation is widely used [20], the second one is also a reasonable approach to the ordered states in the strongly correlated systems [33].

Still, however, both the slave-boson approach and the mean-field decoupling were used in one of their simplest possible versions. For example, first, we assumed that the number of bosons which condense is equally distributed through the lattice which led to the site-independent Gutzwiller factors. On the one hand, we checked that the site-dependent Gutzwiller factors yield similar results for the CDW with period $\lambda = 3$ as obtained in Fig. 2.8. On the other hand, it turned out that the self-consistent mean-field calculations did not converge when we used the site-dependent Gutzwiller factors for the CDW with period $\lambda = 5$. Second, we assumed that the solution was nonmagnetic — clearly introducing the possibility of finite spin polarization would improve the present result. However, as the purpose of the calculations was to investigate the onset

of the CDW order due to the interladder interaction, this was at least partially justified.

*Possible shortcomings of the derivation of the model.*— Distinct approximations and shortcomings are related with the $t$–$J$–$V_1$–$V_2$ Hamiltonian itself. First, one could verify whether the Zhang-Rice singlets do not get destroyed due to the interladder interaction. Although the Zhang-Rice binding energy is of the order of $(4-5)t_{pd}$ (see Table 2.1) which is much bigger than the biggest possible value of the interladder interaction between them ($V_2 \sim 0.7t$), it is internally consistent when the explicit calculations show that this indeed cannot happen. Second, we assumed that the on-site energy for holes on the rung orbital $b$ is the same as the one for holes in the other oxygen orbitals. However, due to a different coordination number for this site, the on-site energy of the $b$ orbital should be somewhat lower. Indeed, it is estimated that the ratio between these two on-site energies is $\varepsilon \sim 0.9$ [52]. Thus, it is interesting to verify whether this asymmetry in the on-site energies of the oxygen orbitals can destabilize the Zhang-Rice singlets. Hence, in the next two sections, we study in more detail the above mentioned possible shortcomings of the derivation of the model.

### 2.5.2 'Rigidity' of the Zhang-Rice singlets

*Purpose of this section.*— In order to verify whether the interladder interaction $V_2$ could influence the stability of the Zhang-Rice singlets we solve the charge transfer model (2.1). In this way we will be able to check how the Zhang-Rice singlets are influenced by the on-site interaction between holes on the same oxygen sites but belonging to two neighbouring ladders.

*The CDW solution of the charge transfer model.*— We solve the Hamiltonian (2.1) for various values of the model parameters $\{U, \Delta, U_p\}$, and for three different hole densities $n_h = 6/5, 5/4, 4/3$ using the mean-field approximation, i.e., we decouple

$$n_{j\alpha\mu\uparrow} n_{j\alpha\mu\downarrow} \rightarrow \langle n_{j\alpha\mu\uparrow}\rangle n_{j\alpha\mu\downarrow} + n_{j\alpha\mu\uparrow}\langle n_{j\alpha\mu\downarrow}\rangle - \langle n_{j\alpha\mu\uparrow}\rangle\langle n_{j\alpha\mu\downarrow}\rangle, \tag{2.56}$$

where $\mu = d, x, y, b$ and a similar decoupling holds for the neighbouring ladders. The ground state was found by diagonalizing the resulting one-particle Hamiltonian in real space for a single ladder with 60 unit cells, separately for spin up and spin down. The classical fields $\{\langle n_{j\alpha\mu\sigma}\rangle\}$ and $\{\langle \bar{n}_{j-\frac{1}{2},\alpha\mu\sigma}\rangle\}$ were determined self-consistently with the initial values for these fields as in Fig. 2.9. While a uniform spin density wave is stable for $n_h = 1$, one finds a CDW superimposed on the spin density wave order for realistic hole densities $n_h \geq 6/5$. The stability of this composite order follows from the 1D polaronic defects in the spin density wave state. We limit the present analysis to the stability of this particular CDW phase, while we do not study here the possible competition with other phases (see Ref. [65] and next section). *Characterization of the CDW state in the charge transfer model.*— For each state we evaluate: (i) the CDW order parameter

$$\begin{aligned} p' \equiv & \sum_{i\in rung} \langle n_{id} + n_{ib} + n_{ix}\rangle - \frac{1}{\lambda - 1} \sum_{i\notin rung} \langle n_{id} + n_{ib} + n_{ix}\rangle \\ & + \sum_{i\in rung} \langle n_{iy}\rangle - \frac{2}{\lambda - 2} \sum_{i\notin rung} \langle n_{iy}\rangle, \end{aligned} \tag{2.57}$$

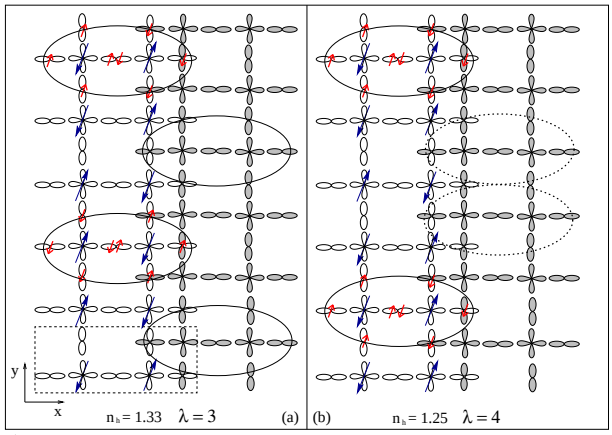


Figure 2.9: Artist's' view of two coupled $Cu_2O_5$ ladders (white and grey) with a CDW order of period: (a) $\lambda = 3$ and (b) $\lambda = 4$. Again (cf. Fig. 2.4) the $Cu_2O_5$ unit cell with two $3d_{x^2-y^2}$, three $2p_x$, and two $2p_y$ orbitals is indicated by dashed line. The arrows stand for hole spins in copper and oxygen orbitals, with their (large) small size corresponding to +1.0 (+0.25) hole charge. The ovals show rungs with enhanced hole density in the CDW phase. The dotted ovals in the grey ladder of (b) show the two possible degenerate states, see text.

where $\lambda$ is the period of the CDW state, and (ii) the second moment of the hole density distribution with respect to the ideal non-orthogonal Zhang-Rice singlet state (to be called also Zhang-Rice dispersion; $n_0 = 0.25$),

$$\sigma^2 \equiv \sum_{i \in rung} \Big\{ (\langle n_{ib} \rangle - 2n_0)^2 + (\langle n_{ix} \rangle - n_0)^2 + (\langle n_{iy} \rangle - n_0)^2 \Big\}. \tag{2.58}$$

Here and in what follows by 'rung' we mean the 'rung with enhanced hole density' which consists of seven oxygen orbitals (four $y$, two $x$ and one $b$) and two copper orbitals (see the ovals in Fig. 2.9). Hence, in both above definitions the mean values of the particle number operators are calculated for these rungs ($i \in rung$) or for all remaining sites in the whole ladder ($i \notin rung$). Note that in the first term in Eq. (2.58) we subtract $2n_0$ hole density as we assume that there are two non-orthogonal Zhang-Rice singlets in the same rung which share the common $b$ oxygen orbital, see Fig. 2.9. Note also that in the ideal CDW phase (shown in Fig. 2.9) $p' = 2$ and $\sigma^2 = 0$, irrespectively of the actual period $\lambda$. We also introduce *rung* hole densities on oxygen and copper sites

$$n_p \equiv \sum_{i \in rung} \langle n_{ib} + n_{ix} + n_{iy} \rangle, \quad n_d \equiv \sum_{i \in rung} \langle n_{id} \rangle. \tag{2.59}$$

Similarly, magnetic order parameters are

$$m_p \equiv \Big| \sum_{i \in rung \cap L} m_{ix} + m_{iy} \Big| + \Big| \sum_{i \in rung \cap R} m_{ix} + m_{iy} \Big|, \tag{2.60}$$

$$m_d \equiv \sum_{i \in rung} |m_{id}|, \tag{2.61}$$

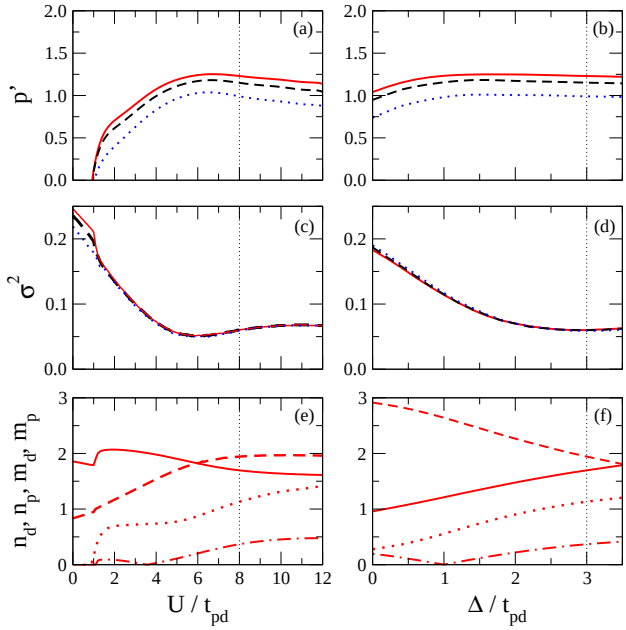


Figure 2.10: Characterization of the CDW ground states obtained with $U_p = 0$ for increasing $U$ (left, $\Delta = 3t_{pd}$) and $\Delta$ (right, $U = 8t_{pd}$): (a), (b) CDW order parameter $p'$, and (c), (d) ZR singlet dispersion $\sigma^2$, for $\lambda = 5, 4, 3$ shown by solid, dashed, and dotted lines, respectively; (e), (f) for $\lambda = 5$ charge (magnetization) in the rung on copper sites shown by solid (dotted) line and on oxygen sites shown by dashed (dashed-dotted) line, see Eqs. (2.59)–(2.61). The realistic values (Ref. [51]) of $U = 8t_{pd}$ and $\Delta = 3t_{pd}$ are marked by vertical lines.

where the magnetization for orbital $\mu$ at site $i$ is $m_{i\mu} = \langle n_{i\mu\uparrow} - n_{i\mu\downarrow} \rangle$. We recall that when holes on the rungs form two localized Zhang-Rice singlets next to each other, then $n_d = m_d \simeq 2$, $n_p \simeq 2$, and $m_p \simeq 1.5$, see Fig. 2.9.

*Results for a single ladder in the charge transfer model.*— First, we investigate the onset of the CDW phase in a single ladder of Fig. 2.9 by assuming $U_p = 0$. In the charge transfer regime (for $\Delta = 3t_{pd}$ following Ref. [51]) the CDW is stable already for $U \geq t_{pd}$ with periods: $\lambda = 5$ for $n_h = 6/5$, $\lambda = 4$ for $n_h = 5/4$, and $\lambda = 3$ for $n_h = 4/3$ [Fig. 2.10(a)]. For higher values of the on-site Coulomb repulsion $U$, $p'$ first increases quite fast irrespectively of the actual CDW period, and next saturates at $p' \sim 1$, being only about 50% of the maximal value $p' = 2$ (a weak decrease of $p'$ for $U > 6t_{pd}$ follows from the charge redistribution). In particular, such a CDW order is robust for the widely accepted value of $U = 8t_{pd}$ for copper oxide ladders [51].

In the strong coupling regime of $U > 4t_{pd}$ the CDW state is formed by holes distributed as in the Zhang-Rice singlets since then $\sigma^2 \sim 0.05$ is indeed very small for all periods [Fig. 2.10(c)]. This is also visible in Fig. 2.10(e) where, in this regime, both the number of holes on oxygen sites ($n_p$) and on copper sites ($n_d$) in the rungs are rather close to their values in the localized Zhang-Rice states. Note that the minimum of $\sigma^2$ would correspond to $n_p = n_d$ which

further motivates the definition of Eq. (2.58). We can also probe the Zhang-Rice character of holes forming the CDW state by looking at the magnetization of holes in the rungs, cf. Fig. 2.10(e). The magnetization $m_d$ grows with increasing $U$ and for large $U \sim 12t_{pd}$ it is still around 30% smaller than that for localized Zhang-Rice singlets. However, even in this range of $U$ the magnetization on the oxygen sites $m_p$ is quite small and much below the value for ideal Zhang-Rice singlets (around 70% smaller). This confirms that the subtle (entangled) nature of the Zhang-Rice singlets can be only partly captured within the classical mean-field approach. Therefore, in what follows we call these states classical Zhang-Rice singlets.

Remarkably, changing the value of $\Delta$ for fixed $U = 8t_{pd}$ does not destabilize the CDW state [Fig. 2.10(b)] irrespectively of the period. This suggests that the charge order is triggered by the on-site Coulomb repulsion. However, the character of the holes forming the CDW state changes and $\sigma^2$ is small ($\sigma^2 \sim 0.07$) only as long as $\Delta$ is large [Fig. 2.10(d)]. This is also visible in Fig. 2.10(f) where a similar discussion as the one concerning Fig. 2.10(e) applies.

To gain a deeper understanding of the results we calculated the charge gap as a function of the Hubbard $U$ (not shown): one finds that the CDW state gains stability when an insulating state is formed. Altogether, one finds that: (i) the Coulomb interaction $U$ can stabilize the CDW in the $Cu_2O_5$ ladders, (ii) the CDW phase can be viewed as an equidistant distribution of the classical Zhang-Rice singlet states in the relevant parameter regime, and (iii) all of the stable periods (even and odd) behave similarly.

*Results for the coupled ladders in the charge transfer model.*— Next, we investigate the influence of the interladder coupling. At finite $U_p$ the 'external' fields $\{\langle \bar{n}_{j-\frac{1}{2},\alpha\mu\sigma}\rangle\}$ in the mean-field version of Eq. (2.1) contribute and were self-consistently determined by iterating the mean-field equations. Thereby, the symmetry of the CDW state was chosen in such a way that the rungs were translated by $\lambda$ Cu-O lattice constants ($\lambda$ odd) in the neighbouring ladders to maximize the distance between them (Fig. 2.9), which minimizes the classical mean-field energy. For even $\lambda = 4$ the numerical calculations performed with the realistic parameters [51] for $Cu_2O_5$ ladder ($U = 8t_{pd}$ and $\Delta = 3t_{pd}$) confirmed that the two topologically equivalent possibilities of such a translation are degenerate, as expected. The effect of the interladder interaction due to $U_p$ was identified by comparing the ground states derived separately in two cases: ($A$) with $\{\langle \bar{n}_{j-\frac{1}{2},\alpha\mu\sigma}\rangle\} = 0$, i.e., using only the (intraorbital) repulsion between oxygen holes on the considered ladder; ($B$) by implementing the 'external' fields $\{\langle \bar{n}_{j-\frac{1}{2},\alpha\mu\sigma}\rangle\}$ calculated self-consistently, i.e. including both the intraorbital and interorbital Coulomb repulsion between holes on oxygen sites.

One finds that in case $A$ the CDW order parameter $p'$ decreases in a similar way for all periods, cf. Fig. 2.11(a), as well as for even period ($\lambda = 4$) when the interladder coupling is switched on (case $B$). Remarkably, a qualitatively distinct behaviour is found for *odd* periods – here the interladder coupling supports the onset of the CDW phase and the order parameter either saturates or even increases with increasing strength of the on-site repulsion $U_p$ (as for $\lambda = 3$), see also Fig. 2.11(c). In fact, the interladder coupling enhances the hole density in the rungs.

Another striking effect is the qualitatively distinct behaviour of the Zhang-Rice dispersion $\sigma^2$ for odd and even periods, see Fig. 2.11(b). While for period

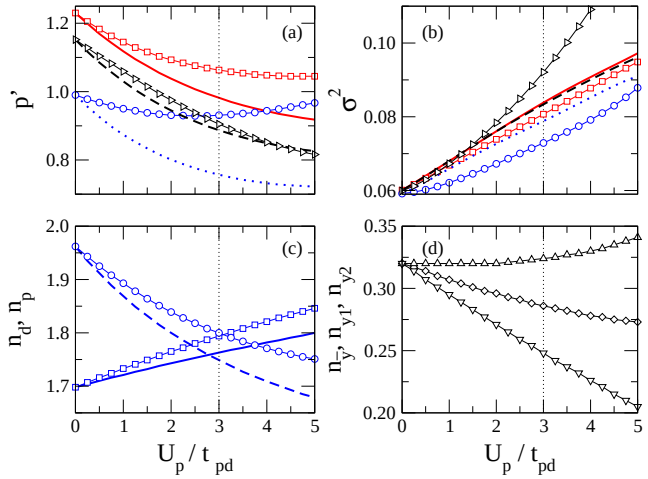


Figure 2.11: The CDW ground state for increasing $U_p$: (a) CDW order parameter $p'$ and (b) Zhang-Rice singlet dispersion $\sigma^2$, for $\lambda = 5, 4, 3$ shown by solid, dashed, and dotted lines (squares, triangles, and circles) in case $A$ ($B$), see text; (c) for $\lambda = 3$ charge on copper (oxygen) sites in the rung shown by solid (dashed) line in case $A$ and by squares (circles) in case $B$, see Eq. (2.59); (d) for $\lambda = 4$ charge in different $y$ orbitals ($n_{\bar{y}}$, $n_{y1}$, and $n_{y2}$, shown by diamonds, triangles down, and up) in the rung in case ($B$), see text. Vertical lines mark the realistic value (Ref. [51]) of $U_p = 3t_{pd}$. Parameters: $\Delta = 3t_{pd}$, $U = 8t_{pd}$.

$\lambda = 4$ switching on the interladder coupling ($B$) drastically increases $\sigma^2$ with respect to the single ladder case ($A$), the results are precisely opposite for odd periods $\lambda = 3, 5$. Furthermore, this increase of $\sigma^2$ with $U_p$ in case ($B$) is large for even period – its value $\sim 0.1$ found for large (but still realistic) $U_p \sim 3.5t_{pd}$ is comparable to the value of the Zhang-Rice dispersion for a single ladder with $\Delta \sim t_{pd}$ [Fig. 2.10(d)], where we do not expect stable Zhang-Rice singlets. This large increase of $\sigma^2$ in this case follows from the geometrical frustration of the CDW state, as for even periods the two $y$ orbitals in the same rung are not equivalent [one of them (say $y1$) is closer than the other one (say $y2$) to the rung in the neighbouring ladder], as shown in Fig. 2.11(d). We have also verified that the mean hole density $n_{\bar{y}} = \frac{1}{2}(n_{y1} + n_{y2})$ almost does not change when the interladder coupling is switched off (not shown).

Thus, the interladder interaction: (i) supports the CDW states with odd periods $\lambda = 3, 5$ and slightly disfavours the frustrated CDW state with even period $\lambda = 4$, (ii) destabilizes (strengthens) the homogeneous Zhang-Rice–type distribution of holes in the rungs for period $\lambda = 4$ ($\lambda = 3, 5$ ), respectively.

*Final conclusions.*—- Altogether, the above calculations show that the Zhang-Rice–type distribution is stable in the odd-period CDW ground state of the charge transfer model. In particular, in such a charge ordered states it is not destroyed due to the interladder interaction, i.e. due to the on-site repulsion between holes on different oxygen $p$ orbitals belonging to two neighbouring ladders.

It is only in the even-period CDW (i.e. $\lambda = 4$) that the interladder in-

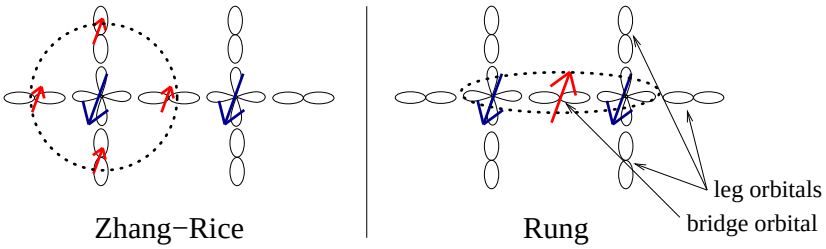


Figure 2.12: Artist's view of the Zhang-Rice singlet (left panel) and rung-centred (rung) hole (right panel) in a $Cu_2O_5$ cluster. Large (small) arrows depict the hole spins for $+1.0$ ($+0.25$) charge. The red arrows stand for spins of doped holes.

teraction destabilizes the homogeneous Zhang-Rice–type distribution of holes. Although, it is not of such an importance for us as we are mainly interested in explaining the onset of the odd-period CDW order, this result does not mean that the true Zhang-Rice singlets will be destabilized in this case. Actually, in reality the Zhang-Rice singlets are even more robust than the ones discussed in this section – the energy gain due to quantum fluctuations and phase coherence are not captured in these classical states (see also Sec. 2.3.3 for more discussion on the binding energy of the true Zhang-Rice singlets).

Thus, we conclude that the Zhang-Rice singlets are rather 'rigid' objects even in their extremely simplified classical version. Their true quantum-mechanical counterpart with much bigger binding energy is expected to be even more 'rigid' and is not destroyed due to the interladder interaction.

### 2.5.3 Rung states or Zhang-Rice singlets

*Purpose of the section.*— The purpose of this section is to investigate the influence of the lower energy of the rung (called also bridge) oxygen orbital, with respect to the on-site energy of the other (called leg) orbitals, on the stability of the Zhang-Rice singlets. Hence, one could expect that instead of the Zhang-Rice state a rung-centred state (rung) could be stabilized with a doped hole residing on the O ($2p$) bridge orbital and bound to the two neighbouring Cu holes via superexchange interactions (cf. Fig. 2.12).

*Zhang-Rice versus rung states in charge transfer model.*— We solve the charge transfer model (2.1) in a somewhat similar way as in the previous section. There are two differences: (i) we do it merely for the single ladder and for only one hole doping $n_h = 4/3$, (ii) we assume that the CDW state with period $\lambda = 3$ is formed by *one* Zhang-Rice singlet or rung state per rung (see Fig. 2.12). Let us note, that this means that the corresponding CDW state has *less* charge (oxygen holes) per every third rung. This stays in contrast with all the previous calculations and with the experimental results [8, 9]. However, the purpose here is to merely verify how the lower value of the bridge orbital energy influences the stability of the Zhang-Rice state.

Qualitatively the results are as follows. For $\varepsilon = 1$ the hole and magnetization distribution resembles the ones in classical Zhang-Rice state (see previous

section): the doped hole is distributed rather isotropically among four oxygen sites surrounding the central copper site occupied by roughly one hole. Also the spin of the doped hole in the oxygen ($2p$) orbitals compensates roughly the spin of the hole in the copper site. On the other hand, for $\varepsilon = 0.8$ the doped hole enters mainly into the $b$ orbital when the holes are transfered from the $p$ orbitals of the leg of the ladder, suggesting a rung character of the doped hole. Let us also note that, in agreement with the assumption of charge order, we find a CDW state with less charge per every third rung of the ladder for the solution with Zhang-Rice or rung character.

In order to quantitatively investigate the role of the specific spin ladder geometry on the stability of the Zhang-Rice and rung states we calculate the densities and magnetization of holes involved in forming:

($i$) the (classical) Zhang-Rice state:

$$n_{\mathrm{ZR}} = n_{ix} + n_{iy_1} + n_{iy_2}, \tag{2.62}$$

for $i$ belonging to the rung with enhanced hole density and $y_1$ as well as $y_2$ orbitals defined as in the previous section and

$$|m_{\mathrm{ZR}}| = |n_{\mathrm{ZR}\uparrow} - n_{\mathrm{ZR}\downarrow}|, \tag{2.63}$$

where we exclude the $b$ orbital from the sum to be able to distinguish between the rung and the Zhang-Rice states;

($ii$) the rung state:

$$n_{\mathrm{Rung}} = n_{ib}, \tag{2.64}$$

for $i$ belonging to the rung with enhanced hole density and

$$|m_{\mathrm{Rung}}| = |n_{\mathrm{Rung}\uparrow} - n_{\mathrm{Rung}\downarrow}|. \tag{2.65}$$

The results are shown in Fig. 2.13(a) as a function of the on-site energy of the bridge orbital $\varepsilon$. We find that with the decreasing value of $\varepsilon$ doped holes tend to occupy the $b$ orbital, and the spins of the holes in the $b$ orbital become polarized. Besides, the spins of the holes involved in forming Zhang-Rice state do not only compensate the spin of the central copper hole but for $\varepsilon < 0.85$ even weakly align ferromagnetically with the copper spin. Hence, we suggest that for $\varepsilon < 0.85$ the doped holes show a rung character while for $\varepsilon > 0.9$ they show a distinctive Zhang-Rice-singlet character separated by a crossover regime. It means that the Zhang-Rice state is stable for the value of $\varepsilon = 0.92$, calculated in Ref. [52], though we are very close to the crossover regime.

*Binding energies for the Zhang-Rice versus those for the rung states.*— Let us now pose the question to what extent our results are relevant for the stability of the real quantum-mechanical Zhang-Rice singlets or rung states. Therefore, using second order perturbation theory in $U$ and $U - \Delta$ [26] (see also Sec. 2.3.3) we calculate the binding energy of a single hole doped into Zhang-Rice and rung states: in the classical case ($E_{\mathrm{ZR}}$ and $E_{\mathrm{Rung}}$, respectively), and in the quantum-mechanical case ($E_{|\mathrm{ZR}\rangle}$ and $E_{|\mathrm{Rung}\rangle}$, respectively). In the classical case, which resembles the states obtained in the mean-field approximation (see above), one

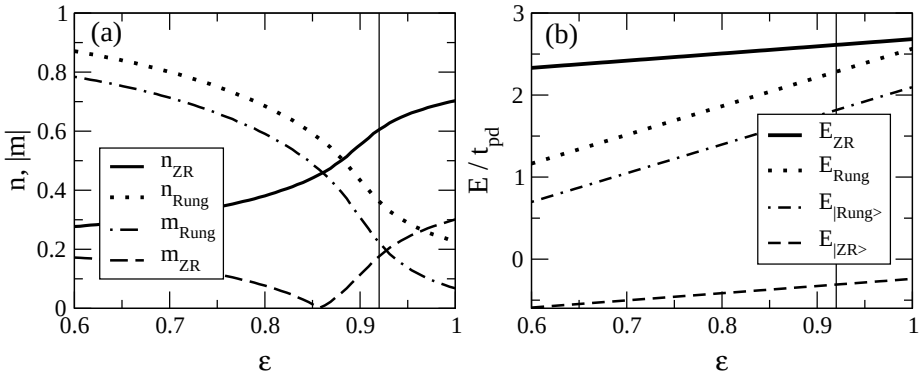


Figure 2.13: (a) Hole density ($n$) and absolute value of magnetization ($|m|$) for holes involved in forming the Zhang-Rice state ($n_{\rm ZR}, |m_{\rm ZR}|$) and the rung states ($n_{\rm Rung}, |m_{\rm Rung}|$) as a function of the ratio of the bridge orbital energy to the leg orbital energy ($\varepsilon$). (b) Binding energies of a single hole in ZR and rung states in the classical case ($E_{\rm ZR}$ and $E_{\rm Rung}$, respectively) and quantum-mechanical case ($E_{|{\rm ZR}\rangle}$ and $E_{|{\rm Rung}\rangle}$, respectively) as a function of the ratio of the bridge orbital energy to the leg orbital energy ($\varepsilon$). The vertical line on both panels depicts the value of $\varepsilon = 0.92$, cf. Ref. [52].

finds:

$$E_{\rm ZR} = \frac{1}{4}(3+\varepsilon)\Delta + J'\Big\langle \sum_{i\in {\rm ZR}} \mathbf{S}_i \cdot \mathbf{S}_{\rm O} - \frac{1}{4}\Big\rangle_{\rm ZR} \ , \tag{2.66}$$

$$E_{\rm Rung} = \varepsilon\Delta + J'\Big\langle \sum_{i\in {\rm Rung}} \mathbf{S}_i \cdot \mathbf{S}_{\rm O} - \frac{1}{4}\Big\rangle_{\rm Rung}, \tag{2.67}$$

where: the superexchange $J' = 2t_1 + 2t_2$,[6] $\mathbf{S}_{\rm O}$ is the spin of the doped oxygen ($2p$) hole, $\mathbf{S}_i$ is the spin of the copper ($3d$) hole, and the sum includes those copper sites which are involved in forming a bound state with the oxygen ($2p$) hole in rung or Zhang-Rice state. The expressions for the energies in the quantum-mechanical case look similar except for the averages of the spin operators which, unlike in the classical case, include also spin fluctuations. In addition, for the real Zhang-Rice singlet we include the phase coherence of holes doped into the oxygen ($2p$) orbitals [26] (i.e. we assume that the holes are distributed among the oxygen orbitals in a symmetric way, see also Sec. 2.3.3). The results are shown in Fig. 2.13(b) as a function of the energy of the bridge orbital $\varepsilon$.

We find for the classical state that for $\varepsilon < 0.97$ the energy difference ($E_{\rm ZR} - E_{\rm Rung}$) is larger than the effective hopping energy $t$ of the oxygen ($2p$) hole ($= t_{pd}^2/U$ or $t_{pd}^2/(U-\Delta)$). Hence for finite bandwidth the rung state could only be stabilized up to the above value of the bridge orbital energy, qualitatively in agreement with the previous mean-field results. However, in the quantum mechanical case the rung state could never be stabilized, and due to the large energy difference ($E_{|{\rm ZR}\rangle} - E_{|{\rm Rung}\rangle}$) the true Zhang-Rice singlet should not be destabilized by finite bandwidth.

[6] Where the very small contribution due to finite $U_p$ is neglected, see also Table 2.1. Besides, $t_1$ and $t_2$ should be slightly modified for $\varepsilon \neq 1$ but the change would be rather small.

*Conclusions.*— In summary, this section shows again a profound stability of the Zhang-Rice singlets in the hole doped spin ladders. First, using the model charge transfer calculations in the mean-field approximation we obtain that the isotropic distribution of doped holes among the oxygen ($2p$) orbitals surrounding the central copper ($3d$) hole is stable. Second, quantum-mechanical calculations of the binding energy of holes forming Zhang-Rice singlets and rung states suggest the Zhang-Rice singlets to be even more stable.

## 2.6 Conclusions

*Purpose of this chapter.*— The purpose of this chapter was to explain theoretically the onset of the CDW state in the telephone number compound for only selected values of $x$ while using a model which merely contains on-site Coulomb interactions. In particular the questions to be answered in this chapter were: (i) what the proper $t$–$J$ model for the coupled $Cu_2O_5$ ladders, which would arise due to the on-site Coulomb interactions, looked like, and (ii) whether this model could explain the onset of the CDW order with particular periods for particular values of $x$ in $Sr_{14-x}Ca_xCu_{24}O_{41}$. Let us now answer these questions.

*Form of the proper model.*— As discussed in Sec. 2.2 the standard $t$–$J$ model solved for the single ladder lead to the results which are incompatible with the experimentally observed CDW state in the coupled $Cu_2O_5$ ladders in $Sr_{14-x}Ca_xCu_{24}O_{41}$. In fact, the $Cu_2O_5$ ladder is a charge transfer system and the Zhang-Rice scheme [26], which enables the derivation of the $t$–$J$ model from the charge transfer system, has never been done (as far as we know) for a single ladder with no $D_{4h}$ symmetry. In addition, the specific geometry of coupled ladders could lead to new interactions due to the on-site repulsion between holes on the different oxygen orbitals belonging to two different ladders (see Fig. 2.4).

Thus, in Sec. 2.3 we derived the proper $t$–$J$ model for coupled ladders, starting from the appropriate charge transfer model (see Sec. 2.3.1) and using the Zhang-Rice scheme [26]. First, we showed that the kinetic $t$ part and the superexchange $J$ part of the new model were similar to the kinetic and superexchange parts in the standard $t$–$J$ model, see Sec. 2.3.3 and 2.3.2. This is because: (i) the holes do not hop between the coupled ladders as the interoxygen hopping can be neglected [39], (ii) the superexchange processes along the $90^0$ bonds are rather weak (see Sec. 2.3.2).

Next, in Sec. 2.3.4 we discussed the repulsion between the Zhang-Rice singlets (or effectively between the copper spins in the new $t$–$J$ model) in the same ladder. This term arises due to the finite on-site interaction $U_p$ between holes on the same orbital in the oxygen sites but belonging to two nearest neighbour Zhang-Rice singlets. Although, a similar term should also be present in the proper $t$–$J$ model for $CuO_2$ planes, it is usually neglected as it is roughly twice smaller then the superexchange term $J$. Actually, a very similar result is obtained for the ladder geometry but this was not *a priori* so clear. Besides, this served as a nice exercise before we we proceeded further to derive the crucial interladder interactions (see below).

The last, but certainly not least, term which constitutes the new proper $t$–$J$ model for coupled ladders is the interladder repulsion between the Zhang-Rice singlets (or again effectively between the copper spins in the new $t$–$J$ model) in

two different ladders, see Sec. 2.3.5. This term also originated from the on-site interactions between holes situated on the same oxygen orbital sites but this time belonging to two different orbitals in the two nearest neighbour Zhang-Rice singlets on *neighbouring* ladders. Since, such Zhang-Rice singlets share two oxygen sites such a term should be four times as big as the intraladder interaction (as the Pauli principle does not prohibit holes with the same spin on the same oxygen site but different orbital). In fact, a detailed check showed that a realistic Hund's exchange reduced this interaction and it turned out that the interladder repulsion is twice stronger than the intraladder repulsion. This, however, means that for realistic charge transfer parameters [39, 51] it is roughly as strong as the superexchange $J$ and cannot be neglected.

*The stability of the CDW state.*— Having derived the proper model, in order to establish whether the CDW state could be stable in the coupled ladders, we presented the solution of this model in Sec. 2.4. The model was solved using the the slave-boson approach (see Sec. 2.4.1) and the mean-field decoupling (see Sec. 2.4.2) and the ground state properties were discussed in Sec. 2.4.3). We showed the the CDW state could be stable in the system entirely due to the interladder interaction. In particular, rather realistic values (see detailed discussion in Sec. 2.4.3) of this interaction led to the stability of the CDW state: (i) with period $\lambda = 3$ for the $n_h = 4/3$ holes ($n = 2/3$ filling), (ii) with period $\lambda = 4$ for the $n_h = 5/4$ holes ($n = 3/4$ filling), (iii) with period $\lambda = 5$ for the $n_h = 6/5$ holes ($n = 4/5$ filling). Thus, the CDW phase with the peculiar periods $\lambda = 3$ or $\lambda = 5$ could indeed be stable in the ladder system. Furthermore, in the slave-boson and mean-field approach it occurred that the CDW state with period $\lambda = 4$ could not be stable in the system merely due to the superexchange $J$ and more sophisticated methods are needed, see Ref. [10].

*Validity of the results.*— In the end of the chapter, we also discussed the validity of the results (Sec. 2.5.1) and of the model itself (Secs. 2.5.2-2.5.3). It is interesting to note that neither (i) the on-site repulsion between holes on different oxygen orbitals belonging to two neighbouring ladders (Sec. 2.5.2), nor (ii) the lower on-site energy of the oxygen site in the middle of the ladder rung (Secs. 2.5.3) lead to the destabilization of the Zhang-Rice singlets. Therefore, the Zhang-Rice scheme indeed could have been used to derive the proper $t$–$J$ model for coupled $Cu_2O_5$ ladders.

*Final remarks.*— To conclude, let us stress that the $t$–$J$ models for the ladders are used frequently [10, 11, 45] as they are computationally simpler than the 2D $t$–$J$ models. Here we showed that for the $t$–$J$ model on a ladder to be indeed physically meaningful, and thus could well describe a realistic ladder subsystem found in $Sr_{14-x}Ca_xCu_{24}O_{41}$, one should add the nearest neighbour interladder repulsive term.

As a postscriptum, let us note that we have not resolved the problem of the peculiar absence of the CDW state with even period in $Sr_{14-x}Ca_xCu_{24}O_{41}$. However, in Sec. 2.7 we describe a toy-system consisting of two coupled chains in which such a CDW could become unstable. Obviously, this does not answer the question of the stability of the CDW state with even period and should be rather treated as an interesting 'side story'.

## 2.7 Postscriptum: destabilizing even-period-CDW state in a toy-model

*Problem with CDW state with period $\lambda = 4$.*— The biggest drawback of the results showed in this chapter is that they do not explain why the CDW order with period $\lambda = 4$ is not stable in the $Cu_2O_5$ coupled ladders in $Sr_{10}Ca_4Cu_{24}O_{41}$ [8]. Indeed, as shown in Fig. 2.8 the CDW state with period $\lambda = 4$ has similar features as the CDW state with odd period $\lambda$ and there are no signatures that this particular state can become unstable. In fact, we could have expected that the CDW state with period $\lambda = 4$ could have become unstable, since for the even period it is impossible to make a CDW state in the neighbouring ladder equally distant from the CDW state in the ladder under consideration. This is visible in Eq. (2.54) where we have some freedom in choosing the CDW state in the neighbouring ladder so that to satisfy the condition that it is as distant as possible from the CDW state in the ladder under consideration. However, this mechanism did not yield any instability, see Fig. 2.8.

On the other hand, it is visible that it is the ratio of the interladder interaction $V_2$ to the kinetic energy which plays a crucial role in the stability of the CDW state, see discussion in Sec. 2.4.3. Since at the same time in the the constraint of the double occupancies is treated at the mean-field level, it may be that we overestimated the kinetic energy in our calculations. Thus, if we were able to reduce it, then it may be that we would discover the different behaviour of the even-period-CDW state (which is now 'covered' by the overestimated kinetic energy).

*Toy-model for two coupled chains.*— In order to verify the above idea, we introduce the model with merely two coupled chains. As here, we will have no rungs, the mobility of the carriers will be reduced and perhaps we would be able to observe a different behaviour of the CDW state with period $\lambda = 4$.

The toy-model for two coupled chains is defined as follows,

$$H_{1\mathrm{D}} = -t \sum_{i\sigma} \left( \tilde{d}^{\dagger}_{i\sigma} \tilde{d}_{i+1,\sigma} + \mathrm{H.c.} \right) + V_2 \sum_{i} \left( \tilde{n}_{id} \tilde{\tilde{n}}_{i+\frac{1}{2},d} + \tilde{n}_{id} \tilde{\tilde{n}}_{i-\frac{1}{2},d} \right), \qquad (2.68)$$

with all the symbols as in Sec. 2.3 and merely the leg-index $\alpha$ skipped (as we have only two interacting legs). This model can be obtained from the $t$–$J$–$V_1$–$V_2$ model (2.2) by putting $V_1 = 0$ and $J = 0$ as well as by neglecting the existence of one of the legs of the ladder. Note that taking $V_1$ and $J$ finite does not introduce any new physics in our mean-field approach, see Sec. 2.4.3.

*Results.*— We solve the model (2.68) in a similar way as model (2.2): (i) we introduce the slave bosons approach, (ii) assume condensation of bosons, (iii) decouple the interaction between the new fermions $f$ in a mean-field way, and finally (iv) assume the existence of the CDW order parameter $p$ (see Sec. 2.4 for more details). The result is shown in Fig. 2.14.

We see that the results resemble those found earlier for the ladder (see Fig. 2.8) with two exceptions: (i) the CDW with $\lambda = 3$ is stable for much smaller value of the ratio $V_2/t$, and (ii) the CDW with period $\lambda = 5$ does not have a 'cusp'. While the latter is due to a distinct (and simpler) band structure for the chain (cf. discussion about the 'cusp' in Sec. 2.4.3) and is not of big importance here, the first difference is striking and needs some more studies. In particular, this results in a very appealing interpretation of Fig. 2.8: since the CDW order

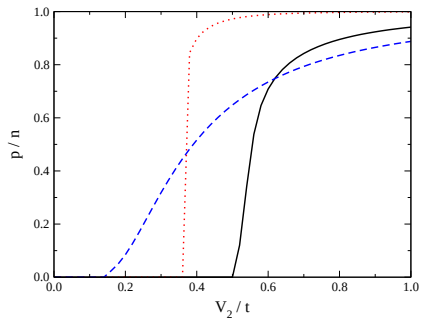


Figure 2.14: The CDW order parameter $p$ as a function of the interladder interaction $V_2$ in the two coupled chains: for filling $n = 2/3$ ($n_h = 4/3$) with period $\lambda = 3$ (dashed line), for filling $n = 3/4$ ($n_h = 5/4$) with period $\lambda = 4$ (solid line), and for filling $n = 4/5$ ($n_h = 6/5$) with period $\lambda = 5$ (dotted line).

with period $\lambda = 3$ is stable for relatively small values of $V_2/t$, it is possible to choose a rather realistic value of $V_2 \sim 0.4t$ [7] that the odd-period-CDW state are already stable while the even-period-CDW state is not yet stable (see Fig. 2.14).

The reason for this distinct behaviour of the CDW state with period $\lambda = 3$ lies in the peculiar band structure for the chains for $n = 2/3$. In fact, this band structure is nested, i.e. the Fermi momentum coincides with the edge of the (folded) Brillouin zone (not shown). Therefore, the system is unstable toward the order already for infinitely small interaction.

*Conclusions.*— Thus, for the toy-model for two coupled chains we indeed obtain that there exists such a realistic value of the interladder interaction parameter $V_2$ where the even-period-CDW state is not stable while the odd-period-CDW states are stable. However, the mechanism for this behaviour lies entirely in the peculiar features of this 1D system (nesting). Therefore, although the phenomenon is interesting itself, it cannot explain the lack of the CDW state with period $\lambda = 4$ in the $Cu_2O_5$ coupled ladders in $Sr_{10}Ca_4Cu_{24}O_{41}$ [8].

[7] Which is only ca. 20% smaller than the $0.5t$ value calculated using Eq. (2.38) and parameters from Ref. [39, 51].

# Chapter 3

# Verifying the idea of orbitally induced hole localization

*This chapter is based on the following publications: (i) K. Wohlfeld, 'Polaron in the t-J models with three-site terms: the SU(2) and the Ising cases', AIP Conference Proceedings* **1014**, *265-269 (2008); and (ii) K. Wohlfeld, M. Daghofer, A. M. Oleś, P. Horsch, 'Spectral properties of orbital polarons in Mott insulators', Physical Review B* **78**, *214423/1-24 (2008).*

## 3.1 Introduction

*Doping Mott insulators with holes.*— The Mott insulators, i.e. such insulators in which electrons localize due to the strong on-site Coulomb repulsion $U$, are best understood in the so-called 'commensurate case' [2, 54]. Then the average number of electrons per site is an integer number and in the low-temperature Mott insulating phase the hopping between the neighbouring sites in the lattice is not allowed as it costs energy $U > W$ (where, as in the previous Chapter, $W = 2zt$ with $t$ being the strength of the largest hopping element while $z$ is the coordination number in the hypercubic lattice). Actually the reason why this state is well understood is the onset of the associated magnetic and/or orbital ordering in such a case: the electrons in the 'commensurate case' can still perform virtual hoppings which lower the total energy of the system and whose magnitude strongly depends on the alignment of the spins of the electrons on the neighbouring sites. Such virtual processes, called superexchange processes, lead to some kind of magnetic ordering and/or orbital ordering.[1] Thus, more precisely, it is the associated magnetic and/or orbital ordering which is well-understood in the 'commensurate case' while the Mott insulating state itself is still far from being understood (despite over 70 years of research [20, 66]).

A somewhat similar situation occurs in the 'non-commensurate' case, i.e. when the number of electrons in the system is not an integer number (see Refs. [20, 28] for a not-up-to-date but nevertheless a thorough review on this extremely broad subject). Since always the limiting cases are the most interesting ones

[1] The detailed form of the magnetic and possibly orbital ordering depends on the details of the band structure.

in physics (as being the easiest to study), one typically looks at the problem when the number of electrons in the Mott insulating systems is very close to the integer number. At this stage one should make a remark on the language: actually when we just take out a fraction of electrons from such a 'commensurate' Mott insulator, then it is easier to talk about introducing *holes* into the Mott system. Anyway, in these hole doped Mott insulators one again faces a similar problem as the one described in the above paragraph. Again, it is difficult to discuss the hole doped Mott insulating state itself. On the other hand, one can relatively easily discuss what happens when the holes are introduced into the associated magnetic and/or orbital ordering.

*Motion of a single hole in Mott insulators.*— The simplest problem which arises when the holes are doped into Mott insulators could be stated as follows: what happens when merely a single hole is introduced into the 'commensurate state' [21, 67]. Would such a hole be confined (localized) or would it rather move coherently through the lattice? As discussed above such a general question would be rather difficult to answer. Instead it would be much easier to verify what happens when a single hole is introduced into the magnetically/orbitally ordered state which could be concomitant with the Mott insulating state itself.

*Inter alia*, one should mention here that there is a very attractive idea that the mere presence of orbital degeneracy in the transition metal oxides leads to the hole confinement in the strongly correlated electron system. As already mentioned in the Preface to the thesis this is backed by the following facts: (i) the manganites show a colossal magnetoresistive effect [12, 13, 14, 15] which can be attributed to the orbital degeneracy [16, 17, 18], and (ii) the transition metal oxides with orbital degeneracy (e.g. manganites or vanadates) have much more stable insulating phases with hole doping [15, 19] than the cuprates without orbital degeneracy [20].

Actually, in two simple magnetically/orbitally ordered states such a problem was already investigated (see below) and (out of the simplest possible orderings) it is only in a peculiar Mott insulator with $t_{2g}$ orbital degrees of freedom that the answer to the problem is not yet settled – it is the purpose of this chapter to investigate this problem. Let us first, however, give a brief overview of these two already investigated cases of the single hole in the magnetically/orbitally ordered states.

*Absence of hole confinement in the AF phase.*— If, in the Mott insulator, the highest occupied orbital in the ions with unfilled electronic shells is not degenerate with any other orbital (which could in principle happen in some particular crystal field, see below) and if the ions themselves form a cubic lattice, then such a Mott insulating state develops an AF order below a critical temperature $T_N$ in the 'commensurate phase' [54]. A typical example is the 2D AF plane formed by $CuO_2$ sheets of atoms in, for example, $La_2CuO_4$ (the parent compound for high-$T_c$ supereconductors) or $Sr_2CuO_2Cl_2$ [68, 69]. When a single hole is inserted into such a state then it forms a defect in the AF background [21]. Naively, i.e., considering the fact that the AF state at temperature $T = 0$ and in 2D has a classical Néel order, one expects that a propagating hole would disturb the AF background and generate a string of broken bonds, with ever increasing energy cost when the hole creates defects moving away from its initial position. This suggests hole confinement as realized already four decades ago [21]. Nevertheless, the quantum nature of this problem leads to a new quality: a hole in the AF Mott insulator can propagate coherently on the superexchange

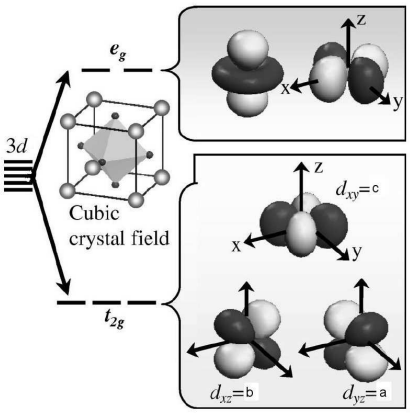


Figure 3.1: The energy splitting of the $3d$ states of the ion placed in the cubic crystal field into: (i) the $t_{2g}$ levels (3 degenerate states: $d_{xy}$, $d_{zx}$ and $d_{yz}$) and (ii) the $e_g$ levels (2 degenerate states: $d_{x^2-y^2}$ and $d_{3z^2-r^2}$). The figure is reproduced after Ref. [71].

scale $J$ which controls AF quantum fluctuations [22, 23, 70], because they heal the defects arising on the hole path. Crucial for this observation is the presence of transverse spin components $\propto (S^+_{\mathbf{i}} S^-_{\mathbf{j}} + S^-_{\mathbf{i}} S^+_{\mathbf{j}})$ in the effective low-energy Heisenberg model derived from the appropriate superexchange interactions.

*Orbital degeneracy.*— Quite often the highest occupied orbital on the ions with unfilled shells in the Mott insulators is energetically degenerate with one or more other orbitals. This gives rise to a rich variety of phenomena [72, 73, 74] which could jointly be termed as 'orbital physics'. For example, if the ions are placed in the cubic crystal field, then for instance the $3d$ levels are split into two distinct degenerate levels: (i) the lower lying $t_{2g}$ levels (3 degenerate states: $d_{xy}$, $d_{zx}$ and $d_{yz}$) and (ii) the $e_g$ levels with higher energy (2 degenerate states: $d_{x^2-y^2}$ and $d_{3z^2-r^2}$); cf. Fig. 3.1. This is due to the high symmetry of the crystal field: obviously in the spherically symmetric field of the nucleus (as is the case of the single hydrogen atom) all $3d$ orbitals are degenerate whereas the less symmetric crystal field could in principle remove the degeneracy of the $t_{2g}$ or $e_g$ levels. In the 'textbook' example of the orbitally degenerate system $LaMnO_3$ the manganese ions have $3d^4$ configuration and, in the ionic picture, the highest occupied level is the degenerate $e_g$ level: in the absence of any other processes (see below) there would be 50% probability to find the electron in the state $d_{x^2-y^2}$ and 50% probability to find the electron in the state $d_{3z^2-r^2}$.

Furthermore, in the orbitally degenerate Mott insulators the superexchange processes are more complicated as they have to involve the orbital and spin degrees of freedom on equal footing [72, 73]. This could lead to the onset of *both* the magnetic and orbital order in the system. The particular kind of this order depends on the symmetries of the orbitally degenerate orbitals. This in turns means that the behaviour of the single hole doped into the Mott insulator with orbital degrees of freedom would depend on the kind of the orbital degeneracy present in the system [75].

*Absence of hole confinement in systems with $e_g$ AO order.*— As already

mentioned above one of the most prominent examples of the orbitally degenerate systems is $LaMnO_3$. There, in this 'commensurate case', the superexchange processes lead to the development of the AO order concomitant with the FM spin alignment in the $ab$ plane and the FO order with spin AF order along the $c$ direction [76].[2] Similarly as in the purely spin case (hole in the AF state, see above), one could think that the doped hole would be confined in the plane of such an ordered state. This time the reason is that the superexchange processes which lead to the AO order are much more classical and the AO order is much more robust than in the spin AF case [29]. However, also here the hole finds a way to propagate: the coherent propagation arises not only due to the very small but still finite quantum fluctuations present in the system but predominantly due to the possibility of the $e_g$ interorbital hopping which allows for the hole motion without disturbing the AO background (which in the spin language would correspond to the spin-flip hopping) [77].

*Main goals of the chapter.*— As the $t_{2g}$ orbitals have naturally distinct symmetries than the $e_g$ orbitals one expects a different behaviour when the hole is doped to the system with $t_{2g}$ orbital degrees of freedom. A natural question arises then: would the hole be confined in such a Mott insulator? This question is of high theoretical importance since the hole confinement in such a system would mean that it is possible to have orbitally induced hole localization in Mott insulators. Of course the reverse is not true: negative answer to the above question would not mean that the hole confinement in the orbital systems were impossible. One could imagine that there exist other mechanisms which localize the hole in the orbital systems – for example due to the interactions induced by the lattice. However, the simplest possible mechanism, as the one discussed in this chapter, would be outruled.

Therefore, the main goals of the chapter are: (i) to establish what the minimal $t$–$J$ model, which contains the $t_{2g}$ orbital degrees of freedom and bears its truly distinctive features, looks like, (ii) what is the undoped ground state of this model (e.g. whether the quantum fluctuations exist in the ground state), and (iii) whether the doped hole can move coherently in such an undoped ground state.

*Structure of the chapter.*— The chapter is organized as follows. In Sec. 3.2 we start the analysis by looking at the anticipated features of the new $t$-$J$ model which is derived in Sec. 3.3. Next, the model in the case of the one hole added to the undoped ground state is solved: (i) we reduce the model to the polaron-type Hamiltonian using the slave fermion approach in Sec. 3.4.1, (ii) we derive the equations for the Green's functions using the SCBA method in Sec. 3.4.2, (iii) we solve the equations obtained in point (ii) numerically on a finite mesh of the momentum $\mathbf{k}$ points (Sec. 3.4.3). Then, in Sec. 3.5 the results are discussed: (i) its validity, see Sec. 3.5.1, (ii) the explanation why the dispersion relation of the doped holes is strictly 1D, see Sec. 3.5.2 (see also Appendix A), and (iii) we analyse how the three-site terms lead to the renormalized dispersion of the dressed hole in Sec. 3.5.3. Finally, the conclusions are written in Sec. 3.6 while in the *Postscriptum* in Sec. 3.7 the experimental consequences of the obtained results are studied (see also Appendix B).

[2] While the Jahn-Teller effect only further stabilizes such an order.

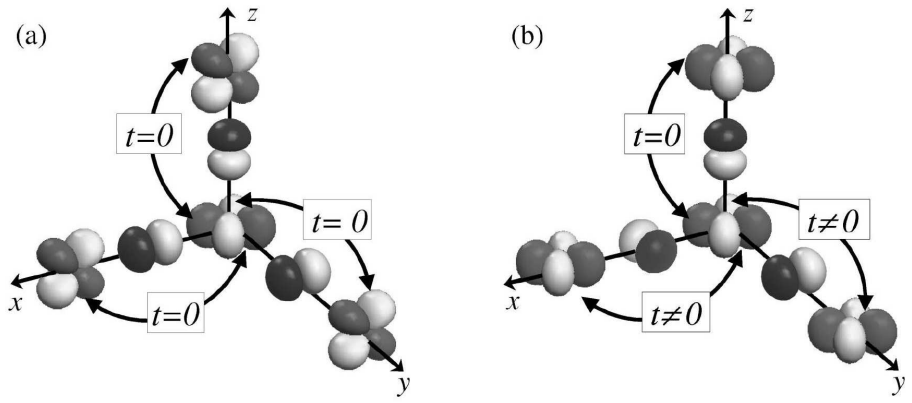


Figure 3.2: The possible hopping elements between the $t_{2g}$ orbitals when the oxygen $p$ orbitals are placed between them: (a) the hopping between different $t_{2g}$ orbitals is zero, (b) the hopping between the same $t_{2g}$ orbital is possible only in the particular plane (the choice of the plane depends on the orbital under considerations: e.g. for the $d_{xy}$ orbital is is the $ab$ plane). Both panels are reproduced after Ref. [71].

## 3.2 The $t_{2g}$ orbital $t$–$J$ model *with* three-site terms

*'Rough' predictions of the new $t$–$J$ model.*— Let us look at the anticipated features of the new $t$–$J$ model. Actually, the choice of the new $t$–$J$ model was somewhat left arbitrary: we have merely noted in the introduction that we intend to study the features of such an orbital $t$–$J$ model that the symmetries of the $t_{2g}$ orbitals would be demonstrated 'at most'. Actually, this not a very transparent condition and thus let us firstly describe what we mean by these distinctive features. In Fig. 3.2 we show the possible hopping elements between various $t_{2g}$ orbitals. Whereas Fig. 3.2(a) merely shows that the interorbital hopping is prohibited the most striking feature is shown in Fig. 3.2(b): the electrons in $d_{xy} \equiv c$ orbital can hop in the $ab$ plane whereas they cannot hop along the $c$ direction. A similar phenomenon occurs for $d_{zx} \equiv b$ (hopping only in the $ac$ plane) and $d_{yz} \equiv a$ (hopping only in the $bc$ plane) orbitals. This means that choosing that the $c$ orbital has higher energy (which could happen in realistic systems, cf. $Sr_2VO_4$) and looking at the plane with electrons only in the $a$ and $b$ orbitals one can get rid of all the quantum fluctuations in the superexchange processes: this is because then the exchange process is impossible as the same electron which performs a virtual hop to the neighbouring site has then to return to the original site. Thus, without any calculations, one can immediately see that the ground state at half-filling of the appropriate $t$–$J$ model for spinless electrons would be the Néel AO state (i.e. an ordered state with two sublattices: one with electrons localized in $a$ orbitals and the other one with electrons in $b$ orbitals) and is an exact ground state, i.e. it does not contain any quantum fluctuations.

What happens when one adds a single hole to such a state? This has already been partially discussed in the Introduction but is also shown schematically in Fig. 3.3. It presents in a schematic way a few first steps in the motion of a

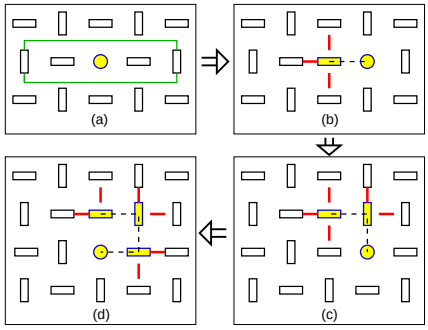


Figure 3.3: Schematic view of the anticipated hole motion in the $t_{2g}$ orbital $t$–$J$ model with AO order formed by $a$ and $b$ orbitals. Circles depict holes while horizontal (vertical) rectangles depict occupied $b$ ($a$) orbitals with electrons that can move only horizontally (vertically), respectively. The hole inserted in the AO state (a) can move via nearest neighbour hopping $t$, and interchanges its position with an electron, so that it has to turn by 90° in each step along its path and leaves behind broken bonds leading to string excitations with ever increasing energy (b) and (c). After moving by 270° around a plaquette (d), the hole cannot return to its initial position as would be necessary to complete the Trugman path [78].

hole inserted at a selected site into such a Néel ordered ground state with no quantum fluctuations. When the hole moves via the nearest neighbour hopping $t$, it creates string excitations in each step that cannot be healed by orbital flips because the orbital superexchange is purely Ising-like. Moreover, it can even not heal the defects by itself because it cannot complete a Trugman loop [78] when the orbital defects are created and three occupied orbitals are moved anticlockwise on a plaquette after the hole moved clockwise by three steps, see Fig. 3.3(d). Thus, the hole is confined in the $t_{2g}$ orbital $t$–$J$ model.

*Reasons for wrong predictions.— A priori* there should be no reason why not to believe in the conjecture written above: provided, the detailed mathematical calculations confirm the above analysis one could indeed make a claim that 'the hole is confined in the $t_{2g}$ AO ordered state'. However, in the last section we discussed in detail how a hole could move in the spin AF state or in the $e_g$ AO state. In both cases the hole at first could be thought to be immobile and only the detailed study and inclusion of some neglected processes (such as quantum fluctuations or interorbital hopping) leads to the conclusion that the coherent hole motion is possible. This 'historical perspective' suggests that also this time one has to be very careful while neglecting any processes which could be essential in the Hamiltonian to faithfully describe the properties of the system.

There is yet, another, more physical, reason. In Ref. [23] it is shown that when one studies the motion of a hole in the model without quantum spin fluctuations, then some approximations which are valid in the $SU(2)$ symmetric case no longer apply. More precisely, in the Ising case the violation of the so-called $C1$ constraint (see Ref. [23]), stating that no hole and magnon can be present at the same site in the effective polaron-model, leads to serious underestimation of the incoherent bandwidth while the same violation of this constraint in the

$SU(2)$ symmetric case does not cause any problem. Thus in the case when the $SU(2)$ symmetry is absent in the model one has to be more careful with all the approximations made.

*More careful approach needed.*— There exists one serious approximation which is already a generic feature of the standard $t$–$J$ model: the so-called three-site terms are neglected there, see Chapter 1. These terms are present in any meaningfull canonical perturbation theory derivation of the $t$–$J$ from the Hubbard model [1, 2]. Actually, 'why the full strong-coupling model [i.e. $t$–$J$ model with three-site terms – note added by K. W.] has received far less attention than the $t$–$J$ model is unclear' as Eskes and Eder write in Ref. [79]. Most probably the reason can be that the three-site terms give a much smaller contribution to the total energy than the superexchange term or the constrained hopping term: the latter two scale as $\propto J(1-\delta)^2$ or $\propto t\delta$ (where $\delta \ll 1$ is the number of doped holes) while the three-site terms are $\propto J\delta$. Indeed, including the three-site terms in the standard $t$–$J$ model does not yield any new qualitative results concerning the hole motion in the AF state [80]. Here, however, in what follows it will be shown that these terms are indeed needed to give a physically relevant answer to the problem of orbitally induced hole confinement. Thus, let us now present the derivation of the physically relevant $t_{2g}$ orbital $t$–$J$ model with three-site terms.

## 3.3 The model

### 3.3.1 The $t_{2g}$ orbital $t$–$J$ Hamiltonian

*Hubbard-like model.*— As the starting point we consider the Hubbard-like model describing electrons in transition metal oxides with active $t_{2g}$ orbitals when the crystal field splits them into $e_g$ and $a_1$ states, and the doublet $e_g$ is filled by one electron per site. This occurs for the $d^1$ configuration (e.g. in the titanates) when the $e_g$ doublet has lower energy than the $a_1$ state, or for $d^2$ configuration when the $e_g$ states have higher energy and are considered here, while the $a_1$ state is occupied by one electron at each site and thus inactive (as in the high-spin ground state of the $R\mathrm{VO}_3$ perovskites [81] where $R$ stands for a rare earth element). More precisely, we consider electrons with two $t_{2g}$ orbital flavours, $a$ and $b$, moving within the $ab$ plane. The electrons in such orbitals can propagate conserving the orbital flavour by the nearest neighbour hopping $t$, but only along one direction in the $ab$ plane, see also Fig. 3.2. Furthermore, we assume that the system has an FM order which means that all the spins are the same and for the purpose of the studies presented below one can safely skip the spin index, see also [82]. This results in the following orbital Hubbard model

$$\mathcal{H} = -t \sum_{\mathbf{i}} \left( b^\dagger_{\mathbf{i}} b_{\mathbf{i}+\hat{\mathbf{a}}} + a^\dagger_{\mathbf{i}} a_{\mathbf{i}+\hat{\mathbf{b}}} + \mathrm{H.c.} \right) + U \sum_{\mathbf{i}} n_{\mathbf{i}a} n_{\mathbf{i}b}, \tag{3.1}$$

where $a^\dagger_{\mathbf{i}}(b^\dagger_{\mathbf{i}})$ creates a spinless electron with orbital flavour $a(b)$ at site $\mathbf{i}$, $\{n_{\mathbf{i}a}, n_{\mathbf{i}b}\}$ are electron density operators, and $t$ is the hopping element along $b$ or $a$ axis. Similarly as in the Introduction $U$ stands for the on-site interaction energy for a doubly occupied configuration. At the filling of one electron in $\{a, b\}$ orbitals per site this interaction corresponds to the high-spin $d^2$ (or $d^3$) state (i.e. it corresponds to $U - 3J_H$ in terms of element of the Coulomb interaction between $3d$

electrons, where $U$ is the intraorbital on-site interaction between two electrons and $J_H$ is the on-site exchange element which causes the Hund's rule energy gain due to the FM alignment of two spins on the same site). As discussed in detail in Sec. 3.2 such a choice of active $t_{2g}$ orbitals guarantees that the $t$–$J$ model would bear all of the desired and distinctive features of the $t$–$J$ model for correlated electrons in $t_{2g}$ orbitals.

*Canonical perturbation expansion.*— The task is now to apply to Eq. (3.1) the canonical perturbation expansion similarly as the one introduced in Chapter 1 for the spin Hubbard model. Actually these calculations are done in the same way as in that chapter and the only difference now is that the parts of the Hamiltonian which describe processes within/between the Hubbard subbands are defined differently. Namely

$$\mathcal{H} = \mathcal{H}_0 + \mathcal{H}_1, \tag{3.2}$$

where $\mathcal{H}_0$ describes the physics within the Hubbard subband:

$$\begin{aligned}
\mathcal{H}_0 =& \mathcal{V} + \mathcal{T}_0, \\
\mathcal{V} =& U \sum_{\mathbf{i}} n_{\mathbf{i}a} n_{\mathbf{i}b}, \\
\mathcal{T}_0 =& -t \sum_{\mathbf{i}} \Big\{ (1 - n_{\mathbf{i}a}) b^\dagger_{\mathbf{i}} b_{\mathbf{i}+\hat{\mathbf{a}}} (1 - n_{\mathbf{i}+\hat{\mathbf{a}},a}) + (1 - n_{\mathbf{i}b}) a^\dagger_{\mathbf{i}} a_{\mathbf{i}+\hat{\mathbf{b}}} (1 - n_{\mathbf{i}+\hat{\mathbf{b}},b}) \\
& + n_{\mathbf{i}a} b^\dagger_{\mathbf{i}} b_{\mathbf{i}+\hat{\mathbf{a}}} n_{\mathbf{i}+\hat{\mathbf{a}},a} + n_{\mathbf{i}b} a^\dagger_{\mathbf{i}} a_{\mathbf{i}+\hat{\mathbf{b}}} n_{\mathbf{i}+\hat{\mathbf{b}},b} + \text{H.c.} \Big\},
\end{aligned} \tag{3.3}$$

while $\mathcal{H}_1$ is responsible for hopping processes between different Hubbard subbands:

$$\begin{aligned}
\mathcal{H}_1 =& \mathcal{T}_+ + \mathcal{T}_-, \\
\mathcal{T}_+ =& -t \sum_{\mathbf{i}} \Big\{ n_{\mathbf{i}a} b^\dagger_{\mathbf{i}} b_{\mathbf{i}+\hat{\mathbf{a}}} (1 - n_{\mathbf{i}+\hat{\mathbf{a}},a}) + n_{\mathbf{i}b} a^\dagger_{\mathbf{i}} a_{\mathbf{i}+\hat{\mathbf{b}}} (1 - n_{\mathbf{i}+\hat{\mathbf{b}},b}) + \text{H.c.} \Big\}, \\
\mathcal{T}_- =& -t \sum_{\mathbf{i}} \Big\{ (1 - n_{\mathbf{i}a}) b^\dagger_{\mathbf{i}} b_{\mathbf{i}+\hat{\mathbf{a}}} n_{\mathbf{i}+\hat{\mathbf{a}},a} + (1 - n_{\mathbf{i}b}) a^\dagger_{\mathbf{i}} a_{\mathbf{i}+\hat{\mathbf{b}}} n_{\mathbf{i}+\hat{\mathbf{b}},b} + \text{H.c.} \Big\}.
\end{aligned} \tag{3.4}$$

*Central Hamiltonian of the chapter.*— Then following the same steps as in Chapter 1 we obtain the appropriate $t_{2g}$ orbital $t$–$J$ model:[3]

$$H = H_t + H_J + H_{3\text{s}}, \tag{3.5}$$

where the $H_t$ is the kinetic energy in the constrained Hilbert space with no double occupancies (see Sec. 3.3.2), $H_J$ describes the superexchange terms (see Sec. 3.3.3), and finally $H_{3\text{s}}$ are the three-site terms which were neglected in the final $t$–$J$ Hamiltonian in Chapter 1 (see Sec. 3.3.4).

### 3.3.2 The kinetic energy term

*Explicit form.*— Using Eq. (3.3) and the canonical perturbation expansion of

[3] In the literature the $t$–$J$ model *with* three-site terms is also called the strong-coupling model [80]. However, to avoid confusion we will not use this name since throughout this thesis we deal with several different extensions of the standard $t$–$J$ model and the strong-coupling model is just another variation of such extended version of the $t$–$J$ model.

Chapter 1 one obtains the kinetic energy term,

$$H_t = -t \sum_{\mathbf{i}} \left( \tilde{b}^{\dagger}_{\mathbf{i}} \tilde{b}_{\mathbf{i}+\hat{\mathbf{a}}} + \tilde{a}^{\dagger}_{\mathbf{i}} \tilde{a}_{\mathbf{i}+\hat{\mathbf{b}}} + \text{H.c.} \right), \tag{3.6}$$

where the use of the operators

$$\tilde{b}^{\dagger}_{\mathbf{i}} = b^{\dagger}_{\mathbf{i}}(1 - n_{\mathbf{i}a}), \tag{3.7}$$

and

$$\tilde{a}^{\dagger}_{\mathbf{i}} = a^{\dagger}_{\mathbf{i}}(1 - n_{\mathbf{i}b}), \tag{3.8}$$

mean that the hopping is allowed only in the constrained Hilbert space with no doubly occupied sites.

### 3.3.3 The Ising superexchange term

*Explicit form.*— Following the same steps as in Chapter 1 and using Eq. (3.4) we obtain that the superexchange processes for the Hubbard model under consideration take the form

$$H_J = \frac{1}{2} J \sum_{\langle \mathbf{ij} \rangle} \left( T^z_{\mathbf{i}} T^z_{\mathbf{j}} - \frac{1}{4} \tilde{n}_{\mathbf{i}} \tilde{n}_{\mathbf{j}} \right), \tag{3.9}$$

where the summation goes over the pairs formed by the nearest neighbour sites $\mathbf{i}$ and $\mathbf{j}$. The parameter $J$ is defined as

$$J = \frac{4t^2}{U}, \tag{3.10}$$

while the pseudospin operators $T^z_{\mathbf{i}}$ is

$$T^z_{\mathbf{i}} = \frac{1}{2}(\tilde{n}_{\mathbf{i}a} - \tilde{n}_{\mathbf{i}b}). \tag{3.11}$$

Here $\tilde{n}_{\mathbf{i}} = \tilde{n}_{\mathbf{i}a} + \tilde{n}_{\mathbf{i}b}$ and the superexchange vanishes when two electrons with the same orbital flavour occupy sites $\mathbf{i}$ and $\mathbf{j}$.

*The Ising character.*— Note the total absence of the pseudospin-flip terms $\propto (T^+_{\mathbf{i}} T^-_{\mathbf{j}} + T^-_{\mathbf{i}} T^+_{\mathbf{j}})$ in the superexchange interactions which are now purely Ising type. This is because along each particular direction only one orbital flavour can hop: the virtual exchange process $\propto \mathcal{T}_- \mathcal{T}_+$ in which an electron with for example $a$ orbital flavour makes a virtual excursion to the neighbouring site (which costs energy $U$) and then an electron with $b$ orbital flavour returns is impossible [see the form of Eq. (3.4)]. Since only such virtual processes contribute to the pseudospin-flip terms, the latter terms are absent. The same phenomenon explains also the prefactor $\frac{1}{2}$ in Eq. (3.9). Nevertheless, the strictly 1D kinetic energy of the electrons in the two orbitals leads to the 2D superexchange.

Let us also note, that the pseudospin-flip processes $\propto (T^+_{\mathbf{i}} T^-_{\mathbf{j}} + T^-_{\mathbf{i}} T^+_{\mathbf{j}})$ would be present in the (not considered here) model for strongly correlated $a$ and $b$ electrons along the $c$ axis. In fact, this is the case in a somewhat more complicated spin-orbital model for cubic vanadates [83] where such pseudospin fluctuations are responsible for the onset of the AF order in the $ab$ plane and the FM order along the $c$ axis in $LaVO_3$ (see Ref. [83] and discussion in Chapter 4).

### 3.3.4 The three-site terms

*Origin of the three-site terms.*— As discussed in Chapter 1 when one derives the $t$–$J$ model from the Hubbard model one obtains also the so-called three-site terms which also originate from the $\propto \mathcal{T}_-\mathcal{T}_+$ virtual processes. These terms are often neglected [e.g. in the standard $t$–$J$ model, see Eq. (1.22)] but here they will turn out to be important and lead to qualitative changes, see discussion in Sec. 3.2.

*Explicit form.*— We cast the three-site terms into two different classes:

$$H_{3\mathrm{s}} = H_{3\mathrm{s}(l)} + H_{3\mathrm{s}(d)}, \tag{3.12}$$

where $H_{3\mathrm{s}(l)}$ are the three-site terms along the line and $H_{3\mathrm{s}(d)}$ are along the diagonal. It is relatively straightforward [using Eq. (3.4) and Eq. (1.18) from Chapter 1] to obtain their explicit form:

$$H_{3\mathrm{s}(l)} = -\tau \sum_{\mathbf{i}} (\tilde{b}^\dagger_{\mathbf{i}-\hat{\mathbf{a}}} \tilde{n}_{\mathbf{i}a} \tilde{b}_{\mathbf{i}+\hat{\mathbf{a}}} + \mathrm{H.c.}) - \tau \sum_{\mathbf{i}} (\tilde{a}^\dagger_{\mathbf{i}-\hat{\mathbf{b}}} \tilde{n}_{\mathbf{i}b} \tilde{a}_{\mathbf{i}+\hat{\mathbf{b}}} + \mathrm{H.c.}), \tag{3.13}$$

$$H_{3\mathrm{s}(d)} = -\tau \sum_{\mathbf{i}} (\tilde{a}^\dagger_{\mathbf{i}\pm\hat{\mathbf{b}}} \tilde{a}_{\mathbf{i}} \tilde{b}^\dagger_{\mathbf{i}} \tilde{b}_{\mathbf{i}\pm\hat{\mathbf{a}}} + \mathrm{H.c.}) - \tau \sum_{\mathbf{i}} (\tilde{a}^\dagger_{\mathbf{i}\mp\hat{\mathbf{b}}} \tilde{a}_{\mathbf{i}} \tilde{b}^\dagger_{\mathbf{i}} \tilde{b}_{\mathbf{i}\pm\hat{\mathbf{a}}} + \mathrm{H.c.}), \tag{3.14}$$

where

$$\tau = \frac{t^2}{U}. \tag{3.15}$$

Note that in principle we could have used $J$ as the energy scale of the three-site terms but for didactic reasons we define a different constant which will be connected solely with the three-site terms. In what follows this will enable us to distinguish between the processes related to the superexchange terms and to the three-site terms.

## 3.4 Method and results

### 3.4.1 The slave-fermion approach

*Slave-fermion approach.*— It is widely recognized that the central difficulty in solving any $t$–$J$ model is the problem of fulfilling the constraint of no double occupancies at each site. There are several methods suggested to overcome this difficulty in an approximate way. One of them is called the slave-boson method and is typically used for systems which are relatively highly doped [20], cf. Chapter 2. On the other hand, for the very lightly doped system the method of choice is the slave-fermion approach as it is quite good in describing the half-filled ground state and its excitations (where it merely amounts to the introduction of Schwinger bosons for spins and/or pseudospins [20]). As in the present chapter we are interested in the properties of the system in the extremely low doped regime we introduce the latter method in what follows and transform the Hamiltonian $H$ into the effective Hamiltonian $H^{eff}$.

*Undoped case: low energy excitations.*— It is easy to verify that the classical undoped ground state of the Hamiltonian Eq. (3.5) is the Néel ordered AO state:

$$|\Phi_0\rangle = \prod_{\mathbf{i}\in A} a^\dagger_{\mathbf{i}} \prod_{\mathbf{j}\in B} b^\dagger_{\mathbf{j}} |0\rangle, \tag{3.16}$$

with $a$ orbitals occupied on the sublattice $A$ and $b$ orbitals occupied on the sublattice $B$ is an exact ground state. Here $|0\rangle$ is the true vacuum state with no electrons, while $|\Phi_0\rangle$ is the physical vacuum at half filling. Next, let us consider the low energy states. Below, we will calculate the orbital excitations (orbitons – see Ref. [84]) at half filling by transforming the pseudospins into the Schwinger bosons and then using the linear orbital wave (LOW) approximation.

First, in the classical state we introduce two sublattices $A$ and $B$ such that all $a$ ($b$) orbitals are occupied in the perfect AO state in sublattice $A$ ($B$). Next we rotate pseudospins on sublattice $A$ so that the symmetry of the lattice is recovered, all the pseudospins in the whole lattice take positive values now, $\langle T^z_{\mathbf{i}}\rangle = 1/2$, and the Hamiltonian changes appropriately.

Second, we introduce Schwinger bosons $t$ such that:

$$T^z_{\mathbf{i}} = \frac{1}{2}(n_{\mathbf{i}tb} - n_{t\mathbf{i}ta}) \tag{3.17}$$

with the local constraint at each site $\mathbf{i}$

$$\sum_{\gamma=a,b} t^\dagger_{\mathbf{i}\gamma} t_{\mathbf{i}\gamma} = 1. \tag{3.18}$$

Third, we transform the Schwinger boson operators into the Holstein-Primakoff bosons $\beta$:[4]

$$t^\dagger_{\mathbf{i}b} = \sqrt{1 - t^\dagger_{\mathbf{i}a} t_{\mathbf{i}a}} \equiv \sqrt{1 - \beta^\dagger_{\mathbf{i}}\beta_{\mathbf{i}}}, \tag{3.19}$$

$$t^\dagger_{\mathbf{i}a} = \beta^\dagger_{\mathbf{i}}, \tag{3.20}$$

where the above constraint is now no longer needed.

Next, we substitute the above transformations into the Hamiltonian $H_J$ and skip higher order terms (LOW approximation). The latter approximation physically means that the number of bosons $\beta$ is small (which is naturally the case for low energy states). This results in the effective substitution

$$T^z_{\mathbf{i}} = \frac{1}{2} - \beta^\dagger_{\mathbf{i}}\beta_{\mathbf{i}}. \tag{3.21}$$

Finally, we introduce Fourier transformation separately for each sublattice ($N$ is the total number of sites on both sublattices while $N/2$ is the number of sites in each sublattice):

$$\beta_{\mathbf{k}A} = \sqrt{\frac{2}{N}} \sum_{\mathbf{j}\in A} e^{i\mathbf{k}\mathbf{j}} \beta_{\mathbf{j}}, \tag{3.22}$$

$$\beta_{\mathbf{k}B} = \sqrt{\frac{2}{N}} \sum_{\mathbf{j}\in B} e^{i\mathbf{k}\mathbf{j}} \beta_{\mathbf{j}}. \tag{3.23}$$

Then, after neglecting constant terms which merely give the classical energy of the undoped ground state, the LOW Hamiltonian for orbitons reads:

$$H^{eff}_J = J \sum_{\mathbf{k}} (\beta^\dagger_{\mathbf{k}A}\beta_{\mathbf{k}A} + \beta^\dagger_{\mathbf{k}B}\beta_{\mathbf{k}B}), \tag{3.24}$$

[4] We denote the orbital excitations with $\beta$ since it is very common in the literature [23] to use $\alpha$ for spin excitations.

where the orbiton energy does not depend on momentum $\mathbf{k}$. The fact that the excited states have higher energy than the ground state proves the stability ground state. In fact, the dispersionless excitations do not generate any quantum corrections and the classical ground state is exact.

*Doped hole: coupling with orbitons.*— We expect that a doped hole does not modify significantly the classical ground state stable for the half-filled case (see above). The situation could be different in the lightly doped regime but in the case of one hole in the whole plane such a modification is negligible and will be neglected below. Instead, the doped hole may modify its neighbourhood by its coupling to the excitations of the classical ground state — orbitons — which renormalize the hole motion. In order to describe it mathematically, we rewrite $H_t$ (see next paragraph) and $H_{3\mathrm{s}}$ (see below) using similar transformations as performed for the half-filled case.

First, we rotate spins and pseudospins on sublattice $A$. Next, using the slave-fermion approach we express the electron operators in terms of the Schwinger bosons introduced above and in terms of the (constrained) fermionic operators representing holes:

$$\tilde{a}^{\dagger}_{\mathbf{i}} = t^{\dagger}_{\mathbf{i}a} h_{\mathbf{i}}, \tag{3.25}$$

$$\tilde{b}^{\dagger}_{\mathbf{i}} = t^{\dagger}_{\mathbf{i}b} h_{\mathbf{i}}. \tag{3.26}$$

Here the constraint on the bosonic operators is as in Eq. (3.18) while $h^{\dagger}_{\mathbf{i}} h_{\mathbf{i}}$ denotes the number of holes at site $\mathbf{i}$.

Next, similarly as above, we transform the Schwinger bosons into the Holstein-Primakoff bosons, skip all terms containing more than two bosons, and perform Fourier transformation for bosons and (additionally) for holons to arrive at the Hamiltonian:

$$H_t^{eff} = \frac{zt}{\sqrt{N}} \sum_{\mathbf{k},\mathbf{q_1}} \left\{ M_x(\mathbf{k},\mathbf{q_1}) h^{\dagger}_{\mathbf{k}A} h_{\mathbf{k}-\mathbf{q_1},B} \beta_{\mathbf{q}_1 A} + M_y(\mathbf{k},\mathbf{q_1}) h^{\dagger}_{\mathbf{k}B} h_{\mathbf{k}-\mathbf{q_1},A} \beta_{\mathbf{q}_1 B} + \mathrm{H.c.} \right\}, \tag{3.27}$$

where $z = 4$ is the coordination number for the 2D square lattice and

$$M_{\mu}(\mathbf{k},\mathbf{q_1}) = \frac{1}{2} \cos(k_{\mu} - q_{1\mu}) \tag{3.28}$$

is the vertex function with $\mu = x, y$. Thus, the hopping term $H_t$, Eq. (3.6), transforms into a scattering of holons on orbitons (orbital excitations), with the momentum conserved in each scattering process.

*Doped hole: free dispersion.*— After performing similar transformations as the ones introduced for the $t$ part of the Hamiltonian one obtains that the *linear* three-site terms, Eq. (4.13), lead to the following Hamiltonian for the holes

$$H_{3\mathrm{s}}^{eff} = \tau \sum_{\mathbf{k}} \left\{ \varepsilon_B(\mathbf{k}) h^{\dagger}_{\mathbf{k}B} h_{\mathbf{k}B} + \varepsilon_A(\mathbf{k}) h^{\dagger}_{\mathbf{k}A} h_{\mathbf{k}A} \right\}, \tag{3.29}$$

where the free dispersion relations are

$$\varepsilon_A(\mathbf{k}) = 2\cos(2k_y), \tag{3.30}$$

and

$$\varepsilon_B(\mathbf{k}) = 2\cos(2k_x). \tag{3.31}$$

Note that we entirely neglect the *diagonal* three-site terms which lead to the coupling between holes and orbitons. This approximation will be discussed further in the next sections.

Thus, in the lightly doped case, when the classical orbital ordered ground state present in the half-filled case survives, the $t$–$J$ model (3.5) can be reduced to an effective model:

$$H^{eff} = H_t^{eff} + H_J^{eff} + H_{3\mathrm{s}}^{eff}, \tag{3.32}$$

see Eqs. (3.24), and (3.27)-(3.29). Actually, this is a polaron-type model with the coupling between fermions (holes) and bosonic excitations (orbitons) which is rather straightforward to solve, cf. next Section. Besides, the validity of the mapping between the two models will be discussed in Sec. 3.5.1.

### 3.4.2 The self-consistent Born approximation

*Green's functions.*— The spectral properties of the hole doped into the AO ground state $|\Phi_0\rangle$ with energy $E_0$ [see Eq. (3.16)] of the $t$–$J$ model Eq. (3.5) at half-filling, treated here as a physical vacuum, follow from the Green's functions:

$$G_a(\mathbf{k},\omega) = \left\langle \Phi_0 \left| a_{\mathbf{k}}^\dagger \frac{1}{\omega + H - E_0} a_{\mathbf{k}} \right| \Phi_0 \right\rangle , \tag{3.33}$$

$$G_b(\mathbf{k},\omega) = \left\langle \Phi_0 \left| b_{\mathbf{k}}^\dagger \frac{1}{\omega + H - E_0} b_{\mathbf{k}} \right| \Phi_0 \right\rangle . \tag{3.34}$$

However, due to the mapping of the $t$–$J$ model onto polaron model (3.32) performed in the last section, it is now convenient to express the above Green's functions in terms of the polaron Hamiltonian $H^{eff}$. This requires that one first writes down the electron operators in terms of the operators used in Eq. (3.32):

$$a_{\mathbf{k}} = \frac{1}{\sqrt{N}} \left( \sum_{\mathbf{j}\in A} e^{i\mathbf{k}\mathbf{j}} h_{\mathbf{j}}^\dagger + \sum_{\mathbf{j}\in B} e^{i\mathbf{k}\mathbf{j}} h_{\mathbf{j}}^\dagger \beta_{\mathbf{j}} \right) , \tag{3.35}$$

$$b_{\mathbf{k}} = \frac{1}{\sqrt{N}} \left( \sum_{j\in A} e^{i\mathbf{k}\mathbf{j}} h_{\mathbf{j}}^\dagger \beta_{\mathbf{j}} + \sum_{\mathbf{j}\in B} e^{i\mathbf{k}\mathbf{j}} h_{\mathbf{j}}^\dagger \right) . \tag{3.36}$$

Second, the ground state $|\Phi_0\rangle$ is now a physical vacuum $|0\rangle$ with respect to the orbiton operators $\beta_{\mathbf{k}}$ with energy $E$ calculated in the LOW approximation. Then, one arrives at the following relations:

$$G_a(\mathbf{k},\omega) = \frac{1}{2} \left\langle 0 \left| h_{\mathbf{k}A} \frac{1}{\omega + H^{eff} - E} h_{\mathbf{k}A}^\dagger \right| 0 \right\rangle \equiv \frac{1}{2}\, G_{AA}(\mathbf{k},\omega), \tag{3.37}$$

$$G_b(\mathbf{k},\omega) = \frac{1}{2} \left\langle 0 \left| h_{\mathbf{k}B} \frac{1}{\omega + H^{eff} - E} h_{\mathbf{k}B}^\dagger \right| 0 \right\rangle \equiv \frac{1}{2}\, G_{BB}(\mathbf{k},\omega), \tag{3.38}$$

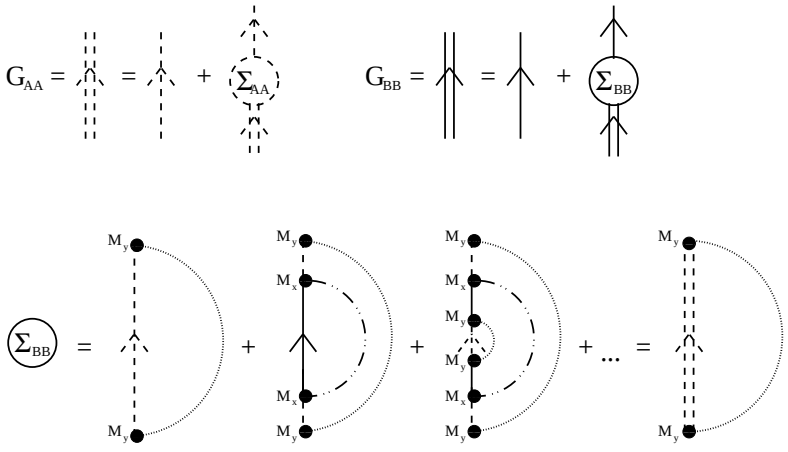


Figure 3.4: Diagrammatic representation of the perturbative procedure used within the SCBA: top — the Dyson's equation for the $G_{BB}(\mathbf{k},\omega)$ and $G_{AA}(\mathbf{k},\omega)$ Green's functions; bottom — the summation of diagrams for the self-energy $\Sigma_{BB}(\mathbf{k},\omega)$. Dashed (dashed-dotted) lines stand for Green's functions for orbitons on sublattice $B$ ($A$). Equation for $\Sigma_{AA}(\mathbf{k},\omega)$ is similar (not shown).

where the above set of equations follows from the fact that $\beta_{\mathbf{k}}|0\rangle = 0$ and the factor $1/2$ is due to the operators $h_{\mathbf{k}A}$ ($h_{\mathbf{k}B}$) being defined separately for each sublattice. Note that here the ground state energy $E$ is taken as a reference in order to be able to compare results of the present approach with those obtained using the variational cluster approach (VCA) for the Hubbard model, see Sec. 3.5.1.

*Equations for the self-energy.*— We calculate the above Green's functions by summing over all possible non-crossing diagrams (i.e. neglecting closed loops), cf. lower part of Fig. 3.4. However, the crossing diagrams do not contribute here since the closed loops (Trugman processes) do not occur, see Fig. 3.3. Since the structure of the present problem makes it necessary that two Green's functions and two self-energies are considered, we obtain the following SCBA equations for the self-energies (see also Fig. 3.4):

$$\Sigma_{AA}(\mathbf{k},\omega) = \frac{z^2t^2}{N}\sum_{\mathbf{q}} M_x^2(\mathbf{k},\mathbf{q})G_{BB}(\mathbf{k}-\mathbf{q},\omega+J), \tag{3.39}$$

$$\Sigma_{BB}(\mathbf{k},\omega) = \frac{z^2t^2}{N}\sum_{\mathbf{q}} M_y^2(\mathbf{k},\mathbf{q})G_{AA}(\mathbf{k}-\mathbf{q},\omega+J). \tag{3.40}$$

The above equations should always be supplemented by the Dyson's equations:

$$G_{AA}(\mathbf{k},\omega) = \frac{1}{\omega + J + \tau\varepsilon_A(\mathbf{k}) - \Sigma_{AA}(\mathbf{k},\omega)}, \tag{3.41}$$

$$G_{BB}(\mathbf{k},\omega) = \frac{1}{\omega + J + \tau\varepsilon_B(\mathbf{k}) - \Sigma_{BB}(\mathbf{k},\omega)}. \tag{3.42}$$

They, together with Eqs (3.39-3.40), form a self-consistent set of equations which has to be solved numerically.

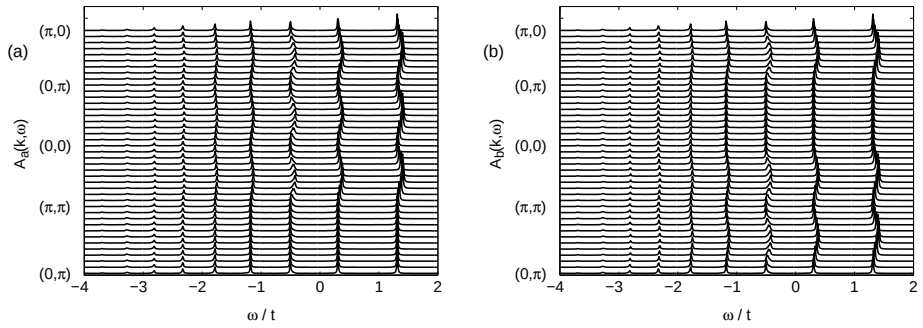


Figure 3.5: The spectral functions as obtained in the SCBA for the $t_{2g}$ orbital $t$–$J$ model (3.5) for a hole doped into: (a) $a$ orbital, and (b) $b$ orbital. Parameters: $J = 0.4t$ and $\tau = 0.1t$. Broadening $\delta = 0.01t$ and cluster size $20 \times 20$.

Finally, once the Green's functions are known, one can calculate the spectral functions for a hole created in $a$ and $b$ orbital:

$$A_a(\mathbf{k},\omega) = -\frac{2}{\pi}\lim_{\delta\to 0}\,\mathrm{Im}\,G_a(\mathbf{k},\omega+i\delta) = -\frac{1}{\pi}\lim_{\delta\to 0}\,\mathrm{Im}\,G_{AA}(\mathbf{k},\omega+i\delta)\,, \quad (3.43)$$

$$A_b(\mathbf{k},\omega) = -\frac{2}{\pi}\lim_{\delta\to 0}\,\mathrm{Im}\,G_b(\mathbf{k},\omega+i\delta) = -\frac{1}{\pi}\lim_{\delta\to 0}\,\mathrm{Im}\,G_{BB}(\mathbf{k},\omega+i\delta)\,, \quad (3.44)$$

where we introduce a factor of 2 in front of the definition of the spectral function $A_\gamma(\mathbf{k},\omega)$ for convenience.

Note that the intersublattice Green's function $G_{AB}(\mathbf{k},\omega)$ vanishes since it would imply that at least one defect was left in the sublattice $B$ after the hole was annihilated in the sublattice $A$, resulting in orthogonal states as there are no processes in the Hamiltonian which cure such defects [cf. the form of the Hamiltonian Eq. (3.32) and Fig. 3.4].

### 3.4.3 The spectral functions and quasiparticle properties

*Spectral functions.*— The system of SCBA equations (3.39)-(3.42) was solved self-consistently on a mesh of $20 \times 20$ **k**-points (besides, the convergence was checked by comparing the results with those obtained for the cluster with $32\times 32$ **k**-points). The spectral functions are displayed in Fig. 3.5. Surprisingly, the spectral density consists of *dispersive* ladder-like spectrum suggesting that the hole doped into any of the two orbitals is mobile. The dispersion is particularly pronounced for the first (low-energy) excitation which can be identified as a quasiparticle state. One finds that the dispersion is strictly 1D and is dictated by the orbital flavour at the site where the hole is originally added, i.e. no dispersion occurs in the complementary direction. For example, a hole added to the $a$ orbital moves only along the $b$ direction.

*Hole propagation due to three-site terms.*— Since removing the three-site terms from the Hamiltonian (3.5) leads to the disappearance of the dispersion (not shown) one can immediately ascribe the onset of this small dispersion $\propto \tau$ to the hole motion via the three-site terms. Furthermore, then the spectral functions (which consist of dispersionless ladder-type peaks) are qualitatively

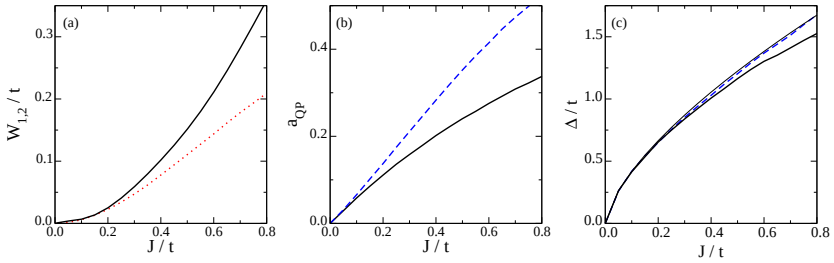


Figure 3.6: Quasiparticle properties obtained for the 2D $t_{2g}$ model within the SCBA for increasing superexchange $J$ (with $\tau = J/4$): (a) the bandwidth of the quasiparticle $W_1$ (solid line) and the second dispersive feature $W_2$ (dotted line), (b) the spectral weight $a_{\rm QP}$, and (c) the distance between the first two peaks in the spectra (pseudogap) $\Delta$. The solid (dashed) lines in (b) and (c) give the results for $\mathbf{k} = (0,0)$ [$\mathbf{k} = (\pi/2, \pi/2)$], respectively. The light solid line in (c) indicates $\Delta = t(J/t)^{2/3}$ law (see text).

similar to the results obtained for a hole doped into the spin $t$–$J$ model with Ising only interaction, see e.g. Fig. 3 of Ref. [23], where the hole is trapped in a string-like potential [22]. This confirms the ideas presented in Sec. 3.2 — indeed in case the three-site terms were not included in the $t$–$J$ model the hole would be immobile, as shown in Fig. 3.3. Furthemore, as predicted in Sec. 3.2, the inclusion of the three-site terms changes this picture qualitatively as the hole can then become mobile and the spectral functions acquire a small dispersion.

*Quasiparticle properties.*— Let us analyse now the characteristic features of the quasiparticle state such as: the bandwidth $W$ and the quasiparticle spectral weight $a_{\rm QP}$. The energy of incoherent excitations (string states) is to some extent characterized by the separation between the quasiparticle state and the next (second) spectral feature at higher energy – it is called here a pseudogap $\Delta$. All these quantities increase with increasing superexchange energy $J$ (here $\tau = J/4$), see Fig. 3.6. One finds that: (i) the bandwidth $W_1$ of the first quasiparticle peak, see Fig. 3.6(a), is proportional to $J^2$ for small $J$ ($J < 0.7$) and to $J$ in the regime of large $J$ ($J > 0.7$) — the bandwidth renormalization is here distinct from the one found either in the spin $SU(2)$ (see Ref. [23]) or in the orbital $e_g$ models [77], (ii) the bandwidth $W_2$ of the second largest dispersive peak [Fig. 3.6(a)] is smaller than that for the first peak and tends to saturate at a value $W_2 \sim 0.25t$ obtained for larger $J > t$ (not shown), (iii) the spectral weight $a_{\rm QP}$ of the quasiparticle peak, shown in Fig. 3.6(b), grows with $J$, and (iv) the pseudogap $\Delta$ shown in Fig. 3.6(c) grows generally like $t(J/t)^{2/3}$, while for higher $J$ values some deviation from this law is observed for the $\mathbf{k} = (0,0)$ point.

*Two problems left, to be studied in next sections.*— Firstly, the lack of the quasiparticle dispersion in one direction, e.g. along the $a$ direction for a hole doped into the $a$ orbital (see Fig. 3.5), is at first instance counterintuitive: One could imagine that it should be allowed that the hole doped into the $a$ orbital switches to a neighbouring site of the $B$ sublattice by the $t$ process, and then propagates freely along the $a$ axis by the three-site effective hopping $\tau$ without generating any further defects. This might in principle lead to some dispersion

in the spectra along the $k_x$ direction. In Sec. 3.5.2 we study this problem in detail.

Secondly, one finds that the bandwidth of the quasiparticle is strongly renormalized as it is much smaller than its free value (calculated from the free three-site term dispersion) $W = 2z\tau = 2J$. Furthermore, the totally different mechanism of hole motion in the considered here $t_{2g}$ orbital model and in the spin model [23, 85, 86] suggest that one cannot explain the renormalization of the quasiparticle bandwidth using any of the ideas proposed previously. In fact, the mere dependence of the bandwidth on the superexchange energy scale $J$ is a convex function of $J$ (see Fig. 3.6) whereas in the spin $t$–$J$ model the bandwidth is a concave function of $J$ [23, 85, 86]. Thus, one needs to understand microscopically how the three-site terms, which lead to the dispersion here, are renormalized — we investigate this issue in Sec. 3.5.3.

## 3.5 Discussion

### 3.5.1 Validity of the results

*General remarks.*— As there are a number of approximations employed while reducing the $t_{2g}$ orbital $t$–$J$ model (3.5) to the polaron Hamiltonian (3.32) and then a slightly new approach was used to solve the latter model using the SCBA method (see below), in what follows: (i) we look at three particular problems connected with the approximations and methods employed in the previous sections, and (ii) we compare the results obtained using the SCBA method for the $t_{2g}$ orbital $t$–$J$ model (3.5) with those obtained in the numerical VCA method for the Hubbard model (3.1).

*Sublattice-dependence of the Green's functions.*— Firstly, as it has been already noted in the previous section, if one skips the flavour-conserving three-site terms (3.13), the calculated spectral functions (not shown) reproduce the well-known ladder spectra and are equivalent to those calculated for the Ising limit of the spin $t$-$J$ model [23]. This means that the zig-zag-like hole trapping in the orbital case is physically similar to the standard hole trapping in the spin case (apart from the modified energy scale due to a different value of the superexchange, the ladder spectra are similar in both cases), whereas for the free hole movement obviously it matters whether the dispersion relation is 1D or 2D. Moreover, this also means that in this special case ($\tau = 0$) the spectra are the same for holes doped into either of the orbitals as the Green's functions are the same for both sublattices. However, *even in this case* it is not allowed to assume *a priori* that $A = B$ and $G_{AA}(\mathbf{k}, \omega) = G_{BB}(\mathbf{k}, \omega)$. In fact, these are two sublattices with two distinct orbital states occupied in the ground state at half filling, and each orbital has entirely different hopping geometry. This does not happen in the standard spin case with isotropic hopping, and for this reason one can eliminate there the sublattice indices.

*Neglected three-site terms.*— Secondly, the result shown in Fig. 3.5 is obtained by neglecting the three-site terms with 90° hopping, see Eq. (3.14). One may wonder whether this approximation is justified whereas the formally quite similar forward hopping term (3.13) is crucial and is responsible for the absence of hole confinement in the ground state with the AO order [85]. Hence, let us look in more detail at these two different kinds of three-site terms, shown in Fig.

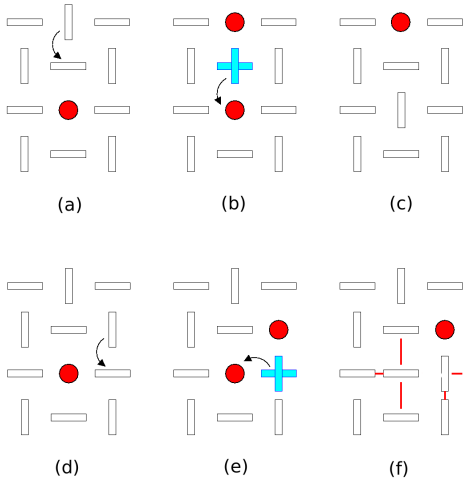


Figure 3.7: Schematic representation of two three-site terms in the $t_{2g}$ orbital model (3.5). Circles depict holes while horizontal (vertical) rectangles depict occupied orbitals with electrons that can move only horizontally (vertically), respectively. Processes shown in panels (a)–(c) result from forward propagation (3.13), while the ones shown in panels (d)–(f) and given by Eq. (3.14) create a defect in the AO order with the energy cost indicated by the lines for the bonds connecting two identical orbital states (broken bonds) in (f).

3.7. The first (linear) hopping term (3.13) transports an $a$ electron along the $b$ axis over a site occupied by a $b$ electron. Such processes are responsible for the 1D coherent hole propagation. As one can see in Figs. 3.7(a)–(c), the AO order remains then undisturbed, so these processes determine the low-energy features in the spectra. Hopping by the other three-site term (3.14), shown in Fig. 3.7(d)–(f), involves an orbital flip at the intermediate site, destroys the AO order on six neighbouring bonds, and thus costs additional energy. As two orbitals are flipped and two excited states are generated, these processes go beyond the lowest order perturbation theory, and it is consistent to neglect them in the SCBA. In any case, they could contribute only to the incoherent processes at high energy and not to the low-energy quasiparticle. Indeed, this interpretation is confirmed by exact diagonalization performed for the $t_{2g}$ orbital $t$–$J$ Hamiltonian (3.5) on $4\times4$ and $4\times6$ clusters, which give the same results for the quasiparticle dispersion, no matter whether the orbital-flipping terms (3.14) are included or not. In addition, the quasiparticle dispersion found in the SCBA agrees with the numerical results obtained by the VCA (see below), which gives further support to the SCBA approach in the present problem.

*Vertex function in the polaron model.*— Lastly, despite several other approximations made in writing down the Hamiltonian Eq. (3.32), the vertex part $H_t$ is *exact*, in contrast to the Ising interaction in the spin $t$–$J^z$ model [23]. The reason is that the constraint $C1$ mentioned in Ref. [23], which states that a hole *and* a boson excitation are prohibited to occur simultaneously at the same site, cannot be violated here, because hopping $t$ is strictly 1D. This can be verified by considering one hole excitation spectra in the limit of $J \to 0$. Indeed, for

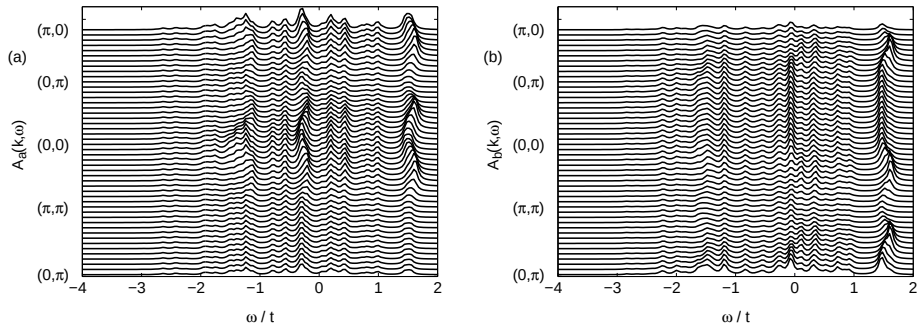


Figure 3.8: Spectral function $A(\mathbf{k},\omega)$ obtained with the VCA method for the 2D $t_{2g}$ Hubbard model (3.1) for: (a) $a$ orbitals, and (b) $b$ orbitals. Parameter: $U = 10t$. This result was obtained by Maria Daghofer.

$J = 0$ one obtains the incoherent spectrum with a bandwidth of $W_{\rm inc} = 4\sqrt{2}t$ (not shown), which (unlike in the spin case) perfectly agrees with the retraceable path approximation result $W_{\rm inc} = 4\sqrt{z-2}t$ from Ref. [67], where $z-2$ is the number of possible forward going steps in the model. However, still the three-site terms $H_{3\rm s}$ and the orbiton terms $H_J$ are not exact in Eq. (3.32) and thus it is necessary to check the present results by comparing them with the numerical spectra obtained for the orbital Hubbard model (3.1) — the results are presented below.

*Comparison with VCA results.*— Since the problem of a hole added to the background with the AO order of $t_{2g}$ orbitals cannot be solved exactly using analytic methods and the SCBA had to be employed in the last section, the numerical VCA calculations are presented below.[5] Actually, we compare the analytic results for the $t_{2g}$ orbital $t$–$J$ Hamiltonian (3.5) presented in Sec. 3.4.3 with those obtained for the $t_{2g}$ Hubbard model (3.1) using the VCA method. This enables us to compare not only the methods employed but also the two models which stand for the same physics in the strongly correlated regime.

Before we analyse the spectral functions, let us recall that the VCA method [87] is appropriate for models with on-site interactions, as for instance the present Hubbard model (3.1) for $t_{2g}$ orbitals, but cannot be easily implemented for models where the interacting part connects different sites, like in the $t$-$J$ model. For the present $t_{2g}$ model (3.1) the VCA method is used with the open boundary conditions [87], which leads to the spectral densities depicted in Fig. 3.8. The results resemble very much the SCBA results of Fig. 3.5 for $t_{2g}$ orbital $t$–$J$ model (3.5), suggesting that not only both models are indeed equivalent in the strongly correlated regime, but also that the implemented SCBA method of Sec. 3.4.3 is of a very good quality. The differences between them, almost exclusively affecting high-energy features, are discussed below.

On the one hand, one sees that the high-energy part of the spectral density in Fig. 3.8 is composed of a number of peaks with a dispersion almost parallel to that of the quasiparticle state. In fact, the spectrum corresponds almost exactly to the ladder spectrum of the spin $t$-$J$ model with Ising superexchange [22, 23] but with a weak dispersion added to the peaks. The peaks at higher-energy are dispersive for the same reason as the quasiparticle state: After hopping a

[5] These calculations were performed by Maria Daghofer.

few times by nearest neighbour hopping $t$ — and creating string excitations, see Fig. 3.7 — the hole can exhibit coherent propagation via three-site terms, leading to the observed dispersion. On the other hand, the VCA spectrum (Fig. 3.8) does not show these distinct peaks and the structure of $A(\mathbf{k},\omega)$ is richer. However, the first moments calculated in separate intervals of $\omega$ follow similar dispersions to those found for the first three peaks obtained in $A(\mathbf{k},\omega)$ within the SCBA [85].

The above difference can be understood as following from the full Hilbert space used in the VCA calculations which results in excitations of doubly occupied sites, weakening of the AO order even for relatively large $U = 10t$. Therefore the spectra of Fig. 3.8 have more incoherent features. In addition, the three-site terms which create two orbiton excitations (3.14) that were neglected in the SCBA, might also influence the high-energy part of the spectrum. The difference to the SCBA results might also be due to the fact that states with longer strings including several orbital excitations, which occur when the hole moves by a few steps via $t$, cannot be directly accommodated within the 10-site cluster solved here, and cannot be therefore reproduced with sufficient accuracy.

Apart from the differences in the high-energy part of the spectrum, one also observes differences in the spectral weight distribution: In the VCA results (Fig. 3.8) the total weight found in photoemission part (hole excitation) strongly depends on momentum $\mathbf{k}$, while no such variation can be seen in the SCBA results in Fig. 3.5. This difference does not originate from different approximate methods used, but stems from the different *models*: In Hubbard-like models, the number of electron states occupied depends on the momentum $\mathbf{k}$ [88]. In contrast, undoped $t$–$J$-like models have exactly one electron per site, which enforces a different sum rule and eliminates the $\mathbf{k}$-dependence from the photoemission part.

### 3.5.2 Understanding the 1D dispersion

*Purpose of the section.*— In order to understand why the dispersion of the hole doped into 2D $t_{2g}$ AO state is strictly 1D (both for the quasiparticle and for the excited states) we introduce below the 1D orbital Hubbard model.

*1D orbital Hubbard model.*— The 1D orbital Hubbard model is defined as

$$\mathcal{H}_{\rm 1D} = -t\sum_i (a_i^\dagger a_{i+1} + \text{H.c.}) + U\sum_i n_{ia}n_{ib}\ , \tag{3.45}$$

where (similarly as in 2D case) $a_i^\dagger$ ($b_i^\dagger$) creates a spinless electron with orbital flavour $a$ ($b$) at site $i$, and $\{n_{ia}, n_{ib}\}$ are electron density operators. On-site Coulomb repulsion $U$ is the energy of a doubly occupied state (it arises as a linear combination of the Coulomb and Hund's exchange in the respective high-spin configuration [84]), and $t$ is the nearest neighbour hopping element. Only electrons with orbital flavour $a$ are mobile while the other ones with flavour $b$ cannot hop. To simplify, we call below the $a$ and $b$ orbitals mobile and immobile ones, respectively. This situation not only describes a toy-model defined for the purpose of understanding better the spectral functions of the 2D $t_{2g}$ orbital model but also corresponds to (spinless) interacting $e_g$ electrons in the FM chain (as along the $c$ direction in the manganites, see Ref. [89]) or to the 1D (spinless) Falicov-Kimball model with degenerate orbitals.

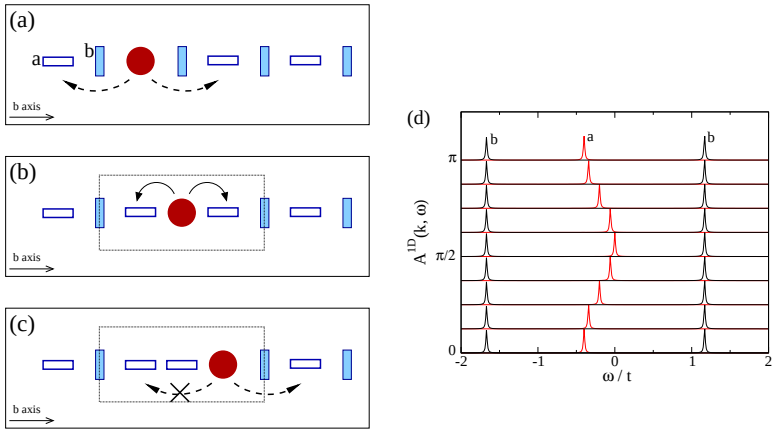


Figure 3.9: Hole propagation in the 1D orbital $t$–$J$ model (3.46). Two top panels show a hole doped into: (a) mobile $a$ orbitals (empty boxes), and (b) immobile $b$ orbitals (filled boxes). Solid (dashed) arrows indicate possible hopping processes with hopping elements $t$ and $\tau$, respectively; in case of a hole added to the $b$ orbital the latter process occurs only after the initial hopping by $t$, see panel (c). Panel (d) shows the exact spectral functions $A_a^{1D}(k,\omega)$ and $A_b^{1D}(k,\omega)$ of a hole added into the $a$ orbital (middle dispersive feature between $\omega = -0.4t$ and $\omega = 0$) and the $b$ orbital (two side dispersionless maxima) as obtained from the 1D orbital $t$–$J$ model (3.46). Parameters: $J = 0.4t$, $\tau = 0.1t$, and peak broadening $\delta = 0.01t$.

*1D orbital $t$–$J$ model.*— In the regime of large $U$, i.e. for $t \ll U$, the canonical perturbation expansion discussed in Chapter 1 (see Sec. 3.3 for a similar derivation in the 2D case) leads to the effective $t$–$J$ Hamiltonian with Ising-like superexchange and three-site terms

$$H_{\rm 1D} = -t\sum_i \left(\tilde{a}_i^\dagger \tilde{a}_{i+1} + {\rm H.c.}\right) + \frac{1}{2}J\sum_i \left(T_i^z T_{i+1}^z - \frac{1}{4}\tilde{n}_i\tilde{n}_{i+1}\right) - \tau\sum_i \left(\tilde{a}_{i-1}^\dagger \tilde{n}_{ib}\tilde{a}_{i+1} + {\rm H.c.}\right) , \quad (3.46)$$

where (again) a tilde above a fermion operator indicates that the Hilbert space is restricted to unoccupied and singly occupied sites and the pseudospin $T_i^z = (\tilde{n}_{ia} - \tilde{n}_{ib})/2$. The superexchange constant $J$ and the three-site term hopping $\tau$ are defined as in Eq. (3.10) and Eq. (3.15), respectively. The 1D $t$–$J$ orbital model defined without the three-site hopping $\tau$, was solved exactly before [89] and all excitations occurred to be dispersionless. Here we generalize this exact solution to the full Hamiltonian (3.46) *including* the three-site terms, and show how the spectral functions change then.

*Spectral function for a hole in the mobile orbital.*— We start with calculating

the Green's function for the hole doped into the $a$ (mobile) orbital,[6]

$$G_a^{\rm 1D}(k,\omega) = \left\langle \Phi_0^{\rm 1D} \left| a_k^\dagger \frac{1}{\omega + H_{\rm 1D} - E_0^{\rm 1D}} a_k \right| \Phi_0^{\rm 1D} \right\rangle , \tag{3.47}$$

where $E_0^{\rm 1D}$ is the energy of the ground state. As in case of $t_{2g}$ orbitals considered above, the occupied orbitals alternate and at half filling form sublattices $\{A, B\}$. The physical vacuum is

$$|\Phi_0^{\rm 1D}\rangle = \prod_{i\in A} a_i^\dagger \prod_{j\in B} b_{\rm j}^\dagger \,|0\rangle, \tag{3.48}$$

where (again) $|0\rangle$ is the true vacuum state with no electrons. Besides, the hole with momentum $k$ is created by the operator

$$a_k = \frac{1}{\sqrt{N}} \sum_j e^{ikj} a_j \,, \tag{3.49}$$

with $N$ being the number of sites in the chain. Then one can easily verify that the state $a_k|\Phi_0^{\rm 1D}\rangle$ in Eq. (3.47) is an eigenstate of the Hamiltonian (3.46). The hopping $\propto t$ is blocked by the constraint of no double occupancy in the Hilbert space and the only two terms that contribute in this state are: (i) the superexchange term ($\propto J$) which gives the energy $\frac{1}{2}J$ of two missing bonds as a correction to $E_0^{\rm 1D}$, and (ii) the three-site hopping term ($\propto \tau$) which contributes to the $k$ dependence due to the processes shown in Fig. 3.9(a) after Fourier transformation. As a result, one finds

$$G_a^{\rm 1D}(k,\omega) = \frac{1}{2} \frac{1}{\omega + \frac{1}{2}J + 2\tau\cos(2k)} \,, \tag{3.50}$$

where the factor 1/2 originates from the fact that $\langle\Phi_0^{\rm 1D}|a_k^\dagger a_k|\Phi_0^{\rm 1D}\rangle = 1/2$. Note that $\tilde{n}_{ib} \equiv 1$ in the three-site terms, as in this case all the sites with $j \in B$ are occupied by $b$ electrons in the ground state (3.16). The hole spectral function,

$$A_a^{\rm 1D}(k,\omega) = -\frac{2}{\pi} \lim_{\delta\to 0} {\rm Im}\, G_a^{\rm 1D}(k,\omega+i\delta) \,, \tag{3.51}$$

consists of a single dispersive state, shown as the middle peak in Fig. 3.9(d). As expected, the hole is mobile thanks to the three-site terms and it propagates coherently with the unrenormalized bandwidth $W = 4\tau$. The result obtained here is *identical* with the one found using the VCA for the corresponding Hubbard model (3.45) (see also Fig. 5 of Ref. [85]). This confirms that both the orbital Hubbard model (3.45) and its $t$–$J$ model *with* three-site terms (3.46) are equivalent and precisely describe the same physics in the regime of $t \ll U$.

*Spectral function for a hole doped into the immobile orbital.*— The calculation of the Green's function for the hole doped into the $b$ (immobile) orbital is considerably more *involved* as one needs to use the continued fraction method.

[6] We calculate the 'mobile case' for didactic reasons. It will be the 'immobile case' (see below) from which we will draw some conclusions concerning the understanding of the 1D dispersion in the 2D case.

Thus, we perform these calculations in Appendix A. We obtain $k$-independent Green's function [compare Eq. (A.10)]

$$G_b^{1\mathrm{D}}(\omega) = \frac{1}{2}\left\{\omega + \frac{1}{2}J - \frac{4t^2}{\omega + \frac{1}{2}J \mp \sqrt{(\omega+J)^2 - 4\tau^2}}\right\}^{-1}, \tag{3.52}$$

from which we calculate the the hole spectral function

$$A_b^{1\mathrm{D}}(\omega) = -\frac{2}{\pi}\lim_{\delta\to 0}\mathrm{Im}\, G_b^{1\mathrm{D}}(\omega + i\delta), \tag{3.53}$$

shown in Fig. 3.9(d). It also does not depend on $k$ and for the realistic parameters with $\tau < t$ it consists of two poles and the incoherent part centred around $\omega = -J$. This latter contribution has rather low intensity and is thus invisible on the scale of Fig. 3.9(d) and the two peaks absorb almost the entire intensity. This result resembles the case of $\tau = 0$ (see Ref. [89]) and might appear somewhat unexpected — we analyse it below.

*Why the three-site terms are suppressed in the immobile case.*— First, we comment on the absence of the $k$ dependence in the spectral function $A_b^{1\mathrm{D}}(\omega)$ (3.53). To understand this result It suffices to analyse the hole doped into the $b$ orbital at any finite value of $J$ which induces the AO ground state (3.48). The hole can only move incoherently, because once it moves away from the initial site $j$ by the hopping $t$ [see Fig. 3.9(b) and (c)], it creates a defect in the AO state which blocks its hopping by the three-site processes over site $j$. Consequently, the hole may hop only in the other direction, i.e. away from the defect in the AO state, and in order to absorb eventually this orbital excitation it has to come back to its original position, retracing its path. In this way a forward and backward propagation along the 1D chain interfere with each other, resulting in the fully incoherent spectrum of Fig. 3.9(d).

Looking at the spectral function $A_b^{1\mathrm{D}}(\omega)$ of a hole doped into the $b$ orbital at finite $\tau = 0.1t$ shown in Fig. 3.9(d) one may be somewhat surprised that the result indicates only two final states of the 1D chain. These are the bonding and the antibonding state of a hole confined within a three-site box and discussed in detail in Ref. [89] in the limit of $\tau = 0$. One finds that the two excitation energies obtained for the present parameters, $\omega = -1.67t$ and $\omega = 1.17t$, are indeed almost unchanged from those given by Eq. (A.9) at $\tau = 0$. We note that the third nonbonding state has a different symmetry and thus gives no contribution to $A_b^{1\mathrm{D}}(\omega)$.

Altogether, one finds that in the realistic regime of parameters with $\tau = J/4$, the incoherent part of the spectrum is extremely small and thus invisible in the scale of Fig. 3.9(d). This implies that the hole is still practically trapped within the three-site box depicted in Fig. 3.9(b), in spite of the potential possibility of its delocalization by finite $\tau$. Only when the value of the three-site hopping $\tau$ is considerably increased, the hole can escape from the three-site box and may delocalize over the entire chain.

A systematic evolution of the spectral function $A_b^{1\mathrm{D}}(\omega)$ with increasing $\tau$ is depicted in Fig. 3.10. One observes that the incoherent spectral weight grows with increasing $\tau$ and is already visible in between the two maxima for $\tau = 0.5t$. When the three-site hopping term approaches $\tau = t$, the spectrum changes in a qualitative way — both peaks are absorbed by the continuum and the spectral density resembles the density of states of the 1D chain with the nearest

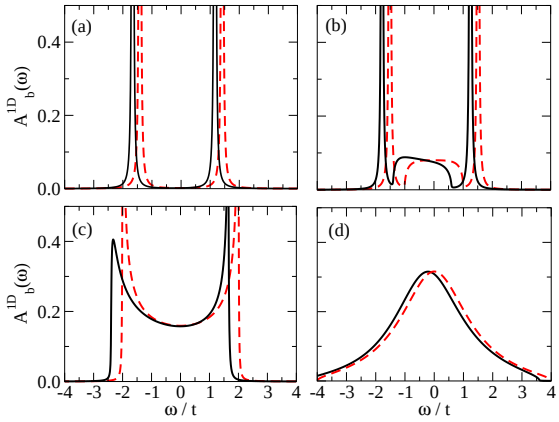


Figure 3.10: Spectral function $A_b^{1D}(\omega)$ of a hole doped into the $b$ orbital in the 1D model with: (a) $\tau = 0$, (b) $\tau = 0.5t$, (c) $\tau = t$, and (d) $\tau = 2t$. Dashed (solid) lines for $J = 0$ ($J = 0.4t$), respectively, with broadening $\delta = 0.01t$.

neighbour hopping. For the extremely large effective hopping $\tau \simeq 2t$ the two peaks corresponding to the energies given by Eq. (A.9) from Appendix A are absorbed by the continuum centered at $\omega \sim 0$, and the spectrum corresponds to the incoherent delocalization of the hole over the 1D chain. Note also that finite $J$ results only in an overall shift of the spectra due to the energy cost of the hole excitation in the ordered ground state (3.16).

*Understanding the 1D dispersion in the 2D model.*— Having understood the 1D case in detail one can now try to understand why the dispersion relation for the hole doped into the 2D $t_{2g}$ AO state is strictly 1D. More precisely, the question which arises here is: why, in the 2D case, a hole doped for example into the $b$ orbital cannot hop along the $b$ direction. In principle one could imagine that the hole doped into the $b$ orbital in the 2D lattice hops by the $t$ process to the neighbouring site, creates one defect in the AO site and then propagates freely along the $b$ direction via the three-site terms. This, however, cannot contribute to any **k**-dependent motion: as shown in the above 1D example the hole always has to return to the original site where it has been doped as it has to erase the defect it has created in the first $t$ step while moving to the other sublattice (otherwise, the hole annihilation operator would not permit to return to the ground state).

A similar phenomenon occurs in the 2D case. One should only note that strictly speaking, in the 1D model there are actually two interrelated reasons why the hole cannot move coherently when it is doped into the $b$ orbital: (i) the creation of the defect after the first $t$ step which has to be erased by the hole before the hole itself is annihilated by the $a_k^\dagger$ operator in Eq. (3.47), and (ii) the fact that this defect blocks the hole motion by three-site terms in one direction. However, in the SCBA treatment the latter constraint is neglected, so it is the point (i) which suffices alone to confine the hole.

Furthermore, the spectrum associated with such a propagation, as described in the above paragraph, is not only **k**-independent but also its spectral weight is extremely small both in the 2D model in the realistic range of parameters

(where it is invisible at the scale of Fig. 3.5) and in the 1D case (as discussed above). Again, the reason why this spectral weight is so small in the 2D case can be understood using the 1D model: the value of the three-site hopping is too small to delocalize the hole from the three-site box.

### 3.5.3 Renormalization of the three-site terms

*Purpose of the section.*— In what follows we will study the extended version of the 1D model, called the 'centipede model', with electrons hopping between $d_{yz}$ and $d_{zx}$ orbitals in $ab$ plane — the model includes two neighbours on every second site and thus has $2N$ sites for the chain of length $N$, see Fig. 3.11. We will show that even the shortest possible strings with the length of one bond which can be excited here when the hole moves in this geometry are sufficient to generate some characteristic features recognized in the spectral properties of the 2D $t_{2g}$ model (see Sec. 3.4.3). In particular, using this toy-model we will show how the renormalization of the three-site terms in the 2D $t_{2g}$ orbital $t$–$J$ model arises due to the peculiar interrelation between the coherent propagation via the three-site terms and the incoherent motion due to the creation of the strings by the nearest neighbour hopping $t$.

*Introducing the centipede model.*— The centipede model of Fig. 3.11(a) consists of a chain along $b$ axis, with the Hamiltonian as described by Eq. (3.45), and two sites being the nearest neighbours of every second site of the chain along the $a$ axis, which could represent radicals added to a linear molecule. We use here the convention introduced already in the previous sections, that $a$ and $b$ orbitals stand for $d_{yz}$ and $d_{zx}$ $t_{2g}$ orbitals, respectively, that permit the electron hopping along the $b$ and $a$ axis in the $ab$ plane. The Hamiltonian of the present model is

$$\mathcal{H}_{ce} = -t\sum_i \left\{ b^\dagger_{2i}(b_{2i,u} + b_{2i,d}) + \text{H.c.} \right\} - t\sum_i (a^\dagger_i a_{i+1} + \text{H.c.}) + U\sum_i n_{ia} n_{ib}. \tag{3.54}$$

The hopping along the bonds parallel to the $a$ axis is allowed only to the orbitals $b$, with the corresponding creation operators $\{b^\dagger_{2i,u}, b^\dagger_{2i,d}\}$, see Fig. 3.11(a). To simplify notation, we call these orbitals $u$ and $d$, and introduce the following operators:

$$u^\dagger_{2i} \equiv b^\dagger_{2i,u}, \qquad d^\dagger_{2i} \equiv b^\dagger_{2i,d}\,. \tag{3.55}$$

In the limit of large $U$ ($U \gg t$) the occupied orbitals form AO order along the chain and we select the Néel state with $b$ ($u$ and $d$) orbitals occupied on the external sites, as shown in Fig. 3.11, since we are interested in their effect on the hole propagation when the hole is doped to an $a$ orbital. This leads to the following 1D centipede $t$–$J$ model (derived using the canonical perturbation expansion discussed in Chapter 1, see also Sec. 3.3 for a similar derivation in the 2D case) :

$$\begin{aligned} H_{ce} = &- t\sum_i \{(\tilde{u}^\dagger_{2i} + \tilde{d}^\dagger_{2i})\tilde{b}_{2i} + \text{H.c.}\} - \tau\sum_i (\tilde{a}^\dagger_{2i}\tilde{n}_{2i+1,b}\tilde{a}_{2i+2} + \text{H.c.}) \\ &- \frac{3}{4}J\sum_i (\tilde{u}^\dagger_{2i}\tilde{u}_{2i} + \tilde{d}^\dagger_{2i}\tilde{d}_{2i})\,. \end{aligned} \tag{3.56}$$

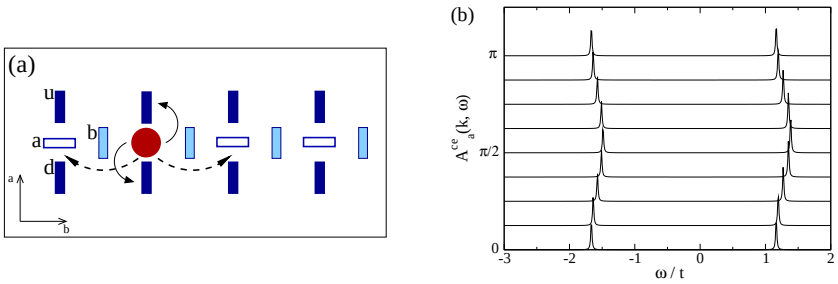


Figure 3.11: Propagation of a hole added into the $a$ orbital in the centipede $t$–$J$ model (3.56): (a) schematic picture of a hole doped at site $a$ and its possible delocalization via hopping $t$ (solid lines) and three-site effective $\tau$ term (dashed lines); (b) spectral function $A_a^{ce}(k,\omega)$. Parameters: $J = 0.4t$, $\tau = 0.1t$, peak broadening $\delta = 0.01t$. The chain is oriented along the $b$ axis, and non-equivalent positions of the orbitals which do not permit hopping along this direction are labelled $b$, $u$ and $d$ in panel (a).

On the one hand, the superexchange interaction for all the bonds within the centipede is not included in Eq. (3.56) as it results only in a rather trivial energy shift of the spectra obtained from the Green's function $G_a^{ce}(k,\omega)$ which is of interest here,[7] cf. Sec. 3.5.2. On the other hand, the last term in Eq. (3.56) is added to to include the energy loss when the hole delocalizes to one of the side sites and a short string is created which as well occurs in the full 2D model of Sec. 3.4.3 (see also discussion below).

Whereas the second term in Eq. (3.56) is once again the three-site hopping derived before in the 1D model (3.46) [cf. Fig. 3.9(a)], the other two terms describe the possibility of creating defects in the AO order when the hole leaves the spine of the centipede (i.e. moves away from the $a$ sites) by creating strings of length one, just as it may happen in the $t_{2g}$ 2D model. Here the hole can leave the chain to its nearest neighbour orbital $u_{2i}$ or $d_{2i}$ [cf. sites attached to the chain along the $a$ axis shown in Fig. 3.11(a)]. Such defects are created by hopping $t$ and cost energy $3J/4$ in each case. Hence, the present 1D model represents an extreme reduction of the full $t_{2g}$ 2D model, allowing only the strings of length one, and each defect has to be deexcited before the hole can hop to another three-site unit along the chain. Note, however, that the energies of these string excitations are properly chosen and are just the same as in the full 2D model.

The model given by Eq. (3.56) constitutes a one-particle problem (after inserting $\tilde{n}_{2i+1,b} \equiv 1$ which is consistent with the Ising nature of the superexchange) and hence can be solved exactly. We will consider the Green's function $G_a^{ce}(k,\omega)$ for $a$ orbitals, defined similarly as in Eq. (3.47), and a hole excitation is created again by the operator $a_k$ of Eq. (3.49). The continued fraction (see also Appendix A for a more elaborate version of the method) terminates after

[7] The Green's function $G_b^{ce}(k,\omega)$ does not show new qualitative features as compared with the solution obtained for the 1D orbital chain of Sec. 3.5.2.

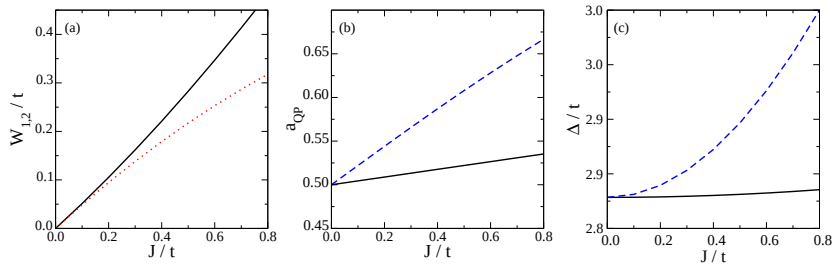


Figure 3.12: Characteristic features in the spectra obtained for the 1D centipede model (Fig. 3.11) for increasing $J$: (a) the bandwidth $W_{1,2}$, (b) the spectral weight $a_{\rm QP}$, and (c) the distance $\Delta$ between the two peaks. The solid (dotted) line in (a) corresponds to the first (second) dispersive peak in $A_a(k,\omega)$ whereas the solid (dashed) lines in the lower panels show results for $k=0$ ($k=\pi/2$), respectively. The light solid line in (a) is merely a guideline for the eye to show that the bandwidth of the first peak is a function with a positive second derivative. Parameter: $\tau = J/4$.

the second step and one finds the exact Green's function

$$G_a^{ce}(k,\omega) = \frac{1}{2}\frac{1}{\omega + 2\tau\cos(2k) - \frac{2t^2}{\omega+\frac{3}{4}J}}\,, \tag{3.57}$$

leading to the corresponding spectral function $A_a^{ce}(k,\omega)$, defined as in Eq. (3.51). The numerical results obtained with $J = 0.4t$ are shown in Fig. 3.11(b). Instead of a single dispersive state of Fig. 3.9(d), the spectral function consists here of two dispersive peaks separated by a gap of roughly $2\sqrt{2}t$. This demonstrates that the larger hopping $t$ suppresses at first instance the hopping along the chain by the element $\tau$, and a hole doped into the $a$ orbital delocalizes in the first place over the three-site unit, discussed in Sec. 3.5.2, consisting of a hole and two $b$ ($u$ and $d$) orbitals. Therefore the hole behaves effectively as a defect created at a $b$ site in the 1D chain of Sec. 3.5.2. This explains that the maxima of $A_a^{ce}(k,\omega)$ are found again for the local bonding and antibonding state, similar to the structure of $A_b^{\rm 1D}(\omega)$ in Sec. 3.5.2. However, at present the corresponding states gain weak dispersion because the hole may as well delocalize along the chain by the three-site hopping $\tau$. Note also that the low-energy (right) peak has slightly higher dispersion (leading to a broader band) than the left one. This case illustrates that the 1D dispersion is broader for the (low energy) quasiparticle state but is also shared by the feature at higher energy. This observation will help us to interpret the spectra for the 2D $t_{2g}$ model (see below).

In addition, we also calculate some characteristic features of the spectra of the centipede model, cf. Fig. 3.12. They will mostly serve for a comparison with the respective results of the 2D $t_{2g}$ model in the next paragraph. However, let us only remark that the renormalization of the bandwidth, shown in Fig. 3.12(a), follows from an intricate interplay between coherent hole propagation and the string excitations. With increasing $\tau = J/4$ the free bandwidth increases but at the same time the energies of the defects (generated by the hole when it moves to 'lower' or 'upper' sites) are $\propto J$; hence, the bandwidth does not depend in a

linear way on $J$, cf. Fig. 3.12(a). Physically this means that the hole motion is gradually more and more confined to just the 1D path along the chain with increasing $J$ (and keeping $\tau = J/4$).

*Renormalization of the three-site terms in the $t_{2g}$ orbital $t$–$J$ models.*— As already noted in Sec. 3.4.3 [see also Fig. 3.6(a)] the quasiparticle bandwidth in the 2D $t_{2g}$ orbital $t$–$J$ model, arising from the superexchange three-site terms, is renormalized as it was found to be much smaller than the respective free value, $W \ll 2J$. Even at $J = t$, the quasiparticle bandwidth is only $W \simeq J/2$, i.e. it is here reduced by a factor of 4.

A similar but considerably weaker reduction of the 1D dispersion by string excitations can be seen in the present centipede model, see Fig. 3.12(a). In addition, the dispersion of the second peak is weaker than that of the quasiparticle. Interestingly, the bandwidth corresponding to the dispersion of the second peak in the centipede model is not only weaker than that of the quasiparticle itself but is also renormalized in a similar way to that found for the full 2D $t_{2g}$ model.

Although it should be noted that in the centipede case the renormalization is almost linear as the length of the string excitations is limited to a single step (within one of the three-atom units along the chain), the centipede model can indeed explain microscopically how the renormalization of the three-site terms in the 2D model arises: The renormalization of the coherent hole propagation in the 2D $t_{2g}$ model, leading to a reduced bandwidth, follows from the creation of string states during the 1D hole propagation via three-site terms. Note that the latter processes were absent in the 1D model, and therefore the hole moved there freely by three-site hopping terms and the bandwidth was unrenormalized [see Eq. 3.50].

*Further comparison between the centipede and the $t_{2g}$ orbital $t$–$J$ model.*— Actually, the other quasiparticle properties in the 2D $t_{2g}$ model and in the centipede model are much more different than the bandwidth: It is only the increase of $a_{\rm QP}(\pi/2, \pi/2)$ with respect to $a_{\rm QP}(0, 0)$ in the 2D case [see Fig. 3.6(b)] which resembles the increase of the spectral weight for the low-energy peak at $k = \pi/2$ over the one at $k = 0$ in the centipede model [see Fig. 3.12(b)]. These differences are due to the fact that both the quasiparticle spectral weight and the pseudogap are heavily related to the string excitations in the system which are entirely different in the 2D case (infinitely long strings possible) and in the centipede model (where only strings of length one are possible).

## 3.6 Conclusions

*Purpose of this chapter.*— The purpose of this chapter was to investigate whether a single hole added to the Mott insulating ground state at half-filling can be confined due to the presence of the orbital degeneracy. Actually, more precisely the idea was to study the simplest possible example, where one could naively expect hole confinement: a 2D Mott insulator with $t_{2g}$ orbital degrees of freedom. It occurred that the hole can never be confined in such a system but instead can move there on a renormalized scale due to the so-called three-site terms. Obviously, this does not imply that the hole confinement in the Mott insulator with orbital degrees of freedom is impossible: one can imagine that there may exist another phenomenon in orbitally degenerate systems which leads to

hole confinement. However, the simplest possible mechanism, as shown here, is outruled.[8]

In what follows, we will now show why the hole is not confined in such an orbitally degenerate system by giving answers to the three questions posed in the introduction to this chapter.

*Form of the $t$–$J$ model with $t_{2g}$ orbital degrees of freedom.*— As discussed in Sec. 3.2 one had some choice in defining the $t$–$J$ model with $t_{2g}$ orbital degrees of freedom. However, the idea was to formulate the model in such a way that the characteristic symmetries of the $t_{2g}$ orbitals, which leads to the lack of the interorbital hopping and the 2D hopping of electrons between a particular $t_{2g}$ orbital, could be visible 'as far as possible'. This is not a very precise statement but nevertheless we demonstrated in Sec. 3.2 that a model with only two active $\{d_{zx}, d_{yz}\}$ orbitals in the $ab$ plane and spinless strongly correlated electrons would indeed bear all these distinctive features.

Altogether this led (see Sec. 3.3) to the $t$–$J$ model with an Ising-type interaction between orbital pseudospins and 1D hopping of electrons with particular orbital flavour. However, it occurred that due to the absence of the $SU(2)$ symmetry in such a model one had to be more careful with any approximations made during the derivation of the model or while solving it. Thus, the frequently neglected three-site terms had to be included in the model.

*Undoped ground state.*— In the half-filled case the above discussed $t_{2g}$ orbital $t$–$J$ model with three-site terms reduced to the Ising-like interaction between pseudospins. As the superexchange constant $J$ was positive in this model, the ground state consisted of alternating pseudospins between two sublattices and had no pseudospin quantum fluctuations, see Sec. 3.4.1. Consequently, the ground state turned out to be a classical AO state with $d_{zx}$ and $d_{yz}$ alternating orbitals.

*Motion of the hole in the undoped ground state.*— In order to investigate motion of a single hole doped into the half-filled AO ground state we reduced the $t_{2g}$ orbital $t$–$J$ model to the effective polaron Hamiltonian using the slave-fermion approach (Sec. 3.4.1). The latter one was rather easy to solve using the SCBA method and we obtained the spectral functions which consisted of the *dispersive* ladder-like peaks (Sec. 3.4.3). While the onset of the ladder spectrum revealed the fact that the hole was trapped in string-like potential, the small dispersive features suggested that the hole was not truely confined. This result was thoroughly checked and confirmed in Sec. 3.5.1 where (in particular) we showed that the Hubbard model led to similar spectral functions with a small 1D dispersion. Furthermore, in Sec. 3.5.2 we explained the lack of the 1D character of the dispersion relations using the auxiliary orbital 1D model.

We emphasize that the mechanism of coherent hole propagation which occurs in the 2D $t_{2g}$ orbital model is completely different from the one known in the spin case. Generally, in orbital systems (with conserved orbital flavours) it originates entirely from the three-site hopping processes, similarly to the discussed 1D case in Sec. 3.5.2. But unlike in the latter case, in the 2D $t_{2g}$ case the quasiparticle bandwidth is strongly reduced from the value given by the amplitude of bare three-site hopping. In order to investigate this problem in more detail, we discussed the subtle interplay between the coherent hole propagation

[8] Note that a different mechanism present in systems with orbital degeneracy (orbital polarization), shown in Ref. [90], leads to the strong reduction of the bandwidth — but the bandwidth is still finite and additional effects are needed to truely localize the hole.

and string excitations in the 1D centipede model (Sec. 3.5.3), where polaronic hole confinement competed with coherent propagation along the chain, which to some extent resembled the realistic 2D $t_{2g}$ case. Indeed, this explained the renormalization as following from incoherent string excitations which dressed the coherent propagation and did not contribute additional momentum dependence.

*Final remarks.*— In the whole chapter we discussed a highly theoretical problem of the hole confinement induced by the presence of the orbital degrees of freedom. However, a natural question arises: could such a problem be relevant for any experiment. Actually, introduction of a single hole to the half-filled system corresponds to the photoemission experiment on the half-filled system: there the photon removes the electron from the crystal (somewhat similarly as in the well-known photoelectric effect), i.e. it creates a hole in the system [69]. Thus, the only problem with which still arises is: can one find a crystal with a plane with two active $\{d_{zx}, d_{yz}\}$ orbitals in the $ab$ plane. As shown in the Postscriptum (Sec. 3.7) there exists a certain class of vanadates and fluorides whose photoemission spectra should bear all of the characteristic features of the spectral functions shown in Figs. 3.5 or 3.8. It remains a challenge for the experimental community to verify this conjecture.

## 3.7 Postscriptum: photoemission spectra of vanadates and fluorides

*Realistic systems with longer range hopping.*— In this section we discuss the possible implications of the results obtained for the $t_{2g}$ orbital model of this chapter on future experiments and make predictions concerning the photoemission spectra of strongly correlated fluorides and vanadates. The first important feature to consider is the interplay of the three-site hopping with the longer-range $\{t_2, t_3\}$ hopping to second and third neighbours which contributes to the electronic structure and may always be expected in any realistic system (for instance, due to hybridization with oxygen orbitals). These hopping elements were neglected in both the Hubbard model (3.1) and in the $t$–$J$ model (3.5) but they could significantly influence the spectral weight distribution. One will see, however, that although features induced by longer-range hopping are small as long as $|t_{2(3)}| < t$, they can be clearly distinguished from the effects of three-site hopping.

*Next nearest neighbour hopping.*– The same requirements for orbital symmetry that are necessary to obtain nearest neighbour hopping, as discussed in this work, also strongly restrict the range of allowed longer-range hopping terms. It is important to recall that the $d$–$d$ hopping elements involve intermediate oxygen orbitals. For next nearest neighbour hopping, the orbital phases of the involved oxygen $2p_\pi$ orbitals make all terms vanish that conserve orbital flavour [75], and only orbital-flipping terms

$$H_{\rm NNN} = -t_2 \sum_{\mathbf{i}} \left( a^\dagger_{\mathbf{i}\pm\hat{\mathbf{b}}} b_{\mathbf{i}\pm\hat{\mathbf{a}}} + a^\dagger_{\mathbf{i}\mp\hat{\mathbf{b}}} b_{\mathbf{i}\pm\hat{\mathbf{a}}} + \text{H.c.} \right) , \tag{3.58}$$

given by hopping element $t_2$, are finite. With realistic parameters one arrives at the estimation of $|t_2| \sim 20$ meV, i.e., $|t_2| \sim J/3$. Similar to the orbital flipping

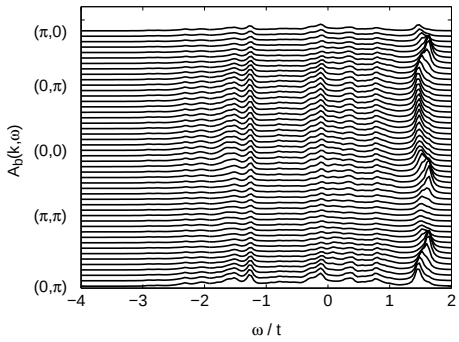


Figure 3.13: Spectral density $A_b(\mathbf{k},\omega)$ obtained within the VCA method for a hole inserted into $b$ orbitals of the $t_{2g}$ model (3.1), supplemented by finite next nearest neighbour hopping (3.58). Parameters: $U = 10t$, and $t_2 = 0.15t$. This result was obtained by Maria Daghofer.

three-site term (3.14), such a hopping process disturbs the AO order stabilized by the superexchange and induces string excitations. For this reason, its impact is largely confined to the high-energy part of the spectrum and is rather small for the low-energy quasiparticle state. This can be seen in Fig. 3.13 where we show the spectral density for $t_2 = 0.15t$ and $J = 0.4t$: While the higher energy part is somewhat affected by finite $t_2$, the intensity and dispersion of the low-energy quasiparticle is almost the same as obtained for $t_2 = 0$, see Fig. 3.8(b).

*Third neighbour hopping.*— The quasiparticle dispersion could also be influenced by the third-neighbour hopping terms $t_3$, where the orbital symmetry leads to the same anisotropy as for nearest neighbour hopping: $a$ orbitals allow only hopping along the $a$ axis, and $b$ orbitals only along the $b$ one:

$$H_{t_3} = -t_3 \sum_{\{\mathbf{imj}\}\|a} b^\dagger_{\mathbf{i}} b_{\mathbf{j}} - t_3 \sum_{\{\mathbf{imj}\}\|b} a^\dagger_{\mathbf{i}} a_{\mathbf{j}} \,. \tag{3.59}$$

Here the unit consisting of three sites $\{\mathbf{imj}\}$, shown in Fig. 3.3(a), is parallel to one of the cubic axes in the $ab$ plane. In contrast to $t_2$ terms, these terms do not induce any string excitations but contribute only to the dispersion of the quasiparticle state itself, so they mix with the three-site effective hopping $\tau$. To illustrate this effect, one can choose $t_3 = \pm J/4$ for the spectra shown in Fig. 3.14. Note that the value of $|t_3|$ is here larger than expected in transition metal oxides where it is in general smaller than the three-site hopping term $\tau = J/4$. The spectral density $A(\mathbf{k},\omega)$ contains now the combined effects of the three-site terms $\propto \tau$ and third-neighbour hopping $\propto t_3$ and one finds that $t_3$, depending on its sign, can either amplify or weaken the quasiparticle dispersion which stems from the effective three-site hopping, see Fig. 3.14.

*Third versus next nearest neighbour hopping.*— From the above example one can see that the longer-range hopping violates the particle-hole symmetry of the spectral functions. The spectra obtained for the original orbital Hubbard model (3.1) with nearest neighbour hopping $t$ obey the particle-hole symmetry. The three-site superexchange terms arise from this model and therefore these terms also have to follow the particle-hole symmetry. This is in marked contrast to

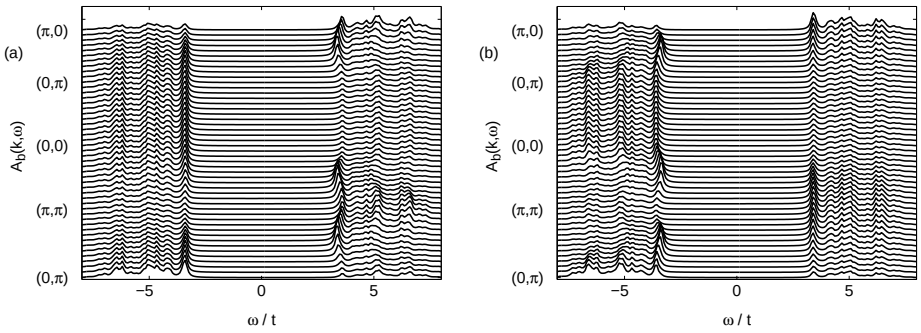


Figure 3.14: Photoemission $[(\omega-\mu)<0]$ and inverse photoemission $[(\omega-\mu)>0]$ part of the spectral density $A_b(\mathbf{k},\omega)$ for a hole inserted into $b$ orbitals obtained within VCA for the $t_{2g}$ model (3.1) with an additional longer-range third-neighbour hopping $t_3$ (3.59). The value $t_3$ is selected so that to suppress dispersion arising from the three-site effective hopping in: (a) the hole (photoemission) sector with $t_3 = 0.1t = J/4$, and (b) in the inverse photoemission sector with $t_3 = -0.1t = -J/4$. Parameter: $U = 10t$. This result was obtained by Maria Daghofer.

the $t_2$ terms that do not respect it [91] or to $t_3$ terms, see Fig. 3.14. As a result, the spectra exhibit a striking *particle-hole asymmetry* — reduced dispersion in the particle (inverse photoemission) sector corresponds to enhanced dispersion in the hole (photoemission) sector and *vice versa*.

It will be shown now that the above asymmetry indeed follows from the difference between the nearest neighbour and next nearest neighbour hopping under particle-hole transformation. While this is transparent for the Hubbard model acting in the full Hilbert space, it is somewhat subtle for the $t$–$J$-like models. Thereby let us focus on the $t_3$ hopping which influences directly the quasiparticle dispersion. The operator for nearest neighbour hopping can be transformed from $\{c_{\mathbf{j}}, c^\dagger_{\mathbf{j}}\}$ electron operators to $\{h^\dagger_{\mathbf{j}}, h_{\mathbf{j}}\}$ hole operators, and one arrives at an identical form for the kinetic energy as long as a phase shift between the two sublattices is introduced:

$$h^\dagger_{\mathbf{j}} = (-1)^{(j_x+j_y)} c_{\mathbf{j}}\,, \qquad h_{\mathbf{i}} = (-1)^{(j_x+j_y)} c^\dagger_{\mathbf{j}}\,, \tag{3.60}$$

where $\mathbf{j} = (j_x, j_y)$ is the lattice site. Hopping along the $a$ axis then becomes

$$\begin{aligned} K_x &= \sum_{\mathbf{j}} (c^\dagger_{\mathbf{j}} c_{\mathbf{j}+\hat{\mathbf{a}}} + c^\dagger_{\mathbf{j}+\hat{\mathbf{a}}} c_{\mathbf{j}}) \\ &= \sum_{\mathbf{j}} \Big\{ (-1)^{j_x+j_y} h_{\mathbf{j}} (-1)^{j_x+1+j_y} h^\dagger_{\mathbf{j}+\hat{\mathbf{a}}} + (-1)^{j_x+1+j_y} h_{\mathbf{j}+\hat{\mathbf{a}}} (-1)^{j_x+j_y} h^\dagger_{\mathbf{j}} \Big\} \\ &= -\sum_{\mathbf{j}} \Big( h_{\mathbf{j}} h^\dagger_{\mathbf{j}+\hat{\mathbf{a}}} + h_{\mathbf{j}+\hat{\mathbf{a}}} h^\dagger_{\mathbf{j}} \Big) \\ &= \sum_{\mathbf{j}} \Big( h^\dagger_{\mathbf{j}} h_{\mathbf{j}+\hat{\mathbf{a}}} + h^\dagger_{\mathbf{j}+\hat{\mathbf{a}}} h_{\mathbf{j}} \Big)\,, \end{aligned} \tag{3.61}$$

and analogously along the $b$ axis. The minus sign for one of the sublattices corresponds to a momentum shift by $\mathbf{q} = (\pi, \pi)$ as can be easily verified in the

Fourier transform.

$$\begin{aligned} h^{\dagger}_{\mathbf{k}} &= \frac{1}{N}\sum_{\mathbf{j}} \mathrm{e}^{\mathrm{i}\mathbf{k}\mathbf{j}}(-1)^{(j_x+j_y)}c_{\mathbf{j}} \\ &= \frac{1}{N}\sum_{\mathbf{j}} \mathrm{e}^{\mathrm{i}(\mathbf{k}+\mathbf{q})\mathbf{j}}c_{\mathbf{j}} = c_{\mathbf{k}+\mathbf{q}}\,. \end{aligned} \tag{3.62}$$

The on-site density-density interaction is not affected by the particle-hole transformation apart from a shift in the chemical potential.

Since the three-site hopping emerges from the Hubbard-like model with nearest neighbour hopping, it respects particle-hole symmetry. Hence it obeys the same rules concerning particle-hole transformation i.e., momentum $(0,0)$ for electrons is mapped to $(\pi,\pi)$ for holes. For the third-neighbour hopping $t_3$ (3.59), however, the above transformation does not work any longer, because both the creation and the annihilation operator act on the same sublattice. Instead the transformation vector would have to be $\mathbf{q}' = (\pi/2,\pi/2)$. Consequently, the combined effect of explicit next nearest neighbour hopping and three-site terms stemming from nearest neighbour processes turns out to be strongly particle-hole asymmetric. For example, negative $t_3$ gives a band in the electron sector with the largest distance from the Fermi energy at momenta $(0,0)$ and $(\pi,\pi)$, and the values nearest to it at $(\pi/2,\pi/2)$, and the same is true for the three-site hopping. Consequently, the two dispersions add together and lead to increased total dispersion, see the photoemission part in Fig. 3.7. On the contrary, in inverse photoemission the direct next nearest neighbour hopping $t_3$ gives a maximal distance at $(\pi/2,\pi/2)$, while maximal energy is still found at $(0,0)$ and $(\pi,\pi)$ for the three-site terms. Therefore, now $t_3$ and three-site hopping $\tau$ compete with each other and the dispersion is weaker. For a particular choice of the model parameters they can even cancel each other, as shown in the inverse photoemission part in Fig. 3.7. Positive $t_3$ leads to the opposite result, see Fig. 3.7. Thus, even large and unphysical values of $t_3$ not only do not destroy the qualitative spectra predicted in the previous sections but generate asymmetry between the photoemission and inverse photoemission part of the spectra, so their contribution can easily be resolved.

*Conclusions concerning the realistic spectra.*— The symmetry arguments leading to Eq. (3.58) and Eq. (3.59) remain valid also for systems with specific $e_g$ orbital degeneracy as observed in certain fluorides with 2D AO order which involves alternating $z^2-y^2$ and $x^2-z^2$ orbitals [92]. In fact, the effective polaron model Eq. (3.32) describes also this case, as we show by a detailed derivation in Appendix B. Hence, we conclude that the photoemission and inverse photoemission spectra for the planar vanadium oxide $Sr_2VO_4$ and for the planar $K_2CuF_4$ or $Cs_2AgF_4$ fluorides should be qualitatively similar to the spectral functions shown in Figs. 3.5 or 3.8.

# Chapter 4

# Understanding hole motion in $LaVO_3$

*This chapter is based on the following publications: (i) K. Wohlfeld, A. M. Oleś, P. Horsch, 'Orbitally induced string formation in the spin-orbital polarons', to appear in Physical Review B* **79** *(2009); and (ii) K. Wohlfeld, 'Spin, orbital, and spin-orbital polarons in transition metal oxides', to appear in AIP Conference Proceedings (2009).*

## 4.1 Introduction

*Cubic vanadates.*— Among the rich class of transition metal oxides, the cubic vanadium oxides (vanadates) are one of the less known 'families' – especially in comparison with their much better investigated 'cousins': the high-$T_c$ cuprate superconductors or the colossal magnetoresistive manganites [20]. Nevertheless, the cubic vandates are worth to look at: As it will be shown below they exhibit the tremendously interesting *orbital* physics phenomena since in this class of compounds spins and orbitals do not decouple and may fluctuate together [93].

*Undoped case.*— Let us be more specific and concentrate on one of the most prominent examples of the cubic vandates: $LaVO_3$. This crystal has a typical perovskite structure in which the vanadium ions can be viewed as effectively forming an almost undistorted cubic lattice [19]. The nominal valence of the vanadium ions is $V^{4+}$ whereas all other ions have filled shells. Thus, the $3d$ orbitals on the vanadium ions are occupied by two electrons and the electronic bands near the Fermi level should be predominantly formed due to the effective hopping $t$ between these orbitals via oxygen ions. In the 'graduate condensed-matter textbook' this would typically mean that such a system would be considered metallic. However, due to the very large on-site Coulomb repulsion $U > W$ between electrons in the $3d$ orbitals the electrons localize and a Mott-Hubbard insulating state is formed [19] (where as before $W = 8t$ while $t$ stands for the effective hopping of $3d$ electrons).

So far, however, $LaVO_3$ can be considered just as another example of the Mott insulators, which, at least to the author, do not seem to be particularly

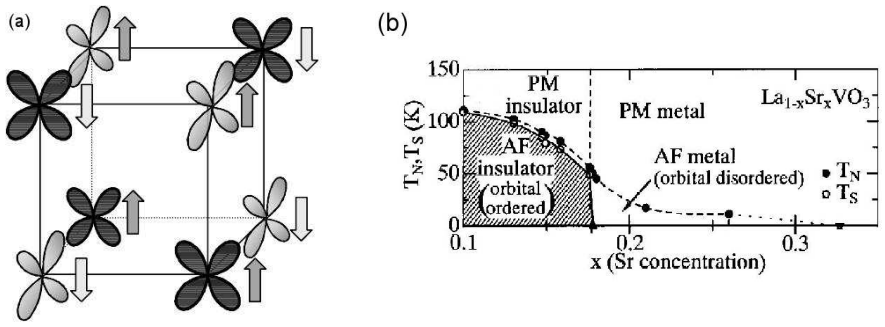


Figure 4.1: Panel (a), reproduced after Ref. [94], shows the magnetic and orbital order stable below ca. 140 K in $LaVO_3$. One electron occupies either the $d_{zx}$ or the $d_{yz}$ orbitals (shown in a very simplified, yet distinguishable, form in the figure) while the other one always occupies the $d_{xy}$ orbital (not shown). Both of them form the $S = 1$ spins which are depicted by arrows. Furthermore, the $dzx$ and $d_{yz}$ occupied orbitals alternate and form the $G$-AO order whereas the $S = 1$ spins are aligned along the $c$ axis and alternating along the $a$ and $b$ directions forming the $C$-AF phase (see also text). Panel (b), reproduced after Ref. [19], shows the phase diagram of $La_{1-x}Sr_xVO_3$. Note the differences between the notation used in the figure (Ref. [94]) and in the text: the temperature in which the $G$-AO orbital order sets in is depicted in the figure by '$T_S$' whereas the $C$-AF phase is denoted with the 'AF' letters in the figure.

interesting, mainly for being very hard to understand.[1] What makes this compound indeed very interesting is the proximity of the onset of the magnetic and orbital ordering which sets in at $T_N \sim 143$ K and $T_O \sim 141$ K, respectively [24, 25], with both of these orderings of relatively complex type. Namely, the magnetic phase is of a $C$-AF–type (AF $ab$ plane with a FM order along the $c$ direction) whereas the orbital order is of a $G$-AO–type (AO order of $d_{zx} \equiv b$ and $d_{yz} \equiv a$ orbitals in all three cubic directions and always occupied $d_{xy}$ orbital); see also Fig. 4.1(a). Since the Jahn-Teller coupling in cubic vanadates is very weak the magnetically and orbitally ordered states could only be explained by some sort of purely electronic mechanism. Indeed, as shown in Ref. [83], the electrons in the Mott insulating phase, although localized, perform virtual hoppings between neighbouring sites leading to such superexchange interactions that the observed experimentally ordered phases could be stable.

*Hole doped case.*— Although these phenomena associated with $LaVO_3$ would alone suffice to justify the above mentioned 'existence of interesting orbital physics phenomena in the cubic vanadates' there are yet even more peculiar experimental observations associated with this class of compounds. They concern the properties of the lightly doped cubic vanadate $La_{1-x}Sr_xVO_3$ [19]. It occurs that in this strongly correlated compound the $C$-AF and $G$-AO ordered Mott insulating phase is not only stable for $x = 0$ but also persists to a relatively high value of hole doping $x = 0.178$ [19]. Rather surprisingly, the $C$-AF phase remains stable up to an even higher value of $x = 0.26$ although in this

[1] Daniel I. Khomskii (unpublished lecture notes on condensed matter theory for graduate students at the University of Groningen).

regime the insulating and orbital ordered phase has already disappeared; see also Fig. 4.1(b) [19]. As, in the ionic picture, $x$ stands for the introduction of holes into the $3d$ orbitals of the vanadium ions (where a nominal valence upon doping changes as $3d^{2-x}$) it remains a challenge to explain why the ordered and insulating states persist to such high dopings.[2] Besides, somewhat similar phase diagrams have been observed in other doped cubic vanadates such as $Pr_{1-x}Ca_xVO_3$, $Nd_{1-x}Sr_xVO_3$ or even to some extent in $Y_{1-x}Ca_xVO_3$ [25]. In fact, in all these cases the lattice distortions contribute significantly [25] to the hole localization and thus we would like to concentrate on the (almost) undistorted compound $La_{1-x}Sr_xVO_3$ in the further analysis.

Actually, one might in principle expect to resolve some of these puzzles by comparing the phase diagram of the doped cubic vanadates to those of the high-$T_c$ superconducting cuprates or the colossal magnetoresistive manganites. However, such a comparison only further enhances the lack of understanding of the doped cubic vanadates. First, in the cuprates such as $La_{2-x}Sr_xCuO_4$ the AF order disappears very quickly with doping $x$, i.e. already for $x \sim 0.02$ [20]. This is despite the fact that the value of the superexchange constant $J$ is relatively high there which would lead to larger magnetic energy in the cuprates than in the vanadates. This suggests that, among other factors, it is the orbital dynamics which could be responsible for the difference between the totally distinct behaviour upon hole doping of these two classes of compounds. Second, a similar conjecture can be drawn from the comparison between the vanadates and the manganites. In the latter ones, e.g. in $La_{1-x}Sr_xMnO_3$ the AO orbital Mott insulating state is stable up to $x \sim 0.18$ [97], i.e. almost to the same level as in $La_{1-x}Sr_xVO_3$. However, $La_{1-x}Sr_xMnO_3$ has FM order already in the insulating planes but $La_{1-x}Sr_xVO_3$ has AF planes – this again suggests that it is the orbital dynamics which governs the behaviour of the doped holes in the doped cubic vanadates.

*Main goals of the chapter.*— Summarizing, perhaps the most important feature of the experimental phase diagram of the lightly ($x < 0.18$) hole doped $La_{1-x}Sr_xVO_3$ is that: the orbital dynamics seems to drive the hole motion there whereas the spins seem to be somewhat 'hidden'. Since the problem of the lightly hole doped cubic vanadates has, with one exception (see below), never been studied before, even the simplest theoretical studies on the hole doped cubic vanadates should shed some light on this issue. Therefore, in this chapter of the thesis, we look at the problem of the motion of a single hole introduced into the orbitally and magnetically ordered plane of $LaVO_3$. It should be noted that the studies presented in Ref. [94] revealed the role of the AO and FM order stable along the third (not studied here) direction in the doped $La_{1-x}Sr_xVO_3$, and explained the differences between the doped $Y_{1-x}Ca_xVO_3$ and $La_{1-x}Sr_xVO_3$ but, by the very nature of that 1D model, could not address the problems mentioned above. This is because, contrary to the problem solved in this chapter, the hole moving along the third ($c$) cubic direction couples to spin and orbital dynamics *separately*: either orbitons (orbital excitations) in the lightly doped $C$-AF phase of $La_{1-x}Sr_xVO_3$, or magnons (spin excitations) in the very lightly doped $G$-AF phase of $Y_{1-x}Ca_xVO_3$ [94].

Thus, the main goals are to investigate: (i) what the proper $t$–$J$ model, which

[2] On the other hand, the unusual coexistence of the $C$-AF phase and the metallic phase in the intermediate hole-doped regime is to some extent explained using the classical double exchange model adopted to the $t_{2g}$ orbital symmetries, see Refs. [95, 96].

governs the hole motion in the 2D AF spin- and AO orbitally-ordered state of $LaVO_3$, looks like, (ii) whether the hole can move coherently in $LaVO_3$, (iii) whether the orbital dynamics indeed seems to influence the hole motion much more than the spin dynamics, and (iv) what is the impact of the results obtained here on the understanding of the experimental phase diagram of the lightly doped cubic vandates. Actually, it will occur that by working out the answers to the above questions we will also predict the main features of the photoemission spectra of the cleaved samples of $LaVO_3$ with polarization corresponding to the *ab* planes.

*Structure of the chapter.*— The chapter is organized as follows. In Sec. 4.2 we start the analysis by looking at the anticipated features of the new *t*-*J* model which is derived in Sec. 4.3. Next, we solve the model in the case of the one hole added to the undoped ground state: (i) we reduce the model to the polaron-type Hamiltonian using the slave fermion approach in Sec. 4.4.1, (ii) we derive the equations for the Green's functions using the SCBA in Sec. 4.4.2, (iii) we solve the equations obtained in point (ii) analytically (in some range parameters) and numerically on a finite mesh of the momentum $\mathbf{k}$ points (Sec. 4.4.3). Then, in Sec. 4.5 the results are discussed where, in particular, we analyse the composite interplay of spin and orbital dynamics on the hole motion. Finally, we draw some conclusions in Sec. 4.6 and add some general statements concerning the hole motion in various spin and/or orbitally ordered states in the *Postscriptum* in Sec. 4.7.

## 4.2 The $t_{2g}$ *spin-orbital* $t$–$J$ model with three-site terms

*'Rough' predictions of the new t-J model.*— It is clear that due to the $t_{2g}$ orbital degeneracy present in the $3d$ states on the vanadium ions in $La_{1-x}Sr_xVO_3$ even the simplest low energy model for correlated electrons should include the orbital degrees of freedom [73, 74]. Thus, the simple Hubbard model which describes the correlated electrons within the $s$ orbitals would not be sufficient and consequently also the standard *t*-*J* model cannot describe properly the phenomena present in lightly doped cubic vanadates (compare appropriate discussion in Chapter 1 and Chapter 3.2). However, before we move on and derive such a model step-by-step (see Sec. 4.3) let us try to anticipate the results obtained there.

Actually, the $J$ part of this new *t*-*J* model is presented in Ref. [83] where the undoped classical ground state is also discussed. This state agrees with the one observed experimentally and is precisely the same as discussed in Sec. 4.1: the $C$-AF and the $G$-AO ordered phase. Next, one can try to imagine what happens when a single hole is doped into the *ab* plane of such a state (this is the limit in which we want to study the solutions of the new *t*-*J* model), cf. Fig. 4.2. In the beginning this seems to be not very hard – one only needs to recall the discussion of Chapter 3. There it was shown that a hole in the AF state is mobile due to spin quantum fluctuation (compare also Ref. [23]) whereas a hole in the $t_{2g}$ AO state was mobile only after the three-site terms were included in the model (see also Ref. [85]). However, then an interesting problem arises: would a hole in a state with both orderings behave rather like the one in an AF

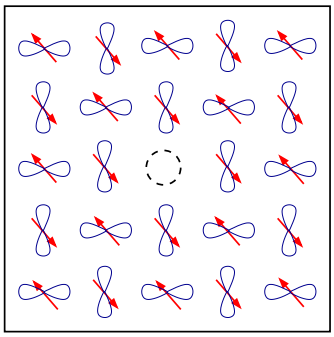

Figure 4.2: Artist's view of a single hole introduced into the spin and orbitally ordered $ab$ plane of $LaVO_3$ [the 3D order present in $LaVO_3$ is shown in Fig. 4.1(a)]. The electrons occupy the $d_{yz}$ and $d_{zx}$ degenerate orbitals forming the classical AO state (their projections along the $a$ and $b$ axis are shown) whereas the electron spins alternate on the neighbouring sites forming the classical AF state. Note that the electrons in the *always* occupied $d_{xy}$ orbitals are not shown for clarity although their spins couple via the Hund's rule to the electron spins in $d_{zx}$ and $d_{yz}$ orbitals and contribute to total spins $S = 1$ in the AF state (besides, at the hole position spin $1/2$ is left).

state or rather like the one in an AO state or in a totally different way? This cannot be answered easily and suggests that a new approach to the solution of this new $t$–$J$ model in the 'one-doped-hole' regime is needed. But let us now try to analyze first why such a problem arises at all.

*Reasons for no 'rough' predictions.*— In fact, here the mere coexistence of the AF and AO order in the undoped case represents a very exotic physics: it formally violates [93] the Goodenough-Kanamori rules [56, 55] that state complementary spin and orbital order in the ground state of a crystal with magnetic and orbital ordering, i.e. either FM spin coexisting with AO order, or AF spin coexisting with FO order. Although these rules are valid on the condition that the orbitals cannot fluctuate and cannot be treated as the dynamical variables they have been very successfull in the prediction of the ordered phase of various compounds, such as e.g. $KCuF_3$ with FM and AO order in the $ab$ planes and the AF and FO order along the $c$ axis. As in the cubic vanadates the Goodenough-Kanamori rules are violated this suggests that most probably[3] the reason for the violations is that the orbitals should be treated as dynamical variables. Actually, indeed there are strong quantum fluctuations of the $\{d_{yz}, d_{zx}\}$ orbitals along the $c$ direction [83] which are responsible for the coexistence of the AO and AF order in the plane [83] which further supports the above claim.

*More careful approach to the problem needed.*— The main lesson from the last paragraph is that a more careful approach to obtain the solutions of the new $t$-$J$ model is needed: one has to *take into account the spins and orbitals on equal footing* as both types of degrees of freedom have to be treated as dynamical variables. Obviously, such approach was not needed for the standard $t$-$J$ model without orbital degrees of freedom but more interestingly it was also not needed

[3] Logically one cannot exclude other reasons for the violation of these rules.

for the $t$-$J$ model describing the situation in the $ab$ planes of the manganites. In the latter case the Goodenough-Kanamori rules were not violated and the undoped ground state was the FM and AO state which meant that the hole could move freely in the spin sector and it solely coupled to the orbital dynamics [82].

Thus not only we need a new $t$-$J$ model to describe the physics present in the lightly doped cubic vanadates but also we need a new approach to get the solutions of this model. More precisely, in the case of the one hole doped to the half-filled state this means that the hole will couple both to the excitations of the AO ordered state (orbitons) and the AF ordered state (magnons). In the following sections we will present the mathematical framework to investigate the ideas of this section.

## 4.3 The model

### 4.3.1 The $t_{2g}$ spin-orbital $t$–$J$ Hamiltonian

*Hubbard-like model.*— The starting point is the multiorbital Hubbard model relevant for the $t_{2g}$ orbitals in the transition metal oxides with the perovskite structure [98, 99],

$$\begin{aligned}\mathcal{H} &= -t\sum_{\langle\mathbf{ij}\rangle||\gamma}\sum_{\mu(\gamma),\sigma}\left(d^{\dagger}_{\mathbf{i}\mu\sigma}d_{\mathbf{j}\mu\sigma}+\text{H.c.}\right)+U\sum_{\mathbf{i}\mu}n_{\mathbf{i}\mu\uparrow}n_{\mathbf{i}\mu\downarrow}\\ &+(U-\frac{5}{2}J_H)\sum_{\mathbf{i},\mu<\nu,\sigma\sigma'}n_{\mathbf{i}\mu\sigma}n_{\mathbf{i}\nu\sigma'}-2J_H\sum_{\mathbf{i},\mu<\nu}\mathbf{S}_{\mathbf{i}\mu}\cdot\mathbf{S}_{\mathbf{i}\nu}\\ &+J_H\sum_{\mathbf{i}\mu\neq\nu}d^{\dagger}_{\mathbf{i}\mu\uparrow}d^{\dagger}_{\mathbf{i}\mu\downarrow}d_{\mathbf{i}\nu\downarrow}d_{\mathbf{i}\nu\uparrow},\end{aligned}\tag{4.1}$$

where $U$ is the intraorbital Coulomb repulsion and $J_H$ is the on-site Hund's exchange interaction. Here the $d^{\dagger}_{\mathbf{i}\mu\sigma}$ operator stands for creation of an electron with spin $\sigma$ in one of the three $t_{2g}$ orbitals, $\mu\in\{d_{xy},d_{yz},d_{zx}\}$. Note that the hopping is allowed only between the same $t_{2g}$ orbitals and $\mu(\gamma)$ (where $\gamma=a,b,c$ is a cubic direction) is chosen in such a way that the electron in each $t_{2g}$ orbital hops only in the allowed plane, cf. Ref. [71] or the more detailed discussion on this issue in Chapter 3. Besides, the summations in the interaction terms are done in such a way that each pair of the orbitals is included only once and the spin operator is defined as:

$$\mathbf{S}_{\mathbf{i}\mu}=\{d^{\dagger}_{\mathbf{i}\mu\uparrow}d_{\mathbf{i}\mu\downarrow},d^{\dagger}_{\mathbf{i}\mu\downarrow}d_{\mathbf{i}\mu\uparrow},\frac{1}{2}(n_{\mathbf{i}\mu\uparrow}-n_{\mathbf{i}\mu\downarrow})\}\tag{4.2}$$

Let us also note, that this Hamiltonian describes rigorously the multiplet structure of the $d^2$ and $d^3$ ions in the $t_{2g}$ subspace as only one Hund's exchange element is involved [99].

*Central Hamiltonian of this chapter.*— Applying the canonical perturbation expansion of Chapter 1 to the Hamiltonian Eq. (4.1) for the case of the two electrons per site, relevant for the planes of lightly doped cubic vanadates, we obtain the Hamiltonian of the spin-orbital $t$–$J$ model with the three-site terms:[4]

$$H=H_t+H_J+H_{3\text{s}},\tag{4.3}$$

[4] In the literature the $t$–$J$ model *with* three-site terms is also called the strong-coupling model [80]. However, we will not use this name since throughout this thesis we deal with

where the $H_t$ is the kinetic energy in the constrained Hilbert space with no 'double occupancies' (see Sec. 4.3.2), $H_J$ describes the superexchange terms (see Sec. 4.3.3) and finally $H_{3s}$ are the three-site terms (see Sec. 4.3.4). Please note that unlike in the previous chapter we will not give here the explicit expressions for the $\mathcal{T}_0$, $\mathcal{T}_+$, and $\mathcal{T}_-$ processes (see Chapter 1 for their definition) as they are rather tedious. This is further backed by the fact that the complicated $J$ part of the $t$–$J$ model has been already derived [100] while for the kinetic and three-site terms will not be needed (see below).

### 4.3.2 The kinetic energy term

*Explicit form.*— The kinetic energy term of the $t_{2g}$ spin-orbital $t$-$J$ model, which describe the hopping of the electrons in the constrained Hilbert space, i.e. in the space with singly occupied or doubly occupied sites (the lowest Hubbard subband of the model), follow in a straightforward way from the unconstrained hopping of electrons residing in the $t_{2g}$ orbitals. Thus in the $ab$ plane, which is under consideration here, electrons in $d_{yz} \equiv a$ ($d_{zx} \equiv b$) orbitals can hop only along the $b$ ($a$) direction. Besides, we will assume here that the $d_{xy}$ orbital does not contribute to hopping elements as it lies lower in energy and is always occupied by one electron in the half-filled and lightly hole-doped regime of cubic vanadates [101]. Hence, we arrive at

$$H_t = -t \sum_{\mathbf{i},\sigma} P \left( \tilde{b}^\dagger_{\mathbf{i},\sigma} \tilde{b}_{\mathbf{i}+\hat{\mathbf{a}},\sigma} + \tilde{a}^\dagger_{\mathbf{i},\sigma} \tilde{a}_{\mathbf{i}+\hat{\mathbf{b}},\sigma} + \text{H.c.} \right) P. \tag{4.4}$$

Here the use of the constrained operators

$$\tilde{b}^\dagger_{\mathbf{i}\sigma} = b^\dagger_{\mathbf{i}\sigma}(1 - n_{\mathbf{i}b\bar{\sigma}})(1 - n_{\mathbf{i}a\bar{\sigma}})(1 - n_{\mathbf{i}a\sigma}), \tag{4.5}$$

and

$$\tilde{a}^\dagger_{\mathbf{i}\sigma} = a^\dagger_{\mathbf{i}\sigma}(1 - n_{\mathbf{i}a\bar{\sigma}})(1 - n_{\mathbf{i}b\bar{\sigma}})(1 - n_{\mathbf{i}b\sigma}), \tag{4.6}$$

means that the hopping is allowed only in the constrained Hilbert space. Besides, since the Hund's coupling dominates over the kinetic processes, $J_H \gg t$, in the cubic vanadates [102] we project the final states resulting from the electron hopping onto the high spin states, which is denoted by the $P$ operators in Eq. (4.4). Note that Eq. (4.4) is a generalization of Eq. (3.6) valid only for spinless fermions in the $t_{2g}$ system under consideration.

### 4.3.3 The spin-orbital superexchange terms

*Explicit form.*— The spin-orbital superexchange in cubic vanadates is derived in Ref. [100] [see Eqs. (6.5)-(6.7) there]. It reads,

$$H_J = H_{J(1)} + H_{J(2)} + H_{J(3)}, \tag{4.7}$$

many different extensions of the standard $t$–$J$ models and the strong-coupling model is just another variation of such extended version of the $t$–$J$ model. See also a similar footnote in Chapter 3.3.1.

where

$$H_{J(1)} = -\frac{1}{6} J r_1 \sum_{\langle \mathbf{ij} \rangle} (\mathbf{S_i} \cdot \mathbf{S_j} + 2) \left( \frac{1}{4} - T_\mathbf{i}^z T_\mathbf{j}^z \right), \tag{4.8}$$

$$H_{J(2)} = \frac{1}{8} J \sum_{\langle \mathbf{ij} \rangle} (\mathbf{S_i} \cdot \mathbf{S_j} - 1) \left( \frac{19}{12} \mp \frac{1}{2} T_\mathbf{i}^z \mp \frac{1}{2} T_\mathbf{j}^z - \frac{1}{3} T_\mathbf{i}^z T_\mathbf{j}^z \right), \tag{4.9}$$

$$H_{J(3)} = \frac{1}{8} J r_3 \sum_{\langle \mathbf{ij} \rangle} (\mathbf{S_i} \cdot \mathbf{S_j} - 1) \left( \frac{5}{4} \mp \frac{1}{2} T_\mathbf{i}^z \mp \frac{1}{2} T_\mathbf{j}^z + T_\mathbf{i}^z T_\mathbf{j}^z \right). \tag{4.10}$$

Here: $\mathbf{S}_i$ is a spin $S = 1$ operator, $T_\mathbf{i}^z = (\tilde{n}_{\mathbf{i}b} - \tilde{n}_{\mathbf{i}a})/2$ is a pseudospin $T = 1/2$ operator, and the superexchange constant $J = 4t^2/U$ with $U$ being the effective repulsion between electrons on the same vanadium site and in the same orbital and with $t \ll U$ being the effective hopping between vanadium ions, see Eq. (4.1). The factors $r_1 = 1/(1-3\eta)$ and $r_3 = 1/(1+2\eta)$ (where $\eta = J_H/U$) account for the Hund's coupling $J_H$ and originate from the energy splitting of various $d^3$ excited states due to the various possible spin and orbital configurations (multiplet structure) [83]. Let us recall, that superexchange Hamiltonian (4.7) was derived [100] with the assumption that the $d_{xy}$ orbital was singly occupied at each vanadium ion (see also discussion in Sec. 4.3.2. Besides, in principle Hamiltonian (4.7) was originally derived for the undoped case and should be modified for the doped case by adding the superexchange interactions due to the existence of the $d_i^1 d_j^1$ and $d_i^1 d_j^2$ nearest neighbour configurations. However, the contributions of these terms should be very small in the discussed here small doping regime and they will be neglected.

### 4.3.4 The three-site terms

*Identification of 'important' three-site terms.*— The three-site terms have not been derived before for the case of the $d^2$ systems with spin and orbital degrees of freedom. These terms, although frequently neglected, can play an important role in the coherent hole propagation in orbital systems (see Chapter 3 or Ref. [85]). However, in the present case the derivation of all possible three-site terms is relatively tedious and leads to a complex expression. Fortunately, it was shown in Chapter 3 or Ref. [85] (for orbital systems) and in Ref. [80] (for spin systems) that the only three-site terms which occurred to be relevant for the lightly doped systems were these which did not contribute to the coupling between hole and orbital or spin excitation but merely contributed to the free hole motion (see also Sec. 4.4.1). Nevertheless, we discuss first the possible role of the neglected three-site terms in Sec. 4.5.1.

*Derivation of the 'important' three-site terms.*— In what follows, using the canonical perturbation theory of Chapter 1, we derive the three-site terms which would contribute to such a motion of a single hole that it does not disturb the AO and AF order present in the undoped ground state (see also discussion in the beginning of Sec. 4.4.1). We start the analysis by looking at the possibility of the free hole motion along the $a$ direction, see Fig. 4.3. We would like to move the electron in the $b$ orbital (the one in the $a$ orbital does not hop along this direction) from the right site to the left site over the middle site in such a way that the spin and orbital order present before the process stays intact (in the language of Chapter 1 this means transfering the electron first with the $\mathcal{T}_+$

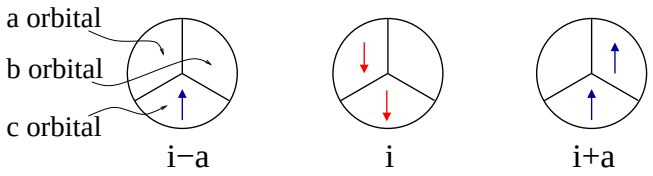


Figure 4.3: Three neighbouring sites along the $a$ direction with such an AO and AF order that the electron on site $\mathbf{i}+\hat{\mathbf{a}}$ can move over the intermediate site $i$ via the superexchange process $\propto J$ to site $\mathbf{i}-\hat{\mathbf{a}}$ without disturbing the AO and AF order.

and then with the $\mathcal{T}_-$ process). This confines the choice of the possible high energy intermediate $d_i^3$ configurations at the middle site to the states with the total spin $|3/2,-1/2\rangle$ (see Fig. 4.3) and the possible states: (i) ${}^4A_2$ with energy $U-3J_H$, (ii) ${}^2E\frac{1}{2}\theta$ state with energy $U$, (iii) ${}^2E\frac{1}{2}\varepsilon$ state with energy $U$. Note that all the intermediate states with orbital singlets are excluded as they would require orbital excitations. Thus, one arrives at the following contribution (see Chapter 1 for more details) to the free hole motion which arises due to the three-site term processes along the $a$ direction,

$$-\left(\frac{1}{3}\frac{1}{1-3\eta}+\frac{2}{3}\right)\frac{t^2}{U}\,P\,\tilde{b}^{\dagger}_{\mathbf{i}-\hat{\mathbf{a}},\sigma}\tilde{n}_{\mathbf{i}a\bar{\sigma}}\tilde{b}_{\mathbf{i}+\hat{\mathbf{a}},\sigma}\,P. \tag{4.11}$$

A similar consideration but for the processes along the $b$ direction yields

$$-\left(\frac{1}{3}\frac{1}{1-3\eta}+\frac{2}{3}\right)\frac{t^2}{U}\,P\,\tilde{a}^{\dagger}_{\mathbf{i}-\hat{\mathbf{b}},\sigma}\tilde{n}_{\mathbf{i}b\bar{\sigma}}\tilde{a}_{\mathbf{i}+\hat{\mathbf{b}},\sigma}\,P. \tag{4.12}$$

However, the $90^0$ processes, called also around 'the corner' (see Chapter 3), such as e.g. first the hopping of an electron along the $b$ direction and then along the $a$ direction would not contribute to the free motion. This is because an electron in a particular orbital can hop only along one particular cubic direction and thus one would have to interchange the hopping of electrons at the intermediate high energy site which would lead to the orbital excitation.

Hence, after adding the sums over all sites $i$ and spins $\sigma$ and the conjugate terms to Eqs. (4.11)-(4.12) one ends up with:

$$\begin{aligned} H_{3s}=&-\frac{1}{12}J\,(r_1+2)\sum_{\mathbf{i},\sigma}P\left(\tilde{b}^{\dagger}_{\mathbf{i}-\hat{\mathbf{a}},\sigma}\tilde{n}_{\mathbf{i}a\bar{\sigma}}\tilde{b}_{\mathbf{i}+\hat{\mathbf{a}},\sigma}+\text{H.c.}\right)P \\ &-\frac{1}{12}J\,(r_1+2)\sum_{\mathbf{i},\sigma}P\left(\tilde{a}^{\dagger}_{\mathbf{i}-\hat{\mathbf{b}},\sigma}\tilde{n}_{\mathbf{i}b\bar{\sigma}}\tilde{a}_{\mathbf{i}+\hat{\mathbf{b}},\sigma}+\text{H.c.}\right)P. \end{aligned} \tag{4.13}$$

Note that these terms are $\propto J$ and hence are of the same order in $t^2/U$ as superexchange terms (4.7).

Finally, one may wonder how Eq. (4.13) could contribute to the free hole motion since it contains four electron operators. However, the number operators which stand in the middle of this equation only reflect the relevant configurations and in fact can be dropped out in the assumed here AO and AF order. More precisely, let us introduce two sublattices $\{A,B\}$ in such a way that e.g. the

intermediate site in Fig. 4.3 belongs to the sublattice $A$ (with all $a$ orbitals occupied and the spins pointing 'downwards'); let us also concentrate on Eq. (4.11). Since we assumed that in this sublattice the electrons have spin 'down' and are located in the $a$ orbital thus if, in addition, one assumes that $\sigma =\uparrow$ in Eq. (4.11), then one is allowed to write $\tilde{n}_{\mathbf{i}a\downarrow} \equiv 1$ and drop out this operator. Obviously, if one assumed $\sigma =\downarrow$ or that $i \in B$, then one would not get any contribution. Thus for some particular choices of $\sigma$ and the sublattice indices Eq. (4.11) would describe the free hole motion whereas in some other cases this equation would not contribute at all. While writing down Eq. (4.45) in Sec. 4.4.1 we take care of this problem.

## 4.4 Method and results

### 4.4.1 The slave-fermion approach

*Slave-particle formalism.*— Similarly as in Chapter 3 also here we will calculate the properties of the half-filled system with one doped hole using the slave fermion method which takes care of the constraint of 'no double occupancies' in the kinetic energy term of the $t$–$J$ model. In fact, this is a method of choice for low doped $t$–$J$ models [20] with some kind of magnetic/orbital order in the half-filled ground state.

*Undoped case: low energy excitations.*— It was shown in Ref. [83] that the classical ground state of the 3D version of the Hamiltonian Eq. (4.7) is a $C$-AF state and $G$-AO ordered state. Thus, the classical undoped ground state of the Hamiltonian Eq. (4.3) is the (Néel ordered) AF state and AO state. Certainly, this is not the eigenstate of the Hamiltonian and thus the full description of the system should also take into account the quantum fluctuations around such a classical ground state. Below, we will calculate them by transforming the spins and pseudospins into the appropriate Schwinger bosons and then using the linear spin wave (LSW) and linear orbital wave (already denoted as LOW, see previous Chapter) approximation. In addition from the LSW and LOW approach, we will obtain the spectrum of the low energy excited states.

First, in the classical state we introduce two sublattices $A$ and $B$ such that: (i) all $a$ ($b$) orbitals are occupied in the perfect AO state in sublattice $A$ ($B$), and (ii) spins pointing 'downwards' ('upwards') are located on sublattice $A$ ($B$). Next we rotate spins and pseudospins on sublattice $A$ so that all the spins and pseudospins in the whole lattice are in the same local eigenstates with eigenvalues of $S^z_{\mathbf{i}}$ and $T^z_{\mathbf{i}}$.

Second, we introduce Schwinger bosons $t$ and $f$ such that:

$$T^z_{\mathbf{i}} = \frac{1}{2}(n_{t\mathbf{i}b} - n_{t\mathbf{i}a}), \tag{4.14}$$

$$S^z_{\mathbf{i}} = \frac{1}{2}(n_{f\mathbf{i}\uparrow} - n_{f\mathbf{i}\downarrow}), \tag{4.15}$$

$$S^+_{\mathbf{i}} = f^\dagger_{\mathbf{i}\uparrow} f_{\mathbf{i}\downarrow}, \tag{4.16}$$

$$S^-_{\mathbf{i}} = f^\dagger_{\mathbf{i}\downarrow} f_{\mathbf{i}\uparrow}, \tag{4.17}$$

with the constraints

$$\sum_{\gamma=a,b} t^\dagger_{\mathbf{i}\gamma} t_{\mathbf{i}\gamma} = 1, \quad \sum_{\sigma=\uparrow,\downarrow} f^\dagger_{\mathbf{i}\sigma} f_{\mathbf{i}\sigma} = 2. \tag{4.18}$$

Third, we transform the Schwinger boson operators into the Holstein-Primakoff bosons $\alpha$ and $\beta$:

$$t^\dagger_{\mathbf{i}b} = \sqrt{1 - t^\dagger_{\mathbf{i}a} t_{\mathbf{i}a}} \equiv \sqrt{1 - \beta^\dagger_{\mathbf{i}} \beta_{\mathbf{i}}}, \tag{4.19}$$

$$t^\dagger_{\mathbf{i}a} = \beta^\dagger_{\mathbf{i}}, \tag{4.20}$$

$$f^\dagger_{\mathbf{i}\uparrow} = \sqrt{2 - f^\dagger_{\mathbf{i}\downarrow} f_{\mathbf{i}\downarrow}} \equiv \sqrt{2 - \alpha^\dagger_{\mathbf{i}} \alpha_{\mathbf{i}}}, \tag{4.21}$$

$$f^\dagger_{\mathbf{i}\downarrow} = \alpha^\dagger_{\mathbf{i}}, \tag{4.22}$$

where the above constraints are now no longer needed.

Next, we substitute the above transformations into the Hamiltonian $H_J$ and skip higher order terms (LSW and LOW approximation). The latter approximation physically means that the number of bosons $\alpha$ and $\beta$, which describe the fluctuations around the ordered state, is small. This results in the effective substitutions:

$$T^z_{\mathbf{i}} = \frac{1}{2} - \beta^\dagger_{\mathbf{i}} \beta_{\mathbf{i}}, \tag{4.23}$$

$$S^z_{\mathbf{i}} = 1 - \alpha^\dagger_{\mathbf{i}} \alpha_{\mathbf{i}}, \tag{4.24}$$

$$S^+_{\mathbf{i}} = \sqrt{2} \alpha_{\mathbf{i}}, \tag{4.25}$$

$$S^-_{\mathbf{i}} = \sqrt{2} \alpha^\dagger_{\mathbf{i}}. \tag{4.26}$$

Finally, we introduce Fourier transformation separately for each sublattice ($N$ is the total number of sites on both sublattices):

$$\beta_{\mathbf{k}A} = \sqrt{\frac{2}{N}} \sum_{\mathbf{j}\in A} e^{i\mathbf{k}\mathbf{j}} \beta_{\mathbf{j}}, \tag{4.27}$$

$$\beta_{\mathbf{k}B} = \sqrt{\frac{2}{N}} \sum_{\mathbf{j}\in B} e^{i\mathbf{k}\mathbf{j}} \beta_{\mathbf{j}}, \tag{4.28}$$

$$\alpha_{\mathbf{k}A} = \sqrt{\frac{2}{N}} \sum_{\mathbf{j}\in A} e^{i\mathbf{k}\mathbf{j}} \alpha_{\mathbf{j}}, \tag{4.29}$$

$$\alpha_{\mathbf{k}B} = \sqrt{\frac{2}{N}} \sum_{\mathbf{j}\in B} e^{i\mathbf{k}\mathbf{j}} \alpha_{\mathbf{j}}, \tag{4.30}$$

define operators

$$\alpha_{\mathbf{k}\pm} = (\alpha_{\mathbf{k}A} \pm \alpha_{\mathbf{k}B})/\sqrt{2}, \tag{4.31}$$

and perform the standard Bogoliubov transformation for magnons [23]

$$\tilde{\alpha}_{\mathbf{k}\pm} = u_{\mathbf{k}} \alpha_{\mathbf{k}\pm} - v_{\mathbf{k}} \alpha^\dagger_{-\mathbf{k}\pm}, \tag{4.32}$$

where

$$u_{\mathbf{k}} = \sqrt{\frac{1+\nu_{\mathbf{k}}}{2\nu_{\mathbf{k}}}}, \quad v_{\mathbf{k}} = -\mathrm{sgn}(\gamma_{\mathbf{k}})\sqrt{\frac{1-\nu_{\mathbf{k}}}{2\nu_{\mathbf{k}}}}, \tag{4.33}$$

with $\nu_{\mathbf{k}} = \sqrt{1-\gamma_{\mathbf{k}}^2}$ and the structure factor for the square lattice

$$\gamma_{\mathbf{k}} = \frac{1}{2}(\cos k_x + \cos k_y). \tag{4.34}$$

Then, after neglecting constant terms which merely give the classical energy of the undoped ground state, the LSW and LOW Hamiltonian for magnons and orbitons reads:

$$H_J^{eff} = H_{\mathrm{LSW}}^{eff} + H_{\mathrm{LOW}}^{eff}, \tag{4.35}$$

$$H_{\mathrm{LSW}}^{eff} = J_S \sum_{\mathbf{k}} \omega_{\mathbf{k}} (\tilde{\alpha}_{\mathbf{k}+}^{\dagger}\tilde{\alpha}_{\mathbf{k}+} + \tilde{\alpha}_{\mathbf{k}-}^{\dagger}\tilde{\alpha}_{\mathbf{k}-} + 1), \tag{4.36}$$

$$H_{\mathrm{LOW}}^{eff} = J_O \sum_{\mathbf{k}} (\beta_{\mathbf{k}A}^{\dagger}\beta_{\mathbf{k}A} + \beta_{\mathbf{k}B}^{\dagger}\beta_{\mathbf{k}B}), \tag{4.37}$$

where

$$J_O = \eta \frac{2-\eta}{(1-3\eta)(1+2\eta)} J, \tag{4.38}$$

and

$$J_S = \frac{-5\eta^2 - 3\eta + 1}{4(1-3\eta)(1+2\eta)} J. \tag{4.39}$$

in agreement with Eq. (6.11) of Ref. [100] and Eq. (11) of Ref. [103]. Besides, the dispersion relation for the magnons is

$$\omega_{\mathbf{k}} = zS\sqrt{1-\gamma_{\mathbf{k}}^2} \tag{4.40}$$

where $z = 4$ is the coordination number, $S = 1$ is the value of the spin. Let us note that in the regime of reasonable values of $\eta \in [0, 0.20]$: $E_O$ is negative whereas $J_O > 0$ and $J_S > 0$, which means that the classical ground state indeed has coexisting AO and AF order. Furthermore, at temperature $T = 0$ the considered here classical 2D AO and AF ground state is stable with respect to the quantum fluctuations, both in spin and orbital channel. In fact, the orbital order is undisturbed by local Ising excitations, while the quantum AF ground state is modified and the order parameter is renormalized with magnon excitations [23].

*Doped hole: coupling with magnons and orbitons.*— We expect that a doped hole does not modify significantly the classical ground state stable for the half-filled case (see above). This could play a role in the lightly doped regime, but in the case of one hole in the whole plane such a modification is negligible and will be neglected below. Instead, the doped hole may modify its neighborhood by its coupling to the excitations of the classical ground state — magnons and orbitons — which renormalize the hole motion. In order to describe it mathematically, we rewrite $H_t$ (see next paragraph) and $H_{3s}$ (see below) using similar transformations as performed for the half-filled case.

First, we rotate spins and pseudospins on sublattice $A$. Next, using the slave-fermion approach we express the electron operators in terms of the Schwinger

bosons introduced above and in terms of the (constrained) fermionic operators representing holes:

$$\tilde{a}^{\dagger}_{\mathbf{i}\sigma} = \frac{1}{\sqrt{2}} f^{\dagger}_{\mathbf{i}\sigma} t^{\dagger}_{\mathbf{i}a} h_{\mathbf{i}}, \tag{4.41}$$

$$\tilde{b}^{\dagger}_{\mathbf{i}\sigma} = \frac{1}{\sqrt{2}} f^{\dagger}_{\mathbf{i}\sigma} t^{\dagger}_{\mathbf{i}b} h_{\mathbf{i}}. \tag{4.42}$$

Here the constraints on the bosonic operators are as in Eq. (4.18) while $h^{\dagger}_{\mathbf{i}} h_{\mathbf{i}}$ denotes the number of holes at site $\mathbf{i}$.

Note that the factor $\frac{1}{\sqrt{2}}$ is not added 'ad hoc' but originates from a detailed check of the validity of the above equations: it should always be present in the spin $S = 1$ case because e.g. when one annihilates one boson in a two-boson state with the $f$ operator, then a factor $\sqrt{2}$ appears. Due to this factor and the above constraint on the number of bosons the high spin projection operators $P$ in $H_t$ are no longer needed (i.e. quantum double exchange [104] factors are implicitly included in this formalism).

Next, similarly as above, we transform the Schwinger bosons into the Holstein-Primakoff bosons, skip all terms containing more than two bosons, perform Fourier transformation for bosons and (additionally) for holons here, introduce $\alpha_{k\pm}$ operators, and finally perform Bogoliubov transformation to arrive at the Hamiltonian:

$$\begin{aligned} H_t^{eff} =& \frac{zt}{2N} \sum_{\mathbf{k},\mathbf{q_1},\mathbf{q_2}} \Big\{ M_x(\mathbf{k},\mathbf{q_1},\mathbf{q_2}) h^{\dagger}_{\mathbf{k}A} h_{\bar{\mathbf{k}}B} (\tilde{\alpha}_{\mathbf{q}_{1+}} + \tilde{\alpha}_{\mathbf{q}_{1-}}) \beta_{\mathbf{q}_2 A} \\ &+ M_y(\mathbf{k},\mathbf{q_1},\mathbf{q_2}) h^{\dagger}_{\mathbf{k}B} h_{\bar{\mathbf{k}}A} (\tilde{\alpha}_{\mathbf{q}_{1+}} - \tilde{\alpha}_{\mathbf{q}_{1-}}) \beta_{\mathbf{q}_2 B} \\ &+ M_x(\mathbf{k},\mathbf{q_1},\mathbf{q_2}) h^{\dagger}_{\mathbf{k}A} h_{\bar{\mathbf{k}}B} (\tilde{\alpha}^{\dagger}_{-\mathbf{q}_{1+}} - \tilde{\alpha}^{\dagger}_{-\mathbf{q}_{1-}}) \beta_{\mathbf{q}_2 A} \\ &+ M_y(\mathbf{k},\mathbf{q_1},\mathbf{q_2}) h^{\dagger}_{\mathbf{k}B} h_{\bar{\mathbf{k}}A} (\tilde{\alpha}^{\dagger}_{-\mathbf{q}_{1+}} + \tilde{\alpha}^{\dagger}_{-\mathbf{q}_{1-}}) \beta_{\mathbf{q}_2 B} + \text{H.c.} \Big\}, \end{aligned} \tag{4.43}$$

where

$$M_{\mu}(\mathbf{k},\mathbf{q_1},\mathbf{q_2}) = u_{\mathbf{q}_1} \gamma_{k_\mu - q_{1\mu} - q_{2\mu}} + v_{\mathbf{q}_1} \gamma_{k_\mu - q_{2\mu}}, \tag{4.44}$$

with $\mu = x, y$. Here $\bar{\mathbf{k}} = \mathbf{k} - \mathbf{q_1} - \mathbf{q_2}$ follows from momentum conservation, and the coefficients $\{u_{\mathbf{q}_1} v_{\mathbf{q}_1}\}$ are the standard Bogoliubov factors (4.33).

*Doped hole: free dispersion.*— After performing similar transformations as the ones introduced for the $t$ part of the Hamiltonian one obtains that the three-site terms, Eq. (4.13), lead to the following Hamiltonian for the holes

$$H_{3\text{s}}^{eff} = \tau \sum_{\mathbf{k}} \Big\{ \varepsilon_B(\mathbf{k}) h^{\dagger}_{\mathbf{k}B} h_{\mathbf{k}B} + \varepsilon_A(\mathbf{k}) h^{\dagger}_{\mathbf{k}A} h_{\mathbf{k}A} \Big\}, \tag{4.45}$$

where

$$\tau = \frac{1}{4} \frac{1-2\eta}{1-3\eta} J, \tag{4.46}$$

and the free hole dispersion relations on the sublattices are

$$\varepsilon_A(\mathbf{k}) = 2\cos(2k_y), \tag{4.47}$$

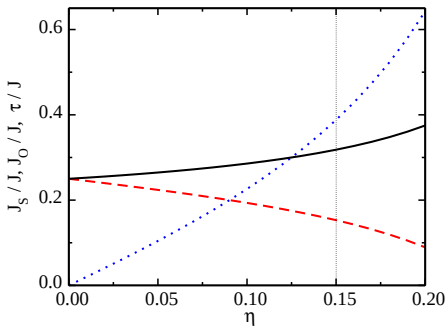


Figure 4.4: The effective spin and orbital exchange interaction $J_S$ (dashed line) and $J_O$ (dotted line) as a function of the Hund's rule coupling $\eta = J_H/U$, respectively. The solid line shows the dependence of the three-site term $\tau$ on $\eta$. The realistic value of $\eta = 0.15$ (cf. Ref. [83]) is indicated by the light dotted line.

and

$$\varepsilon_B(\mathbf{k}) = 2\cos(2k_x). \tag{4.48}$$

Note that, we have neglected all of the three-site terms which lead to the coupling between holes and magnons and/or orbitons. This is physically justified since then such terms would be of the order of $J/4$, i.e. much smaller than the terms in Eq. (4.43). See also Sec. 4.5.1 for further discussion.

Thus in the lightly doped case, when the classical spin and orbital ordered ground state present in the half-filled case is not destroyed, the $t$–$J$ model (4.3) can be reduced to an effective model

$$H^{eff} = H_t^{eff} + H_J^{eff} + H_{3\mathrm{s}}^{eff}, \tag{4.49}$$

see Eqs. (4.35), and (4.43)-(4.45). Actually, this is a polaron-type model with the coupling between fermions (holes) and bosonic excitations (orbitons and magnons), which is relatively easy to solve (see next section). The validity of the mapping between the two models was thoroughly discussed in Ref. [23] and Chapter 3.

Note that the original $t$-$J$ model with three-site terms (4.3) has three parameters $\{J, \eta, t\}$, whereas the effective polaron model given by Eq. (4.49) is more conveniently analysed when using four parameters $\{J_S, J_O, \tau, t\}$, which determine the scale of spin and orbital excitations as well as free hole propagation (due to the three-site terms) and the vertex function ($t$), see below. In what follows we will use either one of these two parameter sets (and only sometimes both of them) depending on the context. Hence, we plot in Fig. 4.4 the functional relation between the parameters $\{J_S, J_O, \tau\}$ on Hund's exchange $\eta$. While the magnon energies $\propto J_S$ decrease with $\eta$, the energy scale of orbitons $\propto J_O$ increases rapidly, so the latter excitations are expected to play an important role in the realistic regime of parameters.

### 4.4.2 The self-consistent Born approximation

*Green's functions.*— The spectral properties of the hole doped into the AF/AO

ground state $|\Phi_0\rangle$ with energy $E_0$ of the $t$–$J$ model Eq. (4.3) at half-filling follow from the Green's functions:

$$G_{a\downarrow}(\mathbf{k},\omega) = \left\langle \Phi_0 \left| a^\dagger_{\mathbf{k}\downarrow} \frac{1}{\omega + H - E_0} a_{\mathbf{k}\downarrow} \right| \Phi_0 \right\rangle , \tag{4.50}$$

$$G_{a\uparrow}(\mathbf{k},\omega) = \left\langle \Phi_0 \left| a^\dagger_{\mathbf{k}\uparrow} \frac{1}{\omega + H - E_0} a_{\mathbf{k}\uparrow} \right| \Phi_0 \right\rangle , \tag{4.51}$$

$$G_{b\downarrow}(\mathbf{k},\omega) = \left\langle \Phi_0 \left| b^\dagger_{\mathbf{k}\downarrow} \frac{1}{\omega + H - E_0} b_{\mathbf{k}\downarrow} \right| \Phi_0 \right\rangle , \tag{4.52}$$

$$G_{b\uparrow}(\mathbf{k},\omega) = \left\langle \Phi_0 \left| b^\dagger_{\mathbf{k}\uparrow} \frac{1}{\omega + H - E_0} b_{\mathbf{k}\uparrow} \right| \Phi_0 \right\rangle . \tag{4.53}$$

However, due to the mapping of the $t$–$J$ model onto the polaron model performed in the last section, it is now convenient to express the above Green's functions in terms of the polaron Hamiltonian $H^{eff}$. This requires that one first writes down the electron operators in terms of the operators used in Eq. (4.49):

$$a_{\mathbf{k}\downarrow} = \frac{1}{\sqrt{N}} \left( \sum_{\mathbf{j}\in A} e^{i\mathbf{k}\mathbf{j}} h^\dagger_{\mathbf{j}} + \sum_{\mathbf{j}\in B} e^{i\mathbf{k}\mathbf{j}} h^\dagger_{\mathbf{j}} \alpha_{\mathbf{j}} \beta_{\mathbf{j}} \right) , \tag{4.54}$$

$$a_{\mathbf{k}\uparrow} = \frac{1}{\sqrt{N}} \left( \frac{1}{\sqrt{2}} \sum_{\mathbf{j}\in A} e^{i\mathbf{k}\mathbf{j}} h^\dagger_{\mathbf{j}} \alpha_{\mathbf{j}} + \sum_{\mathbf{j}\in B} e^{i\mathbf{k}\mathbf{j}} h^\dagger_{\mathbf{j}} \beta_{\mathbf{j}} \right) , \tag{4.55}$$

$$b_{\mathbf{k}\downarrow} = \frac{1}{\sqrt{N}} \left( \sum_{\mathbf{j}\in A} e^{i\mathbf{k}\mathbf{j}} h^\dagger_{\mathbf{j}} \beta_{\mathbf{j}} + \frac{1}{\sqrt{2}} \sum_{\mathbf{j}\in B} e^{i\mathbf{k}\mathbf{j}} h^\dagger_{\mathbf{j}} \alpha_{\mathbf{j}} \right) , \tag{4.56}$$

$$b_{\mathbf{k}\uparrow} = \frac{1}{\sqrt{N}} \left( \sum_{\mathbf{j}\in A} e^{i\mathbf{k}\mathbf{j}} h^\dagger_{\mathbf{j}} \alpha_{\mathbf{j}} \beta_{\mathbf{j}} + \sum_{\mathbf{j}\in B} e^{i\mathbf{k}\mathbf{j}} h^\dagger_{\mathbf{j}} \right) . \tag{4.57}$$

Second, the ground state $|\Phi_0\rangle$ is now a physical vacuum $|0\rangle$, with respect to the Bogoliubov operators $\tilde{\alpha}_{\mathbf{k}\pm}$ and the operators $\beta_{\mathbf{k}}$, with the ground state energy $E$ calculated now in the LSW and LOW approximation. Then, one arrives at the following relations:

$$G_{a\downarrow}(\mathbf{k},\omega) = \frac{1}{2} \left\langle 0 \left| h_{\mathbf{k}A} \frac{1}{\omega + H^{eff} - E} h^\dagger_{\mathbf{k}A} \right| 0 \right\rangle \equiv \frac{1}{2}\, G_{AA}(\mathbf{k},\omega), \tag{4.58}$$

$$G_{b\uparrow}(\mathbf{k},\omega) = \frac{1}{2} \left\langle 0 \left| h_{\mathbf{k}B} \frac{1}{\omega + H^{eff} - E} h^\dagger_{\mathbf{k}B} \right| 0 \right\rangle \equiv \frac{1}{2}\, G_{BB}(\mathbf{k},\omega), \tag{4.59}$$

where the factor $1/2$ is due to the operators $h_{\mathbf{k}A}$ ($h_{\mathbf{k}B}$) being defined separately for each sublattice. Furthermore, the Green's functions

$$G_{a\uparrow}(\mathbf{k},\omega) \ll G_{a\downarrow}(\mathbf{k},\omega)\,, \tag{4.60}$$

$$G_{b\downarrow}(\mathbf{k},\omega) \ll G_{b\uparrow}(\mathbf{k},\omega)\,, \tag{4.61}$$

correspond to excited states and thus can be skipped. Note that the above set of equations follows from the fact that $\beta_{\mathbf{k}}|0\rangle = 0$ and the inequalities are due to

$$\left\langle 0 \left| \frac{\alpha^\dagger_i \alpha_i}{2} \right| 0 \right\rangle \sim \frac{n_0}{2} \sim 0.1\,, \tag{4.62}$$

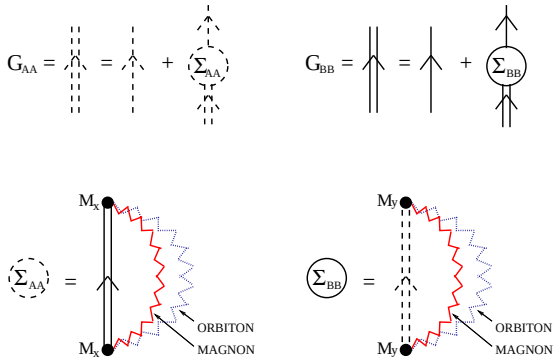


Figure 4.5: Diagrammatic representation of the SCBA equations: top – the Dyson's equation for the $G_{AA}(\mathbf{k},\omega)$ and $G_{BB}(\mathbf{k},\omega)$ Green's functions; bottom – calculation of the respective self-energies. Note the appearance of the two wiggly lines in the calculation of the self-energies coming from the orbiton and the magnon excitations.

where $n_0$ is the average number of spin deviations in the 2D ground state $|0\rangle$. Note that below we will eliminate the ground state energy $E$ to simplify equations.

*Equations for the self-energy.*— As seen in Section 4.4.1 the vertices in the spin-orbital model are more complex than for the standard spin case [23]: (i) one always has two boson and two holon lines at each vertex (instead of just one boson and two holons lines in the standard lowest SCBA order), (ii) one has the sublattice structure (this resembles the orbital case), (iii) one has two kinds of magnons (which we had to introduce in order to keep track of the lattice index). Also, in the LSW and LOW order all the terms $\propto \alpha_i^\dagger \beta_i$ do not contribute (the self-energies for them would require altogether four boson lines instead of just two for $\propto \alpha_i \beta_i$).[5] Hence, we largely follow the route which was proposed for the orbital $t_{2g}$ model in Chapter 3 and obtain the following SCBA equations for the self-energies (see also Fig. 4.5):

$$\Sigma_{AA}(\mathbf{k},\omega) = 2\frac{z^2t^2}{4N^2}\sum_{\mathbf{q_1},\mathbf{q_2}} M_x^2(\mathbf{k},\mathbf{q_1},\mathbf{q_2}) \times G_{BB}(\mathbf{k}-\mathbf{q_1}-\mathbf{q_2},\omega+J_S\omega_{\mathbf{q_1}}+J_0) \tag{4.63}$$

$$\Sigma_{BB}(\mathbf{k},\omega) = 2\frac{z^2t^2}{4N^2}\sum_{\mathbf{q_1},\mathbf{q_2}} M_y^2(\mathbf{k},\mathbf{q_1},\mathbf{q_2}) \times G_{AA}(\mathbf{k}-\mathbf{q_1}-\mathbf{q_2},\omega+J_S\omega_{\mathbf{q_1}}+J_0), \tag{4.64}$$

[5] We have verified analytically that these terms would not lead to any $\mathbf{k}$-dependence in the spectra as in the self-energies describing such processes one can shift the summation over the momenta in such a way that the self-energies are momentum independent (See also Sec. 4.5.1 for a similar calculation concerning the self-energies for two boson lines). Thus, these terms would not change the qualitative feature of the calculated spectra, i.e. that the $\mathbf{k}$-dependence of the quasiparticle states originates entirely from the three-site terms. Besides, one can note that inclusion of such terms would require going beyond the LSW and LOW approximation, i.e. one would have to include the interactions between magnons and/or orbitons.

where the factor 2 in front of the vertex comes from the fact that one has two kinds of magnons (and hence two distinct diagrams). Fortunately, this factor cancels with one of the 2 in the denominator and we obtain that the coupling constant is simply $(t/\sqrt{2})^2$, i.e. we recover the factor $1/\sqrt{2}$ which comes out from the quantum double exchange. The above equations should always be supplemented by the Dyson's equations,

$$G_{AA}(\mathbf{k},\omega) = \frac{1}{\omega + \tau\varepsilon_A(\mathbf{k}) - \Sigma_{AA}}, \tag{4.65}$$

$$G_{BB}(\mathbf{k},\omega) = \frac{1}{\omega + \tau\varepsilon_B(\mathbf{k}) - \Sigma_{BB}}. \tag{4.66}$$

Altogether, Eqs. (4.63)-(4.66) form a self-consistent set of equations which can be solved numerically.

Finally, one can calculate the spectral functions for a hole created in $a$ and $b$ orbital:

$$A_a(\mathbf{k},\omega) = -\frac{2}{\pi}\lim_{\delta\to 0}\,\mathrm{Im}\,G_{a\downarrow}(\mathbf{k},\omega+i\delta) = -\frac{1}{\pi}\lim_{\delta\to 0}\,\mathrm{Im}\,G_{AA}(\mathbf{k},\omega+i\delta)\,, \tag{4.67}$$

$$A_b(\mathbf{k},\omega) = -\frac{2}{\pi}\lim_{\delta\to 0}\,\mathrm{Im}\,G_{b\uparrow}(\mathbf{k},\omega+i\delta) = -\frac{1}{\pi}\lim_{\delta\to 0}\,\mathrm{Im}\,G_{BB}(\mathbf{k},\omega+i\delta)\,, \tag{4.68}$$

where we introduced a factor of 2 in front of the definition of the spectral functions $A_\gamma(\mathbf{k},\omega)$ for convenience.

### 4.4.3 The spectral functions and quasiparticle properties

*Analytic calculations.*— It occurs that in the case when the three-site terms are absent (i.e. for $\tau \equiv 0$) one can easily prove two important properties obtained with the SCBA Eqs. (4.63)-(4.64): (i) the self-energies are $\mathbf{k}$-independent, (ii) the spectral functions contain the quasiparticle state for finite value of the exchange parameter $J$ (equivalently $J_S$ *or* $J_O$).

First, we show property (i). Since we have assumed that $\tau = 0$ we can rewrite SCBA equations (4.63)-(4.64) together with Dyson's equations (4.65)-(4.66) in the following manner:

$$\Sigma_{AA}(\mathbf{k},\omega) = \frac{z^2t^2}{2N^2}\sum_{\mathbf{q_1},\mathbf{q_2}} \frac{M_x^2(\mathbf{k},\mathbf{q_1},\mathbf{q_2})}{\omega + J_S\omega_{\mathbf{q}_1} + J_O - \Sigma_{BB}(\mathbf{k}-\mathbf{q_1}-\mathbf{q_2}, \omega + J_S\omega_{\mathbf{q_1}} + J_0)}, \tag{4.69}$$

$$\Sigma_{BB}(\mathbf{k},\omega) = \frac{z^2t^2}{2N^2}\sum_{\mathbf{q_1},\mathbf{q_2}} \frac{M_y^2(\mathbf{k},\mathbf{q_1},\mathbf{q_2})}{\omega + J_S\omega_{\mathbf{q}_1} + J_O - \Sigma_{AA}(\mathbf{k}-\mathbf{q_1}-\mathbf{q_2}, \omega + J_S\omega_{\mathbf{q_1}} + J_0)}, \tag{4.70}$$

which after substitution $\mathbf{q}_2 \to \mathbf{k} - \mathbf{q}_2$ in the sums leads to

$$\Sigma_{AA}(\mathbf{k},\omega) = \frac{z^2t^2}{2N^2}\sum_{\mathbf{q_1},\mathbf{q_2}} \frac{f^2(\mathbf{q}_1,\mathbf{q}_2)}{\omega + J_S\omega_{\mathbf{q}_1} + J_O - \Sigma_{BB}(\mathbf{q_2}-\mathbf{q_1}, \omega + J_S\omega_{\mathbf{q_1}} + J_0)}, \tag{4.71}$$

$$\Sigma_{BB}(\mathbf{k},\omega) = \frac{z^2t^2}{2N^2}\sum_{\mathbf{q_1},\mathbf{q_2}} \frac{g^2(\mathbf{q}_1,\mathbf{q}_2)}{\omega + J_S\omega_{\mathbf{q}_1} + J_O - \Sigma_{AA}(\mathbf{q_2}-\mathbf{q_1}, \omega + J_S\omega_{\mathbf{q_1}} + J_0)}, \tag{4.72}$$

where we defined

$$f(\mathbf{q}_1,\mathbf{q}_2)=u_{\mathbf{q}_1}\gamma_{q_{2x}-q_{1x}}+v_{\mathbf{q}_1}\gamma_{q_{2x}},\quad g(\mathbf{q}_1,\mathbf{q}_2)=u_{\mathbf{q}_1}\gamma_{q_{2y}-q_{1y}}+v_{\mathbf{q}_1}\gamma_{q_{2y}},\tag{4.73}$$

with $\gamma_{\mathbf{k}}$ defined as in Eq. (4.34). Since the right hand side of the equations for the self-energies do not depend on $\mathbf{k}$ [see Eqs. (4.71)-(4.72)], one is allowed to drop the momentum dependence of the self-energies. Hence, the spectral functions are also momentum independent in the case of $\tau=0$ and the only dependence on $\mathbf{k}$ may originate from the three-site terms.

Second, using the dominant pole approximation [22] we show that the quasiparticle state exists [property (ii)] if $J$ is finite (i.e. $J_S$ *or* $J_O$ are finite). Hence, following Kane *et al.* we assume that the Green's function can be separated into the part containing the pole and the part responsible for the incoherent processes:

$$G_{AA}(\omega)=\frac{a_A}{\omega-\omega_A}+G^{inc}_{AA}(\omega)\tag{4.74}$$

$$G_{BB}(\omega)=\frac{a_B}{\omega-\omega_B}+G^{inc}_{BB}(\omega),\tag{4.75}$$

where

$$a_A=\frac{1}{1-\frac{\partial\Sigma_A}{\partial\omega}\big|_{\omega=\omega_A}},\tag{4.76}$$

$$a_B=\frac{1}{1-\frac{\partial\Sigma_B}{\partial\omega}\big|_{\omega=\omega_B}},\tag{4.77}$$

and the pole positions:

$$\omega_A=\Sigma_{AA}(\omega_A),\tag{4.78}$$

$$\omega_B=\Sigma_{AA}(\omega_B),\tag{4.79}$$

are to be determined self-consistently following Eqs. (4.74)-(4.75).

Next, following Ref. [22] it is straightforward to derive the upper bound for the residues (spectral weights) $\{a_A,a_B\}$:

$$a_A\leq\left\{1+\frac{z^2t^2}{2N^2}\sum_{\mathbf{q_1},\mathbf{q_2}}f^2(\mathbf{q}_1,\mathbf{q}_2)\frac{a_B}{(J_S\omega_{\mathbf{q}_1}+J_0)^2}\right\}^{-1},\tag{4.80}$$

$$a_B\leq\left\{1+\frac{z^2t^2}{2N^2}\sum_{\mathbf{q_1},\mathbf{q_2}}g^2(\mathbf{q}_1,\mathbf{q}_2)\frac{a_A}{(J_S\omega_{\mathbf{q}_1}+J_0)^2}\right\}^{-1}.\tag{4.81}$$

If the sums in the above equations are divergent, then the upper bounds for the residues are equal zero and the Green's functions do not have the quasiparticle pole. Hence, one needs to check the behaviour for small values of the momenta $\mathbf{q}_1$. Then $\omega_{\mathbf{q}_1}\sim|\mathbf{q}_1|$ but e.g. $(u_{\mathbf{q}_1}\gamma_{q_{2y}-q_{1y}}+v_{\mathbf{q}_1}\gamma_{q_{2y}})^2\sim|\mathbf{q}_1|(\gamma_{q_{2y}}-\widehat{q}_1\cdot\nabla\gamma_{q_{2y}})^2$. Thus, if at least either $J_S$ or $J_O$ is finite, then there are no divergences in Eqs. (4.80)-(4.81). Consequently, under the same conditions the quasiparticle state exists.

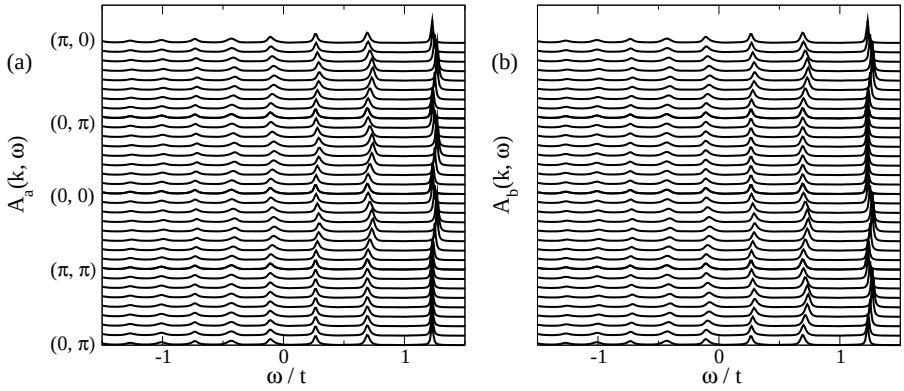


Figure 4.6: The spectral functions for the hole doped into the $a$ (left panel) and $b$ orbital (right panel). Parameters: $J = 0.2t$ and $\eta = 0.15$ (i.e. $J_S = 0.03t$, $J_O = 0.08t$, and $\tau = 0.06t$). Broadening $\delta = 0.01t$ and cluster size $16 \times 16$.

*Numerical calculations.*— We calculate the spectral functions $A_a(\mathbf{k}, \omega)$ and $A_b(\mathbf{k}, \omega)$ by solving SCBA equations (4.63)-(4.64) on a mesh of $16 \times 16$ $k$-points. The results for two different values of the superexchange constant $J = 0.2t$ and $J = 0.6t$ are shown in Figs. 4.6 and 4.7, respectively. Also we assume the Hund's coupling to be quite strong, i.e. $\eta = 0.15$.[6] However, such a value of the Hund's coupling is not only realistic but together with the observed value of $J = 0.2t$ gives a reasonable value of the spin-only exchange constant $J_S = 0.03t$ (which is in agreement with the observed Néel temperature in $LaVO_3$), cf. Sec. VIB of Ref. [100] for more detailed discussion on this issue. Thus, the spectral functions shown in Fig. 4.6 are calculated for the the realistic values of parameters in $LaVO_3$ whereas those shown in Fig. 4.7 are merely calculated for comparison.

Let us first discuss the results in Fig. 4.6. The quasiparticle peak in the low energy part of the spectrum is clearly visible and confirms the analytic predictions presented above. However, the quasiparticle state has a small 1D dispersion: along the $k_x$ direction for holes doped into the $b$ orbitals and along the $k_y$ direction for holes doped into the $a$ orbital. Since such a dispersion is not present when the three-site terms are neglected (compare the above analytic considerations) one can immediately ascribe the onset of the 1D dispersion in the spectra to the three-site terms. Furthermore, this phenomenon is quite well understood and we refer to Chapter 3 or Refs. [85] for a more detailed discussion of this problem.

Besides, the excited states form a ladder-like spectrum, also with a small 1D dispersion. Similarly as for the quasiparticle state the excited states resemble qualitatively the spectral functions calculated for the purely orbital model, see Chapter 3 or Ref. [85]. However, here one sees that quantitatively the spin-orbital spectra are different than the orbital ones. In particular, they are quite similar to those obtained for $J = 0.4t$ in the purely orbital model (see Fig. 3.5 in Chapter 3) although this observation has no physical meaning since all of the exchange constants used in the spin-orbital model ($J$, $J_S$ or $J_O$) are much

[6] Note that only for didactic purpose in Secs. 4.5.2–4.5.3 we calculate the spectral functions for $\eta = 0$. However, one should bear in mind that such a value is unphysical and inconsistent with the assumed infinite value of the Hund's coupling in Eq. (4.4).

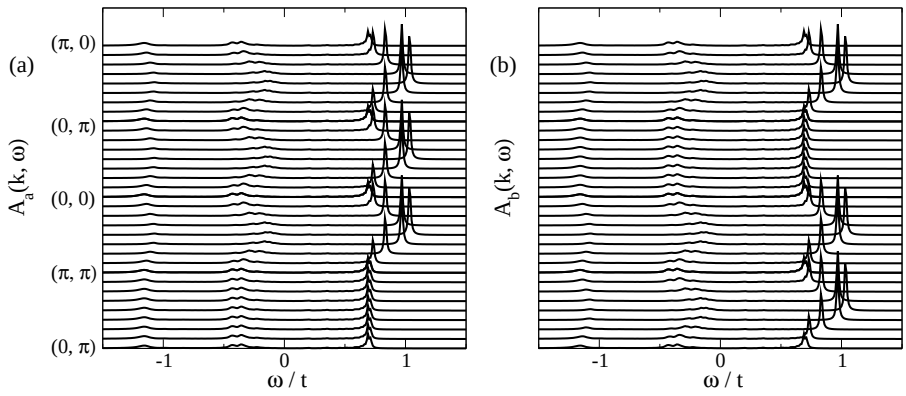


Figure 4.7: The spectral functions for the hole doped into the $a$ (left panels) and $b$ orbital (right panel). Parameters: $J = 0.6t$ and $\eta = 0.15$ (i.e. $J_S = 0.09t$, $J_O = 0.23t$, and $\tau = 0.19t$). Broadening $\delta = 0.01t$ and cluster size $16 \times 16$.

smaller than $0.4t$.

Looking at the spectral functions shown in Fig. 4.7 one notes that the ladder-like spectrum almost disappears when the value of the superexchange constant is increased to $J = 0.6t$. However, the qualitative properties of the dispersive quasiparticle peak stay mostly unchanged and the 1D character of the dispersion relation is preserved. Quantitatively, the quasiparticle spectral weight and the bandwidth increases quite drastically.

To conclude, the spin-orbital spectral functions form ladder-like spectra with a small 1D dispersion and have many similarities with the purely orbital spectra of the $t_{2g}$ model, cf. Chapter 3 or Ref. [85]. Still, however, there are a few relatively important differences with the orbital model which suggest that the spin-orbital is definitely more complex than the purely orbital model. For the understanding of this problem we refer to Sec. 4.5 whereas in what follows we will further investigate the properties of the spectral functions of the spin-orbital model.

*Quasiparticle properties.*— Now we analyze in more detail the quasiparticle properties of the spectral functions of the spin-orbital model, cf. Fig. 4.8. In addition, we compare these properties with those calculated for the spin $t$–$J$ model with three-site terms of Ref. [80] and the orbital $t$–$J$ model with three-site terms of Ref. [85] or Chapter 3.

By looking at the results for the spin-orbital model in Fig. 4.8 one sees that: (i) the quasiparticle bandwidth $W$ is strongly renormalized from its respective free value ($W = 8\tau$ as it may only originate from the three-site term dispersion relation, see above) and is proportional to $J^2$ for small $J$ ($J < 0.6t$) and to $J$ in the regime of large $J$ ($J > 0.6t$); (ii) the quasiparticle spectral weight $a_{QP}$ grows considerably with increasing $J$; (iii) the pseudogap $\Delta$ (the energy distance between the quasiparticle state and the first excited state) exists and roughly scales as $t(J/t)^{2/3}$ although for larger values of superexchange $J$ there are some discrepancies from this law.

Thus, one sees that the quasiparticle properties of the spin-orbital model differ qualitatively from than those of the spin model. We should stress that although the spin model used here is the $S = 1/2$ $t$-$J$ model with the three-site

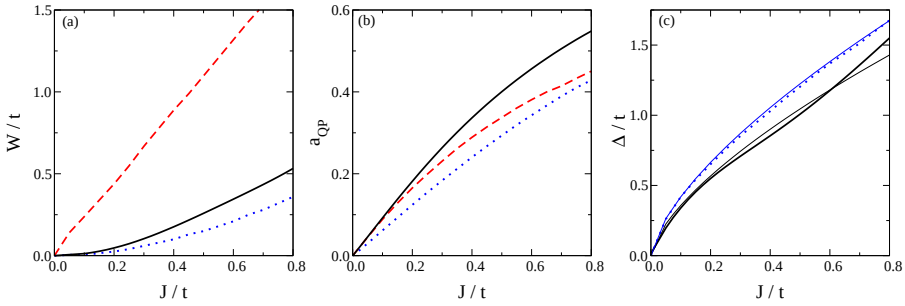


Figure 4.8: Dependence on $J$ of the quasiparticle properties: for the spin-orbital model discussed in the present chapter with the Hund's coupling $\eta = 0.15$ (solid line), for the spin model of Ref. [80] (dashed line), and for the orbital model of Ref. [85] or Chapter 3 (dotted line). Panel (a) shows the quasiparticle bandwidth $W$, (b) – the quasiparticle spectral weight $a_{QP}$ averaged over the 2D Brillouin zone, (c) – the pseudogap $\Delta$ (energy distance between the quasiparticle state and the first excited state) at $\mathbf{k} = (\pi/2, \pi/2)$. Note that $\Delta$ is not shown for the spin model as it cannot be defined there. The two light solid lines on panel (c) show the $(J/t)^{2/3}$ curves fitted to the data for the orbital and the spin-orbital model.

terms [80] but one expects similar generic behaviour in the case of spin $S = 1$ (see also Sec. 4.5.2). Hence, as there is no qualitative agreement with the model for spin $S = 1/2$ there would neither be a qualitative agreement with the model for spin $S = 1$.

On the other hand, we should note significant similarities between the present model and the orbital model (see also Fig. 4.8); the generic behaviour of the bandwidth, the spectral weight, and of the pseudogap seems to be the same in both models. There are, however, two differences. First, the $t(J/t)^{2/3}$ law does not describe the behaviour of the spin-orbital pseudogap so well as in the orbital case. Second, if one assumes that the spin-orbital model is just qualitatively similar to the orbital model, then it should be possible to rescale all the quasiparticle properties with such an effective value of the superexchange $J$ that they would coincide with the results for the orbital model. This, however, is not possible. For example, from the fits to the $t(J/t)^{2/3}$ law one can deduce that such an effective value of the superexchange would be $J_{eff} = (a_{SO}/a_O)^{2/3} = 0.79J$, where $a_{SO} = 1.94$ ($a_O = 1.66$) is the fitted coefficient which multiplies the $t(J/t)^{2/3}$ law in the spin-orbital (orbital) case. On the other hand, a similar fit to the quasiparticle spectral weight would require that such a $J_{eff}$ would be bigger than $J$.

In summary, the properties of the quasiparticle state in the spin-orbital model resemble those found for the quasiparticle in the purely orbital $t_{2g}$ model of Chapter 3. However, some detailed analysis presented in this section reveals that such a correspondence is rather 'superficial' and that few of the qualitative features of both models are different. We refer to the next section for the thorough understanding of this phenomenon.

## 4.5 Discussion

### 4.5.1 Validity of the results

*General remarks.*— In order to solve the $t_{2g}$ spin-orbital $t$–$J$ model in the case of one hole doped in the half-filled ground state we have introduced several approximations. Actually, they can be cast into two distinct classes: (i) those related with the introduction of the slave fermions, and (ii) those related with the SCBA method. However, the shortcomings of these two approximations were studied in detail by many authors (cf. Refs. [28, 105, 106] or Chapter 3 of this thesis) and it occurred that none of them were severe. On the other hand, there could potentially be a problem with the $t$-$J$ model itself: although, following suggestion in Chapter 3 or Ref. [85], we included those three-site terms which lead to the free hole dispersion (see Sec. 4.3.4) we neglected all of the others. Thus, below we take a closer look at this problem.

*Neglected three-site terms.*— A careful analysis leads to the conclusion that all the three-site terms which do not contribute to the free hole motion would lead to the coupling between a hole and either two magnons or two orbitons. Since orbitons are local excitations, see Eq. (4.37), the latter contribution would only slightly enhance the string potential in the present model and consequently the spectral functions would bear even more signatures of the ladder spectrum. However, this effect will be quantitatively very small as the three-site terms would contribute to the vertex as $\propto (J/4)$ (see below) whereas the magnon-orbiton vertices considered in this chapter are of the order of $t$. Thus, one can safely neglect these terms.

On the other hand, neglecting the terms which would lead to the interaction between a hole and two magnons is not *a priori* justified. One could imagine that it might lead to the hole motion by coupling to the quantum spin fluctuations – similarly as in the standard spin case with the coupling between a hole and a single magnon. Thus, we investigate this problem in detail: (i) we derived the respective three-site terms, and (ii) we performed all the transformations as in Sec. 4.4.1 which lead to the Hamiltonian written in the polaron representation. Since all these calculations are relatively tedious we do not explicitly write down all the steps but merely present the final Hamiltonian which describes the coupling between a hole and two magnons

$$
\begin{aligned}
H_{2m}^{eff} &= \frac{1}{4}\frac{\eta Jz}{1-3\eta}\,\frac{1}{2N}\sum_{\mathbf{k},\mathbf{q_1},\mathbf{q_2}}\Big\{V_{1y}(\mathbf{k},\mathbf{q_1},\mathbf{q_2})h^{\dagger}_{\mathbf{k}A}h_{\bar{\mathbf{k}}A}\\
&\times\ (\tilde{\alpha}_{\mathbf{q}_{1+}}\tilde{\alpha}_{\mathbf{q}_{2+}}+\tilde{\alpha}_{\mathbf{q}_{1+}}\tilde{\alpha}_{\mathbf{q}_{2-}}-\tilde{\alpha}_{\mathbf{q}_{1-}}\tilde{\alpha}_{\mathbf{q}_{2-}}-\tilde{\alpha}_{\mathbf{q}_{1-}}\tilde{\alpha}_{\mathbf{q}_{2+}})\\
&+\ V_{1x}(\mathbf{k},\mathbf{q_1},\mathbf{q_2})h^{\dagger}_{\mathbf{k}B}h_{\bar{\mathbf{k}}B}(\tilde{\alpha}_{\mathbf{q}_{1+}}\tilde{\alpha}_{\mathbf{q}_{2+}}+\tilde{\alpha}_{\mathbf{q}_{1+}}\tilde{\alpha}_{\mathbf{q}_{2-}}\\
&-\ \tilde{\alpha}_{\mathbf{q}_{1-}}\tilde{\alpha}_{\mathbf{q}_{2-}}-\tilde{\alpha}_{\mathbf{q}_{1-}}\tilde{\alpha}_{\mathbf{q}_{2+}})+\text{H.c.}\Big\}\\
&-\ \frac{1}{4}\frac{Jz}{1-3\eta}\,\frac{1}{2N}\sum_{\mathbf{k},\mathbf{q_1},\mathbf{q_2}}\Big\{V_{2y}(\mathbf{k},\mathbf{q_1},\mathbf{q_2})h^{\dagger}_{\mathbf{k}A}h_{\bar{\mathbf{k}}A}\\
&\times\ (\tilde{\alpha}_{\mathbf{q}_{1+}}\tilde{\alpha}_{\mathbf{q}_{2+}}+\tilde{\alpha}_{\mathbf{q}_{1+}}\tilde{\alpha}_{\mathbf{q}_{2-}}+\tilde{\alpha}_{\mathbf{q}_{1-}}\tilde{\alpha}_{\mathbf{q}_{2-}}+\tilde{\alpha}_{\mathbf{q}_{1-}}\tilde{\alpha}_{\mathbf{q}_{2+}})\\
&+\ V_{2x}(\mathbf{k},\mathbf{q_1},\mathbf{q_2})h^{\dagger}_{\mathbf{k}B}h_{\bar{\mathbf{k}}B}(\tilde{\alpha}_{\mathbf{q}_{1+}}\tilde{\alpha}_{\mathbf{q}_{2+}}-\tilde{\alpha}_{\mathbf{q}_{1+}}\tilde{\alpha}_{\mathbf{q}_{2-}}\\
&+\ \tilde{\alpha}_{\mathbf{q}_{1-}}\tilde{\alpha}_{\mathbf{q}_{2-}}-\tilde{\alpha}_{\mathbf{q}_{1-}}\tilde{\alpha}_{\mathbf{q}_{2+}})+\text{H.c.}\Big\}\,,
\end{aligned}
\tag{4.82}
$$

where

$$V_{1\mu}(\mathbf{k},\mathbf{q_1},\mathbf{q_2}) = \frac{1}{2}u_{\mathbf{q}_1}u_{\mathbf{q}_2}\cos(2k_\mu - 2q_{1\mu} - q_{2\mu}) + \frac{1}{2}v_{\mathbf{q}_1}v_{\mathbf{q}_2}\cos(2k_\mu - q_{2\mu}), \tag{4.83}$$

and

$$V_{2\mu}(\mathbf{k},\mathbf{q_1},\mathbf{q_2}) = \frac{1}{4}u_{\mathbf{q}_1}v_{\mathbf{q}_2}\cos(2k_\mu - 2q_{1\mu}), \tag{4.84}$$

with all the symbols defined as those in Eq. (4.43). Note that above we have neglected all terms of the type $\propto \tilde{\alpha}^\dagger\tilde{\alpha}$ as they would lead to the four boson line diagrams (the self-energies with two magnon lines are very small, see below, and hence the self-energies with four magnon diagrams would be even smaller).

Next, we implement the processes derived above into the SCBA method and obtain the following equations for the additional self-energies:

$$\begin{aligned}
\Sigma^{'}_{AA}(\mathbf{k},\omega) &= \frac{z^2\lambda^2}{2N^2}\sum_{\mathbf{q_1},\mathbf{q_2}}\left\{\eta V_{1y}(\mathbf{k},\mathbf{q_1},\mathbf{q_2}) - V_{2y}(\mathbf{k},\mathbf{q_1},\mathbf{q_2})\right\}^2 \\
&\quad \times G_{AA}(\mathbf{k}-\mathbf{q_1}-\mathbf{q_2},\omega + J_S\omega_{\mathbf{q_1}} + J_S\omega_{\mathbf{q_2}}) \\
&+ \frac{z^2\lambda^2}{2N^2}\sum_{\mathbf{q_1},\mathbf{q_2}}\left\{\eta V_{1y}(\mathbf{k},\mathbf{q_1},\mathbf{q_2}) + V_{2y}(\mathbf{k},\mathbf{q_1},\mathbf{q_2})\right\}^2 \\
&\quad \times G_{AA}(\mathbf{k}-\mathbf{q_1}-\mathbf{q_2},\omega + J_S\omega_{\mathbf{q_1}} + J_S\omega_{\mathbf{q_2}})\Big\},
\end{aligned} \tag{4.85}$$

$$\begin{aligned}
\Sigma^{'}_{BB}(\mathbf{k},\omega) &= \frac{z^2\lambda^2}{2N^2}\sum_{\mathbf{q_1},\mathbf{q_2}}\left\{\eta V_{1x}(\mathbf{k},\mathbf{q_1},\mathbf{q_2}) - V_{2x}(\mathbf{k},\mathbf{q_1},\mathbf{q_2})\right\}^2 \\
&\quad \times G_{BB}(\mathbf{k}-\mathbf{q_1}-\mathbf{q_2},\omega + J_S\omega_{\mathbf{q_1}} + J_S\omega_{\mathbf{q_2}}) \\
&+ \frac{z^2\lambda^2}{2N^2}\sum_{\mathbf{q_1},\mathbf{q_2}}\left\{\eta V_{1x}(\mathbf{k},\mathbf{q_1},\mathbf{q_2}) + V_{2x}(\mathbf{k},\mathbf{q_1},\mathbf{q_2})\right\}^2 \\
&\quad \times G_{BB}(\mathbf{k}-\mathbf{q_1}-\mathbf{q_2},\omega + J_S\omega_{\mathbf{q_1}} + J_S\omega_{\mathbf{q_2}}),
\end{aligned} \tag{4.86}$$

where

$$\lambda = \frac{1}{1-3\eta}\frac{J}{4}. \tag{4.87}$$

This requires that one substitutes for the self-energies:

$$\Sigma_{AA}(\mathbf{k},\omega) \to \Sigma^{'}_{AA}(\mathbf{k},\omega) + \Sigma_{AA}(\mathbf{k},\omega), \tag{4.88}$$

$$\Sigma_{BB}(\mathbf{k},\omega) \to \Sigma^{'}_{BB}(\mathbf{k},\omega) + \Sigma_{BB}(\mathbf{k},\omega), \tag{4.89}$$

in the Dyson's equations (4.65)-(4.66) which changes the SCBA equations.

Finally, we solve the modified SCBA equations on a mesh of $16\times16$ points. It occurs that the spectral functions obtained with the additional self-energies Eqs. (4.85)-(4.86) are virtually similar to those obtained without them (unshown). The only small difference is the very small enhancement of the incoherent part. This can be understood in the following way. First, the added contributions scale as $(J/4)^4$ and are very small as $J < t$. Second, the vertices, Eqs. (4.83)-(4.84), are singular at e.g. $\mathbf{q}_1 = (0,0)$ and $\mathbf{q}_2 = (0,0)$ points. Therefore, the self-energies associated with these vertices could only contribute to the incoherent

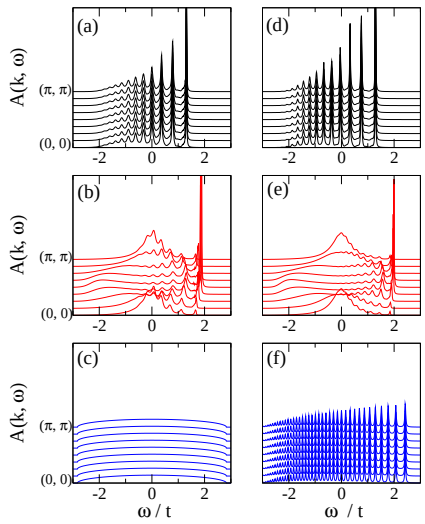


Figure 4.9: Spectral function along the $\Gamma - M$ direction of the Brillouin zone for: the spin-orbital model (top panels), spin toy-model (middle panels), orbital toy-model (bottom panels). $J = 0.2t$ and $\eta = 0$ (i.e. $J_S = 0.05t$, $J_O = 0$, but $\tau \equiv 0$, see text) on the left panels whereas $J = 0.2t$ and $\eta = 0.15$ (i.e. $J_S = 0.03t$, $J_O = 0.08t$, but $\tau \equiv 0$, see text) on the right panels. Note that $\tau \equiv 0$ implies (see Chapter 3) $A_a(\mathbf{k}, \omega) = A_b(\mathbf{k}, \omega) \equiv A(\mathbf{k}, \omega)$. Broadening $\delta = 0.01t$ [$\delta = 0.02t$ on panel (f)] and cluster size $16 \times 16$.

part of the spectrum [the divergent vertices lead to the divergences in denominators of equations (4.80)-(4.81) yielding the upper bounds for the quasiparticle residues in the dominant pole approximation]. The physical interpretation of this phenomenon is as follows: (i) the hole produces two magnon excitations at each step it moves forward, (ii) the hole always moves by two sites in a single step (as the three-site terms lead to the next nearest neighbour hopping), (iii) magnons 'travel' in the system and cure the defects created by the hole at a 'velocity' one site per each step. Thus, the magnons are not 'fast' enough to erase the defects created by the hole.

In conclusion, neglecting the three-site terms which do not lead to the free hole motion is entirely justified. Such processes are not only quantitatively small but also they do not change the physics qualitatively.

### 4.5.2 The role of the joint spin-orbital dynamics

*Purpose of this section.*— The main task of this and the next section is to understand the spectral functions and the quasiparticle properties of the spin-orbital model. In particular, we not only want to understand the peculiar similarities or rather small differences between the spin-orbital model and its purely orbital counterpart, which were discussed in Sec. 4.4.3, but also we want to understand why the spin physics seems to be 'hidden' in the present spin-orbital system. Note that for the sake of simplicity in this section we will entirely neglect the three-site terms (4.13) in the spin-orbital model (4.3) (or in other words we will

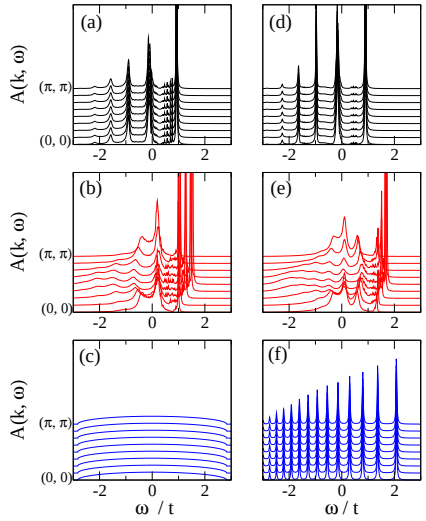


Figure 4.10: Spectral function along the $\Gamma - M$ direction of the Brillouin zone for: the spin-orbital model (top panels), spin toy-model (middle panels), orbital toy-model (bottom panels). $J = 0.6t$ and $\eta = 0$ (i.e. $J_S = 0.15t$, $J_O = 0$, but $\tau \equiv 0$, see text) on the left panels whereas $J = 0.6t$ and $\eta = 0.15$ (i.e. $J_S = 0.09t$, $J_O = 0.23t$, but $\tau \equiv 0$, see text) on the right panels. Note that $\tau \equiv 0$ implies (see Chapter 3) $A_a(\mathbf{k}, \omega) = A_b(\mathbf{k}, \omega) \equiv A(\mathbf{k}, \omega)$. Broadening $\delta = 0.01t$ [$\delta = 0.02t$ on panel (f)] and cluster size $16 \times 16$.

put $\tau \equiv 0$). This is motivated by the fact that the role of the three-site terms is solely to provide dispersion in the spectra (see Sec. 4.4.3) and the mechanism of this dispersion is quite well understood, see Chapter 3.

*Introducing auxiliary toy-models.*— We start the analysis with the introduction of two artificial toy-models whose results will be later compared to those of the $t$–$J$ spin-orbital model. First, we define the following $t$–$J_S$ spin toy-model

$$H_S = -t \sum_{\langle \mathbf{ij} \rangle, \sigma} P(\tilde{c}^\dagger_{\mathbf{i}\sigma} \tilde{c}_{\mathbf{j}\sigma} + \text{H.c.}) P + J_S \sum_{\langle \mathbf{ij} \rangle} \mathbf{S_i} \cdot \mathbf{S_j}, \tag{4.90}$$

where spin $S = 1$, the constrained operators $\tilde{c}^\dagger_{\mathbf{i}\sigma} = c^\dagger_{\mathbf{i}\sigma}(1 - n_{\mathbf{i}\bar{\sigma}})$, and the operators $P$ project onto the high spin states. Note that here the superexchange energy scale is $J_S$ [see Eq. (4.39)] and not $J$. Hence, it is defined in such a way that it mimics the formation of the AO order. On the other hand, the kinetic energy is blind to the AO here and Eq. (4.4) reduces to the kinetic part of Eq. (4.90) only if the orbitals form an orbital liquid state. This is an obvious logical inconsistency but the aim here is to see what happens when the joint spin-orbital dynamics in the kinetic energy is entirely neglected. It is also the reason why we call model (4.90) the toy-model.

Second, we define the following $t$-$J_O$ orbital toy-model

$$H_O = -t \sum_{\mathbf{i}} (\tilde{b}^\dagger_{\mathbf{i}} \tilde{b}_{\mathbf{i}+\hat{\mathbf{a}}} + \tilde{a}^\dagger_{\mathbf{i}} \tilde{a}_{\mathbf{i}+\hat{\mathbf{b}}} + \text{H.c.}) + J_O \sum_{\langle \mathbf{ij} \rangle} T^z_{\mathbf{i}} T^z_{\mathbf{j}}, \tag{4.91}$$

with pseudospin operator $T = 1/2$, and the constrained operators $\tilde{b}^{\dagger}_{\mathbf{i}} = b^{\dagger}_{\mathbf{i}}(1 - n_{\mathbf{i}a})$ and $\tilde{a}^{\dagger}_{\mathbf{i}} = a^{\dagger}_{\mathbf{i}}(1 - n_{\mathbf{i}b})$. Similarly as in the spin toy-model defined above, the superexchange energy scale is not $J$ but $J_O$ [Eq. (4.38)] which mimics the formation of the AF order. Also, the kinetic energy is blind now to the AF order and Eq. (4.4) reduces to the kinetic part of Eq. (4.91) only if the spins form the FM order. This again is logically inconsistent – see, however, discussion above.

Next, we solve these models using the SCBA method in the case of the one hole doped into the AF (AO) state for the spin (orbital) toy-model. We do not show here the respective SCBA equations as these follow from those written in Ref. [23] (Chapter 3) in the case of the spin (orbital) toy-model. One only has to substitute in the respective SCBA equations $J \to -J_S$, $S \to 1$ and (due to the double exchange factor) also $t \to t/\sqrt{2}$ in Ref. [23] in the spin case and $J \to -J_O$, $E_0 \to 0$, and $\tau \to 0$ in Chapter 3 in the orbital case. We then calculate the respective spectral functions on a mesh of $16 \times 16$ $\mathbf{k}$-points. Note that since $\tau \equiv 0$ the spectral functions for both orbital flavours are equal, i.e. $A_a(\mathbf{k}, \omega) = A_b(\mathbf{k}, \omega) \equiv A(\mathbf{k}, \omega)$.

Finally, we compare the results obtained for the above toy-models with those obtained for the spin-orbital model $t$-$J$ model, Eq. (4.4)-(4.7). We show the results for two different values of $J$, see Figs. 4.9 and 4.10. In addition, we calculate the results for two different values of the Hund's coupling $\eta = 0$ and $\eta = 0.15$ (see left and right panels of each figure).

*Comparison between toy-models and the spin-orbital model.*— Let us first look at the physical regime of $\eta = 0.15$ and $J = 0.2t$, see Fig. 4.9(d)-4.9(f). One sees that the spin-orbital spectral function [panel (d)] resembles qualitatively the ladder spectrum found in the orbital model [panel (f)] although the quantitative comparison reveals strong differences between the two models. Still, the spin-orbital spectral function is entirely different from the $\mathbf{k}$-dependent spin spectral function [panel (e)]. Next, somewhat similar behaviour is found for the case of $\eta = 0.15$ and $J = 0.6t$, see Fig. 4.10(d)-4.10(f). Here, however, the spin-orbital spectrum is qualitatively different than the orbital spectrum.

Even more inquiring behaviour is found in the unphysical regime of $\eta = 0$ (which, however, is an interesting limit, see also footnote 6 in this chapter). Then neither of the panels shown in Fig. 4.9(a)-4.9(c) or Fig. 4.10(a)-4.10(c) is similar to each other. This means that even the orbital model is entirely different in this regime than the spin-orbital model. This is because in this limit the hole moves in the orbital model incoherently as $J_O = 0$ for $\eta = 0$, see e.g. Fig. 4.9(c). However, apparently in the spin-orbital model with $J_O = 0$ and small but finite $J_S$ the hole moves in string-like potential, see e.g. Fig. 4.9(a). This means that the onset of the ladder-like spectrum in the spin-orbital model in this regime cannot be explained easily in terms of the purely orbital model.

In addition, one sees that whereas one gets similar spin-orbital spectra for different values of $\eta$ but the same values of $J$, the spectra found for the orbital model are different. On the contrary, for different values of $J$ and the same values of $\eta$ the spin-orbital spectra are rather distinct but the spin spectra do not change much. This is another argument which suggests that neither the spin toy-model nor the orbital toy-model can explain the properties of the spin-orbital spectra.

*Conclusions.*— To conclude, we note that the joint spin-orbital dynamics in the kinetic part of the spin-orbital model plays a significant role for the

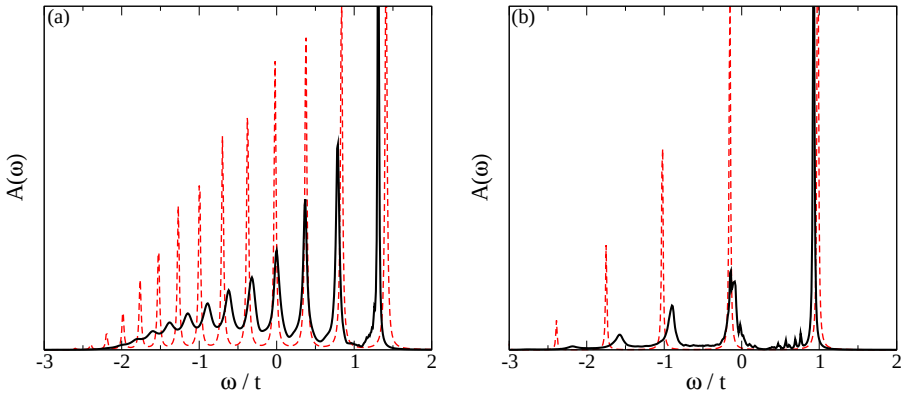


Figure 4.11: Comparison between the spectral functions of the classical limit (dashed lines) and full quantum (solid lines) version of the spin-orbital model at a single point in the Brillouin zone. Panel (a) shows results for $J = 0.2t$ and $\eta = 0$ (i.e. $J_S = 0.05t$, $J_O = 0$, but $\tau \equiv 0$, see text) whereas panel (b) shows results for $J = 0.6t$ and $\eta = 0$ (i.e. $J_S = 0.15t$, $J_O = 0$, but $\tau \equiv 0$, see text). Note that $\tau \equiv 0$ implies (see Chapter 3) $A_a(\omega) = A_b(\omega) \equiv A(\omega)$. Broadening $\delta = 0.01t$ ($\delta = 0.015t$) in panel (a) [(b)] and cluster size $16 \times 16$.

coherent hole motion. The purely spin or orbital toy-models cannot reproduce the spectral function found for the spin-orbital $t$-$J$ model. Hence, indeed the spin-orbital spectral functions resemble the orbital ones only superficially and it is the peculiar interplay of the spins and orbitals, studied in the next section, which leads to the calculated spectra.

### 4.5.3 Suppression of quantum fluctuations

*Classical limit.*— In this section we attempt to understand the spin-orbital spectra by assuming that the spins $S = 1$ are purely classical objects. Hence, we skip all the spin flip terms $\propto S^+_{\mathbf{i}} S^-_{\mathbf{j}}$ in the Hamiltonian Eq. (4.7), we rewrite SCBA equations (4.63)-(4.64) in this case, and finally try to compare the spectral functions calculated in this regime with the ones obtained for the full model, Eq. (4.3). In addition, we not only assume $\tau \equiv 0$ as in the previous section but we also take $\eta = 0$ (which implies $J_O = 0$ in particular), see also footnote 6 in this chapter. In the end of this section we discuss the impact of the finite value of these parameters on the results obtained here.

Since $u_{\mathbf{q}_1} = 1$, $v_{\mathbf{q}_1} = 0$, and $\omega_{\mathbf{q}_1} = 4$ for the $S = 1$ classical spins [23] we can rewrite self-energy equations (4.69)-(4.70),

$$\Sigma_{AA}(\mathbf{k},\omega) = \frac{z^2 t^2}{2N^2} \sum_{\mathbf{q_1},\mathbf{q_2}} \frac{\gamma^2_{q_1 x}}{\omega + J_S z S - \Sigma_{BB}(\mathbf{q}_1, \omega + J_S z S)}, \tag{4.92}$$

$$\Sigma_{BB}(\mathbf{k},\omega) = \frac{z^2 t^2}{2N^2} \sum_{\mathbf{q_1},\mathbf{q_2}} \frac{\gamma^2_{q_1 y}}{\omega + J_S z S - \Sigma_{AA}(\mathbf{q}_1, \omega + J_S z S)}, \tag{4.93}$$

where we already substituted $\mathbf{q}_1 \to \mathbf{k} - \mathbf{q}_1 - \mathbf{q}_2$ in the sums. Then the above

self-consistent equations are momentum independent and one obtains

$$\Sigma_{AA}(\omega) = \Big(\frac{t}{\sqrt{2}}\Big)^2 \frac{z/2}{\omega + J_S z S - \Sigma_{BB}(\omega + J_S z S)}, \tag{4.94}$$

$$\Sigma_{BB}(\omega) = \Big(\frac{t}{\sqrt{2}}\Big)^2 \frac{z/2}{\omega + J_S z S - \Sigma_{AA}(\omega + J_S z S)}, \tag{4.95}$$

since $1/N \sum_{\mathbf{q}_1} \gamma^2_{q_1\nu} = 1/2z$, where $\nu = x, y$.

*Classical and quantum limits coincide.*— We solve Eqs. (4.94)-(4.95) selfconsistently. The respective spectral functions are shown in Fig. 4.11 for $J = 0.2t$ (i.e. $J_S = 0.05t$) and $J = 0.6t$ (i.e. $J_S = 0.15t$). As expected, one obtains a typical ladder spectrum. However, one sees that the results resemble those obtained for the full spin-orbital model Eq. (4.3) with $\eta = 0$ and $\tau = 0$: Although the spectrum of the full spin-orbital model contains some incoherent part, the ladder peaks of the full spin-orbital model and of its classical version almost coincide. In addition, the incoherent bandwidth in the $J = 0$ limit is $W = 4t$ in the classical case whereas it is only slightly reduced in the quantum model ($W \sim 3.7t$). [7] For finite $J$ this results in the small shift of the peaks in the full spin-orbital model with respect to its classical counterpart. This all suggests that the classical and the full (quantum) versions of the spin-orbital models are to a large extent equivalent.

*Interpretation of the classical limit.*— On the other hand, Eqs. (4.94)-(4.95) are almost identical to the SCBA equations for the hole moving in the $S = 1/2$ spin Ising model [cf. Eq. (20) in Ref. [23]]. The only differences are: the self-consistent dependence of the self-energies on two different sublattices, the reduction of the nearest neighbours by a factor 1/2 (in the numerator), a factor $1/\sqrt{2}$ in the hopping element, and the increase of the magnon excitation energy by a factor of 2. Whereas the first two imply the zig-zag hole motion in the ordered state (see Chapter 3) the two others merely mean that the hole moves in the spin $S = 1$ system. Thus altogether, the hole motion in the full spin-orbital model with $\eta = 0$ and $\tau = 0$ can be quite well approximated by the zig-zag hole motion in the $S = 1$ spin Ising model.

*Orbitally induced spin strings.*— The whole analysis written above leads us to conclusion that in the limit of $J_O = 0$ and $\tau = 0$ the hole moves in the spin and orbitally ordered plane in the following way: (i) the orbitals force the hole to move along the zig-zag paths even in the limit of $J_O = 0$, (ii) the orbitals force the hole to retrace its path again even in the limit of $J_O = 0$ – this is similar to the situation discussed by Brinkman and Rice [67] where the hole in the Ising spin model with $J = 0$ always has to retrace its path, (iii) the coherent hole motion by coupling to the spin fluctuations is impossible in the ground state as then the hole would not retrace its path, (iv) instead the hole creates strings in the spin sector which are erased when the hole retraces its path. Thus, one

[7] The obtained value of the incoherent bandwidth $W = 4t$ in the classical limit well agrees with the retracebale path approximation formula $W = 4t_{\rm eff}\sqrt{l}$, where the effective hopping $t_{\rm eff} = t/\sqrt{2}$ due to the double exchange and $l = 2$ is the number of possible forward going steps in the classical spin-orbital model, cf. discussion in Chapter 3.4.3. Note also that the narrowing of the bandwidth in the quantum case is due to the fact that the effective number of forward going steps, which the hole can make so that the spins become misaligned (which is the essence of retraceable path approximation), is slightly reduced. This is because some of the spins are already overturned due to the quantum spin fluctuations in the full quantum model.

notes here a complex interplay of spins and orbitals. In particular, due to point (ii) the orbitals constrain the spin dynamics and force the spins to effectively act on the hole as the classical objects.

*Subtle issues.*— Finally, there are only two subtle issues. First, the model of the zig-zag hole motion in the $S = 1$ spin Ising model does not explain the appearance of the small momentum independent incoherent part in the excited part of the spectrum in the quantum spin-orbital model. This can be understood in the following way: although the hole has to return to the original site (due to the orbitals) the magnons present in the excited states can travel freely in the system. Hence, the energies of the excited states can no longer be classified merely by the length of the retraceable paths (as it would be the case in the classical model with no dispersion in the magnon spectrum). This results in the small incoherent spectrum which surrounds each of the peak of the ladder spectrum, cf. Fig. 4.11. Furthermore, this incoherent spectrum grows with increasing $J_S$ as then the velocity of the magnons increases.

Second, one may wonder how to extend the above understanding of the spin-orbital polarons to the case of finite values of orbital exchange interaction $\eta$ (which results in the finite value of $J_O$, see Fig. 3.4) or finite three-site hopping term $\tau$. Actually, including the nonzero value of $J_O$ merely leads to the substitution of $J_S zS \to J_S zS + J_O$ in Eqs. (4.92)-(4.93) and consequently (4.94)-(4.95); this means that an additional string-like potential, coming this time from the orbital sector, acts on the hole. On the other hand, including the three-site term results in the shift $\omega \to \omega + \varepsilon_A(\mathbf{k})$ and $\omega \to \omega + \varepsilon_B(\mathbf{k})$ in Eqs. (4.92)-(4.93) which means that these equations cannot be reduced to the momentum-independent equations (4.94)-(4.95). However, one can still solve the model. The results (not shown) resemble those found in Figs. 4.6 and 4.7: it is again only the incoherent part which is slightly enhanced in the full spin-orbital model (4.3) whereas in its classical counterpart it is suppressed. Furthermore, all of the quasiparticle properties of the full spin-orbital model shown in Fig. 4.8 are *almost perfectly* reproduced by the classical spin-orbital model (not shown) – with the only slight discrepancy being in the region of the slight deviation from the $t(J/t)^{2/3}$ law for the pseudogap of the full spin-orbital model.

*Conclusions.*— To conclude, one should note that the quantum spin fluctuations are to a large extent suppressed in the spin-orbital model by the simultaneous coupling of the hole to *both* spin and orbital excitations. In particular, they do not affect the quasiparticle state and merely add as a small incoherent spectrum in the incoherent high-energy part of the ladder spectrum. This is due to the classical character of the orbitals which confine the hole motion and prohibit its coherent motion by the coupling to the quantum spin fluctuations. On the other hand, the hole still couples to the spin degrees of freedom, mostly, in a classical way, i.e. by generating string potential due to defects created by hole motion. Thus, *the string* which acts on the hole moving in the plane with AO and AF order *is of the composite orbital and spin character*. This not only explains the peculiar correspondence between the orbital and spin-orbital model but also explains that the spins 'do not hide behind the orbitals' but play an active role in the lightly doped spin-orbital system.

## 4.6 Conclusions

*Purpose of this chapter.*— The purpose of this chapter was to study the motion of a single hole doped into the Mott insulating AF and AO ordered plane of $LaVO_3$ [83], shown schematically in Fig. 4.2. In what follows we will answer this problem by discussing in subsequent paragraphs the answers to the four tasks posed in the introduction to this chapter.

*Form of the proper model.*— First, in Sec. 4.3 we showed that such a hole motion is governed by the respective $t$–$J$ model [100] with $S = 1$ spin and $t_{2g}$ orbital degrees of freedom supplemented by the required here three-site terms, see Ref. [85] or Chapter 3 (which were derived in Sec. 4.3.4 and 4.5.1) and we used this model as the starting point of the analysis. Similarly as in Chapter 2 and 3 one had to be very careful while studying the newly derived extended $t$–$J$ model. As discussed in detail in Sec. 4.2 due to the violation of the Goodenough-Kanamori rules [93] we had to take into account the spin and orbital dynamics on equal footing. This was explicitly showed in Sec. 4.4.1 where we reduced this model to the polaron-type model and showed that indeed the hole couples simultaneously to the collective excitations of *both* the AF state (magnons) and the AO state (orbitons).

*Coherent hole motion in $LaVO_3$.*— Second, we solved the model using the SCBA method and calculated both analytically using the dominant pole approximation and numerically using the SCBA equations that the spectral functions contain a stable quasiparticle peak, provided the value of the superexchange $J$ was finite (see Sec. 4.4.2-4.4.3. Thus, the added hole can move coherently in $LaVO_3$. Let us note that this was not a trivial result as it was not *a priori* clear whether a coupling between a hole and two excitations would lead to a stable quasiparticle state – e.g. the coupling between hole and two magnons does not lead to the stable quasiparticle peak, cf. Ref. [80] and Sec. 4.5.1. However, since the orbitons are massive excitations the hole does not scatter too much on the excitations and the quasiparticle solution exists.

*Influence of the spin and orbital dynamics on the hole motion.*— Furthermore, apart from verifying all the approximations leading to the obtained results (Sec. 4.5.1) we studied in detail the properties of the quasiparticle states (see second part of Sec. 4.4.3). In particular, we looked at the differences between the well-known spin [23] or the $t_{2g}$ orbital (see Chapter 3 or Refs. [82, 85]) polarons and the obtained here spin-orbital polarons. We checked that all of the typical quasiparticle properties of the spin-orbital polarons such as the bandwidth, the quasiparticle spectral weight, and the pseudogap (the distance between the quasiparticle peak and the next excited state) are qualitatively similar to those of the $t_{2g}$ orbital polarons and it is the string picture which dominates in the quasiparticle properties. For example the bandwidth scales as $t(J/t)^2$ and arises solely due to the renormalization of the three-site terms, similarly as in the purely orbital $t_{2g}$ model, see chapter 3. [8]

However, a more detailed investigation (Secs. 4.5.2- 4.5.3) led to the conclusion that microscopically the spin-orbital polarons are much more complex and resemble the orbital polarons only superficially. Actually, we showed that the spin degrees of freedom also play a significant role in the formation of the

[8] Note that the occurrence of the small but still finite bandwidth confirms the idea of the absence of hole confinement in transition metal oxides with orbital degeneracy presented in Chapter 3 or Ref. [85].

spin-orbital polarons although they are forced by the orbitals to act on the hole as the classical Ising spins. This is because the orbitals confine the hole motion by forcing the hole to retrace its path which means that the hole motion by coupling to the quantum spin fluctuations is prohibited. Thus, the string picture which dominates in the spin-orbital polarons is enforced by the orbitals but it is of a joint spin-orbital nature. Lastly, it occurred that it is only in the excited spectrum that the quantum spin fluctuations contribute and are responsible for a small incoherent dome in the spectral function.

Let us also make a side but important remark: actually, the suppression of quantum spin fluctuations by orbitals could be understood as a topological effect. This is due to the fact that it happens even if the energy of the orbital excitations is turned to zero, i.e. when the hole can move in the orbital sector freely. Hence, the mere presence of orbitals is enough to obtain the (almost) classical behaviour of a hole doped into the ground state with AF and AO order.

*Extensions to finite doping.*— Certainly, the extension of the one-hole result to the finite doping is always 'shaky' and, thus, to further verify the problem why the orbital dynamics seems to drive the hole motion in the lightly hole-doped $La_{1-x}Sr_xVO_3$ more theoretical studies on the doped cubic vanadates are needed. Still, the results presented here seem to capture the generic role of the orbital and spin dynamics in the lightly doped cubic vanadates.

*Final remarks.*— An important prediction of this chapter is that if a photoemission spectrum was measured on the cleaved $LaVO_3$ sample, then it would look as the one obtained in Fig. 4.6. The reader may wonder whether (apart from the matrix-elements effects responsible for certain redistribution of spectral intensity) any other processes, such as for example the electron-phonon interaction, would affect hole motion to such an extent that the spectral functions calculated here would change qualitatively. Although we have not made any calculations for such a more complex case so far, we suggest that they would only enhance the ladder spectrum obtained here, since typically the studied mechanisms are only responsible for further localization of the hole.[9]

## 4.7 Postscriptum: spin, orbital and spin-orbital polarons

*General considerations.*— In this section we intend to give a brief overview of what happens when a single hole is doped to one of the following magnetically and/or orbitally ordered ground states: (i) the AF-type of order, (ii) the AO-type of order with $e_g$ alternating orbitals, (iii) the AO-type of order with $t_{2g}$ alternating orbitals, (iv) the coexisting AF and $t_{2g}$ AO ordered state. Actually, the last two cases were thoroughly discussed in the previous and this chapter (respectively) while the first two cases were studied in Ref. [23] and Ref. [82] (respectively). Thus, here we only repeat the results already obtained — in order to get a better insight into various processes which lead to the hole motion in the spin and/or magnetically ordered states.

*Spin polaron.*— A single hole doped into the half-filled Mott insulating ground state with AF order (which could correspond to the undoped planes

[9] Apart from considered here processes connected with the hopping $t$ (string formation) other coupling mechanisms, e.g. due to the electron-phonon interaction, may contribute to orbital polaron formation, see e.g. Ref. [90].

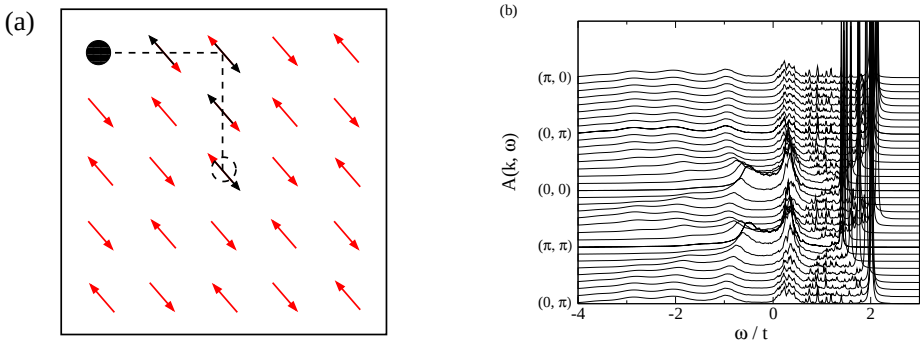


Figure 4.12: Panel (a): Artist's view of the defects created by a single hole doped into the spin AF ordered state. Red arrows denote the AF ordered ground state at half-filling, while black arrows denote overturned spins due to the hole propagation from the point where it was originally doped (dashed empty circle) to the arbitrarily chosen point at the upper-left corner (full circle). Note that the quantum spin fluctuations can flip the spins and (pairwise) erase the defects created by the hole (therefore, in the figure, the overturned black spins have the red arrows as well). Panel (b): spectral density $A(\mathbf{k},\omega)$ (independent of the spin of the removed electron) of the spin $t$–$J$ model [23] with $J = 0.4t$ along the particular directions of the 2D Brillouin zone.

of the high-$T_c$ cuprates such as e.g. $La_2CuO_4$ or $Sr_2CuO_2Cl_2$ [20]) does not move freely as its motion disturbs the spin order [21]. Instead, it couples to the collective (delocalized) excitations of the AF ordered phase (magnons), and it propagates through the lattice together with a 'cloud' of magnons [22]. Thereby the energy scale of the 'coherent' hole propagation is strongly renormalized and is given by the AF superexchange constant $J$. In this way a quasiparticle is formed which is frequently called in the literature a *spin polaron* [23]. Figure 4.12 shows in more detail the most characterstic type of motion here [i.e. how the hole moves by coupling to the spin fluctuations, see panel (a)] and what the corresponding spectral function looks like [panel (b)].

$e_g$ *orbital polaron.*— A slightly different behaviour can be found in the planes with FM spin order and $e_g$ AO orbital order (as in the $ab$ planes of $LaMnO_3$, see Ref. [76]). It has been shown [82] that although the hole introduced into such a state does not disturb the FM spin order, it couples to the collective excitations of the AO state (orbitons). Here again a quasiparticle is formed which is called this time an $e_g$ *orbital polaron*. It should be noted, however, that the orbital polaron has an even smaller bandwidth than the spin polaron [82], as the orbitons are in general much less mobile than the magnons (or even immobile) due to the lack of the $SU(2)$ symmetry in the orbital systems [107] and almost directional Ising-like superexchange [76, 84]. Actually, one can understand the hole motion in this case in terms of the string picture:[10] The hardly mobile orbitons cannot repair the string of the misaligned orbitals in the AO state, which arises due to the hole propagation on the corresponding path. Thus, it is the hole which has to return to the original site and cure

[10] Note that although the string picture alone cannot explain the previously mentioned hole motion in the AF ordered state, it may serve as a perfect starting point for the investigation of the behaviour of holes doped into the AF phase, see Ref. [108].

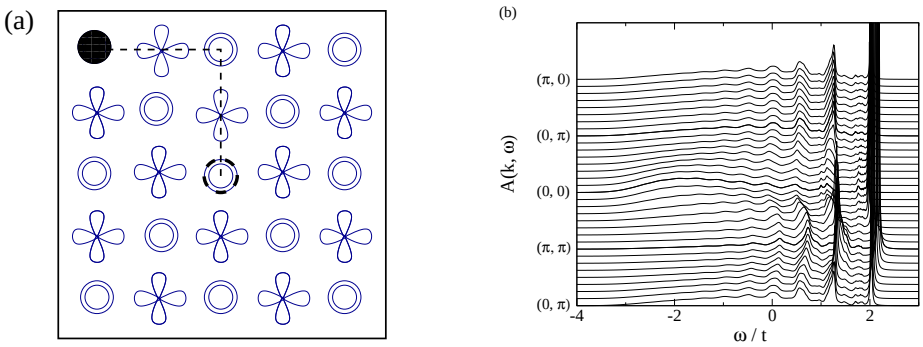


Figure 4.13: Panel (a): Artist's view of the defects created by a single hole doped into the $e_g$ AO state (with alternating $d_{3z^2-r^2}$ and $d_{x^2-y^2}$ orbitals. Black orbitals denote the AO ordered ground state at half-filling. The hole moves from the point where it was originally doped (dashed empty circle) to the arbitrarily chosen point at the upper-left corner (full circle). Note that the AO order at half-filling can in principle stay unchanged due to the possibility of the very small interorbital hopping (shown) although the hole also moves by creating defects in the AO state which can be 'sometimes' cured by the very small quantum pseudospin fluctuations (not shown). Panel (b): spectral density $A(\mathbf{k},\omega)$ (independent on the orbital flavour of the removed electron) of the $e_g$ orbital $t$–$J$ model [82] with $J = 0.1t$ (i.e. $J = 0.4t$ in the convention used in this thesis) along the particular directions of the 2D Brillouin zone.

the defects by retracing its path, unless it propagated due to small off-diagonal hopping in an $e_g$ system [82] and no defects were created on its path (the latter process also contributes to the above mentioned very small bandwidth of the orbital polaron). Figure 4.13 shows in more detail the most characteristic type of motion here [i.e. how the the hole moves by the small interorbital hopping, see panel (a)] and what the corresponding spectral function looks like [panel (b)].

*$t_{2g}$ orbital polaron.*— In the previous chapter an even more extreme situation of the system with orbital order was investigated: The case of a hole doped into the plane with FM spin order accompanied by the $t_{2g}$ AO order (which could correspond not only to the hole introduced into the ordered ground state of $Sr_2VO_4$ with $t_{2g}$ orbitals but also, surprisingly, to those of $K_2CuF_4$ or $Cs_2AgF_4$ with $d_{z^2-y^2}$ and $d_{x^2-z^2}$ active orbitals). Also here a quasiparticle (*$t_{2g}$ orbital polaron*) is formed due to the dressing of a hole by the collective excitations of the ground state with AO order. However, due to the specific $t_{2g}$ orbital symmetries the orbitons are not mobile at all, the off-diagonal hopping is prohibited, and the quasiparticle acquires a finite bandwidth only due to the frequently neglected three-site terms. Thus, the string picture dominates the character of the $t_{2g}$ orbital polarons even more than in the case of systems with $e_g$ orbital degrees of freedom. Figure 4.14 shows in more detail a representative path arising due to hole propagation [i.e. the hole trapping due to the creation of strings by the hole motion, see a representative path on panel (a)] and what the corresponding spectral function looks like [panel (b)].

*$t_{2g}$ spin-orbital polaron.*— Finally, in this chapter we investigated what happens when a hole is introduced into the plane with both $t_{2g}$ AO order and AF

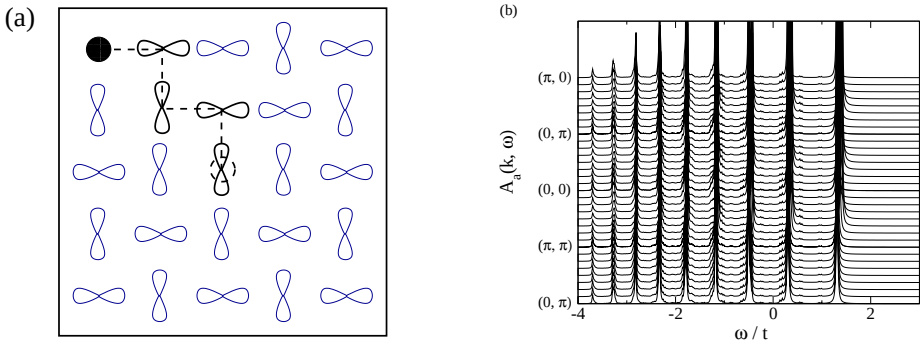


Figure 4.14: Panel (a): Artist's view of the defects created by a single hole doped into the $t_{2g}$ AO state. Blue orbitals denote the AO ordered ground state at half-filling, while black orbitals denote overturned pseudospins due to the hole motion from the point where it was originally doped (dashed empty circle) to the arbitrarily chosen point at the upper-left corner (full circle). Note that there are no quantum pseudospin fluctuations which can erase the defects created by the hole. Panel (b): spectral density $A_a(\mathbf{k},\omega)$ of the $t_{2g}$ orbital $t$–$J$ model (3.5) with $J = 0.4t$ along the particular directions of the 2D Brillouin zone.

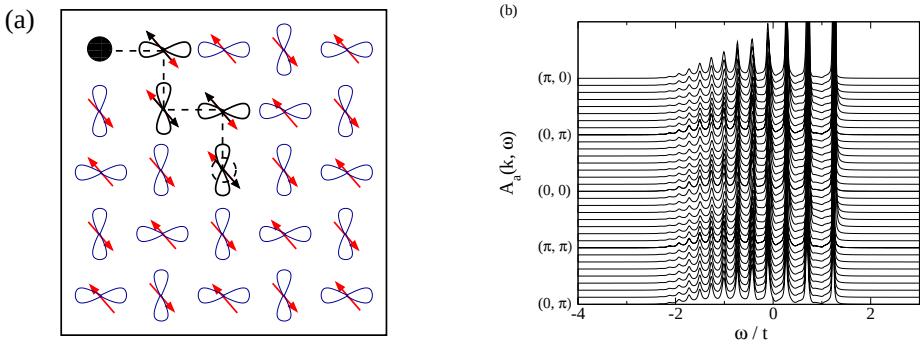


Figure 4.15: Panel (a): Artist's view of the defects created by a single hole doped into the $t_{2g}$ AO and $S = 1$ spin AF ordered state. Red arrows and blue orbitals denote the AF and AO ordered ground state at half-filling, while black arrows and black orbitals denote overturned spins and pseudospins due to the hole motion from the point where it was originally doped (dashed empty circle) to the arbitrarily chosen point at the upper-left corner (full circle). Note that there are no quantum pseudospin fluctuations which can erase the defects created by the hole while the quantum spin fluctuations are suppressed by the orbitals. Panel (b): spectral density $A_a(\mathbf{k},\omega)$ of the $t_{2g}$ spin-orbital $t$–$J$ model (4.3) with $J = 0.2t$ and $\eta = 0.15$ along the particular directions of the 2D Brillouin zone.

spin order (which corresponds to the hole introduced into the $ab$ planes of cubic vanadates such as e.g. $LaVO_3$). Here, the quasiparticle is also formed ($t_{2g}$ *spin-orbital polaron*) but unlike in all of the above cases the hole is dressed here by two types of bosons: orbitons and magnons. Surprisingly, it occurs that the orbital physics dominates here and the spin-orbital polaron resembles the or-

bital polaron to a large extent. This is due to the fact that the orbitals force the hole to retrace its path and hole motion by coupling quantum spin fluctuations is here blocked. Figure 4.15 shows in more detail a representative path arising due to hole propagation [i.e. the hole trapping due to the creation of strings by the hole motion, see panel (a)] ] and what the corresponding spectral function looks like [panel (b)].

*Conclusions.*— The common feature of all these four polarons (quasiparticles) is that all of them have rather large spectral weights (i.e. the incoherent processes are rather small for hole doped into the spin/orbitally ordered states) and small dispersion. However, it is easily visible that the dispersion is significantly larger for the spin polaron than for all of the orbital-type polarons. This is due to the fact that it is much harder for the hole to move in the orbitally ordered state as the latter one is more classical (robust).

# Summary

*Main result.*— The main result of this thesis is the solution of the three strongly correlated electron problems posed in the Preface, which was done using three distinct extended versions of the standard $t$–$J$ model of Chapter 1 or Refs. [1, 2, 3]. More precisely we studied in three consecutive Chapters of the thesis the following problems:

*1. Explaining charge order in* $Sr_{14-x}Ca_xCu_{24}O_{41}$.— Since the $Cu_2O_5$ coupled ladder plane in $Sr_{14-x}Ca_xCu_{24}O_{41}$[4] is a charge-transfer system [41], one needs to use the Zhang-Rice scheme [26] to derive the $t$–$J$ model which would describe the low-energy physics. However, the obtained model (which merely is a $t$–$J$ model on a single ladder) did not reproduce the charge order observed experimentally in $Sr_{14-x}Ca_xCu_{24}O_{41}$ [5, 6, 7, 8]. The reason was that this model omits the repulsion between holes at the same oxygen sites but on different orbitals belonging to two different ladders. Including this term in the Zhang-Rice scheme is crucial — it led to adding the effective interladder interaction between holes in two neighbouring ladders in the new $t$–$J$ model for *coupled* ladders.

The new extended spin $t$–$J$ model was then solved, using the slave-boson approach [20], in the mean-field approximation. The results showed that due to the interladder Coulomb interaction between holes the charge density wave of the peculiar odd period ($\lambda = 3, 5$) could indeed be stable in the $Cu_2O_5$ coupled ladders in $Sr_{14-x}Ca_xCu_{24}O_{41}$ in agreement with the experiment [7, 8].

*2. Verifying the idea of orbitally induced hole localization.*— When one chooses a 2D strongly correlated electron system with $t_{2g}$ degenerate orbitals with the $d_{xy}$ orbital having higher energy, then one is left with a system where along each direction in the $ab$ plane only electrons with one orbital flavour can hop [72, 71]. Therefore, the obtained orbital $t$–$J$ model did not contain pseudospin quantum fluctuation, its $J$ part was purely of the Ising-type, and the model could be regarded as a prototypical example where the orbitals induce hole localization [21, 67]. However, one can have some doubts concerning this result since for instance if the $SU(2)$ symmetry is absent in the system (as is the case here), then one should be more careful with all approximations used (see Sec. 2.2 for more detailed discussion). One of the approximations used in this orbital $t$–$J$ model was the ommitance of the three-site terms which should always be present in any $t$–$J$ model [1, 2] but since their contribution to the total energy is small, one often neglects them. Adding the properly derived three-site terms to the model led to the new $t_{2g}$ orbital $t$–$J$ model *with* three-site terms.

The new extended orbital $t$–$J$ model was then solved, using the slave-fermion approach [20], in the SCBA approximation [23]. The results showed that the hole added to the half-filled AO ordered ground state of the orbital model moved coherently through the lattice due to the three-site terms. Thus, in the simplest

model, in which the orbitally induced hole localization naively would be possible, the added hole was not localized.

*3. Understanding hole motion in $LaVO_3$.*— Due to the $t_{2g}$ orbital degeneracy in the vanadium ions in $La_{1-x}Sr_xVO_3$, the proper $t$–$J$ model for the $ab$ planes of cubic vanadates had to include not only the spin but also orbital degrees of freedom. Furthermore, it should also contain the three-site terms which are required for a faithful represention of the low energy physics in the $t$–$J$ models with the Ising-type interaction between pseudospins (cf. the problem discussed in point 2.). This led to the new $t_{2g}$ *spin-orbital* $t$–$J$ model with three-site terms.

The new extended spin-orbital $t$–$J$ model was then solved, using the slave-fermion approach [20], in the SCBA approximation [23]. This, however, was not so straightforward since one had to take the spin *and* orbital degrees of freedom on equal footing. The reason for that was that the Goodenough-Kanamori rules [55, 56] are violated in the planes of cubic vanadates [93] and both the orbitals and spins should be treated as dynamical variables. Therefore, the SCBA [23] had to be modified to include the coupling between the added hole and the orbital as well as spin excitations simultaneously. The results showed that the hole added to the half-filled AO ordered ground state of the spin-orbital model was not localized but could move merely due to the three-site terms. Since this result resembled the one obtained in point 2. (purely orbital problem, see above), one could easily explain the conjecture from the experiment [19] that the orbital dynamics played a significant role in the doped cubic vanadates. On the other hand, a detailed investigation showed that the spin dynamics was quenched and the spins were forced to act on the hole like orbital pseudospins (i.e. more classical) merely by the orbitals.

*Careful approach needed.*— It is visible from the above discussion that one indeed had to go 'beyond the standard $t$–$J$ model' to obtain reasonable explanations of the problems. However, as just discussed this had to be done rather carefully. First, one had to take into account the charge transfer regime (in the first case) or the orbital degrees of freedom (in two other cases) in the derivation of the respective $t$–$J$ model. Notably, in all three cases this did not turn out to be the 'full story'. Therefore, in order to get physical insights into these situations, one also had to include additional interactions due to the specific geometry of coupled ladders (in the first case), the three-site terms (in two other cases) or develop a new theoretical approach to solve the model (in the third case).

*'Powerfulness' of the $t$–$J$ concept.*– A 'side' but perhaps very important result of the thesis is that it shows how powerful the concept of the $t$–$J$ model is based either on the canonical perturbation expansion [1, 2] or on the Zhang-Rice scheme [26]. Although all of these three problems could have been solved (and at least the first two of them *were* solved) using the Hubbard-like model, it was demonstrated that the extended $t$–$J$ models gave a better insight into them — the problems of Chapter 2 and 3 were solved also using the Hubbard-like model but it was much harder to deduce from these solutions the microscopic picture. For example: (i) to study the role of the interladder interaction in the Hubbard-like model one had to introduce rather complicated order parameters in Chapter 2, or (ii) from the Hubbard-like model it was hard to reveal the peculiar ('three-site-term-type') nature of the hole motion in the AO ordered state in Chapter 3.

The natural question which arises in this context is whether there is a deeper

reason for this 'powerfulness'. Why the concept of the $t$–$J$ model is so successful? Some first hints were already given in Chapter 1 where we stated that any $t$–$J$ model is easier to solve than the Hubbard model as it spans a smaller Hilbert space [28]. Obviously such a feature helps a lot but there is still some deeper (i.e. qualitative) reason – the fermionic systems can be best understood: (i) if they are not interacting (Fermi gas) or (ii) if they are transformed to some kind of bosonic/classical matter [109]. Otherwise the fermion sign problem means that is is hard to obtain reasonable solutions [110] and merely the Fermi liquid phenomenology can be applied [109].

Here, this second possibility needs some clarification and therefore let us give some examples of such transformations 'available on the market' [33, 109, 111, 112]: (a) the weak-coupling scheme in which one introduces (using the mean-field decoupling or the variational Ansatz) the classical ground state which is not the eigenstate of the Hamiltonian at the cost of introducing collective bosonic excitations of the system; then these two together describe the quantum ground state (e.g. BCS theory of superconductivity, spin- or charge- density waves in the Hubbard-like model) [33, 111]; (b) the strong-coupling scheme in which one performs the canonical perturbation expansion [1, 2] or the Zhang-Rice scheme [26] to reduce the dimension of the Hilbert space by introducing spin/pseudospins and then one performs all the steps as in point (a) (e.g. antiferromagnetism in the Hubbard model or much of this thesis) [33, 111]; (c) the true bosonization procedure, valid only for 1D systems [113]; or (d) reduction of the fermionic interacting problem to the Kondo-type impurity problems (the fundament of the dynamical mean-field theory) [114]. Hence, if one wants to understand the interacting fermions, one is anyway bound to introduce some kind of the transformation to classical and/or bosonic matter. It is then a matter of convenience which way to choose and it merely occurs that for example the strong-coupling scheme is more convenient than the weak-coupling scheme. This is because the transformation suggested in point (a) is more complicated in the momentum-space (in the weak coupling regime) than in the real space (in the strong coupling regime) [33]. Here lies the success of the $t$–$J$ model concept.

Thus, summarizing, this thesis is just a canonical example of the paradigm that to explain peculiar phenomena found in the strongly *interacting* fermions (electrons) one needs to somehow 'get rid as much as possible' of the Fermi statistics. It is the $t$–$J$ model that does it in one of the easiest and most transparent possible ways.

*Postscriptum.*— Let us note that for the detailed discussion of the peculiar connections between the problems studied in Chapter 3 and Chapter 4 we refer to Sec. 4.7. There we compare four distinct types of spin and orbital polarons — the well-known spin polaron [23], the $e_g$ orbital polaron [82], and the two polarons discussed in this thesis. The latter ones are: (i) the $t_{2g}$ orbital polaron which is formed when a single hole is doped into the plane with the $d_{zx}/d_{yz}$ alternating orbitals and which is dressed with the excitations of the AO ordered ground state (Chapter 3), and (ii) the $t_{2g}$ spin-orbital polaron which is formed when a single hole is doped into the plane with the $d_{zx}/d_{yz}$ alternating orbitals and the AF order spins and which is dressed with the excitations of the AO and AF ordered ground state (Chapter 4). It is shown there that the dispersion for the spin polarons is significantly larger than for all of the orbital-type polarons. This is because the orbital order is more classical (robust) and it is much harder for the hole to move in such a state.

# Appendix A

# The continued fraction method for the 1D orbital model

*Purpose of the appendix.*— This appendix shows how to calculate the Green's function for the hole doped into the immobile $b$ orbital in the 1D AO ground state (3.16) of the model Eq. (3.46) of Sec. 3.5.2.

*Choice of convenient basis.*— When one attempts to calculate the Green's function for a hole doped in the immobile $b$ orbital

$$G_b^{\rm 1D}(k,\omega) = \left\langle \Phi_0^{\rm 1D} \left| b_k^\dagger \frac{1}{\omega + H_{\rm 1D} - E_0^{\rm 1D}} b_k \right| \Phi_0^{\rm 1D} \right\rangle , \tag{A.1}$$

one finds immediately that the state

$$|\psi_k^{(1)}\rangle \equiv b_k |\Phi_0^{\rm 1D}\rangle = \frac{1}{\sqrt{N}} \sum_j e^{ikj} b_j |\Phi_0^{\rm 1D}\rangle , \tag{A.2}$$

is not an eigenstate of the Hamiltonian $H_{\rm 1D}$. Here a hole is doped in each Fourier component in an occupied $b$ orbital at site $j$ in the ground state $|\Phi_0^{\rm 1D}\rangle$ with AO order (3.16). When a hole is doped, it can delocalize to its neighbours in the 1D chain, as depicted in Fig. 3.9(b), so one has to introduce appropriate basis of states obtained when the single hole delocalizes along the 1D chain. The hopping term $\propto t$ acting on $|\psi_k^{(1)}\rangle$ generates the state

$$|\psi_k^{(2)}\rangle \equiv \frac{1}{\sqrt{2N}} \sum_j e^{ikj} (a_{j-1} + a_{j+1}) a_j^\dagger b_j |\Phi_0^{\rm 1D}\rangle , \tag{A.3}$$

with the hole delocalized to the neighbouring $j-1$ ($j+1$) sites of the $A$ sublattice, i.e. to the the left (right) from the initial hole position $j$ in each Fourier component $b_j|\Phi_0^{\rm 1D}\rangle$ included in Eq. (A.2). The remaining states $\{|\psi_k^{(n)}\rangle\}$ with $n > 2$, which occur in the continued fraction expansion needed to evaluate the Green's function $G_b^{\rm 1D}(k,\omega)$ (see below), are generated by acting $(n-2)$ times on $|\psi_k^{(2)}\rangle$ with the three-site hopping term $\propto \tau$. In this way one finds the set of symmetric states, with a superposition of the hole propagating forward (either

to the left or to the right from the initial defect), i.e. along the same direction as that given by the first hop which leads to $|\psi_k^{(2)}\rangle$, cf. Fig. 3.9(c). This structure of the basis set explains the absence of the $k$ dependence in the Green's function for $b$ orbitals, so we adopt the simplified notation $G_b^{\rm 1D}(\omega)$ below.

*Continued fraction method.*— In the infinite basis generated by the above described procedure, the Hamiltonian matrix of the Hamiltonian (3.46) reads:

$$\begin{aligned}\langle\psi_k^{(m)}|\,\omega + H_{\rm 1D} - E_0^{\rm 1D}|\psi_k^{(n)}\rangle = \\ = \frac{1}{2}\begin{pmatrix} \omega+J/2 & \sqrt{2}t & 0 & 0 & ... \\ \sqrt{2}t & \omega+3J/4 & \tau & 0 & ... \\ 0 & \tau & \omega+J & \tau & ... \\ 0 & 0 & \tau & \omega+J & ... \\ ... & ... & ... & ... & ... \end{pmatrix}.\end{aligned} \tag{A.4}$$

In order to obtain the relevant Green's function $G_b^{\rm 1D}(\omega)$, it suffices to calculate the $(1,1)$ element of the inverse of this matrix.[1] Due to the tridiagonal form of the Hamiltonian, this can be done even for an infinite Hilbert space and one arrives at a continued fraction result:

$$\begin{aligned}G_b^{\rm 1D}(\omega) &= \left\{\left\langle\psi_k^{(m)}\right|\left(\omega + H_{\rm 1D} - E_0^{\rm 1D}\right)^{-1}\left|\psi_k^{(n)}\right\rangle\right\}_{1,1} \\ &= \frac{1}{2}\left\{\omega + \frac{1}{2}J - \frac{2t^2}{\omega+\frac{3}{4}J - \frac{\tau^2}{\omega+J-\frac{\tau^2}{\omega+J-...}}}\right\}^{-1},\end{aligned} \tag{A.5}$$

where the whole self-similar part can be summed up to the self-energy which does not depend on $k$ [67]:

$$\Sigma(\omega) \equiv \frac{\tau^2}{\omega + J - \frac{\tau^2}{\omega+J-\frac{\tau^2}{\omega+J-...}}} = \frac{\tau^2}{\omega + J - \Sigma(\omega)}. \tag{A.6}$$

This, together with Eq. (A.10), leads to a quadratic equation for $\Sigma(\omega)$ with two solutions:

$$\Sigma(\omega) = \frac{1}{2}\left\{(\omega+J) \pm \sqrt{(\omega+J)^2 - 4\tau^2}\right\}. \tag{A.7}$$

The proper sign may be determined using the Green's function $G_b^{\rm 1D}(\omega)$ obtained before [89] in the limit of $\tau = 0$,

$$G_b^{\rm 1D(0)}(\omega) = \frac{1}{2}\left\{\omega + \frac{1}{2}J - \frac{2t^2}{\omega+\frac{3}{4}J}\right\}^{-1}. \tag{A.8}$$

In this limit the self-energy vanishes, $\Sigma(\omega) = 0$, and the Green's function has two poles at energies

$$\omega = -\frac{5}{8}J \pm \sqrt{2}t\sqrt{1 + \frac{1}{128}\left(\frac{J}{t}\right)^2}. \tag{A.9}$$

[1] This relation holds up to a constant due to the fact that the basis $\{|\psi_k^{(n)}\rangle\}$ is not normalized – however, we take care of this problem.

Finally, one arrives at the general result for $\tau > 0$:

$$G_b^{1\mathrm{D}}(\omega) = \frac{1}{2}\left\{\omega + \frac{1}{2}J - \frac{4t^2}{\omega + \frac{1}{2}J \mp \sqrt{(\omega+J)^2 - 4\tau^2}}\right\}^{-1}, \tag{A.10}$$

where the sign convention is fixed by comparing this result with the Green's function $G_b^{1\mathrm{D}(0)}(\omega)$ (A.8) — this implies that one has to select $-$ $(+)$ sign for $\omega < -J$ $(\omega > -J)$, respectively.

# Appendix B

# The effective polaron model for fluorides

*Purpose of the appendix.*— Here we show that the effective polaron model developed in Chapter 3 (see Eq. 3.32) may also be applied to certain fluorides with FM planes and $e_g$ AO order. Thus, we will prove that the experimental predictions concerning the photoemission spectra of certain vanadates (see Sec. 3.7) are also valid for a particular class of fluorides.

*Dependence of $e_g$ AO order on the crystal field.*— In contrast to the $t_{2g}$ orbitally degenerate systems, in the systems with $e_g$ orbital degeneracy the lattice distortions in the cubic phases are usually quite large. In particular, the *static* distortions may counteract to some extent the AO order favoured by the superexchange interactions as e.g. in undoped manganites $R\mathrm{MnO_3}$ [76] or fluorides $\mathrm{Cs_2AgF_4}$ [92]. However, the crystal field does not suppress the orbital order present in these systems but instead it only modifies the occupied orbitals which form the AO state. They have to be optimized in a microscopic model by choosing particular linear combinations of the $e_g$ orbitals, which form the AO order, in order to fit best to the superposition of the superexchange and the Jahn-Teller terms generated by ligand fields [100]. In certain situations this 'modification' could be quite substantial and could even lead to such a selection of $e_g$ orbitals that the resulting state is modified towards a FO-type order [84].

At finite crystal field splitting $\propto E_z$, it is convenient to describe the changes in the occupied orbital states by making two complementary transformations at both sublattices [84], rotating the orbitals by an angle $\theta = \frac{\pi}{4} - \phi$ on sublattice $A$, and by an angle $\theta = \frac{\pi}{4} + \phi$ on sublattice $B$, so that the relative angle between the *occupied* orbitals is $\frac{\pi}{2} - 2\phi$ and decreases with increasing $\phi$, i.e. with increasing $E_z$

$$\begin{pmatrix} |\mu\rangle_{\mathbf{i}} \\ |\nu\rangle_{\mathbf{i}} \end{pmatrix} = \begin{pmatrix} \cos(\frac{\pi}{4} - \phi) & \sin(\frac{\pi}{4} - \phi) \\ -\sin(\frac{\pi}{4} - \phi) & \cos(\frac{\pi}{4} - \phi) \end{pmatrix} \begin{pmatrix} |\mathrm{z}\rangle_{\mathbf{i}} \\ |\mathrm{x}\rangle_{\mathbf{i}} \end{pmatrix}, \tag{B.1}$$

$$\begin{pmatrix} |\mu\rangle_{\mathbf{j}} \\ |\nu\rangle_{\mathbf{j}} \end{pmatrix} = \begin{pmatrix} \cos(\frac{\pi}{4} + \phi) & \sin(\frac{\pi}{4} + \phi) \\ -\sin(\frac{\pi}{4} + \phi) & \cos(\frac{\pi}{4} + \phi) \end{pmatrix} \begin{pmatrix} |\mathrm{z}\rangle_{\mathbf{j}} \\ |\mathrm{x}\rangle_{\mathbf{j}} \end{pmatrix}, \tag{B.2}$$

where the 'old' orthogonal (basis) orbitals are defined as $|\mathrm{x}\rangle_{\mathbf{i}} = \frac{1}{\sqrt{2}}|x^2 - y^2\rangle_{\mathbf{i}}$ and $|\mathrm{z}\rangle_{\mathbf{i}} = \frac{1}{\sqrt{6}}|3z^2 - r^2\rangle_{\mathbf{i}}$ for *every* sublattice site $\mathbf{i}$. Due to the above transformation the AO order is formed now by $|\mu\rangle_{\mathbf{i}}$ and $|\nu\rangle_{\mathbf{j}}$ occupied orbitals at sublattices, $\mathbf{i} \in$

$A$ and $\mathbf{j} \in B$, respectively. Let us stress that although the transformation defined by Eqs. (B.1–B.2) is orthogonal, this does not imply that orbitals on different sublattices, such as e.g. the occupied orbitals $|\mu\rangle_{\mathbf{i}}$ and $|\nu\rangle_{\mathbf{j}}$ are orthogonal — in fact they would be orthogonal only for certain discrete values of $\phi$, for instance for $\phi = \pi/4$.

For the 2D FM systems with active $e_g$ orbitals which are considered here, the relation between the crystal field $E_z$ and the optimal orbital configuration defined by the angle $\phi$ [see Eqs. (12) and (13) of Ref. [84]] is given by:

$$E_z = 4J \sin 2\phi, \tag{B.3}$$

where $J$ is the superexchange constant. In the case of fluorides such as $Cs_2AgF_4$ (Ref. [92]) or $K_2CuF_4$ (Ref. [115]) discussed here, the filling is one $e_g$ electron per site and the crystal field would select the angle $\phi = \pi/12$ (for the reason of looking at this angle see below) since the convenient basis adapted to the actual AO order looks as follows:

$$\begin{aligned}
\forall\, \mathbf{i} \in A: \ & \left|\mu\left(\phi = \frac{\pi}{12}\right)\right\rangle_{\mathbf{i}} = \frac{1}{\sqrt{2}}|y^2 - z^2\rangle_{\mathbf{i}} \equiv |x\rangle_{\mathbf{i}}\,, \\
& \left|\nu\left(\phi = \frac{\pi}{12}\right)\right\rangle_{\mathbf{i}} = \frac{1}{\sqrt{6}}|3x^2 - r^2\rangle_{\mathbf{i}} \equiv |z\rangle_{\mathbf{i}}\,, \\
\forall\, \mathbf{j} \in B: \ & \left|\mu\left(\phi = \frac{\pi}{12}\right)\right\rangle_{\mathbf{j}} = \frac{1}{\sqrt{6}}|3y^2 - r^2\rangle_{\mathbf{j}} \equiv |z\rangle_{\mathbf{j}}\,, \\
& \left|\nu\left(\phi = \frac{\pi}{12}\right)\right\rangle_{\mathbf{j}} = \frac{1}{\sqrt{2}}|x^2 - z^2\rangle_{\mathbf{j}} \equiv |x\rangle_{\mathbf{j}}\,,
\end{aligned} \tag{B.4}$$

where the occupied (empty) orbitals for this type of AO order are denoted as $|x\rangle$ ($|z\rangle$) on both sublattices.

*'Particular' $e_g$ AO order similar to $t_{2g}$ AO order.*— The reason why these particular pairs of basis orbitals (B.4) are interesting here is that this is the only choice of occupied $e_g$ flavours which forms a two-sublattice AO order with the interorbital hopping between occupied orbitals vanishing by symmetry and where the interactions described by pseudospin operators do not allow for any quantum fluctuations. This resembles the $t_{2g}$ case discussed in Chapter 3. There is, however, one subtle difference: two occupied $\{|x\rangle_{\mathbf{i}}, |x\rangle_{\mathbf{j}}\}$ orbitals on sublattices $A$ and $B$ are not orthogonal and do not form the global basis in the $e_g$ orbital space. The choice made in Eq. (B.4) means that one considers two different pairs of orbitals for both sublattices and the interorbital hopping between the *unoccupied* orbitals is also rather small but remains finite.[1] Hence, the respective $t$–$J$ Hamiltonian is richer than the one for the $t_{2g}$ case and we need to check under which conditions it can be reduced to a similar polaron Hamiltonian as the one given by Eq. (3.32).

*$t$–$J$ model for 'particular' $e_g$ orbitals.*— The $e_g$ orbital $t$–$J$ Hamiltonian for the FM planes without the three-site terms but including the crystal field is given e.g. in Ref. [116]. Here we rewrite the kinetic term in a slightly different form (there it is already written in the slave-fermion representation) and substitute $\phi = \pi/12$ to obtain:

$$H_{e_g} = H_t + H_J + H_z\,, \tag{B.5}$$

[1] The physical reason for this is just that the crystal field does not fully prohibit interorbital hopping.

where

$$H_t = -\frac{1}{2}t\sum_{\mathbf{i}}(\tilde{z}^\dagger_{\mathbf{i}}\tilde{z}_{\mathbf{i}+\hat{\mathbf{a}}} + \tilde{z}^\dagger_{\mathbf{i}}\tilde{z}_{\mathbf{i}+\hat{\mathbf{b}}} + \text{H.c.}) - \frac{\sqrt{3}}{2}t\sum_{\mathbf{i}\in A}(\tilde{z}^\dagger_{\mathbf{i}}\tilde{x}_{\mathbf{i}+\hat{\mathbf{a}}} + \tilde{z}^\dagger_{\mathbf{i}}\tilde{x}_{\mathbf{i}+\hat{\mathbf{b}}} + \text{H.c.})$$
$$- \frac{\sqrt{3}}{2}t\sum_{\mathbf{i}\in B}(\tilde{x}^\dagger_{\mathbf{i}}\tilde{z}_{\mathbf{i}+\hat{\mathbf{a}}} + \tilde{x}^\dagger_{\mathbf{i}}\tilde{z}_{\mathbf{i}+\hat{\mathbf{b}}} + \text{H.c.})\,, \tag{B.6}$$

$$H_J = \frac{1}{2}J\sum_{\langle\mathbf{ij}\rangle||\hat{a}}\left(T^z_{\mathbf{i}}T^z_{\mathbf{j}} + \sqrt{3}T^z_{\mathbf{i}}T^x_{\mathbf{j}}\right) + \frac{1}{2}J\sum_{\langle\mathbf{ij}\rangle||\hat{b}}\left(T^z_{\mathbf{i}}T^z_{\mathbf{j}} - \sqrt{3}T^x_{\mathbf{i}}T^z_{\mathbf{j}}\right)\,, \tag{B.7}$$

$$H_z = -\frac{1}{4}J\sum_{\mathbf{i}\in A}(T^z_{\mathbf{i}} + \sqrt{3}T^x_{\mathbf{i}}) + \frac{1}{4}J\sum_{\mathbf{i}\in B}(T^z_{\mathbf{i}} - \sqrt{3}T^x_{\mathbf{i}})\,. \tag{B.8}$$

Here $T^z_{\mathbf{i}} = \frac{1}{2}(\tilde{n}_{\mathbf{i}z} - \tilde{n}_{\mathbf{i}x})$ for $\mathbf{i}\in A$, $T^z_{\mathbf{j}} = \frac{1}{2}(\tilde{n}_{\mathbf{j}x} - \tilde{n}_{\mathbf{j}z})$ for $\mathbf{j}\in B$, and $T^x_{\mathbf{i}} = \frac{1}{2}(\tilde{x}^\dagger_{\mathbf{i}}\tilde{z}_{\mathbf{i}} + \tilde{z}^\dagger_{\mathbf{i}}\tilde{x}_{\mathbf{i}})$ for every site $\mathbf{i}$, see Ref. [84]. As before, a tilde above a fermion operator indicates that the Hilbert space is restricted to unoccupied and singly occupied sites, e.g. $\tilde{x}^\dagger_{\mathbf{i}} = x^\dagger_{\mathbf{i}}(1-n_{\mathbf{i}z})$. The last term $H_z$ represents the above mentioned crystal field with the strength of the interaction written according to Eq. (B.3) with $\phi = \pi/12$.

*Three-site terms for 'particular' $e_g$ orbitals.*— As far as we know, the three-site terms have not been derived for the $e_g$ orbital systems. Thus, we use again the canonical perturbation theory of Chapter 1 applied to the Hubbard model for spinless $e_g$ electrons in a FM plane [107] with the basis rotated by $\phi = \pi/12$, following Eqs. (12) and (13) of Ref. [84]. This leads to the following three-site terms for the $e_g$ orbital $t$–$J$ model with $\phi = \pi/12$:

$$H_{3\text{s}} = H_{3\text{s},a} + H_{3\text{s},b} + H_{3\text{s},ab}, \tag{B.9}$$

where

$$H_{3\text{s},a} =$$
$$-\frac{1}{4}\tau\sum_{\mathbf{i}\in A}\Big[\tilde{z}^\dagger_{\mathbf{i}-\hat{\mathbf{a}}}\tilde{n}_{\mathbf{i}x}\tilde{z}_{\mathbf{i}+\hat{\mathbf{a}}} + \underline{3\tilde{x}^\dagger_{\mathbf{i}-\hat{\mathbf{a}}}\tilde{n}_{\mathbf{i}x}\tilde{x}_{\mathbf{i}+\hat{\mathbf{a}}}} + \underline{\underline{\sqrt{3}\tilde{x}^\dagger_{\mathbf{i}-\hat{\mathbf{a}}}\tilde{n}_{\mathbf{i}x}\tilde{z}_{\mathbf{i}+\hat{\mathbf{a}}}}} + \underline{\underline{\sqrt{3}\tilde{z}^\dagger_{\mathbf{i}-\hat{\mathbf{a}}}\tilde{n}_{\mathbf{i}x}\tilde{x}_{\mathbf{i}+\hat{\mathbf{a}}}}}\Big]$$
$$-\frac{1}{4}\tau\sum_{\mathbf{i}\in B}\Big[\tilde{z}^\dagger_{\mathbf{i}-\hat{\mathbf{a}}}\tilde{n}_{\mathbf{i}x}\tilde{z}_{\mathbf{i}+\hat{\mathbf{a}}} + 3\tilde{z}^\dagger_{\mathbf{i}-\hat{\mathbf{a}}}\tilde{n}_{\mathbf{i}z}\tilde{z}_{\mathbf{i}+\hat{\mathbf{a}}} - \sqrt{3}\tilde{z}^\dagger_{\mathbf{i}-\hat{\mathbf{a}}}\tilde{z}^\dagger_{\mathbf{i}}\tilde{x}_{\mathbf{i}}\tilde{z}_{\mathbf{i}+\hat{\mathbf{a}}} - \sqrt{3}\tilde{z}^\dagger_{\mathbf{i}-\hat{\mathbf{a}}}\tilde{x}^\dagger_{\mathbf{i}}\tilde{z}_{\mathbf{i}}\tilde{z}_{\mathbf{i}+\hat{\mathbf{a}}}\Big]$$
$$+\,\text{H.c.}\,, \tag{B.10}$$

$$H_{3\text{s},b} =$$
$$-\frac{1}{4}\tau\sum_{\mathbf{i}\in A}\Big[\tilde{z}^\dagger_{\mathbf{i}-\hat{\mathbf{b}}}\tilde{n}_{\mathbf{i}x}\tilde{z}_{\mathbf{i}+\hat{\mathbf{b}}} + 3\tilde{z}^\dagger_{\mathbf{i}-\hat{\mathbf{b}}}\tilde{n}_{\mathbf{i}z}\tilde{z}_{\mathbf{i}+\hat{\mathbf{b}}} - \sqrt{3}\tilde{z}^\dagger_{\mathbf{i}-\hat{\mathbf{b}}}\tilde{z}^\dagger_{\mathbf{i}}\tilde{x}_{\mathbf{i}}\tilde{z}_{\mathbf{i}+\hat{\mathbf{b}}} - \sqrt{3}\tilde{z}^\dagger_{\mathbf{i}-\hat{\mathbf{b}}}\tilde{x}^\dagger_{\mathbf{i}}\tilde{z}_{\mathbf{i}}\tilde{z}_{\mathbf{i}+\hat{\mathbf{b}}}\Big]$$
$$-\frac{1}{4}\tau\sum_{\mathbf{i}\in B}\Big[\tilde{z}^\dagger_{\mathbf{i}-\hat{\mathbf{b}}}\tilde{n}_{\mathbf{i}x}\tilde{z}_{\mathbf{i}+\hat{\mathbf{b}}} + \underline{3\tilde{x}^\dagger_{\mathbf{i}-\hat{\mathbf{b}}}\tilde{n}_{\mathbf{i}x}\tilde{x}_{\mathbf{i}+\hat{\mathbf{b}}}} + \underline{\underline{\sqrt{3}\tilde{x}^\dagger_{\mathbf{i}-\hat{\mathbf{b}}}\tilde{n}_{\mathbf{i}x}\tilde{z}_{\mathbf{i}+\hat{\mathbf{b}}}}} + \underline{\underline{\sqrt{3}\tilde{z}^\dagger_{\mathbf{i}-\hat{\mathbf{b}}}\tilde{n}_{\mathbf{i}x}\tilde{x}_{\mathbf{i}+\hat{\mathbf{b}}}}}\Big]$$
$$+\,\text{H.c.}\,, \tag{B.11}$$

$$
\begin{aligned}
&H_{3\mathrm{s},ab} = \\
&-\frac{1}{4}\tau\sum_{\mathbf{i}\in A}\Big[\tilde{z}^{\dagger}_{\mathbf{i}\pm\hat{\mathbf{a}}}\tilde{n}_{\mathbf{i}x}\tilde{z}_{\mathbf{i}\pm\hat{\mathbf{b}}} - 3\tilde{x}^{\dagger}_{\mathbf{i}\pm\hat{\mathbf{a}}}\tilde{x}^{\dagger}_{\mathbf{i}}\tilde{z}_{\mathbf{i}}\tilde{z}_{\mathbf{i}\pm\hat{\mathbf{b}}} + \underline{\underline{\sqrt{3}\tilde{x}^{\dagger}_{\mathbf{i}\pm\hat{\mathbf{a}}}\tilde{n}_{\mathbf{i}x}\tilde{z}_{\mathbf{i}\pm\hat{\mathbf{b}}}}} - \sqrt{3}\tilde{z}^{\dagger}_{\mathbf{i}\pm\hat{\mathbf{a}}}\tilde{x}^{\dagger}_{\mathbf{i}}\tilde{z}_{\mathbf{i}}\tilde{z}_{\mathbf{i}\pm\hat{\mathbf{b}}} \\
&+\tilde{z}^{\dagger}_{\mathbf{i}\pm\hat{\mathbf{a}}}\tilde{n}_{\mathbf{i}x}\tilde{z}_{\mathbf{i}\mp\hat{\mathbf{b}}} - 3\tilde{x}^{\dagger}_{\mathbf{i}\pm\hat{\mathbf{a}}}\tilde{x}^{\dagger}_{\mathbf{i}}\tilde{z}_{\mathbf{i}}\tilde{z}_{\mathbf{i}\mp\hat{\mathbf{b}}} + \underline{\underline{\sqrt{3}\tilde{x}^{\dagger}_{\mathbf{i}\pm\hat{\mathbf{a}}}\tilde{n}_{\mathbf{i}x}\tilde{z}_{\mathbf{i}\mp\hat{\mathbf{b}}}}} - \sqrt{3}\tilde{z}^{\dagger}_{\mathbf{i}\pm\hat{\mathbf{a}}}\tilde{x}^{\dagger}_{\mathbf{i}}\tilde{z}_{\mathbf{i}}\tilde{z}_{\mathbf{i}\mp\hat{\mathbf{b}}}\Big] \\
&-\frac{1}{4}\tau\sum_{\mathbf{i}\in B}\Big[\tilde{z}^{\dagger}_{\mathbf{i}\pm\hat{\mathbf{a}}}\tilde{n}_{\mathbf{i}x}\tilde{z}_{\mathbf{i}\pm\hat{\mathbf{b}}} - 3\tilde{z}^{\dagger}_{\mathbf{i}\pm\hat{\mathbf{a}}}\tilde{z}^{\dagger}_{\mathbf{i}}\tilde{x}_{\mathbf{i}}\tilde{x}_{\mathbf{i}\pm\hat{\mathbf{b}}} + \underline{\underline{\sqrt{3}\tilde{z}^{\dagger}_{\mathbf{i}\pm\hat{\mathbf{a}}}\tilde{n}_{\mathbf{i}x}\tilde{x}_{\mathbf{i}\pm\hat{\mathbf{b}}}}} - \sqrt{3}\tilde{z}^{\dagger}_{\mathbf{i}\pm\hat{\mathbf{a}}}\tilde{z}^{\dagger}_{\mathbf{i}}\tilde{x}_{\mathbf{i}}\tilde{z}_{\mathbf{i}\pm\hat{\mathbf{b}}} \\
&+\tilde{z}^{\dagger}_{\mathbf{i}\pm\hat{\mathbf{a}}}\tilde{n}_{\mathbf{i}x}\tilde{z}_{\mathbf{i}\mp\hat{\mathbf{b}}} - 3\tilde{z}^{\dagger}_{\mathbf{i}\pm\hat{\mathbf{a}}}\tilde{z}^{\dagger}_{\mathbf{i}}\tilde{x}_{\mathbf{i}}\tilde{x}_{\mathbf{i}\mp\hat{\mathbf{b}}} + \underline{\underline{\sqrt{3}\tilde{z}^{\dagger}_{\mathbf{i}\pm\hat{\mathbf{a}}}\tilde{n}_{\mathbf{i}x}\tilde{x}_{\mathbf{i}\mp\hat{\mathbf{b}}}}} - \sqrt{3}\tilde{z}^{\dagger}_{\mathbf{i}\pm\hat{\mathbf{a}}}\tilde{z}^{\dagger}_{\mathbf{i}}\tilde{x}_{\mathbf{i}}\tilde{z}_{\mathbf{i}\mp\hat{\mathbf{b}}}\Big] \\
&+\mathrm{H.c.}\,. \qquad \text{(B.12)}
\end{aligned}
$$

Here we underline (doubly underline) terms which do not require orbital excitations (require orbital excitations), respectively, i.e.

$$H_{3\mathrm{s}(0)} = \underline{H_{3\mathrm{s}}}, \qquad H_{3\mathrm{s}(1)} = \underline{\underline{H_{3\mathrm{s}}}}. \qquad \text{(B.13)}$$

The physical reason for this is just that the crystal field does not fully prohibit interorbital hopping.

*Effective polaron model.*— Next, we perform the same standard transformation to obtain the polaron Hamiltonian from the $t$–$J$ model [23] for the lightly doped ordered states as done in Chapter 3, i.e. we introduce Schwinger boson operators $\{t^{\dagger}_{\mathbf{i}a}, t^{\dagger}_{\mathbf{i}b}\}$ and fermion operators $h_{\mathbf{i}}$ (holons) which are related to the $\tilde{x}^{\dagger}_{\mathbf{i}}$ and $\tilde{z}^{\dagger}_{\mathbf{i}}$ operators in the following way:

$$\tilde{x}^{\dagger}_{\mathbf{i}} \equiv t^{\dagger}_{\mathbf{i}a}h_{\mathbf{i}}, \qquad \tilde{z}^{\dagger}_{\mathbf{i}} \equiv t^{\dagger}_{\mathbf{i}b}h_{\mathbf{i}}. \qquad \text{(B.14)}$$

Please note, however, that here we do not have to perform rotation of the pseudospins since we define distinct electron operators for the occupied and empty orbitals, cf. Eq. (B.4).

Again, as in Chapter 3, we introduce the Holstein-Primakoff bosons $\beta$ and skip higher-order terms in the Hamiltonian (the LOW approximation for bosons and only three-particle interaction in the mixed boson-holon terms). This means that e.g. the three-site terms are reduced only to the terms which were either underlined or doubly underlined in Eqs. (B.10)–(B.12), i.e. to either $H_{3\mathrm{s}(0)}$ or $H_{3\mathrm{s}(1)}$. Here, however, we have to use yet another approximation which was unnecessary for the $t_{2g}$ model: as these terms were absent in Chapter 3 we skip $H_{3\mathrm{s}(1)}$. This approximation is allowed since these terms contribute to the vertex as $\propto \tau$ and not as $\propto t$, resulting typically in much reduced energy scale for the new vertex contributions. Furthermore, we showed in Sec. 3.7 that such terms [cf. Eq. (3.59) and Fig. 3.13] did not change the energy of the quasiparticle and merely modify the incoherent spectrum. Eventually, one arrives at the polaron Hamiltonian for the holes doped into the $e_g$ orbitals of the fluorides with the hopping terms:

$$
\begin{aligned}
H^{eff}_{t} =& \sqrt{3}t\frac{1}{\sqrt{N}}\sum_{\mathbf{k},\mathbf{q}}\Big\{\cos(k_x-q_x)h^{\dagger}_{\mathbf{k}A}h_{\mathbf{k}-\mathbf{q},B}\beta_{\mathbf{q}A} \\
&+\cos(k_y-q_y)h^{\dagger}_{\mathbf{k}B}h_{\mathbf{k}-\mathbf{q},A}\beta_{\mathbf{q}B} + \mathrm{H.c.}\Big\}, \qquad \text{(B.15)}
\end{aligned}
$$

$$H^{eff}_{3\mathrm{s}} = \frac{3}{2}\tau\sum_{k}\Big\{\cos(2k_y)h^{\dagger}_{\mathbf{k}A}h_{\mathbf{k}A} + \cos(2k_x)h^{\dagger}_{\mathbf{k}B}h_{\mathbf{k}B}\Big\}, \qquad \text{(B.16)}$$

and the remaining terms resulting in the energy renormalization

$$H_J^{eff} + H_z^{eff} = \frac{3}{4} J \sum_k \left( \beta_{\mathbf{k}A}^\dagger \beta_{\mathbf{k}A} + \beta_{\mathbf{k}B}^\dagger \beta_{\mathbf{k}B} \right) . \tag{B.17}$$

Therefore, the Hamiltonian given by Eqs. (B.15)–(B.17) reduces to the polaron Hamiltonian (3.32) after substituting $\sqrt{3}t/2 \to t$, and consequently $3J/4 \to J$ and $3\tau/4 \to \tau$. This substitution stems from the different definitions of the hopping $t$ in the $e_g$ and in the $t_{2g}$ systems — in the former case it is the $(dd\sigma)$ hopping between the $3z^2 - r^2$ orbitals along the $c$ direction, whereas in the latter case it is the hopping element between a pair of active $t_{2g}$ orbitals, e.g. $yz$ orbitals in the $(a, b)$ plane.

*Conclusions.*— In summary, we have shown that the Hamiltonian given by Eqs. (B.15)–(B.17) provides the framework to analyse the behaviour of certain lightly doped $e_g$ systems with FM planes and AO order which suppresses the interorbital hopping between occupied orbitals. Its equivalence to the polaron model (3.32) demonstrates that the results obtained and discussed in Chapter 3 should also apply to the case of a hole doped into the fluoride plane with the AO order of $e_g$ orbitals.

# Bibliography


[1] K. A. Chao, J. Spałek, and A. M. Oleś, J. Phys. C **10**, L271 (1977).

[2] K. A. Chao, J. Spałek, and A. M. Oleś, Phys. Rev. B **18**, 3453 (1978).

[3] P. W. Anderson, Science **235**, 1196 (1987).

[4] G. Blumberg, P. Littlewood, A. Gozar, B. S. Dennis, N. Motoyama, H. Eisaki, and S. Uchida, Science **297**, 584 (2002).

[5] T. Vuletić, B. Korin-Hamzić, S. Tomić, B. Gorshunov, P. Haas, T. Room, M. Dressel, J. Akimitsu, T. Sasaki, and T. Nagata, Phys. Rev. Lett. **90**, 257002 (2003).

[6] T. Vuletić, T. Ivek, B. Korin-Hamzić, S. Tomić, B. Gorshunov, P. Haas, M. Dressel, J. Akimitsu, T. Sasaki, and T. Nagata, Phys. Rev. B **71**, 012508 (2005).

[7] P. Abbamonte, G. Blumberg, A. Rusydi, A. Gozar, P. G. Evans, T. Siegrist, L. Venema, H. Eisaki, E. D. Isaacs, and G. A. Sawatzky, Nature **431**, 1078 (2004).

[8] A. Rusydi, P. Abbamonte, H. Eisaki, Y. Fujimaki, G. Blumberg, S. Uchida, and G. A. Sawatzky, Phys. Rev. Lett. **97**, 016403 (2006).

[9] A. Rusydi, M. Berciu, P. Abbamonte, S. Smadici, H. Eisaki, Y. Fujimaki, S. Uchida, M. Rübhausen, and G. A. Sawatzky, Phys. Rev. B **75**, 104510 (2007).

[10] S. R. White, I. Affleck, and D. J. Scalapino, Phys. Rev. B **65**, 165122 (2002).

[11] G. Roux, E. Orignac, S. R. White, and D. Poilblanc, Phys. Rev. B **76**, 195105 (2007).

[12] R. M. Kusters, J. Singleton, D. A. Keen, R. McGreevy, and W. Hayes, Physica B **155**, 362 (1989).

[13] R. von Helmolt, J. Wecker, B. Holzapfel, L. Schultz, and K. Samwer, Phys. Rev. Lett. **71**, 2331 (1993).

[14] S. Jin, T. H. Tiefel, M. McCormack, R. A. Fastnacht, R. Ramesh, and L. H. Chen, Science **264**, 413 (1994).

[15] P. Schiffer, A. P. Ramirez, W. Bao, and S.-W. Cheong, Phys. Rev. Lett. **75**, 3336 (1995).

[16] P. Horsch, J. Jaklič, and F. Mack, Phys. Rev. B **59**, 6217 (1999).

[17] K. Held and D. Vollhardt, Phys. Rev. Lett. **84**, 5168 (2000).

[18] M. S. Laad, L. Craco, and E. Müller-Hartmann, Phys. Rev. B **63**, 214419 (2001).

[19] S. Miyasaka, T. Okuda, and Y. Tokura, Phys. Rev. Lett. **85**, 5388 (2000).

[20] M. Imada, A. Fujimori, and Y. Tokura, Rev. Mod. Phys. **70**, 1039 (1998).

[21] L. N. Bulaevski, E. L. Nagaev, and D. I. Khomskii, Sov. Phys. JETP **27**, 836 (1968).

[22] C. L. Kane, P. A. Lee, and N. Read, Phys. Rev. B **39**, 6880 (1989).

[23] G. Martinez and P. Horsch, Phys. Rev. B **44**, 317 (1991).

[24] S. Miyasaka, Y. Okimoto, M. Iwama, and Y. Tokura, Phys. Rev. B **68**, 100406 (2003).

[25] J. Fujioka, S. Miyasaka, and Y. Tokura, Phys. Rev. B **72**, 024460 (2005).

[26] F. C. Zhang and T. M. Rice, Phys. Rev. B **37**, 3759 (1988).

[27] J. Hubbard, Proc. R. Soc. A **276**, 238 (1963).

[28] E. Dagotto, Rev. Mod. Phys. **66**, 763 (1994).

[29] M. Daghofer and A. M. Oleś, Acta Physica Polonica A **111**, 497 (2007).

[30] D. J. Klein and W. A. Seitz, Phys. Rev. B **8**, 2236 (1973).

[31] H. Eskes, A. M. Oleś, M. B. J. Meinders, and W. Stephan, Phys. Rev. B **50**, 17980 (1994).

[32] J. Spałek, Acta Physica Polonica A **111**, 409 (2007).

[33] J. Zaanen, *The Classical Condensates: from Crystals to Fermi-liquids*, Lecture Notes of the Lorentz Insitute for Theoretical Physics (Leiden), 1997.

[34] A. Gellé and M.-B. Lepetit, Phys. Rev. B **74**, 235115 (2003).

[35] T. Osafune, N. Motoyama, H. Eisaki, and S. Uchida, Phys. Rev. Lett. **78**, 1980 (1997).

[36] K. Magishi, S. Matsumoto, Y. Kitaoka, K. Ishida, K. Asayama, M. Uehara, T. Nagata, and J. Akimitsu, Phys. Rev. B **57**, 11533 (1998).

[37] N. Nücker, M. Merz, C. A. Kuntscher, S. Gerhold, S. Schuppler, R. Neudert, M. S. Golden, J. Fink, D. Schild, S. Stadler, V. Chakarian, J. Freeland, Y. U. Idzerda, K. Conder, M. Uehara, T. Nagata, J. Goto, J. Akimitsu, N. Motoyama, H. Eisaki, S. Uchida, U. Ammerahl, and A. Revcolevschi, Phys. Rev. B **62**, 14384 (2000).

[38] M. Uehara, T. Nagata, J. Akimitsu, H. Takahashi, N. Môri, and K. Kinoshita, J. Phys. Soc. Jpn. **65**, 2764 (1996).

[39] J. B. Grant and A. K. McMahan, Phys. Rev. B **46**, 8440 (1992).

[40] J. M. Tranquada, J. D. Axe, N. Ichikawa, A. R. Moodenbaugh, Y. Nakamura, and S. Uchida, Phys. Rev. Lett. **78**, 338 (1997).

[41] J. Zaanen, G. A. Sawatzky, and J. W. Allen, Phys. Rev. Lett. **55**, 418 (1985).

[42] A. M. Oleś, J. Zaanen, and P. Fulde, Physica B+C **148**, 260 (1987).

[43] J. Dutka and A. M. Oleś, Phys. Rev. B **42**, 105 (1990).

[44] S. Notbohm, P. Ribeiro, B. Lake, D. A. Tennant, K. P. Schmidt, G. S. Uhrig, C. Hess, R. Klingeler, G. Behr, B. Büchner, M. Reehuis, R. I. Bewley, C. D. Frost, P. Manuel, and R. S. Eccleston, Phys. Rev. Lett **98**, 027403 (2007).

[45] E. Dagotto, J. Riera, and D. Scalapino, Phys. Rev. B **45**, 5744 (1992).

[46] R. M. Noack, S. R. White, and D. J. Scalapino, Phys. Rev. Lett. **73**, 882 (1994).

[47] C. A. Hayward and D. Poilblanc, Phys. Rev. B **53**, 11721 (1996).

[48] E. Orignac and T. Giamarchi, Phys. Rev. B **56**, 7167 (1997).

[49] T. Siller, M. Troyer, T. M. Rice, and S. R. White, Phys. Rev. B **63**, 195106 (2001).

[50] A. M. Oleś and W. Grzelka, Phys. Rev. B **44**, 9531 (1991).

[51] S. Nishimoto, E. Jeckelmann, and D. J. Scalapino, Phys. Rev. B **66**, 245109 (2002).

[52] T. F. A. Müller, V. Anisimov, T. M. Rice, I. Dasgupta, and T. Saha-Dasgupta, Phys. Rev. B **57**, R12655 (1998).

[53] J. Zaanen and A. M. Oleś, Phys. Rev. B **37**, 9423 (1988).

[54] P. W. Anderson, Phys. Rev. **115**, 2 (1959).

[55] J. Kanamori, J. Phys. Chem. Solids **10**, 87 (1959).

[56] J. B. Goodenough, *Magnetism and the Chemical Bonds*, Interscience (Wiley), 1963.

[57] L. F. Feiner, J. H. Jefferson, and R. Raimondi, Phys. Rev. B **51**, 12797 (1995).

[58] L. F. Feiner, J. H. Jefferson, and R. Raimondi, Phys. Rev. B **53**, 8751 (1996).

[59] R. Raimondi, J. H. Jefferson, and R. Raimondi, Phys. Rev. B **53**, 8774 (1996).

[60] G. Kotliar and A. E. Ruckenstein, Phys. Rev. Lett. **57**, 1362 (1986).

[61] E. Barnes, J. Phys. F **6**, 1375 (1976).

[62] M. C. Gutzwiller, Phys. Rev. **137**, A1726 (1965).

[63] F. C. Zhang, C. Gros, T. M. Rice, and H. Shiba, Supercond. Sci. Technol. **1**, 36 (1988).

[64] H. Eskes, G. Sawatzky, and L. Feiner, Physica C **160**, 424 (1989).

[65] K. Wohlfeld, A. M. Oleś, and G. A. Sawatzky, Physica C **460-462**, 1043 (2007).

[66] R. Peierls, Proc. Phys. Soc. London **A 49**, 72 (1937).

[67] W. F. Brinkman and T. M. Rice, Phys. Rev. B **2**, 1324 (1970).

[68] A. Nazarenko, K. J. E. Vos, S. Haas, E. Dagotto, and R. J. Gooding, Phys. Rev. B **51**, 8676 (1995).

[69] A. Damascelli, Z. Hussain, and Z.-X. Shen, Rev. Mod. Phys. **75**, 473 (2003).

[70] S. Schmitt-Rink, C. M. Varma, and A. E. Ruckenstein, Phys. Rev. Lett. **60**, 2793 (1988).

[71] A. B. Harris, T. Yildirim, A. Aharony, O. Entin-Wohlman, and I. Y. Korenblit, Phys. Rev. B **69**, 035107 (2004).

[72] K. I. Kugel and D. I. Khomskii, Sov. Phys. Solid State **17**, 285 (1975).

[73] K. I. Kugel and D. I. Khomskii, Sov. Phys. Usp. **25**, 231 (1982).

[74] Y. Tokura and N. Nagaosa, Science **288**, 462 (2000).

[75] J. Zaanen and A. M. Oleś, Phys. Rev. B **48**, 7197 (1993).

[76] L. F. Feiner and A. M. Oleś, Phys. Rev. B **59**, 3295 (1999).

[77] J. van den Brink, P. Horsch, and A. M. Oleś, Phys. Rev. Lett. **85**, 5174 (2000).

[78] S. A. Trugman, Phys. Rev. B **37**, 1597 (1988).

[79] H. Eskes and R. Eder, Phys. Rev. B **54**, R14226 (1996).

[80] J. Bała, A. M. Oleś, and J. Zaanen, Phys. Rev. B **52**, 4597 (1995).

[81] P. Horsch, G. Khaliullin, and A. M. Oleś, Phys. Rev. Lett. **91**, 257203 (2003).

[82] J. van den Brink, P. Horsch, and A. M. Oleś, Phys. Rev. Lett. **85**, 5174 (2000).

[83] G. Khaliullin, P. Horsch, and A. M. Oleś, Phys. Rev. Lett. **86**, 3879 (2001).

[84] J. van den Brink, P. Horsch, F. Mack, and A. M. Oleś, Phys. Rev. B **59**, 6795 (1999).

[85] M. Daghofer, K. Wohlfeld, A. M. Oleś, E. Arrigoni, and P. Horsch, Phys. Rev. Lett. **100**, 066403 (2008).

[86] K. Wohlfeld, A. M. Oleś, M. Daghofer, and P. Horsch, Acta Physica Polonica A **115**, 110 (2009).

[87] M. Potthoff, M. Aichhorn, and C. Dahnken, Phys. Rev. Lett. **91**, 206402 (2003).

[88] W. Stephan and P. Horsch, Phys. Rev. Lett. **66**, 2258 (1991).

[89] M. Daghofer, A. M. Oleś, and W. von der Linden, Phys. Rev. B **70**, 184430 (2004).

[90] R. Kilian and G. Khaliullin, Phys. Rev. B **60**, 13458 (1999).

[91] M. Fleck, A. M. Oleś, and L. Hedin, Phys. Rev. B **56**, 3159 (1997).

[92] H. Wu and D. I. Khomskii, Phys. Rev. B **76**, 155115 (2007).

[93] A. M. Oleś, P. Horsch, L. F. Feiner, and G. Khaliullin, Phys. Rev. Lett. **96**, 147205 (2006).

[94] S. Ishihara, Phys. Rev. Lett. **94**, 156408 (2005).

[95] K. Wohlfeld and A. M. Oleś, Physica Status Solidi (b) **243**, 142 (2006).

[96] K. Wohlfeld, AIP Conf. Proc. **846**, 295 (2006).

[97] T. Chatterji, editor, *Colossal Magnetoresistive Manganites*, Kluwer Academic Publishers, 2004.

[98] A. M. Oleś, Phys. Rev. B **28**, 327 (1983).

[99] A. M. Oleś, P. Horsch, and G. Khaliullin, Phys. Rev. B **75**, 184434 (2007).

[100] A. M. Oleś, G. Khaliullin, P. Horsch, and L. F. Feiner, Phys. Rev. B **72**, 214431 (2005).

[101] J. Fujioka, S. Miyasaka, and Y. Tokura, Phys. Rev. Lett. **97**, 196401 (2006).

[102] T. Mizokawa and A. Fujimori, Phys. Rev. B **54**, 5368 (1996).

[103] G. Khaliullin, P. Horsch, and A. M. Oleś, Phys. Rev. B **70**, 195103 (2004).

[104] A. Weisse, J. Loos, and H. Fehske, Phys. Rev. B **64**, 054406 (2001).

[105] M. Brunner, F. F. Assaad, and A. Muramatsu, Phys. Rev. B **62**, 15480 (2000).

[106] M. Bejas, A. Greco, and A. Foussats, Phys. Rev. B **73**, 245104 (2006).

[107] L. F. Feiner and A. M. Oleś, Phys. Rev. B **71**, 144422 (2005).

[108] P. Wróbel, W. Suleja, and R. Eder, Phys. Rev. B **78**, 064501 (2008).

[109] J. Zaanen, Science **319**, 1205 (2008).

[110] M. Troyer and U.-J. Wiese, Phys. Rev. Lett. **94**, 170201 (2005).

[111] P. W. Anderson, *Basic Notions of Condensed Matter Physics*, Benjamin/Cummings, 1984.

[112] J. Zaanen, F. Krueger, J.-H. She, D. Sadri, and S. I. Mukhin, preprint cond-mat/0802.2455 (2008).

[113] T. Giamarchi, *Quantum Physics in One Dimension*, Oxford Science Publications, 2004.

[114] A. Georges, G. Kotliar, W. Krauth, and M. J. Rozenberg, Rev. Mod. Phys. **68**, 13 (1996).

[115] M. Hidaka, K. Inoue, I. Yamada, and P. J. Walker, Physica B+C **121**, 343 (1983).

[116] J. Bała, A. M. Oleś, and P. Horsch, Phys. Rev. B **65**, 134420 (2002).

# Streszczenie

W niniejszej pracy zostały poruszone trzy problemy dotyczące silnie oddziałujacych elektronów w tlenkach metali przejściowych. Pierwszy z nich dotyczył wyjaśnienia obecności fali gęstości ładunku o nieparzystym okresie (3 oraz 5) w płaszczyznie złożonej z zachodzących na siebie drabin $Cu_2O_5$ w związku $Sr_{14-x}Ca_xCu_{24}O_{41}$ (przy domieszkowaniu odpowiadającym związkom $x = 0$ oraz $x = 11$). Drugie zagadnienie, poruszone w niniejszej pracy, dotyczyło (potencjalnej) możliwości lokalizacji pojedynczej dziury w tlenkach metali przejściowych z degeneracją orbitalną. Trzeci problem to podanie odpowiedzi na pytanie w jaki sposób może poruszać się pojedyncza dziura w płaszczynie *ab* ze wsółistniejącym uporządkowaniem spinowym (antyferromagnetycznym) oraz orbitalnym (z alternującymi orbitalami) w związku $LaVO_3$.

W celu rozwiązanie wyżej wymienionych problemów zostały wyprowadzone rozszerzone wersje modelu $t$–$J$ dla każdej z tych sytuacji: dla pierwszego zagadnienia – model $t$–$J$ dla zachodzących na siebie drabin, dla drugiego problemu – orbitalny model $t$–$J$ z oddziaływaniem typu Isinga pomiędzy orbitalnymi pseudospinami oraz z wyrazami trójwęzłowymi, dla trzeciego zagadnienia – spinowo-orbitalny model $t$–$J$ z wyrazami trójwęzłowymi. Okazało się, że rozwiązania powyższych modeli w formalizmie niewolniczych cząstek oraz w przybliżeniu średniego pola lub samozgodnym przybliżeniu Borna doprowadziło do wyjaśnienia problemów postawionych w niniejszej pracy: (1) na skutek efektywnego odpychania pomiędzy dziurami znajdującymi się na sąsiadujących ze sobą miejscach w zachodzących na siebie dwóch sąsiednich drabinach fala gęstości ładunku o nieparzystym okresie okazała się stanem podstawym układu; (2) włączenie wyrazów trójwęzłowych do orbitalnego modelu $t$–$J$ pokazało, że możliwy jest koherentny ruch dziury w tlenkach metali przejściowych z degeneracją orbitalną; oraz (3) szczegółowa analiza oddziaływania pomiędzy dziurą a kolektywnymi wzbudzeniami (w porządku antyferromagnetycznym oraz z alternującymi orbitalami) pokazała, że dziura w płaszczyznie *ab* w $LaVO_3$ zachowuje się podobnie jak dziura dodana do płaszczyzny jedynie z porządkiem orbitalnym ale bez porządku spinowego. Łacznie w niniejszej pracy zostało pokazane, że pewne niewielkie rozszerzenia modelu $t$–$J$ prowadzą do wyjaśnienia szerokiej klasy zjawisk w tlenkach metali przejściowych z silnie oddziałującymi elektronami.

# The author's list of publications

1. K. Wohlfeld, A. M. Oleś, 'Double exchange model in cubic vanadates', Physica Status Solidi (b) **243**, 142-145 (2006).
2. K. Wohlfeld, 'Double exchange model for correlated electrons in systems with $t_{2g}$ orbital degeneracy', AIP Conference Proceedings **846**, 295-303, (2006).
3. K. Wohlfeld, A. M. Oleś, G. A. Sawatzky, 'Charge density wave in the spin ladder of $Sr_{14-x}Ca_xCu_{24}O_{41}$', Physica C **460-462**, 1043-1044 (2007).
4. K. Wohlfeld, 'Doped Spin Ladder: Zhang-Rice Singlets or Rung-centred Holes?', AIP Conference Proceedings **918**, 337-341, (2007).
5. K. Wohlfeld, A. M. Oleś, G. A. Sawatzky, 'Origin of charge density wave in the coupled spin ladders of $Sr_{14-x}Ca_xCu_{24}O_{41}$', Physical Review B **75**, 180501(R)/1-4 (2007).
6. M. Daghofer, K. Wohlfeld, A. M. Oleś, E. Arrigoni, P. Horsch, 'Absence of hole confinement in transition metal oxides with orbital degeneracy', Physical Review Letters **100**, 066403/1-4 (2008).
7. K. Wohlfeld, 'Polaron in the t-J models with three-site terms: the SU(2) and the Ising cases', AIP Conference Proceedings **1014**, 265-269, (2008).
8. K. Wohlfeld, M. Daghofer, A. M. Oleś, P. Horsch, 'Spectral properties of orbital polarons in Mott insulators', Physical Review B **78**, 214423/1-24 (2008).
9. K. Wohlfeld, A. M. Oleś, M. Daghofer, P. Horsch, 'Reiter's wavefunction applied to a $t_{2g}$ orbital $t$–$J$ model', Acta Physica Polonica A **115**, 110-113 (2009).
10. K. Wohlfeld, P. Horsch, A. M. Oleś, 'Orbitally induced string formation in the spin-orbital polarons', to appear in Physical Review B **79** (2009).
11. K. Wohlfeld, 'Spin, orbital, and spin-orbital polarons in transition metal oxides', to appear in AIP Conference Proceedings (2009).

While the thesis is based on papers no. 4-5, 7-8 and 10-11 (see beginning of each main chapter for a detailed list), papers no. 1-3, 6, and 9 were cited as Refs. [95], [96], [65], [85], and [86] (respectively) in the thesis.

# Acknowledgments

I would like to thank my supervisor Professor Andrzej M. Oleś whose constant help and support made this thesis possible. He also introduced me to all the complex phenomena related to strongly correlated electron systems, paper publishing, scientific community, and (just generally) with the mature life. Besides, it is a great pleasure to acknowledge the scientific collaboration with Doctor Maria Daghofer, Doctor Peter Horsch and Professor George A. Sawatzky – without their research this thesis would not have been completed (at least in the current form).

At this point many people also list their friends, colleagues, and family members whose help and support had also great impact on the shape of the thesis. However, I am not going to make such a list. Simply, those who helped me will guess that I indeed have in mind their Names while writing down these words.

Finally, I also wish to acknowledge financial support by: the Jagellonian University, the Foundation for Polish Science (FNP), the Polish Ministry of Science and Higher Education under Project No. N202 068 32/1481, the Max Planck Society, and the F. Kogutowska Foundation of the Jagellonian University.